



National Library
of Canada

Bibliothèque nationale
du Canada

Canadian Theses Service Service des thèses canadiennes

Ottawa, Canada
K1A 0N4

NOTICE

The quality of this microform is heavily dependent upon the quality of the original thesis submitted for microfilming. Every effort has been made to ensure the highest quality of reproduction possible.

If pages are missing, contact the university which granted the degree.

Some pages may have indistinct print especially if the original pages were typed with a poor typewriter ribbon or if the university sent us an inferior photocopy.

Reproduction in full or in part of this microform is governed by the Canadian Copyright Act, R.S.C. 1970, c. C-30, and subsequent amendments.

AVIS

La qualité de cette microforme dépend grandement de la qualité de la thèse soumise au microfilmage. Nous avons tout fait pour assurer une qualité supérieure de reproduction.

S'il manque des pages, veuillez communiquer avec l'université qui a conféré le grade.

La qualité d'impression de certaines pages peut laisser à désirer, surtout si les pages originales ont été dactylographiées à l'aide d'un ruban usé ou si l'université nous a fait parvenir une photocopie de qualité inférieure.

La reproduction, même partielle, de cette microforme est soumise à la Loi canadienne sur le droit d'auteur, SRC 1970, c. C-30, et ses amendements subséquents.

Leached Chrysotile Asbestos:
Characterization, Leaching Mechanism
and Use in the Synthesis of Zeolites

Anne Vaillancourt

A Thesis
in
The Department
of
Chemistry

Presented in Partial Fulfillment of the Requirements
for the Degree of Master of Science at
Concordia University
Montréal, Québec, Canada

September 1991

© Anne Vaillancourt, 1991



National Library
of Canada

Bibliothèque nationale
du Canada

Canadian Theses Service Service des thèses canadiennes

Ottawa, Canada
K1A 0N4

The author has granted an irrevocable non-exclusive licence allowing the National Library of Canada to reproduce, loan, distribute or sell copies of his/her thesis by any means and in any form or format, making this thesis available to interested persons.

The author retains ownership of the copyright in his/her thesis. Neither the thesis nor substantial extracts from it may be printed or otherwise reproduced without his/her permission.

L'auteur a accordé une licence irrévocable et non exclusive permettant à la Bibliothèque nationale du Canada de reproduire, prêter, distribuer ou vendre des copies de sa thèse de quelque manière et sous quelque forme que ce soit pour mettre des exemplaires de cette thèse à la disposition des personnes intéressées.

L'auteur conserve la propriété du droit d'auteur qui protège sa thèse. Ni la thèse ni des extraits substantiels de celle-ci ne doivent être imprimés ou autrement reproduits sans son autorisation.

ISBN 0-315-68769-X

Canada

CONCORDIA UNIVERSITY

Division of Graduate Studies

This is to certify that the thesis prepared

By: Anne Vaillancourt

Entitled: Leached Chrysotile Asbestos:
Characterization, Leaching Mechanism
and Use in the Synthesis of Zeolites


and submitted in partial fulfilment of the requirements for
the degree of

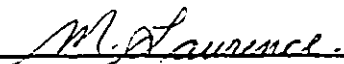
Master in Chemistry

complies with the regulations of this University and meets the
accepted standards with respect to originality and quality.

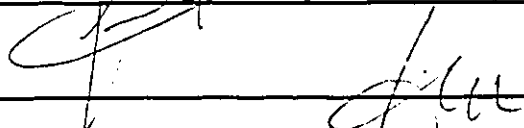
Signed by the final examining committee:


Chair

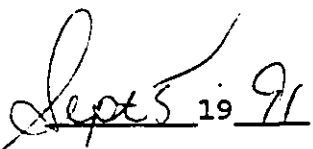

Examiner


Examiner


Thesis Supervisor


Thesis Supervisor

Approved by 
Chair of Department or Graduate Program Director


Sept 5 19 91


Dean of Faculty

ABSTRACT

LEACHED CHRYSOTILE ASBESTOS:
CHARACTERIZATION, LEACHING MECHANISM
AND USE IN THE SYNTHESIS OF ZEOLITES.

ANNE VAILLANCOURT

The controversy regarding commercial use of asbestos has resulted in the banning of most applications in North America because of the carcinogenicity of most fibrous asbestos minerals. The work presented in this thesis is concerned with the transformation of the raw asbestos mineral to an intermediate material which is used for the synthesis of zeolites which are health safe and have wide applications in industry.

First, a complete indexation of the X-ray diffraction pattern of chrysotile was proposed. This was followed by the use of techniques such as X-ray diffraction and bulk density measurements for the study of the mechanism of transformation of chrysotile to amorphous silica hemihydrate. The results are discussed in relation to the fibrous structure of chrysotile.

In the second part, three types of zeolites were synthesized (Na-Y, Na-X and Na-A) using as starting material both silica gel (conventional method) and leached asbestos (new method). In a kinetic study of the crystallization of

Na-A zeolite, it was found that leached asbestos is clearly more efficient than silica gel for the preparation of zeolites. The results are discussed in terms of the degree of polymerization of the type of silica used.

ACKNOWLEDGEMENTS

I wish to express my sincere gratitude and appreciation to my thesis supervisors, Dr. G. Denes and Dr. R. Le Van Mao, for their guidance, cooperation and patience throughout this research project.

I would like to thank the members of my research committee for their cooperation.

I am very grateful to all of my colleagues and especially to Mr. B. Sjiariel for his constant technical assistance.

I also wish to acknowledge in a special way, Mr. P. Kipkemboi whose past involvement in this field was a determining factor in permitting me to obtain interesting results throughout this project.

These acknowledgements would be incomplete if I did not also express my gratitude to Mr. Sid Yousri from Pratt and Whitney for his continuous encouragement and support.

In addition, I would like to thank my parents and my husband for their continuous support and understanding.

TABLE OF CONTENT

	PAGE
TABLE OF CONTENTS.....	vi
LIST OF FIGURES.....	x
LIST OF TABLES.....	xiv
INTRODUCTION	1
CHAPTER I Earlier studies of chrysotile	5
and zeolites	
CHAPTER 2 EXPERIMENTAL SECTION.....	12
2.1 Preparation of Leached Asbestos	12
Materials, Alix	
2.2 Synthesis of Zeolites	12
2.3 X-Ray Powder Diffraction	19
2.3.1 Introduction	19
2.3.2 Degree of Crystallinity	20
Measurements	
2.3.2.1 Chrysotile Asbestos and ..	20
Alix Materials	
2.3.2.2 Na-A zeolite	24
2.3.3 Reproducibility	26
Study of DC	
2.3.4 Instrumentation	26
2.3.5 Sample Preparations	28
for XRD Experiments	
2.4 Bulk Density Measurements	30
2.4.1 Introduction	30
2.4.2 Apparatus and Procedure	31
2.4.3 Calculation of the Bulk Density.	36
2.5 BET: Specific Surface Area Measurements ..	38

2.6	Electron Microscopy	42
2.7	Elemental Analysis by Atomic Absorption Spectroscopy	43
2.8	^{29}Si MAS-NMR Spectroscopy	43
3.0	RESULTS AND DISCUSSIONS.....	44
3.1	Chrysotile Asbestos: X-Ray	44
	Powder Diffraction	
3.1.1	Assignment of the X-Ray Powder Diffraction Pattern of Chrysotile Asbestos	44
3.1.2	Interpretation of the Width ... of the Diffraction Peaks of Chrysotile	53
3.1.2.1	Common Reasons for..... Broadening of the Bragg Peaks	53
3.1.2.2	Line Broadening in Chrysotile Asbestos	57
3.2	Leached Chrysotile Asbestos:	69
	Alix Materials	
3.2.1	The Leaching Process	69
3.2.2	Definition of the MLD	71
3.2.3	Leaching Process with Strong Mineral Acids	72
3.2.4	X-Ray Diffraction	74
3.2.4.1	Effect of Leaching on Chrysotile Asbestos	74
3.2.4.2	Degree of Crystallinity... Studies by XRD: Case of Leaching with Strong Mineral Acids	78
3.2.5	Bulk Density and Surface Area of Chrysotile Asbestos Leached by Strong Mineral Acids	88
3.2.6	Secondary Leaching of Chrysotile Asbestos with Weak Organic Acids	102

3.2.7	Degree of Crystallinity of Alix Materials Leached with Weak Organic Acids	104
3.2.8	Bulk Density of Asbestos Chrysotile Leached with weak Organic acids	111
3.2.9	A Proposed Mechanism	116
3.3	Zeolite Syntheses	128
3.3.1	General Information	128
3.3.2	Na-Y Chrysozeolites	132
3.3.3	Na-X Chrysozeolites	142
3.3.4	Na-A Chrysozeolites	152
3.4	A Study of the Kinetics of the Crystallization of Na-A Zeolite	167
3.4.1	Introduction	167
3.4.2	Comparative Kinetic Study by XRD	173
3.4.3	Solubility Experiment of Silica	186
3.4.4	Study of the Kinetics of Crystallization of Na-A Zeolite: Sigmoid Shaped Curve	191
3.4.5	Evaluation of the Crystallization Constant	193
3.4.6	Morphological Study and Particulate Size Distribution By SEM	198
3.4.7	Kinetic Study by Bulk Density Measurements	214
3.4.8	Specific Surface Area of Na-A Zeolites by BET	216
3.4.9	²⁹ Si Magic Angle Spinning Solid State NMR Study of the Formation of Na-A Zeolite	219
Chapter 4	CONCLUSIONS	224

REFEPENCES	239
APPENDICES.....	246

LIST OF FIGURES

	Page
0.1 Main types of asbestos	2
1.1 Projection of the crystal structure of chrysotile asbestos along the fiber axis	7
1.2 Idealized representation of fibril packing in chrysotile	8
2.1 Hydrothermal synthesis reactor	16
2.2 Steps involved in the synthesis of zeolites	17
2.3 X-ray powder diffraction peaks used for the degree of crystallinity experiments for chrysotile asbestos and Alix materials	22
2.4 X-ray powder diffraction peaks used for the degree of crystallinity experiments of Na-A zeolite	25
2.5 Estimated maximum error allowed on the degree of crystallinity	27
2.6 The bulk density apparatus	32
2.7 Weighing setting	34
2.8 Setting of the density apparatus on the vacuum line	35
3.1 Assignment of the X-ray powder diffraction pattern of 7TF12 chrysotile asbestos	45
3.2 X-ray powder diffraction pattern of Canadian chrysotile asbestos reported in the literature	46
3.3 Effect of lattice strain on the width and position of Bragg peaks	56
3.4 Enlargement of the X-ray powder diffraction pattern of 7TF12 batch of chrysotile asbestos used for line broadening study	59
3.5 Orientation of the b axis in the direction of curvature of the sheets	62

3.6	Spiral winding of chrysotile sheet that produces the tubular shape of the fibril	64
3.7	High-resolution electron micrograph of section of chrysotile asbestos	64
3.8	Comparison between the distorted and ideal unit-cells	67
3.9	X-ray powder diffraction pattern of leached chrysotile asbestos versus MLD	75
3.10	Chrysotile degree of crystallinity (DC) versus the normality of the acid used for leaching at 80 °C for 4 hours	79
3.11	Corrected chrysotile degree of crystallinity (DC) versus the normality of the acid used for leaching at 80 °C for 4 hours	81
3.12	Relationship between the corrected degree of crystallinity and MLD for HCl and H ₂ SO ₄ acid solutions for a reaction time of 4 hours at 80 °C	83
3.13	Bulk density of chrysotile asbestos versus acid normality for a reaction time of 4 hours at 80 °C	89
3.14	Bulk density versus MLD for chrysotile leached by using H ₂ SO ₄ solutions at 80 °C for 4 hours	94
3.15	Bulk density versus MLD for chrysotile leached using HCl solutions at 80 °C for 4 hours	95
3.16	BET specific surface area versus bulk density for chrysotile leached with HCl and H ₂ SO ₄ solutions at 80 °C for 4 hours	98
3.17	Corrected degree of crystallinity versus the normality of the weak acid used for secondary leaching of chrysotile at 80 °C for 4 hours.....	105
3.18	Corrected degree of crystallinity versus MLD for chrysotile after secondary leaching with OXA and ACA at 80 °C for 4 hours	109
3.19	Bulk density of chrysotile versus the normality of the acid used for secondary leaching at 80 °C for 4 hours	112
3.20	Bulk density of chrysotile versus MLD in the case of secondary leaching at 80 °C for 4 hours	115

3.21	Proposed steps for acid leaching of chrysotile asbestos	118
3.22	Interpretation of the ratio MgO/SiO_2 during leaching of chrysotile with strong acids	125
3.23	Schematic free energy relations between reaction mixtures and various zeolite phases, represented by a,b,c	129
3.24	X-ray powder diffraction patterns of the synthesized Na-Y zeolites	134
3.25	X-ray powder diffraction patterns of the synthesized Na-X zeolites	144
3.26	X-ray powder diffraction patterns of the synthesized Na-X chrysozeolites	149
3.27	X-ray powder diffraction patterns of the synthesized Na-A zeolites and chrysozeolites	154
3.28	Condensation of precursor aluminosilicates to give 4 ring units	169
3.29	Polymerization of 4-membered aluminosilicate rings to give more complex units	170
3.30	X-ray powder diffraction patterns of Na-A zeolite samples used for the comparative kinetic study	174
3.31	X-ray powder diffraction patterns of Na-A chrysozeolite samples used for the comparative kinetic study	178
3.32	Plot of the degree of crystallinity (DC) of Na-A zeolite versus reaction time from 0 to 72 hours.....	184
3.33	Plot of the degree of crystallinity (DC) of Na-A zeolite versus reaction time from 0 to 2 hours.....	185
3.34	Plot of log (DC) versus reaction time	195
3.35	Scanning electron micrographs of the solid obtained in the Na-A zeolite synthesis versus reaction time, for the two sources of silica.....	199
3.36	Average particle dimension of Na-A zeolite versus reaction time	211

- 3.37 Average particle dimension of Na-A zeolite
versus reaction time in the first two hours212
- 3.38 ^{29}Si Magic Angle Spinning NMR of Na-A zeolite
samples obtained from silica gel and Alix 168221

LIST OF TABLES

	Page
2.1 Chemical compositions of Alix materials used for zeolite syntheses (wt%, on dried oxides basis). The chrysotile asbestos was 7TF12 batch from Asbestos, Québec	13
3.1 Crystalline compounds with the formula $Mg_3Si_2O_5(OH)_4$ listed in the JCPDS powder diffraction file	47
3.2 Assignment of the X-ray diffraction pattern of batch 7TF12 chrysotile asbestos from Asbestos, Québec	49
3.3 Unit-cell parameters for orthochrysotile- 20_{c1}	50
3.4 Average particle dimensions determined from the broadening of the X-ray diffraction lines	60
3.5 Relationship between the degree of crystallinity (DC) and the corrected degree of crystallinity (corrected DC) versus acid normality and MLD, for a reaction time = 4 hours, a reaction temperature = 80 °C in HCl	84
3.6 Relationship between the degree of crystallinity (DC) and the corrected degree of crystallinity (corrected DC) versus acid normality and MLD for a reaction time = 4 hours, a reaction temperature = 80 °C in H_2SO_4	85
3.7 Bulk density of chrysotile asbestos when HCl was used as leaching reagent (Temperature = 80 °C, reaction time = 4 hours)	90
3.8 Bulk density of chrysotile asbestos when H_2SO_4 was used as leaching reagent. (Temperature = 80 °C, reaction time = 4 hours)	91
3.9 Bulk density values of various types of silica	96
3.10 Specific surface area of Alix samples. (Temperature = 80 °C, reaction time = 4 hours)	99

3.11	Corrected degree of crystallinity (corrected DC) versus MLD and the normality of the acetic acid used for secondary leaching of chrysotile at 80 °C for 4 hours	106
3.12	Corrected degree of crystallinity (corrected DC) versus MLD and the normality of the oxalic acid used for secondary leaching of chrysotile at 80 °C for 4 hours	107
3.13	Effect of secondary leaching at 80 °C for 4 hours on bulk density	113
3.14	Theoretical MgO/SiO ₂ ratios of the intermediate species formed according to the proposed mechanism.....	121
3.15	MgO/SiO ₂ ratio versus MLD in leached chrysotile based on analytical results	123
3.16	Experimental parameters for zeolite Na-Y syntheses. The reaction time was 72 hours, the reaction temperature was 100 °C, and the source of silica was silica gel. An aging time of the reaction mixture was used for VY03 sample	133
3.17	Experimental parameters used for zeolite Na-X syntheses. The reaction time used was 72 hours and temperature was 100 °C for all reactions. Two sources of silica were used (silica gel and Alix materials	143
3.18	Experimental parameters used for zeolite Na-A syntheses. The reaction time and temperature used were 72 hours and 100 °C respectively for all samples. The source of silica was silica gel, sodium silicate, or Alix materials	153
3.19	Experimental parameters used for the kinetic study of the crystallization of zeolite Na-A. Two sources of silica were used i.e. silica gel and Alix 168 (MLD=94). The reaction temperature was kept at 100 °C for all samples	171
3.20	Effect of reaction time on the degree of crystallinity. The reaction temperature was kept at 100 °C for all samples	183
3.21	Solubility of Alix 168 and silica gel in the reaction mixture used for the synthesis of Na-A zeolite	188

3.22	Evaluation of the crystallization constant for Na-A zeolites. Alix 168 and silica gel were the two sources of silica compared in this study	196
3.23	Study of the average particle dimension of Na-A zeolite versus reaction time. The reaction temperature was kept constant at 100 °C	210
3.24	Bulk density of Na-A zeolites versus reaction time and the source of silica used	215
3.25	Specific surface area measurements of Na-A zeolite using the BET technique	217
3.26	²⁹ Si Solid State NMR results of synthesized Na-A zeolite. Silica gel and Alix 168 were the two sources of silica used	220

INTRODUCTION

Chrysotile asbestos is a cheap and abundant natural resource of Québec. This material exhibits a large number of desirable properties such as : a fibrous form, an internal structure that is mechanically strong yet elastic and flexible, low thermal and electrical conductivities, an excellent thermal stability and some interesting surface characteristics. Chrysotile belongs to the serpentine asbestos group and its normal chemical composition is reported in Figure 0.1. Because of its wide range of useful properties, chrysotile is an important constituent of a large number of manufactured products. It actually accounts for 95 % of all the asbestos produced in the world. Chrysotile is used in a wide range of industrial applications such as : construction, automobiles, ship building, aeronautics, aerospace, pharmaceuticals, and the nuclear industries [1-3]. Products which contain chrysotile may be classified according to five distinctive categories of applications: asbestos cement, papers and felts, friction materials, asbestos textiles, and additives.

In the last two decades, the highly publicized health problems caused by chrysotile fibers have resulted in a considerable decrease of its economical use and in official bans in several countries (U.S.A. and western Europe). Industry has shifted more and more to using a number of substitute fibers. In addition, considerable attention has been paid not only to safer ways of using chrysotile based

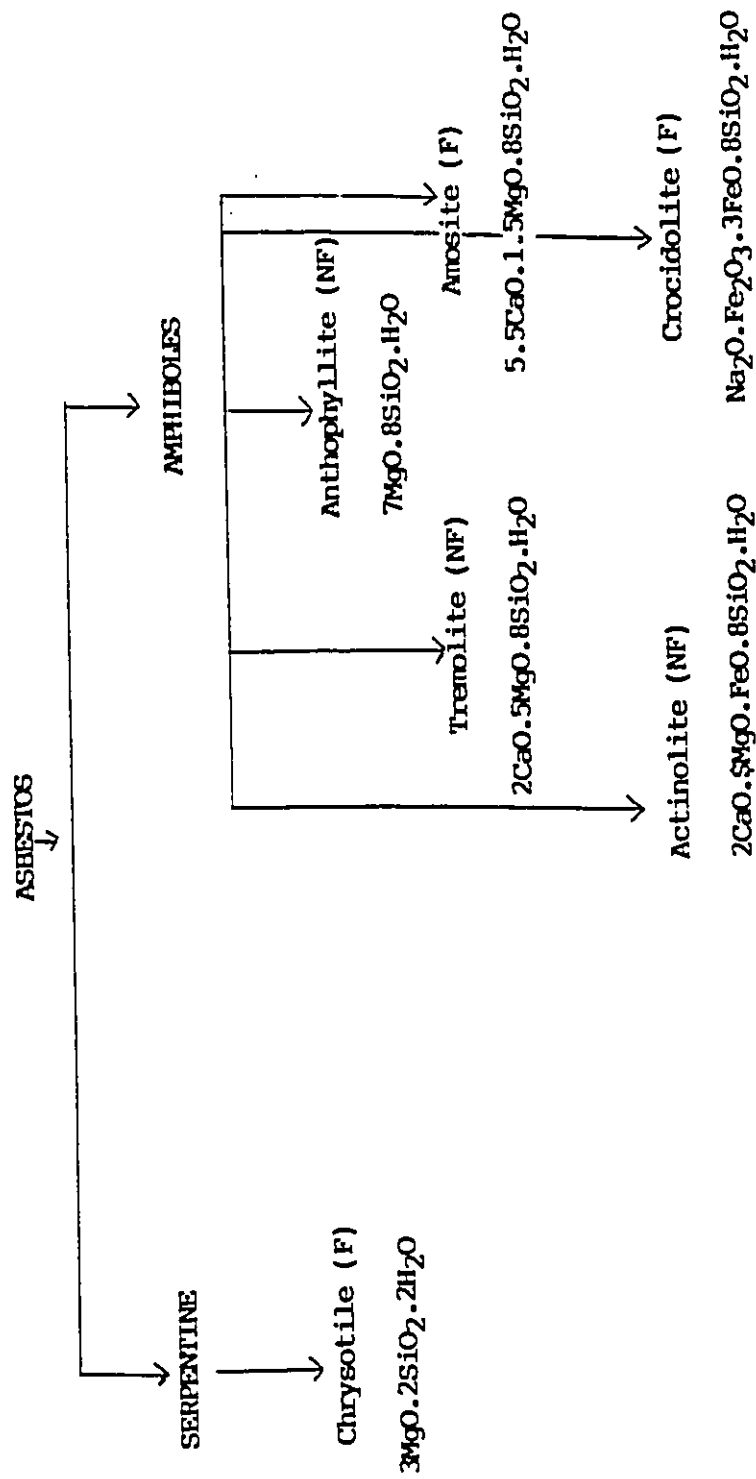


Figure 0.1 Main Types of asbestos [11]
(F): fibrous
(NF): non fibrous

products but also to its conversion to new non-toxic materials. The successful synthesis of zeolites from processed chrysotile by Le Van Mao et al [4,5] has led to founded hopes for interesting industrial applications. Zeolites and their counterparts, chryso-zeolites (zeolites prepared using chrysotile), do not show any cytotoxicity [6] which is believed to be the source of the carcinogenic activity of asbestos. The commercial interest in zeolites originates from their important applications as selective adsorbents, catalysts and ion-exchangers [7,8]. Today's market of zeolites accounts for several billions US dollars a year.

Immediately following the discovery of the chryso-zeolites, a vast research and development program was devised in early 1982. ZSM-5 chryso-zeolite was synthesized and tested in several reactions including the methanol-to-gasoline process [4,5,9,10]. Since the synthesis of chryso-zeolites is a two-step process, it was decided in 1985 to investigate the details of the first step, which is the acid leaching of the asbestos fibers. Results from Kipkempoi's work [11] provided a technological view of the influence of the leaching parameters (strength and nature of the acid media, temperature and time of the leaching operation) on some of the characteristics of the resulting Alix materials, especially the chemical composition (and the related magnesium leaching degree), the surface area, the infrared spectrum and some preliminary information on the solid state

^{29}Si NMR spectrum.

The aim of the present work is to provide additional information and a better understanding of the leaching mechanism and the probable influence of the Alix structural and textural properties on the zeolite synthesis. The zeolites investigated in this work are of the A and X types, the structures and properties of which are well-known [7,12-17]. The conditions for the synthesis of such zeolites is not as demanding, in terms of temperature and presence of specific ions, as that for the ZSM-5 zeolite, and thus from the examination of their properties, the link between the two preparation steps of the chryso-zeolites could be easily established.

This thesis is organized as follows.

Chapter I : EARLIER STUDIES OF CHRYSOTILE AND ZEOLITES

In this chapter, results from our laboratory and from other research groups, necessary for the understanding of our own results, are reported. This is done by carefully examining the properties of the leached materials and the chryso-zeolites, which are the most likely to help elucidating the corresponding mechanisms of formation.

Chapter II: EXPERIMENTAL

Details about the procedures of preparation and some particular characterization techniques are given.

Chapter III: RESULTS AND DISCUSSION.

Chapter IV : CONCLUSIONS

CHAPTER 1 Earlier studies of chrysotile and zeolites.

Chryso-zeolites are prepared from chrysotile fibers in a two step process. The preliminary step consists of leaching out some magnesium from the asbestos. The structural and textural changes within the chrysotile fibers allow the exposure of the silicon atoms. These atoms or aggregates of the same are the sites for the formation of zeolite nuclei in the subsequent step of preparation.

i) This is not the first report on magnesium leaching [18]. However, in the past, it was done with the aim of modifying the surface properties of the chrysotile fibers. The ultimate objective of these acid leaching studies was to decrease the toxicity of the asbestos fibers which is partially associated to the presence of magnesium at the outermost layer of the fibers. Some leaching experiments were carried out with concentrated acids with the aim of removing Mg as completely as possible. The first systematic studies of acid leaching of chrysotile began only with our research program.

For the purpose of understanding the Results and Discussion chapter and the way the chrysotile fibers undergo structural and morphological changes upon acid leaching, it is necessary to refer to the crystal structure and texture of chrysotile. Bragg [19,20] and Warren et al [19,21] determined that chrysotile has a layered type structure, which consists of two parallel sheets, one made of SiO_4

tetrahedra and the other of Mg (O or OH)₆ octahedra, as shown on Figure 1.1. The backbone of the structure is an infinite silica sheet (Si₂O₅)_n, made of SiO₄ tetrahedra all pointing in the same direction. Each SiO₄ tetrahedron is linked to an octahedrally coordinated Mg through bridging oxygens. One of every three Mg(O or OH)₆ octahedra is not connected to a SiO₄ tetrahedron and therefore, is coordinated by an additional hydroxyl group on the inner side of the layer. Investigations using X-ray diffraction [22,23] and electron microscopy [22,24] showed that the single fiber was made of a sheet rolled up around itself, with an internal cavity in the center of the fiber such that the fiber looks like a tube (Figure 1.2). In fact, the internal surface of these tubes is not as empty as it was first seemed. Indeed, the presence of some poorly crystallized fragments of chrysotile, other types of silicates and some other oxides such as iron and nickel oxide, have been confirmed [25]. The theoretical bulk density of chrysotile, assuming empty cavities, has been calculated to be 1.9 g/cm³ [26]. In the kaolinite flat sheets, there is a perfect dimensional fit between the tetrahedral and the octahedral layers [27], and as a result, the sheets do not roll up around themselves. In chrysotile, some distortions are caused by the mismatch between the tetrahedral and octahedral layers, caused by the replacement of 2 Al³⁺ ions (in kaolinite) by 3 Mg²⁺ ions (in chrysotile) which are significantly larger. The larger size of magnesium and the orientations of all the octahedra in the same

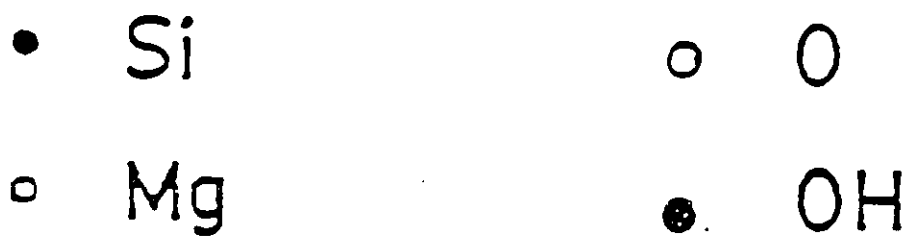
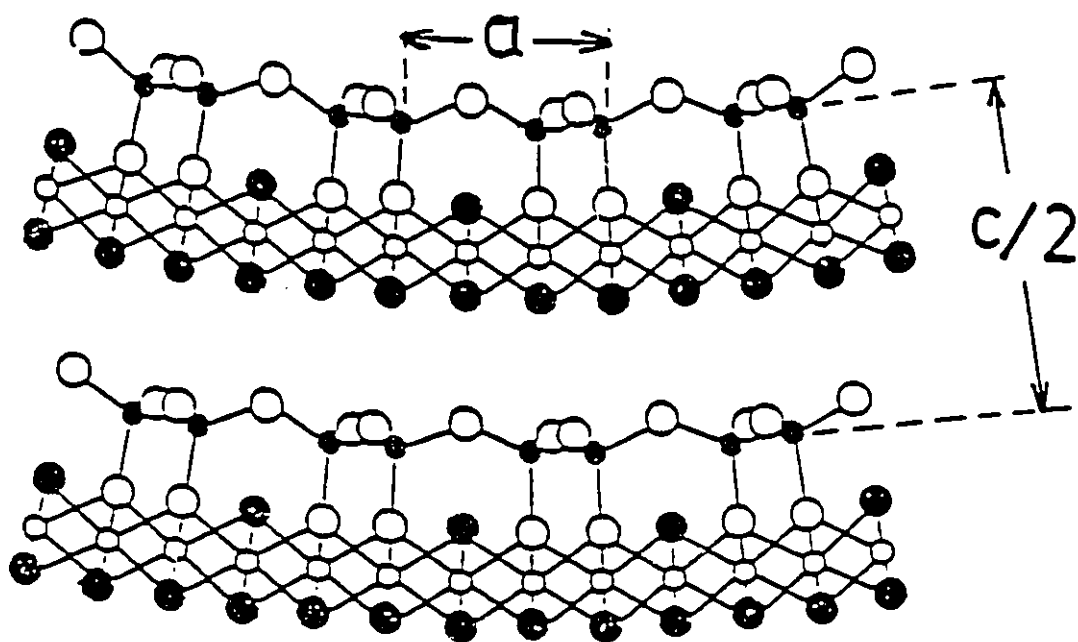


Figure 1.1 Projection of the crystal structure of chrysotile asbestos along the fiber axis.

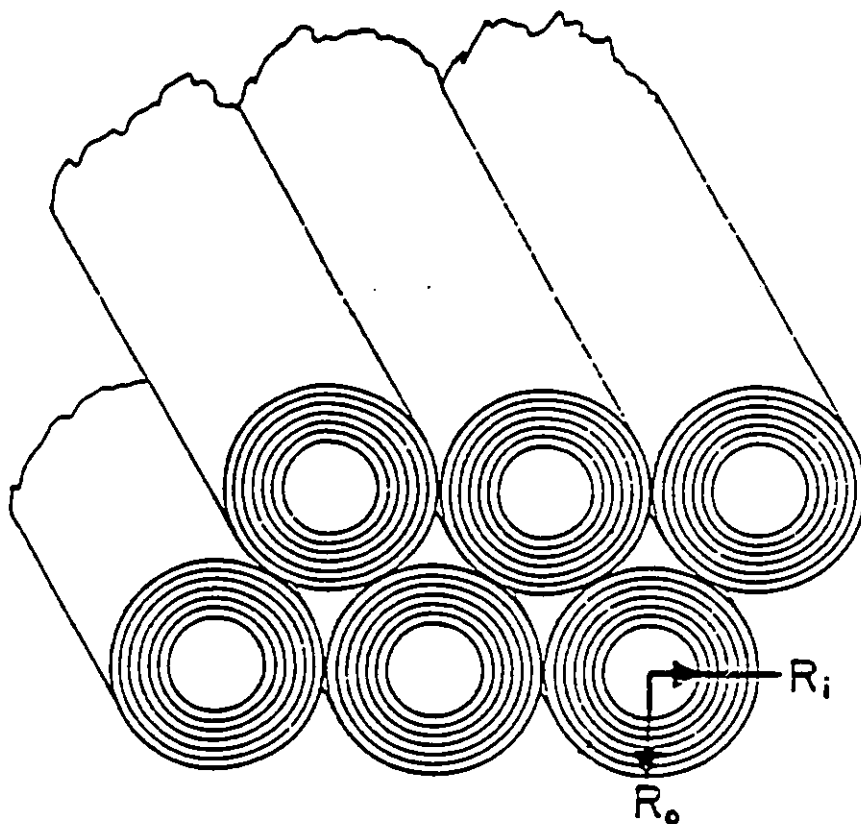


Figure 1.2 Idealized representation of fibril packing in chrysotile. 11.

direction force the sheets to curve in order to relieve the strain and allow a snug fit of Mg in the octahedral sites. As a result, the sheets are wound up helicoidally, giving rise to a fibrous texture. The external side of the curved layers is coated with the axial hydroxyl groups from both kinds of Mg. The internal position of silicate sheets makes them less vulnerable to chemical attack in comparison to the magnesium containing layer. The hydroxyl layer is fully exposed on the external side of the fibers, resulting in a strong basic character. The strong basicity of the hydroxyl groups makes them more susceptible than bridging oxygens to acid attack in the leaching process.

As pointed out by Le Van Mao et al [4,5,10,11,28,29], the chrysotile fibers undergo deep morphological, textural and structural changes during the acid leaching. To determine the extent of the magnesium removal, the magnesium leaching degree or MLD was defined and first used in references 4, 5, and 10. It was found that the correspondence of the MLD with the Alix properties, such as surface area and degree of crystallinity, was fairly good at higher values of MLD [6,11,28]. However, at lower values of MLD, good agreement was not always obtained. Therefore, it was decided to use the X-ray diffraction techniques to identify all of the compounds which contain magnesium, but which do not belong to the structure of the chrysotile. These "impurities" which may represent up to 7 wt % of the chrysotile composition, have a solubility rate in acidic media which is quite different from

that of the chrysotile magnesium component. Once these compounds are identified, one can determine at what moment, and under what conditions, they are removed from the original asbestos material under upon acid attack. Then, it is possible to have a comprehensive understanding of the leaching mechanism.

ii) The first zeolite synthesized by Le Van Mao et al [4,10] was a ZSM-5 type zeolite. It was destined to catalytic applications. Its synthesis requires severe conditions, such as high temperature and high (autogeneous) pressure, as well as, the use of a special organic compound (tetrapropylammonium ions). The latter plays the role of templating or directing components in the synthesis medium [29]. The mechanism of nucleation and crystal growth of the ZSM-5 zeolite is still a matter of discussion [29,30]. Therefore, it is obvious that ZSM-5 zeolite cannot be chosen as a model for the investigation of the "Alix to zeolite" conversion. Among the hundred of synthetic zeolite structures known, the A and X types have been studied most [29-37]. Nucleation and crystal growth of these two types of zeolites have been described in details. Two other advantages associated with these two zeolites are the following: mild synthesis conditions (moderate temperature and pressure) and no need for an organic template in the synthesis medium. This is the reason why zeolites A and X are used as models in this work. The objective of the present work is very clear: to compare the process of zeolite

crystallization using leached asbestos as starting material, with processes using other sources of silica for the synthesis. The result is not only interesting from a theoretical viewpoint, but also for its potential industrial applications. It became obvious that X-ray diffraction and solid state NMR are the techniques of choice for the characterization of the solid materials obtained in our syntheses.

CHAPTER 2 Experimental section.

2.1 Preparation of leached asbestos materials.

Alix.

Chrysotile asbestos, 7TF-12 short fiber commercial grade type, was leached with mineral and organic acids under variable conditions of temperature, acid concentration and/or time of leaching, by Kipkemboi [11].

The first leaching operation was involved with strong mineral acid such as HCl and H₂SO₄.

The second type of leaching process, involves a two step process. In a two step leaching process, chrysotile asbestos fibers were first leached with a mildly acidic HCl solution in order to attain a medium MLD value of around 50-60%, and then treated with an organic acid such as oxalic acid (OXA), acetic acid (ACA) and ethylene diamine tetraacetic acid (EDTA).

Table 2.1 contains the Alix compositions used for the syntheses of zeolites.

2.2 Synthesis of zeolites.

The general requirements for the synthesis of zeolites can be found in [16,38-40], however, since the nature of the product(s) obtained is very sensitive to the exact conditions of preparation, it is necessary to specify the conditions we used.

Alix	SiO ₂	MgO	Al ₂ O ₃	Fe ₂ O ₃	Na ₂ O	MLD
066	96.06	0.50	0.24	3.06	0.14	99.0
162	92.74	2.78	1.30	2.79	0.39	94.8
167	98.57	0.68	0.34	0.20	0.21	98.7
071	90.37	8.50	0.29	0.76	0.08	84.2
168	90.83	3.22	0.35	5.83	0.14	94.0

Table 2.1 Chemical compositions of Alix materials used for zeolite syntheses (wt%, on dried oxides basis). The chrysotile asbestos was 7TF12 batch from Asbestos, Quebec..

The three types of zeolites chosen for synthesis in this work were selected because of their low crystallization temperature of 100 °C. Zeolite A, X and Y were obtained by a hydrothermal synthesis technique using mainly Alix materials of different compositions (Table 2.1) and silica gel as sources of silica, and hydrated sodium aluminate as source of alumina, in a caustic medium, by adding a NaOH solution. However, for comparison purposes with previous works [41-44], various sources of silica such as sodium silicate and specially silica gel were used. Silica gel was also used in the optimization of the experimental parameters such as oxides ratios ($\text{H}_2\text{O}/\text{Na}_2\text{O}$, $\text{Na}_2\text{O}/\text{SiO}_2$, $\text{SiO}_2/\text{Al}_2\text{O}_3$), since these ratios are responsible for the type of zeolite obtained in a synthesis; slight variations of these ratios may have a considerable effect on the purity of the desired material. For example, mixtures of zeolite and/or the presence of other non-zeolitic phases can be obtained.

The preparation procedure for zeolites did first consist in dissolving sodium hydroxide pellets in water; this solution was added to and mixed with a previously weighed source of silica (silica gel, Alix material or sodium silicate). In addition, in the two sample containers (used for synthesis), a previously determined quantity of sodium aluminate was weighed and dissolved in water prior the addition of one of the two silica source solutions, already prepared as above. A vigorous mixing of the reactants was then very important; the systems were stirred until any gel

which formed was broken into nearly homogeneous mixes. The sample containers were well sealed to prevent the loss of water. Two sample containers were simultaneously placed into the glassware synthesis unit or reactor (fig. 2.1), in order to ensure that enough synthesized zeolitic particles would be available for further testing. The reactor temperature was increased until a stable value of 100 °C was reached in the system. A cooling refrigerant was connected to the apparatus in order to avoid evaporation of the water bath, and to prevent melting of the sample containers and loss of the sample. The reaction time could vary from a few minutes to three days, depending on what type of experiment was considered. Figure 2.2 summarizes the complete steps of the synthesis.

After reaction, the two sample containers, containing the polycrystalline zeolite and the mother liquor, respectively, were removed from the hydrothermal synthesis apparatus, and the pressure was released. After adequate cooling, the reaction medium containing the crystallized zeolitic particles was filtered and then washed with distilled water, until the effluent water was in equilibrium with the zeolite has a pH between 9 to 12. Proper washing results in zeolitic particles free of extra sodium ions, which would change the analytical $\text{Na}_2\text{O}/\text{Al}_2\text{O}_3$ ratio of the synthesized zeolite. Then, the crystalline material was dried in a vented oven at a temperature of around 110 - 120 °C for a 24 hour period and stored in a closed container. Each was

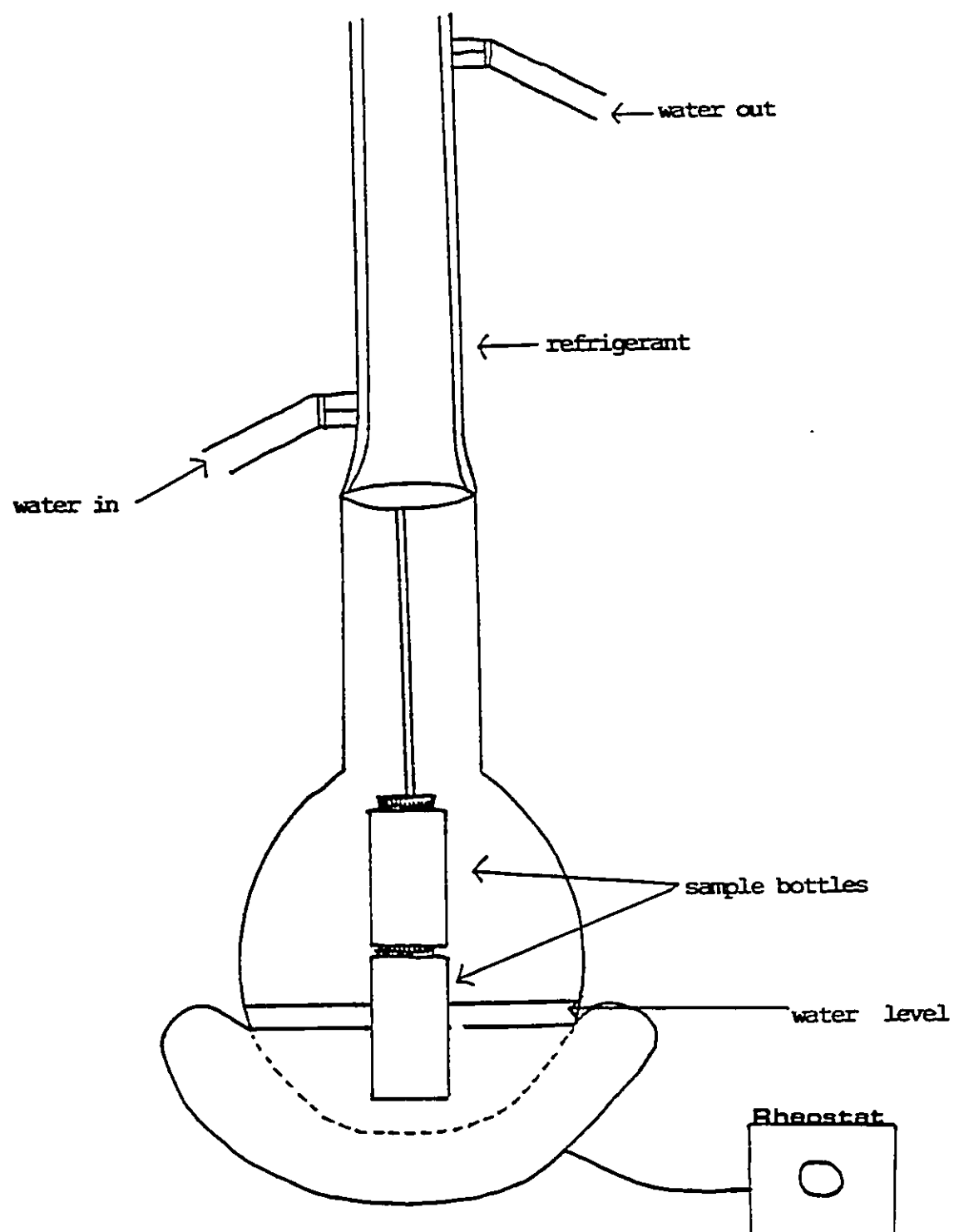


Figure 2.1 Hydrothermal synthesis reactor.

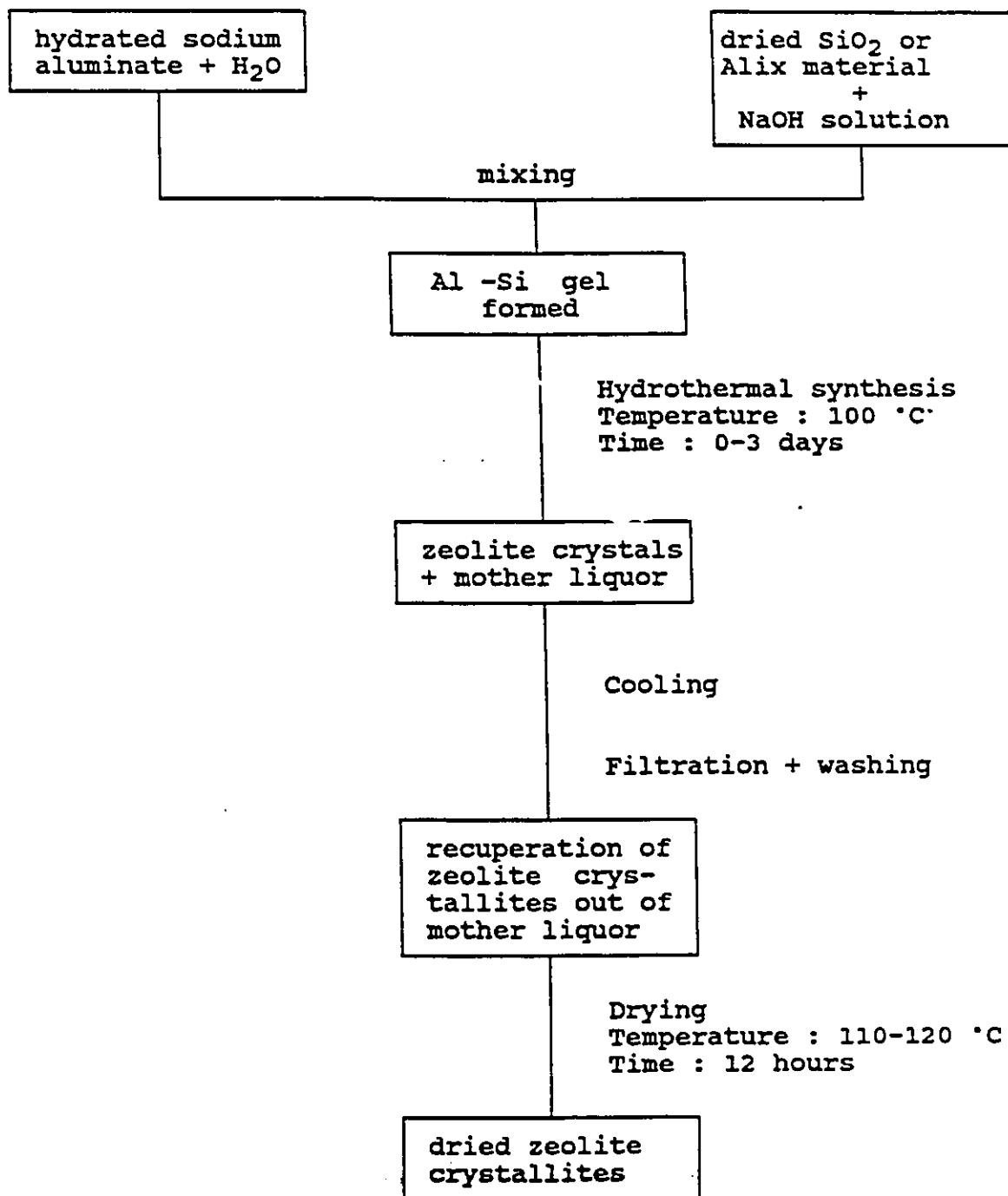


Figure 2.2 Steps involved in the synthesis of zeolites.

identified by XRD powder diffraction and some by chemical analysis (AA).

In the synthesis of X, Y and A zeolites, it was found that the composition of the reacting mixture is critical since it is directly related to the type of zeolite. The reaction time, when crystallization temperature is kept constant, is an important variable in determining the yield in crystalline material [45]. Under some conditions, for example, when too low a temperature is used for too short a time, no crystalline material may be produced, whereas extreme conditions may also result in the production of materials other than the desired zeolite [41,42].

2.3 X-Ray Powder Diffraction.

2.3.1 Introduction

X-Ray diffraction has many very useful applications for the study of solids. We used this technique for the identification of crystalline phases, the measurement of the degree of crystallinity, for the study of progression of reactions, and for the investigation of strain and microcrystallinity in powders. Because chrysotile asbestos and the different zeolites synthesized in this work are crystalline materials, X-ray diffraction is an ideal method for their characterization.

In this work, X-ray powder diffraction was primarily used for phase identification of chrysotile asbestos, prior to, and after leaching, and for the different zeolites synthesized (A, X, and Y). The second application of powder XRD in this research was for the measurement of the degree of crystallinity of chrysotile asbestos (degree of progression of the destruction of the chrysotile structure during acid leaching) and of the zeolites synthesized (degree of progression of crystallization of Na-A zeolites).

Phase identification for the solid materials investigated in this work was carried out by comparison to literature results tabulated in the Powder Diffraction File by the Joint Committee on Powder Diffraction Standards (JCPDS, Swarthmore, USA), previously known as the ASTM file. Other reference sources such as original publications were also used for this purpose [46,47].

2.3.2 Degree of crystallinity measurements.

2.3.2.1 Chrysotile asbestos and Alix materials.

Degree of crystallinity measurements were performed, using a method similar to that of the ASTM [48]. In this work, the "intensity of an X-ray powder diffraction (XRD) peak" means the "integral intensity", obtained by integrating the number of counts versus diffraction angle, when scanning over the peak, and removing the background counts.

Based on earlier works [48,49], chrysotile asbestos of same origin has been chosen as the external standard, which is taken as being 100 percent crystalline. The internal standard used was NaCl. This choice was dictated by its high crystallinity, its stability and the low number of Bragg peaks (cubic system, F lattice), in order to avoid overlapping with the peaks of the sample. The internal standard provides a normalization which accounts for differences in the amount of sample, intensity of incident X-ray beam and response of the counting system, from one measurement to another. Sample preparation consisted in mixing in a weight ratio of 1:2 the internal standard, with the sample previously ground in a mechanical mill for a two minutes period.

All leached chrysotile asbestos used in this study was leached for a 4 hour period, with an experimental temperature of 80 °C.

The measurements we performed involved the following steps:

- 1) manual grinding of the Alix material (or chrysotile asbestos) mixed with the internal standard (NaCl) and drying at 105-110 °C for 12 hours, then cooling to room temperature in a dessicator.
- 2) sample preparation for XRD experiment as described in section 2.3.5.
- 3) recording the complete XRD pattern of the sample for peak position determination, using a goniometer speed of 1° 2 θ /min and a chart speed of 600 mm/h.
- 4) intensity measurements of the two peaks of interest, i.e. (0 0 2) for Alix materials and chrysotile and the (2 0 0) for NaCl, by measuring the number of counts recorded by the digital integrating system, using a goniometer speed of 1° 2 θ /min and a chart speed of 300 mm/h (fig.2.3):
 - i) scan the background for 2 θ sec before and after each peak, in order to get the baseline counts per sec. Repeat the above measurements three time and calculate the average values.
 - ii) scan the two peaks three times and calculate the average value in counts.
- 5) calculation of the degree of crystallinity
$$C_{\text{peak}_1} = \text{average XRD peak intensity of (0 0 2) line of leached or unleached chrysotile in counts.}$$
$$C_{\text{peak}_2} = \text{average XRD peak intensity of NaCl indexed as}$$

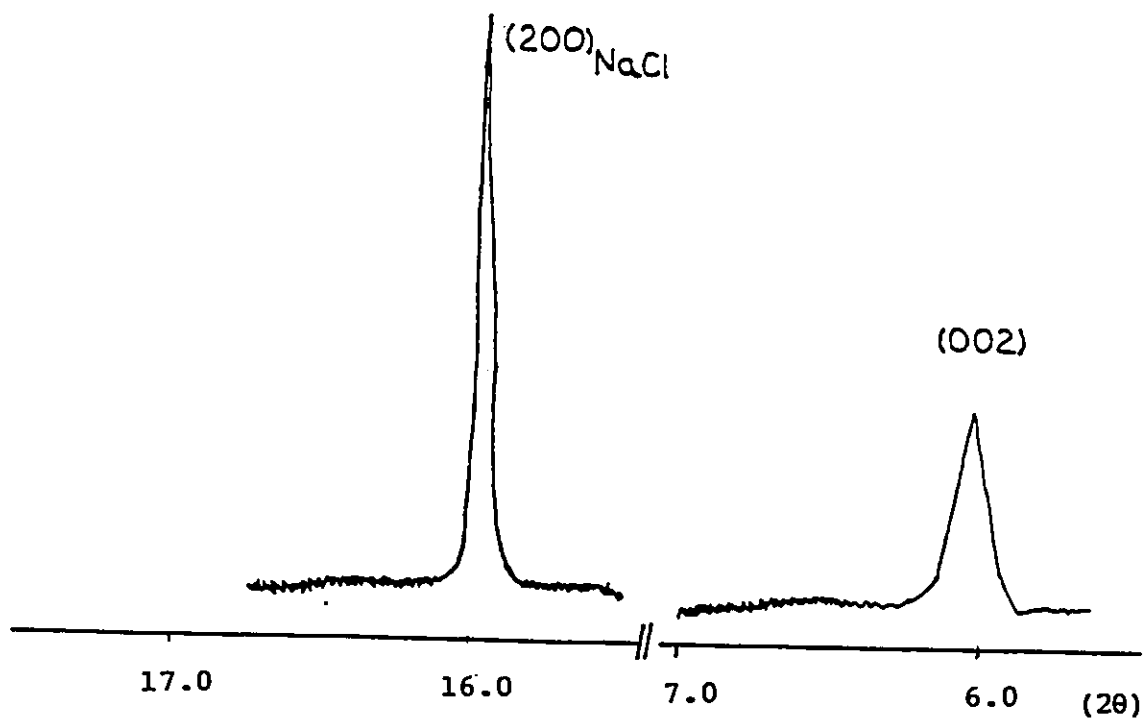


Figure 2.3 X-ray powder diffraction peaks used for the degree of crystallinity (DC) experiments for chrysotile asbestos and Alix materials.

(2 0 0) in counts.

C_{base_1} = average baseline in counts of the (0 0 2) peak of leached or unleached chrysotile.

C_{base_2} = average baseline in counts of the (2 0 0) peak of NaCl.

- i) Absolute intensity of the peaks (C_1 and C_2) expressed as counts are obtained by subtracting the values recorded for the baselines such as:

$$C_{peak_1} - C_{base_1} = C_1 \quad (2.1)$$

and

$$C_{peak_2} - C_{base_2} = C_2 \quad (2.2)$$

- ii) Relative intensity of the peak of the sample (C sample): it is the ratio of the intensity of the (0 0 2) peak of the Alix material or chrysotile and the (2 0 0) peak of the internal standard NaCl:

$$C \text{ sample} = \frac{C_1}{C_2} \quad (2.3)$$

- iii) Determination of the degree of crystallinity, relative to the external standard unleached chrysotile asbestos:

$$\% \text{ crystallinity of the sample} = \frac{C_{\text{sample}}}{C_{\text{asbestos}}} \times 100 \quad (2.4)$$

in which,

$$C_{\text{asbestos}} = \frac{C_1 \text{ unleached chrysotile}}{C_2 \text{ NaCl}} \quad (2.5)$$

2.3.2.2 Na-A zeolite

The measurement of the degree of crystallinity of Na-A zeolites was carried out using a similar method. The external standard was pure commercial Na-A zeolite (Type 4A LINDE) with pore size of 4 Å, which was assumed to be fully crystalline and therefore, was assigned a relative DC of 100%. The internal standard used was KCl. The KCl peak used was (2 0 0), because of its proximity with the concerned θ range of the Na-A zeolites, and its high intensity. About 1g of Na-A zeolite was dried in an oven at 110 °C for at least 2 hours, to eliminate adsorbed water. Then 0.5g of zeolite was mixed with 0.25g of KCl; the mixture was ground manually, dried, and diffraction measurements were made using the same procedure that was used for the leached materials. Overgrinding has to be avoided since it results in microcrystallinity and even destruction of the zeolite. The (2 0 0) line of KCl and two strong peaks of the Na-A zeolite located in the angular range of 20-32 deg (2 θ) were measured. These lines were selected because of their high intensity and the absence of visible splitting due to K alpha ₁ and K alpha ₂ (fig. 2.4).

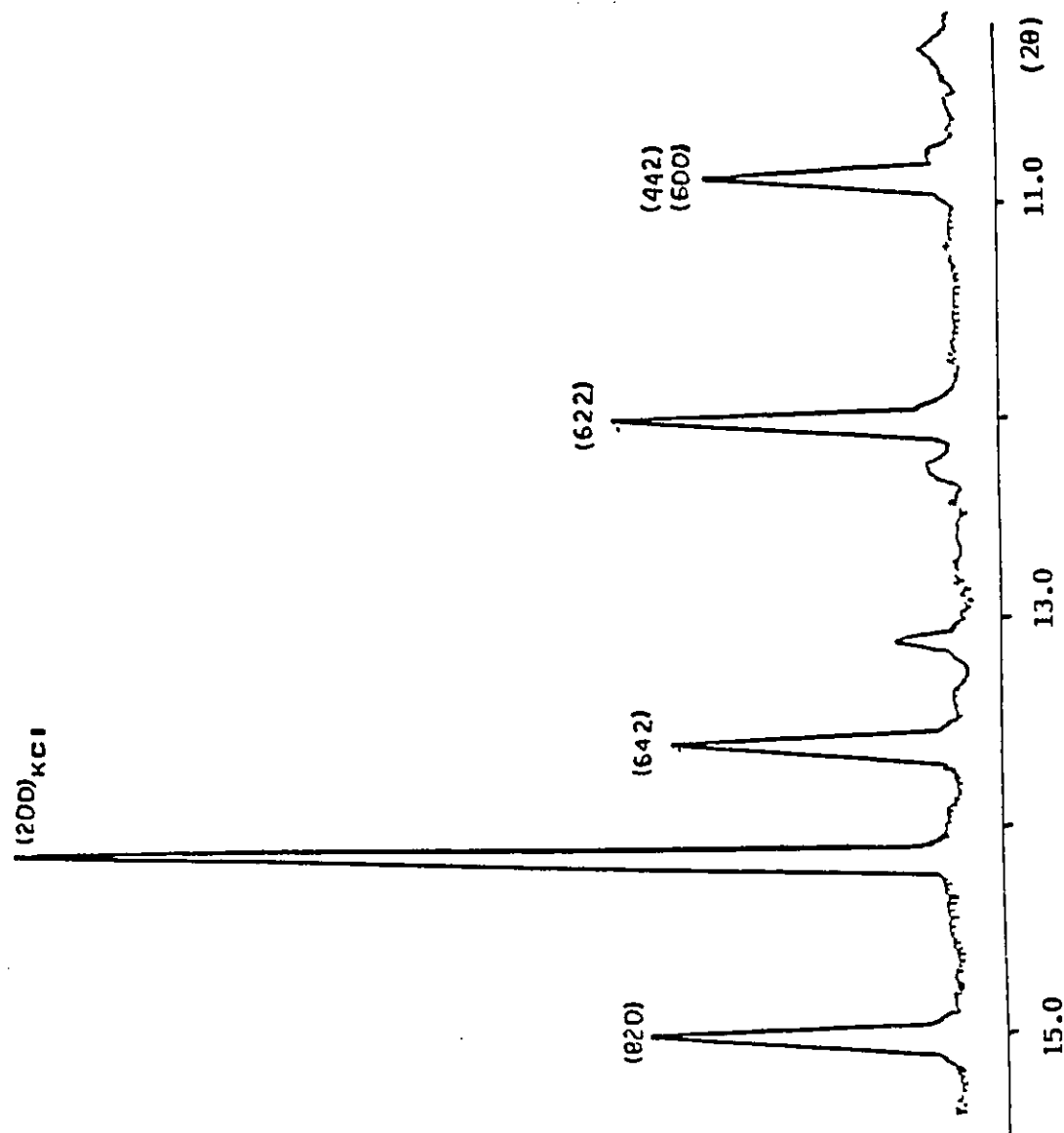


Figure 2.4 X-ray powder diffraction peaks used for the degree of crystallinity experiments of Na-A zeolite.

Calculation was performed as for the leached asbestos, with the difference that the calculation of C sample used the sum of the intensities of the two zeolite peaks used. The percent degree of crystallinity of Na-A zeolite (DC) relative to the external standard is obtained by:

$$DC = \frac{C \text{ sample}}{C \text{ Na-A commercial}} \times 100 \quad (2.6)$$

2.3.3 Reproducibility study of DC

The reproducibility of duplicate samples in this type of determination should be considered suspicious if they differ by more than 5% for values of DC=50% and higher, and by 3% in the vicinity of DC values of 10% [48,49]. In order to estimate the maximum error allowed on DC (ΔDC), in the full range (0 to 100%), we have used the values at 10% and at 50% to determine the following linear relationship between DC and $\Delta(DC)$:

$$\Delta(DC) = 0.05 \times DC + 2.5 \quad (2.7)$$

It can be seen on Figure 2.5 that for DC values close to 100%, the maximum percent difference in DC between duplicate samples should not be higher than 7.5% of DC, and at DC close to zero, $\Delta(DC)$ is equal to 2.5% of DC.

2.3.4 Instrumentation.

A Philips PW 1050-25 diffractometer, with a moveable counter was used in the $\theta - 2\theta$ mode. Monochromatic X-ray

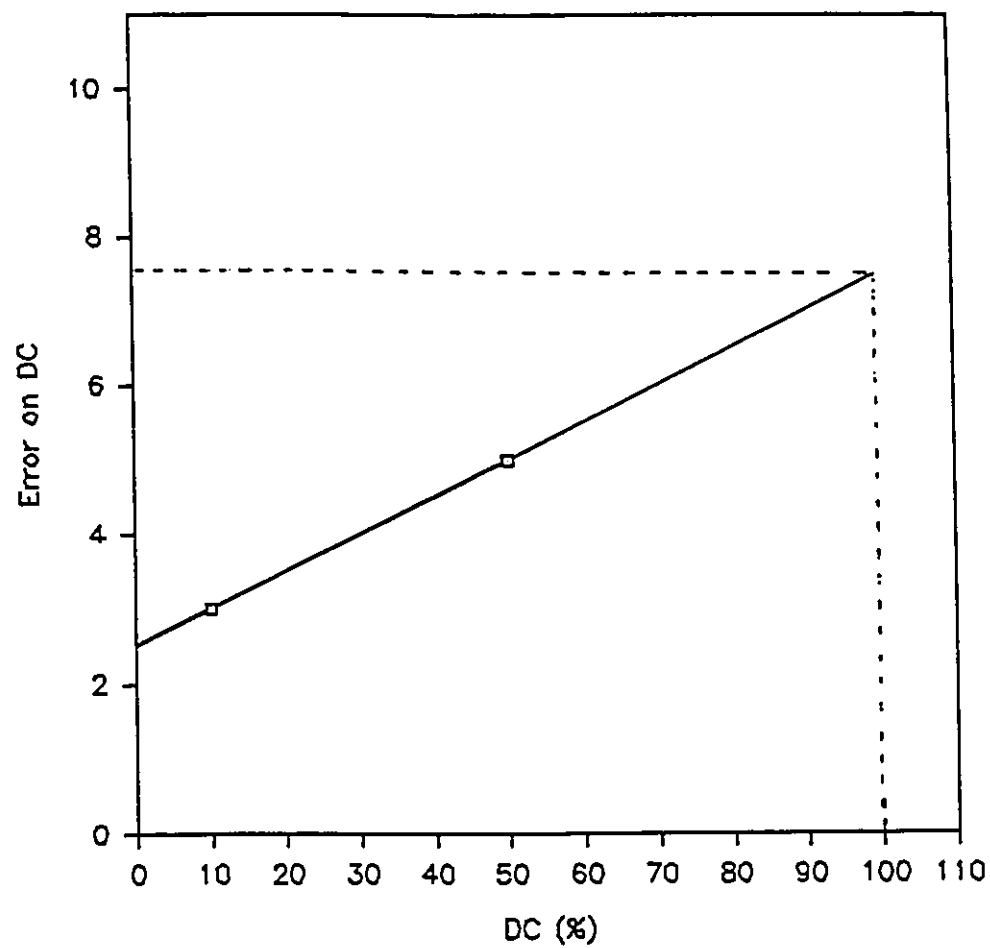


Figure 2.5 Estimated error allowed on the degree of crystallinity [48,49].

radiation of CuK alpha with $\lambda = 1.54178 \text{ \AA}$ was obtained with the use of a Ni filter in order to eliminate the K beta radiation. The sample was rotated at half the speed of the counter.

The scanning speed used varied from $0.125^\circ 2\theta/\text{min}$ to $1^\circ 2\theta/\text{min}$, depending on the type of experiment. The signal from the detector, a Xe/CO₂ scintillation counter, was fed to a pulse amplifier and a pulse height analyzer. The patterns were plotted on a strip chart recorder in the form of number of counts/second, as a measure of intensity, versus diffractometer angles, (θ). The chart speed was constant in order to provide a linear θ scale. The chart speed was usually set at 600 mm/h, however for some applications, a lower speed (300 mm/h) was used.

Towards the end of this work, the X-ray diffractometer was automated with the Sietronics SIE112 system and the patterns were processed on an IBM AT computer and plotted on a NEC Pinwriter PS200 printer.

2.3.5 Sample preparations for XRD experiments.

First, the powdered samples were ground to a fine powder in a mortar, then pressed in a plexiglass holder with a glass microscope slide. This procedure, which is very convenient, has the disadvantage of inducing some preferred orientation, i.e. unequal distribution of orientations of crystallites, in anisotropic crystallites.

Manual grinding in a mortar did not result in any perceptible broadening of the peaks which indicates that the particle size after manual grinding is larger than 1000 \AA . The surface roughness can also have an important effect on the peak position and their relative intensities. If it is too rough, the intensity of the low angle reflections might be to abnormally low. The only way to avoid this type of problem, is to provide an effective grinding of the sample specimen to a fine powder.

It should be noted that since the area of the sample irradiated by the incident beam varies with the Bragg angle, it is important to use an homogeneous sample large enough to catch the whole incident beam at grazing angles (i.e. the lowest and highest Bragg angles to be used). The surface area of the samples in all experiments was fixed by the dimensions of the window in the sample holder (2 cm wide by 1 cm high).

2.4 Bulk density measurements.

2.4.1 Introduction

The density of a material is the ratio of its mass to its volume. The mass is easily obtained by weighing, however, accurate determination of the volume of a small amount (around 1g) of a powder presents serious difficulties. The method we used was adapted and improved in our laboratory from the technique used in the Laboratoire de Chimie Minérale D, Université de Rennes, France. The technique had not been previously described in the literature.

The bulk density measurements of the Alix, asbestos and zeolites powdered samples were carried out by using the Archimedean's method, which consist in the measurement of the volume of liquid displaced by the powder, which is equal to the volume of the powder provided proper wetting is achieved [50,51]. The liquid used to immerse the sample must be totally non-solvent and non-reactive with the sample. In addition, it should have a reasonably low viscosity and surface tension in order to wet the powders efficiently. Furthermore, its volatility should be low enough to avoid a temperature decrease upon evaporation and to allow an accurate setting of the level of liquid. Carbon tetrachloride, CCl_4 , was chosen since it meets best the above criteria, despite its non-negligible volatility. It is particularly unreactive with all of the inorganic solids that we have studied and it is an excellent wetting agent.

The materials tested can be polycrystalline, amorphous

or even single crystals. The sample size is usually close to 1 g, i.e. enough to fill slightly more than half of the crucible used in the measurement.

2.4.2 Apparatus and procedure.

The density apparatus consists of a special glassware designed in our laboratory and illustrated on Figure 2.6. It is divided into three sections, A, B and C. The sample, contained in the crucible E hanging by a metal rod to an analytical balance during weighing, is located in section A. The liquid, CCl_4 , contained in the flask of section B, is slowly admitted into section A, upon opening slightly valve V1. The valve V2 in section C is wide open during measurements, it drains the excess CCl_4 and therefore keeps the level of the liquid constant. This precaution is necessary in order to have the same length of the metal rod in the liquid at each stage of the measurement, in order to have always the same volume of liquid displaced by the rod. In fact, during measurements, CCl_4 from section B is allowed to flow dropwise into section A, to compensate for evaporation. The overflow is recuperated in the flask F (fig.2.7) which is connected to the valve V2 of section C when valve V2 is opened, and evacuated out of the system, in a recuperation flask. The recuperation flask is not open to the atmosphere in order to avoid spreading CCl_4 vapor into the room. In order to have always the same length of metal

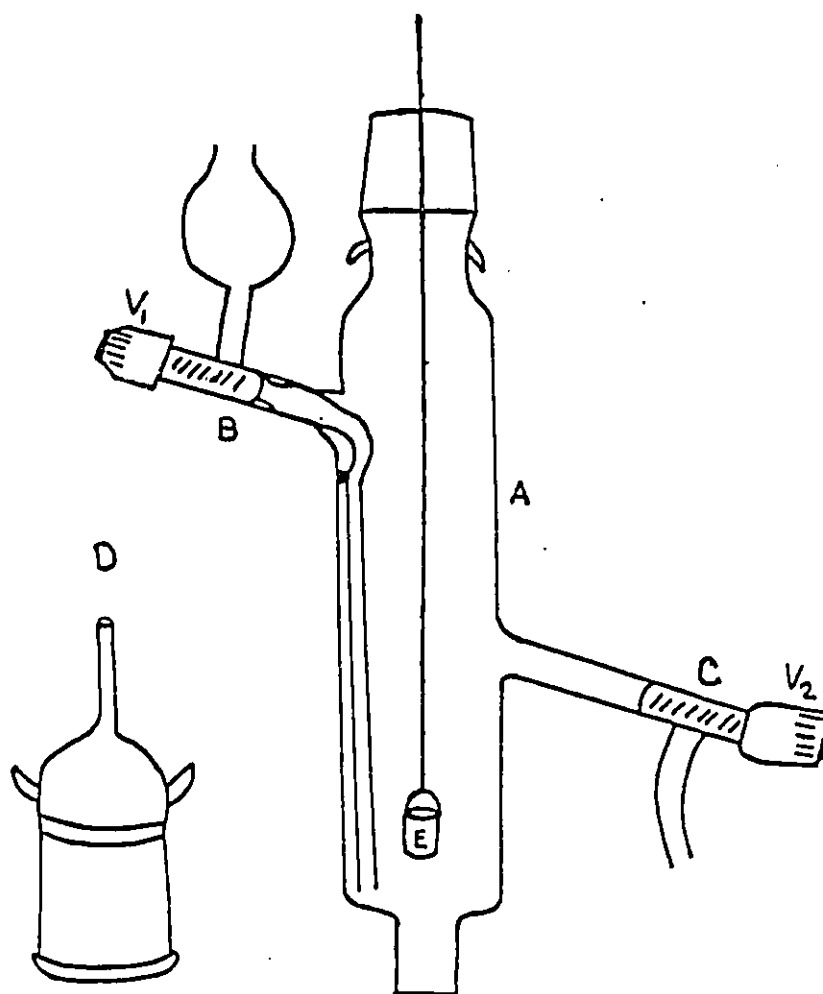


Figure 2.6 The bulk density apparatus.

rod in CCl_4 , it was also necessary to have a precise positioning of the glass vessel relative to the balance. This was achieved by using a metal stand with a precisely machined moving arm (G on fig. 2.7).

Each measurement requires the use of two different settings, as shown in fig. 2.7 and 2.8. The first one is the weighing setting (fig. 2.7) for measuring the weight of the sample in air and in CCl_4 .

One difficulty commonly encountered with the measurement of the weight of liquid displaced by a powder is the elimination of air trapped between the particles, due to imperfect wetting of the sample. This is the largest source of error, since it results in a value of the density of the powder that is too large, and thus an abnormally lower density. To eliminate this problem, the second setting is used (fig. 2.8). The glassware shown on fig. 2.6, with the crucible E containing the powdered sample resting at the bottom of section A, is fitted with part D (fig. 2.6) to a vacuum line (fig. 2.8). The vessel is evacuated very slowly, in order to prevent sucking the powder into the vacuum line. When a low pressure of 10^{-3} Torr is achieved, the sample is maintained under dynamic vacuum for minimum of 30 minutes. Then, the vessel is isolated from the vacuum line (valve V3 is closed) and CCl_4 is allowed into section A of the vessel, which is still under vacuum until the sample is completely immersed. Then air is allowed in the vessel by opening valve V2 causing the disconnection of the vessel from the vacuum line. The

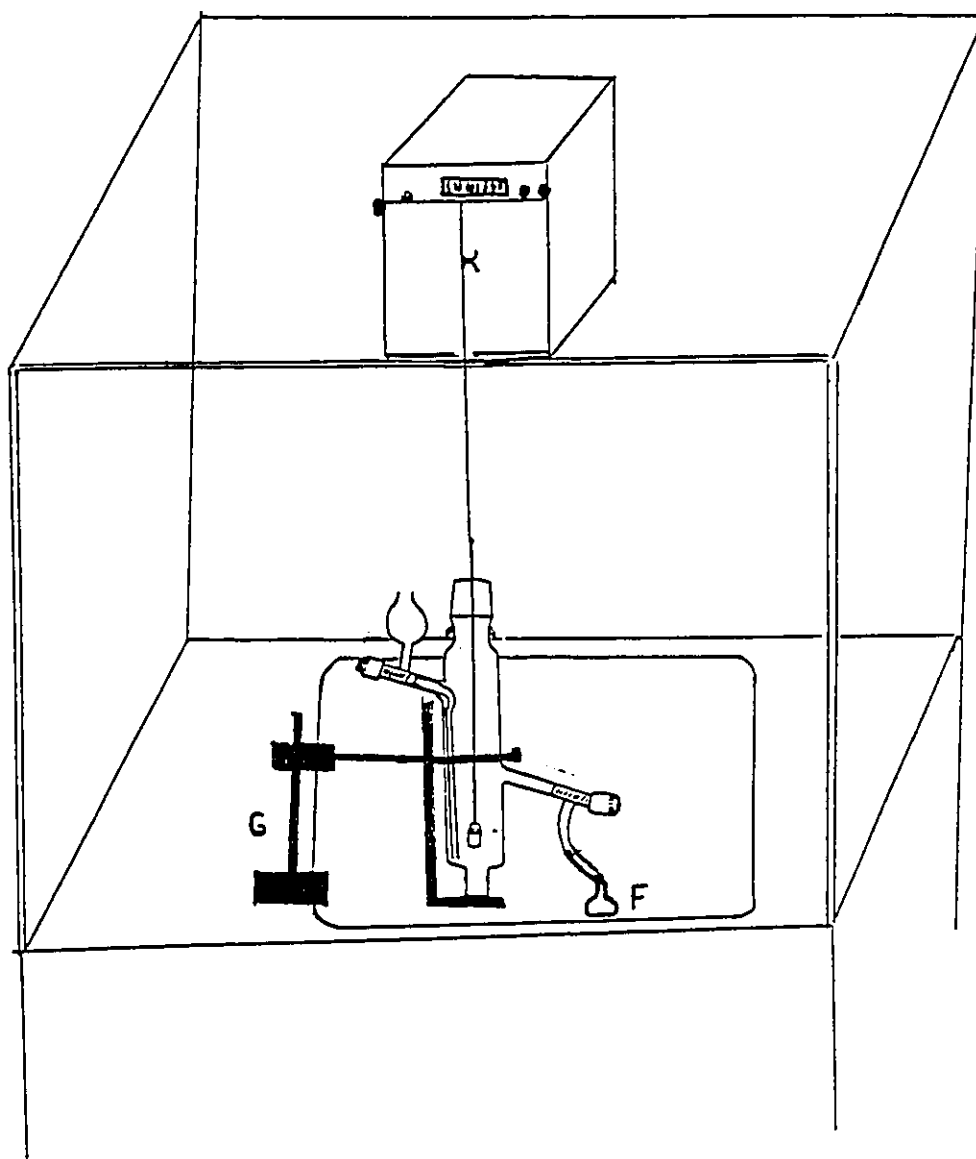


Figure 2.7 Weighing setting.

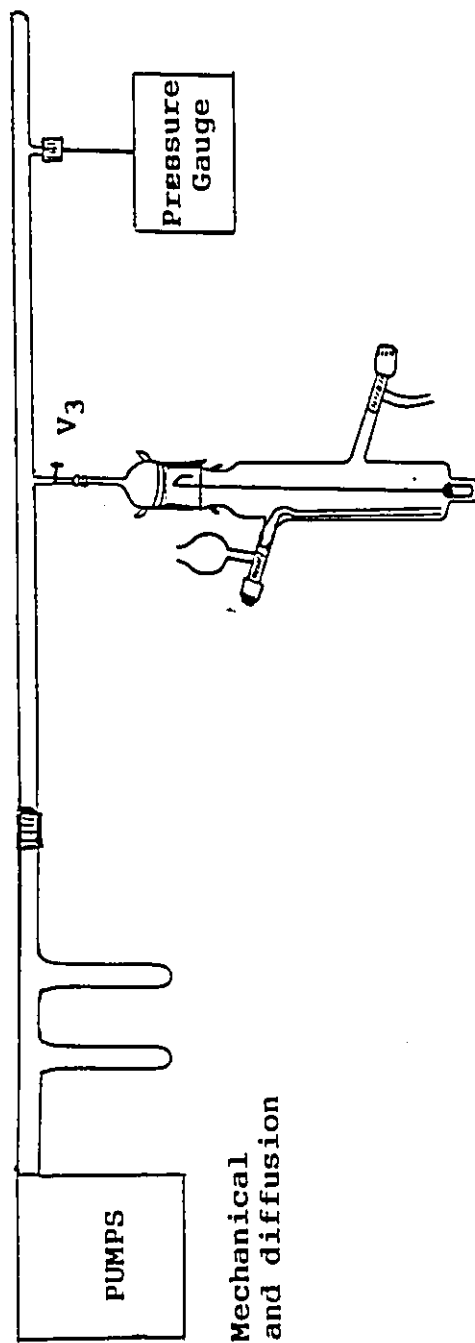


Figure 2.8 Setting of the density apparatus on the vacuum line.

sample holder is "fished out" of the bottom of section A and hanged to the balance (setting 1, fig. 2.7). The level of CCl_4 in the vessel is adjusted as described above and the weight of the immersed sample is measured. Then, the sample is removed from section A and CCl_4 is allowed to evaporate for a few days (until constant weight is reached) and the procedure is repeated at least twice in order to have at least three experimental values of the density for each sample.

Since the vacuum line is in a fume hood, where the slow procedure of wetting under vacuum is carried out, and since the recuperation flask for overflow of CCl_4 is not open to the atmosphere of the room, exposure to CCl_4 , a suspected carcinogenic, is minimized.

Since the above methods allow a wetting as perfect as possible of the samples, only the volume of the bulk of the solid is measured, the density which is obtained is the "bulk density".

2.4.3 Calculation of the bulk density.

The bulk density is calculated from the expression:

$$\rho = \frac{(m_3 - m_1) \times \rho(\text{CCl}_4)}{m_3 - m_4 - m_1 + m_2} \quad (2.8)$$

where,

$$\rho = \frac{\text{mass of the sample}}{\text{volume of the sample}} = \text{density} = \frac{m}{v} \quad (2.9)$$

$\rho(\text{CCl}_4)$ = density of the wetting agent (CCl_4)

m_1 = mass of the empty crucible

m_2 = mass of the empty crucible immersed in CCl_4

m_3 = mass of crucible and powdered sample

m_4 = mass of crucible and powdered sample immersed in CCl_4

and since

$$v = \frac{m_3 - m_4 - m_1 + m_2}{\rho(\text{CCl}_4)} \quad (2.10)$$

$$m = m_3 - m_1 \quad (2.11)$$

and applying (2.10) and (2.11) to equation (2.9), we obtain equation (2.8).

As shown above, four different weighings have to be done for bulk density determination of a single sample.

The experimental error on the measurement of the density of a sample weighing about 1 g, when CCl_4 is used as a wetting agent, is estimated to be 1-2%, since the error on the density of CCl_4 is determined to be 0.005 ($\Delta\rho(\text{CCl}_4) = 0.005$), as shown in appendix 1 [52].

2.5 BET : specific surface area measurement.

BET surface area measurements were performed on the Na-A zeolite we have synthesized and on commercial Na-A zeolites with pores sizes of 4 Å and 5 Å respectively.

Calculations were done using the BET equation:

$$\frac{X}{v_a (1-X)} = \frac{1}{v_m c} + \frac{c-1}{v_m c} \times X \quad (2.12)$$

where

v_a is the adsorbed volume of the adsorbate per unit mass of adsorbent;

v_m is the volume of adsorbate just sufficient to cover, with a complete monolayer of molecules in close packed array, the surface developed by the unit mass of adsorbent;

X is the relative pressure p/p_0 ;

c is a constant varying with the adsorbent - adsorbate interactions. It is related to the differential heat of adsorption E_1 and to the heat of liquefaction E_L , of the adsorbate at the adsorption temperature by the following relation

$$c = \frac{\exp (E_1 - E_L)}{RT} \quad (2.13)$$

where R is the ideal gas constant and T the absolute temperature.

The BET equation shows that the graph of

$$y = \frac{X}{v_a (1-X)} \quad (2.14)$$

versus X , where X varies from 0.05 to 0.35 , should give a

straight line of the form

$$y = NX + B \quad (2.15)$$

if the BET model is valid, where N is the slope and B is the intercept at the origin. From such a BET plot, v_m and c can be derived as

$$c = \frac{m}{b} + 1 \quad (2.16)$$

and

$$v_m = \frac{1}{m + b} \quad (2.17)$$

The v_m value is directly proportional to the specific surface area (s) of the adsorbent:

$$s = \frac{a_m v_m N_A}{V_m} \quad (2.18)$$

where s is the specific surface area

v_m is the monolayer capacity of the unit mass of solid expressed in m^3 STP of N_2/kg of solid if adsorbate is nitrogen

N_A is the Avogadro constant

V_m is the molar volume of the adsorbate

a_m is the surface area covered by one molecule of adsorbate.

In our case, liquid nitrogen was used as adsorbate, and at that temperature of 77°K , the area occupied by a nitrogen molecule is

$$a_m (\text{N}_2) = 16.2 \cdot 10^{-20} \text{ m}^2 \quad (2.19)$$

In these conditions, if N_A and V_m are taken respectively equal to $6.025 \cdot 10^{23} \text{ mole}^{-1}$ and $22.414 \cdot 10^{-3} \text{ m}^3 \text{ mole}^{-1}$, the

specific surface area of the solid is given by the expression

$$S_{\text{BET}} = 4.37 \cdot 10^6 v_m \quad (\text{in m}^2/\text{kg}) \quad (2.20)$$

The measurements were carried out in a classical multipoint BET volumetric apparatus at boiling point of nitrogen (77 °K). The basic apparatus and the method have already been described [11].

The steps involved in the experimental determination of BET nitrogen adsorption of Na-A zeolites include the following (see reference 11 for a description of the set up):

- 1) Weighing of the empty adsorption sampling tube.
- 2) Weighing of the sample sitting in the sampling tube.
- 3) Evacuating the apparatus, until a suitable low pressure of 10^{-3} Torr is recorded.
- 4) Outgassing of the Na-A zeolite sample at elevated temperature, ranging from 220-230 °C, under high vacuum.
- 5) Cooling the sample while still connected to the vacuum line.
- 6) Sample weighing (dried outgassed sample).
- 7) Introducing helium into the gas burette, adjust the mercury level and take pressure readings.
- 8) Monitoring of the temperature of the room.
- 9) Determination of the "dead space" by introduction of helium from calibrated burette to the sample section.
- 10) Pumping to remove helium from the system.
- 11) Then, the sampling tube was then isolated nitrogen was

introduced into the gas burette. The mercury was adjusted and the pressure readings taken.

- 12) The nitrogen from the gas burette was admitted to the sample section and the sampling tube was immersed in a Dewar flask filled with liquid nitrogen (77 °K). When adsorption was complete, usually after 10-20 minutes as indicated by steady pressure readings, the measurements were taken.

Calculation of adsorption from N₂ gas introduced, and correction for dead space, were computed by using law of perfect gases. The specific surface area of the sample was calculated from the experimental readings by using the computer program listed on Appendix A of reference 11.

The main sources of experimental errors were imperfect stability control on the outgassing temperature, variation in temperature of the sample during the adsorption, uncertainties on the level of liquid nitrogen level in the Dewar flask, measurement of the dry degassed weights of samples and incidence of leaks in the apparatus. In general, the method was quite accurate and reproducible results were obtained.

2.6 Electron microscopy.

Synthetic Na-A zeolites were studied by Scanning Electron Microscopy (SEM), for visual inspection, when the effect of the use of two sources of silica for the synthesis were compared (silica gel and Alix materials), for the study of the kinetic of crystallization of Na-A zeolite.

Some dried solid powdered sample was sprinkled on a metal support called "stub", of about 1 cm in diameter, and pressed onto an adhesive surface that was firmly attached to the top of the stub. Extra powder, not fixed or loosely held on the adhesive surface was blown away by a gentle helium flow. Then, the sample was coated with a thin layer of gold metal in a vacuum deposition apparatus, in order to ensure a sufficiently high electric conduction of the sample. This prevents the built-up of static charges on the surface of the samples, which tend to blur the pictures. Then, the sample was placed inside the electron microscope, evacuated under very high vacuum and scanned by a beam of electrons. The thickness of the sample is not relevant since SEM is a reflection experiment and only electrons back scattered by the surface are used to build up the image.

The microscope was a Hitachi S-S20 SEM equipped with a polaroid camera located in the Biology Department at Concordia University.

2.7 Elemental analysis by atomic absorption spectrometry.

Atomic absorption spectrometry was used for the elemental analysis of Si, Al, Fe, Mg and Na in Na-A zeolites. The instrument used was a Perkin-Elmer 503 atomic absorption spectrometer.

2.8 ^{29}Si MAS-NMR spectroscopy.

^{29}Si MAS-NMR spectra were obtained on a Varian VXR 300 FT - NMR spectrometer operating at 59.592 MHz, using superconducting solenoid magnets. A VXR4000 Model computer system was used for data acquisition and amplifiers for the final rf pulse generation. ^{29}Si MAS-NMR spectra were obtained using KEL-F Doty probes (Doty Sc.) with a spinning rates of 2.82 to 4.51 KHz depending on the samples. All ^{29}Si line positions (chemical shifts) were referred to TMS (tetramethylsilane) as zero chemical shift. These experiments were carried out at the Université de Montréal. ^{29}Si MAS - NMR spectra of leached chrysotile asbestos (Alix materials) and of the formation of Na-A zeolite (kinetic study) are reported in this work.

CHAPTER 3 RESULTS AND DISCUSSIONS

3.1 CHRYOTILE ASBESTOS: X-RAY POWDER DIF- FRACTION.

3.1.1 Assignment of the X-ray powder diffraction pattern of chrysotile asbestos.

For the first time, a complete assignment of all Bragg peaks, up to $60^\circ (2\theta)$, of chrysotile asbestos from Asbestos, Quebec (batch 7TF12) has been done. Our experimental X-ray powder diffraction pattern (figure 3.1) is very similar to those found in the literature for Canadian chrysotile asbestos (figure 3.2) [53,54], both in terms of line position and linewidth, with only minor exceptions. For comparison purposes, it should be pointed out that, in Figure 3.2 (b), the Bragg angle 2θ increases from right to left, whereas it increases from left to right in Figures 3.1 and 3.2 (a).

Table 3.1 gives the crystalline phases which have the formula $Mg_3Si_2O_5(OH)_4$, listed in the JCPDS Powder Diffraction File (JCPDS= Joint Committee for Powder Diffraction Standards) [55]. Differentiating between asbestos phases is made somewhat difficult by the fact that 16 crystalline compounds with the same formula, $Mg_3Si_2O_5(OH)_4$, have been identified (Table 3.1) and that most of them have the same set of three strongest peaks, i.e. (i) one at 7.10 to 7.40 Å, (ii) one at 3.55-3.66 Å, and (iii) another at 2.33-2.53 Å.

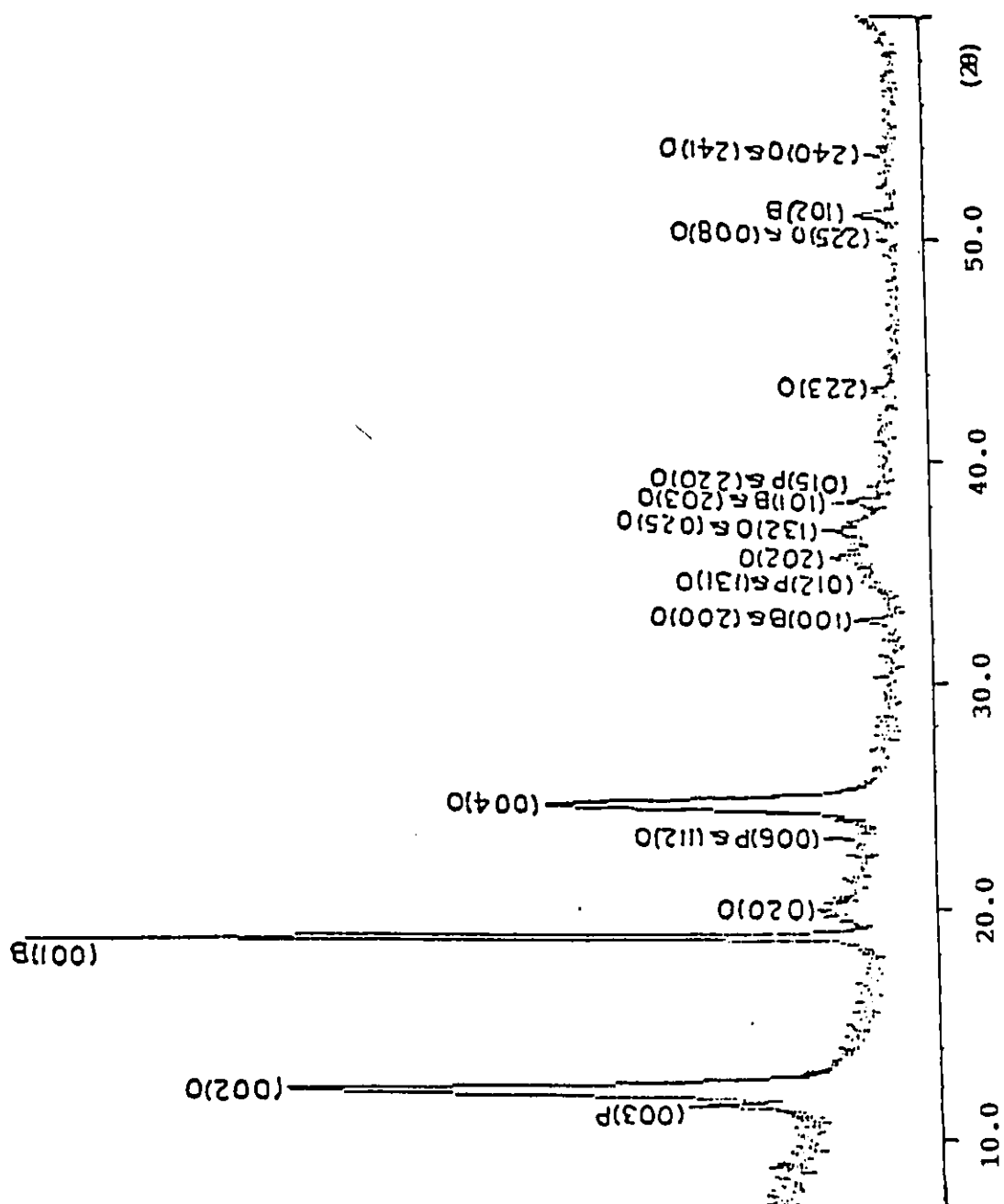


Figure 3.1 Assignment of the X-ray powder diffraction pattern of 7TF12 chrysotile asbestos.

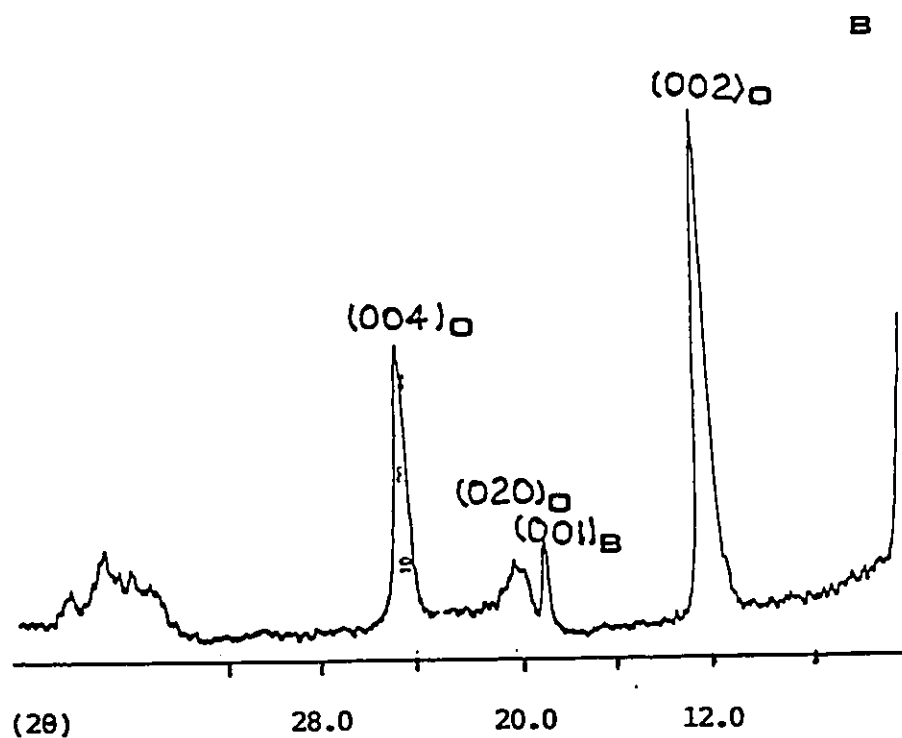
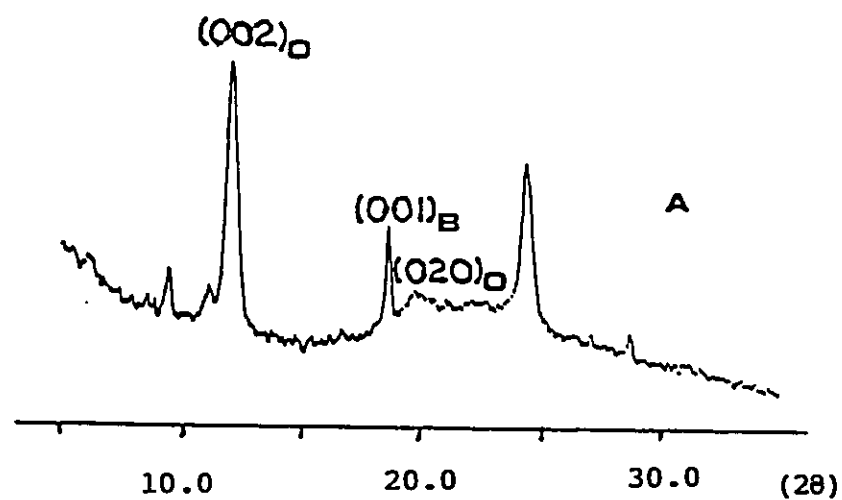


Figure 3.2 X-ray powder diffraction pattern of Canadian chrysotile asbestos reported in the literature.
a: [53] b: [54]

Table 3.1 Crystalline compounds with the formula $\text{Mg}_3\text{Si}_2\text{O}_5(\text{OH})_4$
listed in the JCPDS powder file. [55]

Magnesium Silicate Hydroxide :/Lizardite-1T	$\text{Mg}_3\text{Si}_2\text{O}_5(\text{OH})_4$	7.40 _x	2.51 _x	4.60 _g	18- 779
Magnesium Silicate Hydroxide :/Orthochrysotile-2O _{c1}	$\text{Mg}_3\text{Si}_2\text{O}_5(\text{OH})_4$	7.36 _x	3.66 _g	2.45 ₇	25- 645
Magnesium Silicate Hydroxide :/Lizardite-6T	$\text{Mg}_3\text{Si}_2\text{O}_5(\text{OH})_4$	7.33 _x	3.66 _x	2.50 _x	9- 444
Magnesium Silicate Hydroxide :/Clinochrysotile-2M _{c1}	$\text{Mg}_3\text{Si}_2\text{O}_5(\text{OH})_4$	7.31 _x	3.65 ₇	4.57 ₃	31- 808
Magnesium Silicate Hydroxide :/Anligorite-1M	$\text{Mg}_3\text{Si}_2\text{O}_5(\text{OH})_4$	7.29 _x	2.53 _x	3.61 _g	21- 963
Magnesium Silicate Hydroxide :	$\text{Mg}_3\text{Si}_2\text{O}_5(\text{OH})_4$	7.10 _x	2.50 _x	3.55 ₇	22-1155
Magnesium Silicate Hydroxide :	$\text{Mg}_3\text{Si}_2\text{O}_5(\text{OH})_4$	7.10 _x	2.50 _x	3.55 ₇	22-1156
Magnesium Silicate Hydroxide :	$\text{Mg}_3\text{Si}_2\text{O}_5(\text{OH})_4$	7.10 _x	2.50 _x	3.55 ₇	22-1159
Magnesium Silicate Hydroxide :	$\text{Mg}_3\text{Si}_2\text{O}_5(\text{OH})_4$	7.10 _x	2.33 _g	3.55 ₇	22-1160
Magnesium Silicate Hydroxide :/Orthochrysotile-2O _{c1}	$\text{Mg}_3\text{Si}_2\text{O}_5(\text{OH})_4$	7.10 _x	2.33 _g	3.55 ₇	22-1162
Magnesium Silicate Hydroxide :/Clinochrysotile-2M _{c1}	$\text{Mg}_3\text{Si}_2\text{O}_5(\text{OH})_4$	4.54 _x	7.28 _g	1.53 ₃	21-1262
Magnesium Silicate Hydroxide :	$\text{Mg}_3\text{Si}_2\text{O}_5(\text{OH})_4$	2.50 _x	7.10 _g	3.55 _g	22-1158
Magnesium Silicate Hydroxide :	$\text{Mg}_3\text{Si}_2\text{O}_5(\text{OH})_4$	2.50 _x	7.10 _g	3.55 _g	22-1157
Magnesium Silicate Hydroxide :/Lizardite-1T, syn	$\text{Mg}_3\text{Si}_2\text{O}_5(\text{OH})_4$	2.50 _x	7.10 _g	3.55 _g	22-1161
Magnesium Silicate Hydroxide :	$\text{Mg}_3\text{Si}_2\text{O}_5(\text{OH})_4$	2.39 _x	7.10 _g	3.55 _g	22-1163
Magnesium Silicate Hydroxide :	$\text{Mg}_3\text{Si}_2\text{O}_5(\text{OH})_4$	2.39 _x	7.10 _g	3.55 _g	22-1164

Four of these 16 phases are chrysotiles, i.e. two are orthochrysotiles and the two others are clinochrysotiles.

The peak assignment given in Table 3.2 was established by computer comparison of the experimental peak list obtained using the Sie Ray 112 automation system from Sietronics with the JCPDS Powder Diffraction File [55] using the μ PDMS (Micro Powder Diffraction Search Match) software manufactured by Fein-Marquat Associates. Table 3.2 shows that the powder pattern of our sample can be fully accounted for by a mixture of orthochrysotile-20_{C1} $\text{Mg}_3\text{Si}_2\text{O}_5(\text{OH})_4$ (JCPDS file # 22-1162), brucite $\text{Mg}(\text{OH})_2$ (JCPDS file # 7-0239) and pyroaurite $\text{Mg}_6\text{Fe}_2\text{CO}_3(\text{OH})_{16}\cdot 4\text{H}_2\text{O}$ (JCPDS file # 25-0521). Brucite has already been identified as an impurity in Canadian chrysotile (figure 3.2), however, new information were obtained from this study:

(i) Until the present work, it was not known which variety of chrysotile was mined in Asbestos. We have identified it as being orthochrysotile-20_{C1}. The unit-cell parameters are significantly different from those published in the JCPDS Powder Diffraction File (Table 3.3). This is not surprising, considering the possibility of ion substitutions (Fe/Mg for example), and is in agreement with the observation in the literature that "precise d values will vary with chemical variations" [56]. Table 3.3 shows that the a and c parameters are slightly larger than the literature values, however, their increase is more than compensated for by a more substantial decrease of b. Overall, the volume of the

Peak	I/I ₀	d _o (Å)	d _t (Å)	Phase	h k l
1	13	7.616	7.77	P	0 0 3
2	60	7.155	7.10	O	0 0 2
3	100	4.706	4.77	B	0 0 1
4	7	4.423	4.625	O	0 2 0
5	5	3.852	3.89	O	1 1 2
			3.875	P	0 0 6
6	38	3.610	3.550	O	0 0 4
7	3	2.714	2.725	B	1 0 0
			2.670	O	2 0 0
8	4	2.581	2.624	P	0 1 2
			2.62	O	1 3 1
9	7	2.512	2.499	O	2 0 2
10	8	2.429	2.499	O	1 3 2
			2.420	O	0 2 5
11	6	2.358	2.365	B	1 0 1
			2.326	O	2 0 3
12	1	2.317	2.33	P	0 1 5
			2.312	O	2 2 0
13	2	2.092	2.078	O	2 2 3
14	1	1.812	1.793	O	2 2 5
			1.775	O	0 0 8
15	4	1.787	1.794	B	1 0 2
16	3	1.708	1.748	O	2 4 0
			1.735	O	2 4 1

Notes: 1. d_o: d-spacing observed for the sample;
d_t: theoretical d-spacing, from the the JCPDS Powder Diffraction File for free brucite and pyroaurite, and calculated using the unit-cell parameters of Table 3.3 for orthochrysotile.
2. Phase: B= Brucite, Mg(OH)₂;
O= Orthochrysotile-20C₁, Mg₃Si₂O₅(OH)₄;
P= Pyroaurite, Mg₆Fe₂CO₃(OH)₁₆·4H₂O.

Figure 3.2 Assignment of the X-ray diffraction pattern of batch 7TF12 chrysotile asbestos from Asbestos, Québec

	JCPDS 22-1162	7TF12 batch from Asbes- tos, Quebec	Difference (%)
a (Å)	5.340	5.428	1.62
b (Å)	9.249	8.846	-4.56
c (Å)	14.20	14.40	1.66
Alpha (°)	90.0	90.0	0
Beta (°)	90.0	90.0	0
Gamma (°)	90.0	90.0	0
V (Å ³)	701.3	691.4	-1.41
crystal system	Orthorhom- bic	Orthorhom- bic	
space group	Ccm2 ₁ (#36)	Ccm2 ₁ (#36)	

Table 3.3 Unit-cell parameters for ortho-
chrysotile-20_{C1}.

unit-cell measured on our sample is just 1.41% smaller than that of the literature. These variations are most likely due to chemical variations as well as to stacking irregularities, which are due to the rolled up sheet structure that results in the fibrous texture [57]. In addition, the significant shift of the (0 2 0) peak to higher angles is also probably due to strain in the crystallites (see section 3.1.2).

(ii) Brucite is a well known impurity of chrysotile, and is present in the powder patterns from the literature (Fig. 3.2), however, to our knowledge, this is the first time that pyroaurite has been identified as an impurity of chrysotile asbestos. It should be noted that the first and strongest peak of pyroaurite, (0 0 3) at $2\theta = 11.62^\circ$ is clearly visible on fig. 3.2 (a), and is also present as a shoulder on the beginning of the (0 0 2) peak of chrysotile on fig. 3.2 (b). In both cases, this peak was not assigned. The presence of pyroaurite could account for the small amount of CO_2 (0.44-2.13% wt) that has been found to be present in chrysotile asbestos ores of various origins [58]. Since pyroaurite contains 6.65 % wt CO_2 and chrysotile from Thetford King Beaver Mine contains 0.48 % wt CO_2 [55], if all the carbonate is in the form of pyroaurite, it contains 7.2 % pyroaurite. Unfortunately, such a calculation could not be performed for chrysotile from Asbestos, since its CO_2 content is not known.

In addition, another non-assigned peak is present in Figure 3.2 (a) at about $2\theta = 9.50^\circ$. This peak, which was not observed for the batch 7TF12 from Asbestos, cannot be

accounted for by any of the three crystalline phases identified. It has been reported [57] that the normal impurities in chrysotile are magnetite Fe_3O_4 , brucite $\text{Mg}(\text{OH})_2$, magnesite MgCO_3 , and pyrrhotite Fe_7S_8 . Brucite was observed but the others were not. The (0 0 1) peak of brucite is much stronger in our diffraction pattern (fig. 3.1) than in those from the literature (fig. 3.2), which shows that our sample is much richer in brucite. Magnetite is also present in the 19712 batch from Asbestos, and this was evident because it was attracted to a magnet (it adhered to the stirring bar in the acid leaching experiments), however, since its diffraction pattern was not observed, it was probably present in small quantity or in the microcrystalline state. It should be pointed out that Fe fluoresces when irradiated with the λ alpha line of copper: this reduces drastically the intensity of the Bragg peaks of iron containing species and makes the detection of small quantities more difficult.

3.1.2 Interpretation of the width of the diffraction peaks of chrysotile.

3.1.2.1 Common reasons for broadening of the Bragg peaks.

Bragg peaks cannot have an infinitely small width for the following reasons:

a: Theoretical reason: Although characteristic X-ray emission lines are very narrow, their narrowness is limited by Heisenberg's uncertainty principle, i.e. by the precision of measuring the energy of the electronic levels involved in the production of the X-ray photons. This gives the peaks a natural linewidth, which is very narrow.

b: Instrumental broadening:

b.1: The K alpha emission line of copper is not a single line; it is a doublet, K alpha 1 and K alpha 2. In the conditions of our experiments, this doublet is not resolved and it results in a slightly broadened line.

b.2: Since the geometry of the X-ray powder diffractometer uses the line focussing arrangement, high intensities and good resolution are achieved. However, the slits which prevent radiations scattered at angles other than the Bragg angles from entering the detector, cannot be infinitely narrow, otherwise the intensity reaching the detector would be infinitely small, therefore the finite width of the slits gives rise to a finite linewidth for the Bragg peaks.

c: Broadening due to the sample:

c.1. Microcrystallinity : For certain specialized applications, the shape of the peaks may yield valuable information [59-62]. Extra broadening, i.e. broadening in addition to instrumental broadening may occur if the size of the crystallites is too small, usually below 1000 \AA in diameter. Below an average particle size of about 40 \AA , the peaks are so broad that they cannot be distinguished from the background counts and therefore no diffraction pattern is observed. From measurements of this extra broadening, an average particle size may be obtained by using the accepted formula for particle size broadening known as the Scherrer formula,

$$t = \frac{0.9 \lambda}{B \cos \theta_p} \quad (3.1)$$

where

t : thickness of the crystal (\AA), i.e. the average particle diameter

λ : the X-ray wavelength (CuK alpha = 1.54178 \AA)

θ_p : the Bragg angle.

B : extra broadening due to small particle size.

The linewidth is measured at half the peak height. The extra broadening B giving the correction for instrumental broadening is done by using Warren's formula:

$$B^2 = B_n^2 - B_s^2 \quad (3.2)$$

where

B_n : is the measured peak width in radians at half peak height, for the sample.

B_s : is the corresponding width of a peak of a standard well crystalline material, mixed in with the sample, whose particle size is considerably greater than 2000 \AA and which has a diffraction close enough to the relevant peak of the sample to make the difference in θ_b negligible.

c.2. Strain [63] : When a crystal is subjected to a strain, changes result in the d-spacing, which can have a marked effect on the diffraction pattern. Figure 3.3 [63] shows that a uniform strain (compression or elongation of the crystal) results in a uniform change of d-spacing, and therefore shifts the Bragg peak without broadening. On the other hand, a nonuniform strain distorts the crystals; it results in domains with variable values of d-spacing; the resulting distribution of d-spacings gives a distribution of Bragg angles, and therefore it results in highly broadened peaks. The direction of the strain is obtained from the families of Bragg peaks that show significant broadening. The strain responsible for lineshift and/or broadening can be external (i.e. applied) or internal (i.e. due to the crystal structure or some physical properties driven by cooperative phenomena, such as ferroelectricity, antiferroelectricity, ferroelasticity, antiferroelasticity or piezoelectricity [64]).

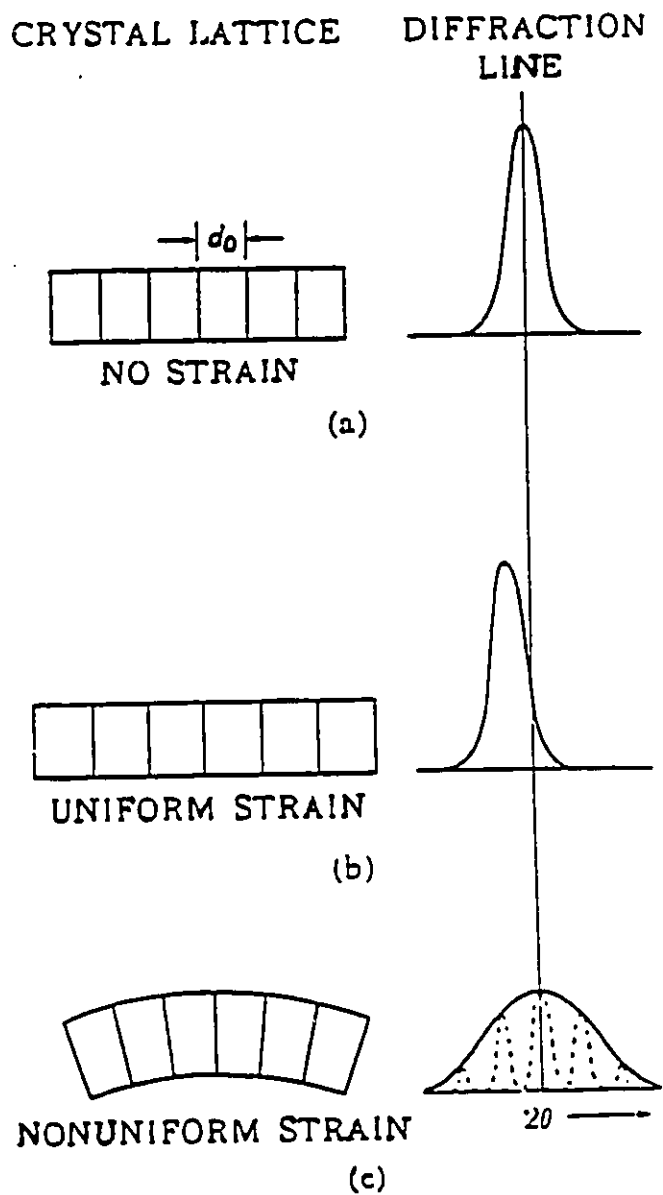


Figure 3.3 Effect of lattice strain on the width and position of Bragg peaks.

c.3. Disorder: Stacking irregularities can result in a non-uniform d-spacing in given directions and give rise to linebroadening. Layered structures which have only weak attractions between neighboring layers are particularly prone to this phenomenon.

3.1.2.2. Line broadening in chrysotile asbestos.

Ordinarily, the powder diffraction pattern of a crystalline material contains a collection of peaks which have the same linewidth within a range of a few degrees 2θ . However, a careful examination of such a diffraction pattern over a wider angular range reveals the presence of a slow but continuous increase of linewidth as the Bragg angle increases; this is due to the non-linearity of Bragg law and the progressive splitting of the Bragg peaks at high angles because the K alpha line is a doublet. Figure 3.1 shows that the diffraction pattern of the 7TF12 batch of chrysotile from Asbestos, Quebec contains very large irregularities of linewidth. For example, if one considers only the lines for $2\theta < 34^\circ$, i.e. in the angular range where overlapping is minimal, it is clear that the brucite and pyroaurite lines are much narrower than those of chrysotile. In addition, the broadening of the chrysotile lines is strongly direction dependent: moderate broadening of the (0 0 1) peaks is observed, which indicates a significant disturbance in the direction of the c axis, whereas the very large width of the

(0 2 0) line shows the presence of considerable trauma along the \vec{b} axis. Chrysotile samples from other sources show also a similar broadening pattern (Fig. 3.2), however, although the types of broadening described above seem to be the rule for chrysotile, its presence has not been explained and is not even mentioned in the literature [53,54]. Distinguishing between the various possible causes of line broadening described above can be difficult if no other type of information is available. Fortunately, the crystal structure and texture of chrysotile have been extensively studied, mostly in an effort to understand the reasons for its carcinogenic properties, and these results can help in explaining the types of line broadening observed.

Figure 3.4 shows an enlargement of the powder diffraction pattern of the 7TF12 batch of chrysotile from Asbestos, in the angular range $2\theta = 9$ to 27° . The linewidths at half height measured on fig. 3.4 were corrected from instrumental broadening by Warren's method, as explained in section 3.1.2.1, using the linewidth of the (2 0 0) peak of KCl, which was recorded separately under identical experimental conditions. Then, the average particle dimension was calculated from each peak using Scherrer's formula. The results are summarized in Table 3.4.

The (0 0 1) line of brucite is as narrow as the KCl line, which shows that there is no detectable microcrystallinity, strain or disorder in the \vec{c} direction of brucite, therefore, the particle dimension along \vec{c} is larger than

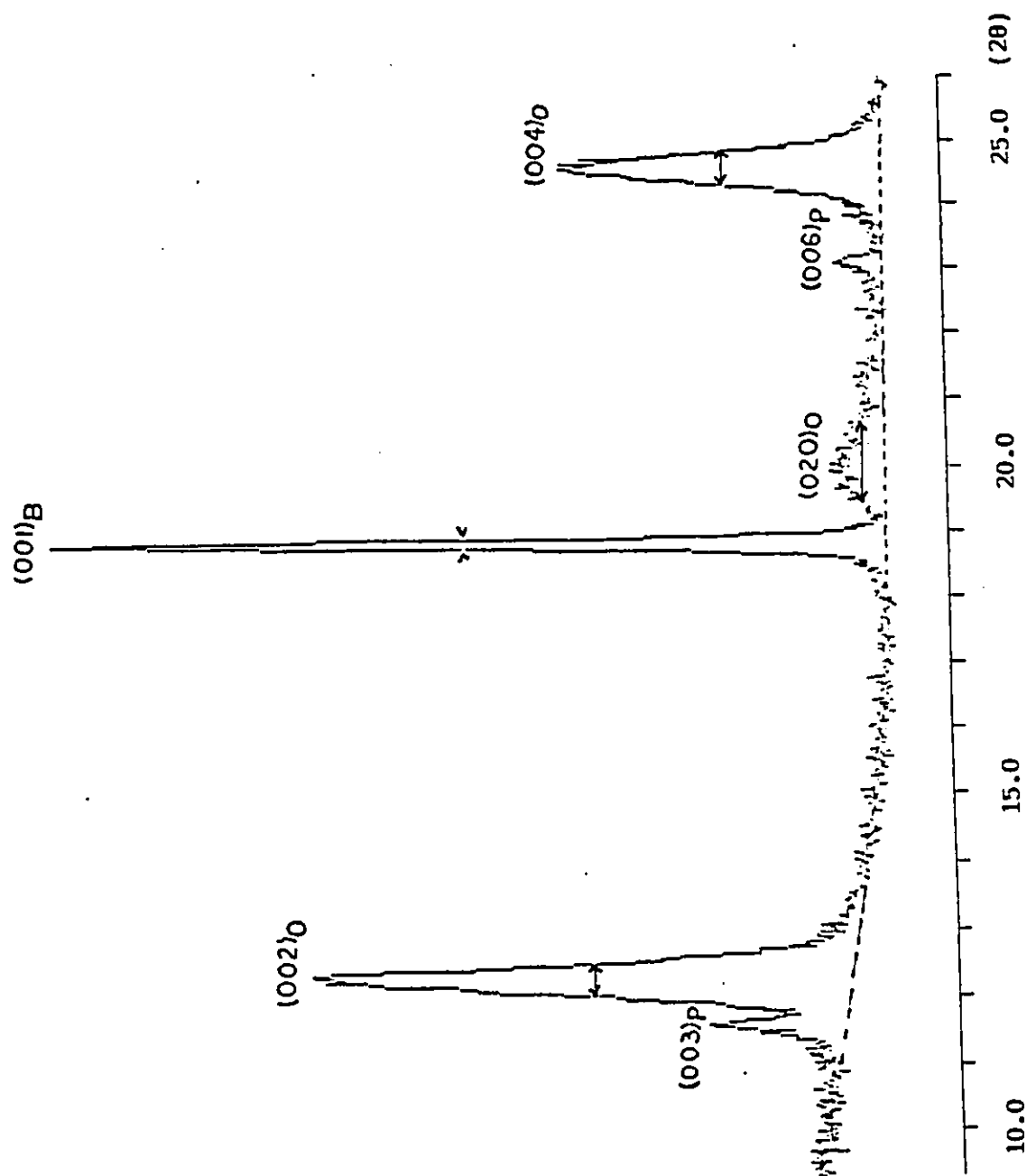


Figure 3.4 Enlargement of the X-ray powder diffraction pattern of 7TF12 batch of chrysotile asbestos used for line broadening study.

Bragg peak	B_M or B_S (2 θ in radians)	B (radians)	t (Å)
(2 0 0) KCl	0.0028	-	-
(0 0 1) brucite	0.0028	0	>1,000
(0 0 2) chrysotile	0.0084	0.0079	177
(0 2 0) chrysotile	0.0211	0.0209	67
(0 0 4) chrysotile	0.0091	0.0087	164

Table 3.4

Average particule dimensions determined from the broadening of the X-ray diffraction lines. Note: The average particle diameters calculated in the table above were determined by assuming that all non-instrumental line broadening was due to microcrystallinity. The results are discussed in the text.

1,000 Å. The (1 0 0) and (1 0 2) peaks which are located at higher angles, although they are weak, and seem unbroadened, therefore one can conclude that the average dimension in the a direction of brucite is also larger than 1,000 Å. For pyroaurite, only the (0 0 3) and (0 0 6) peaks are clearly visible. Since (0 0 3) overlaps with the (0 0 2) peak of chrysotile and (0 0 6) is very weak, the linewidth cannot be measured accurately. However, the two lines look slightly broadened, which indicates an average particle size slightly smaller than 1,000 Å or the presence of moderate strain or stacking disorder along c.

The linebroadening for chrysotile is very highly anisotropic; our results can be fully explained in terms of structure and texture of chrysotile. First, in order to understand the directionality of line broadening, it is essential to locate the crystallographic axes relative to the fiber axes. Figure 3.5 shows the orientation determined from crystallographic and electron microscopic studies [25,58,65].

a. Direction of the \vec{a} axis: No unambiguously identified (h 0 0) peak is observed (those with h odd are not allowed by the C Bravais lattice), therefore, one cannot draw firm conclusions regarding the features in the direction of the \vec{a} axis. The \vec{a} axis is aligned with the fiber axis, and since fibers are long (often 10 μm to 1 mm), the average fiber length is well above 1,000 Å and will not give rise to broadening. Internal strain along a is unlikely since there is no physical constraint to the free growth of the fibers in

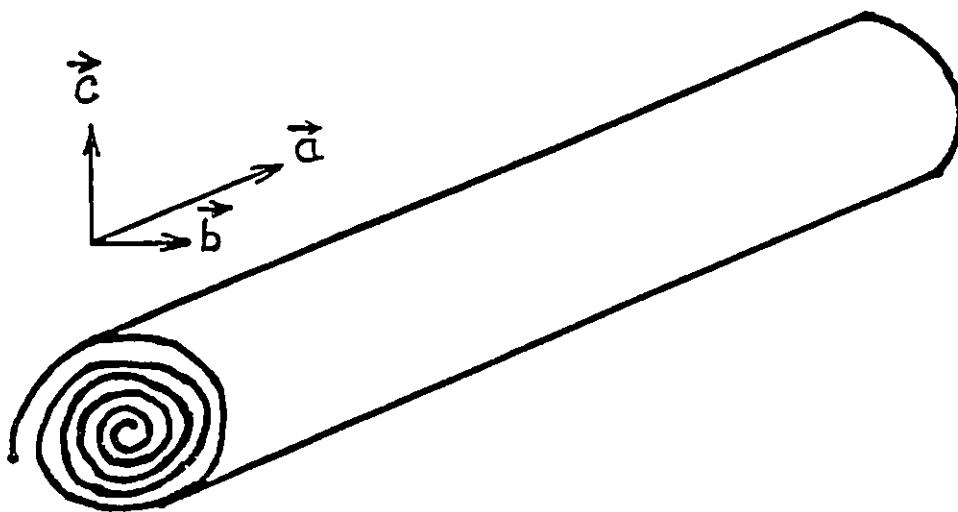


Figure 3.5 Orientation of the b axis in the direction of curvature of the sheets.

that direction. Stacking faults are the most probable sources of a spread in d-spacing in the direction of the \vec{a} axis. Indeed, the sheet structure, which is wound around itself to produce the fibers, winds helicoidally (see fig. 3.6 [57]) in such a way that the unit-cells of subsequent layers are shifted along the \vec{a} direction relative to one another. This could actually lead to nearly complete absence of periodicity along a when one compares successive layers, even though the periodicity is undisturbed within each layer. It would result in a spread of $(h\ 0\ 0)$ peaks over such a wide angle that they would not be observed. This could explain the absence of $(h\ 0\ 0)$ peaks.

b. Direction of the \vec{b} axis: Figure 3.5 shows that the \vec{b} axis lies in the direction of curvature of the sheets. The curvature is induced by the the presence of magnesium near the outer surface of the sheets; the magnesium ions are a little too bulky to fit in their octahedral positions and they create a large amount of non-uniform strain in the direction of the \vec{b} axis. This strain forces the sheets to curve and results in tubular shaped crystallites. This situation is described in fig. 3.3 (c) and is expected to result in a considerable broadening of the $(0\ k\ 0)$ Bragg peaks. This is exactly what is observed on the diffraction pattern (fig. 3.4). Therefore, the average particle size of $67\ \text{\AA}$ calculated from the broadening of the $(0\ 2\ 0)$ line is not correct, since this calculation assumed that only microcrystallinity contributed to the broadening due to the

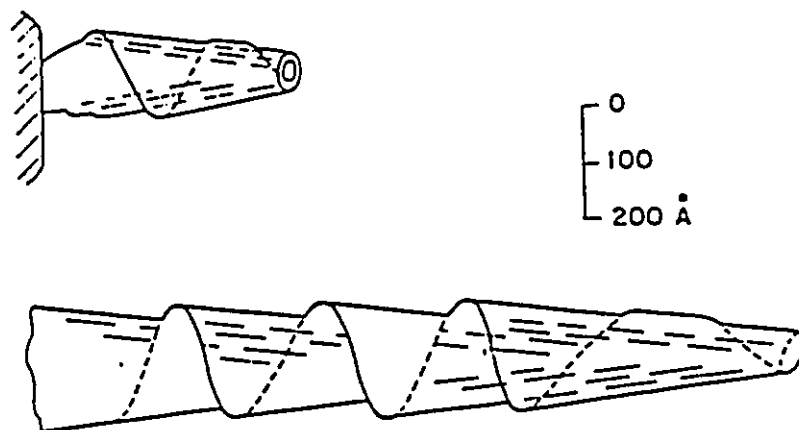


Figure 3.6 Spiral winding of chrysotile sheet that produces the tubular shape of the fibril.

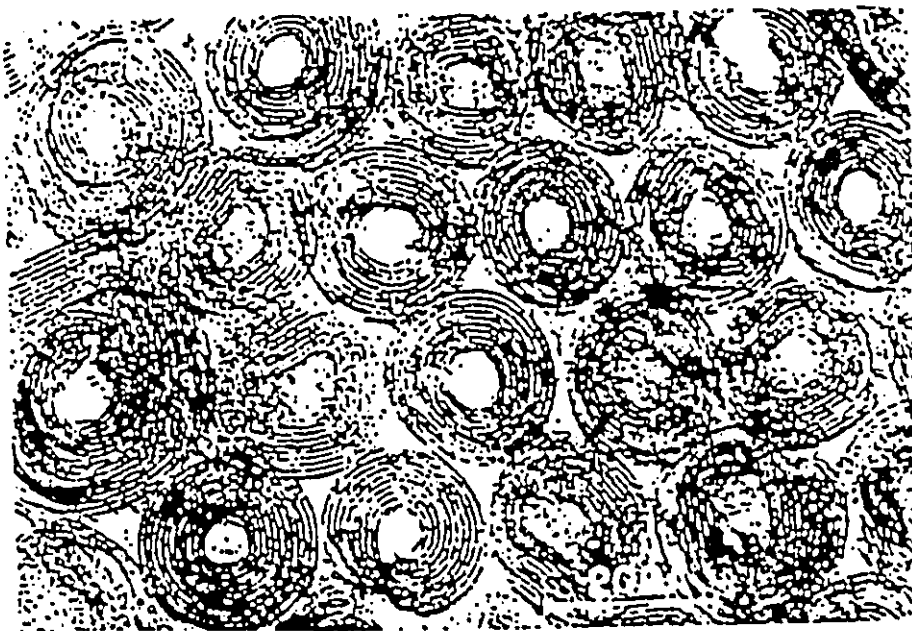


Figure 3.7 High-resolution electron micrograph of transverse section of chrysotile asbestos.

d-spacing of the (0 k 0) peaks, and therefore result in a peak shift to higher angles. It is most likely that the total strain is the sum of both kinds, and variations in the relative amount of each would result in the following features:

- an uniform strain larger than a nonuniform strain would lead to a large shift to higher angles, and to a broadening not as pronounced as the case below;
- an uniform strain smaller than a nonuniform strain would lead to smaller shift to higher angles, and to a much more pronounced broadening.

This could explain the smaller b parameter found in this study, together with a highly broadened line. It can also account for the significant differences in linewidth for the (0 2 0) peak between different literature data; for example, the (0 2 0) peak is much broader on fig. 3.2 (a) than on fig. 3.2 (b).

c. Direction of the \vec{c} axis: Figure 3.5 shows that the \vec{c} direction is perpendicular to the layers and therefore the particle size in this direction is the diameter of the fibers. The average particle diameter in the \vec{c} direction, calculated from the line broadening of peaks (0 0 2) and (0 0 4), was found to be 177 Å using (0 0 2) and 164 Å using (0 0 4) (Table 3.4). The two values are in excellent agreement with each other (average diameter= 170 Å) and with the value of about 200 Å obtained from high resolution

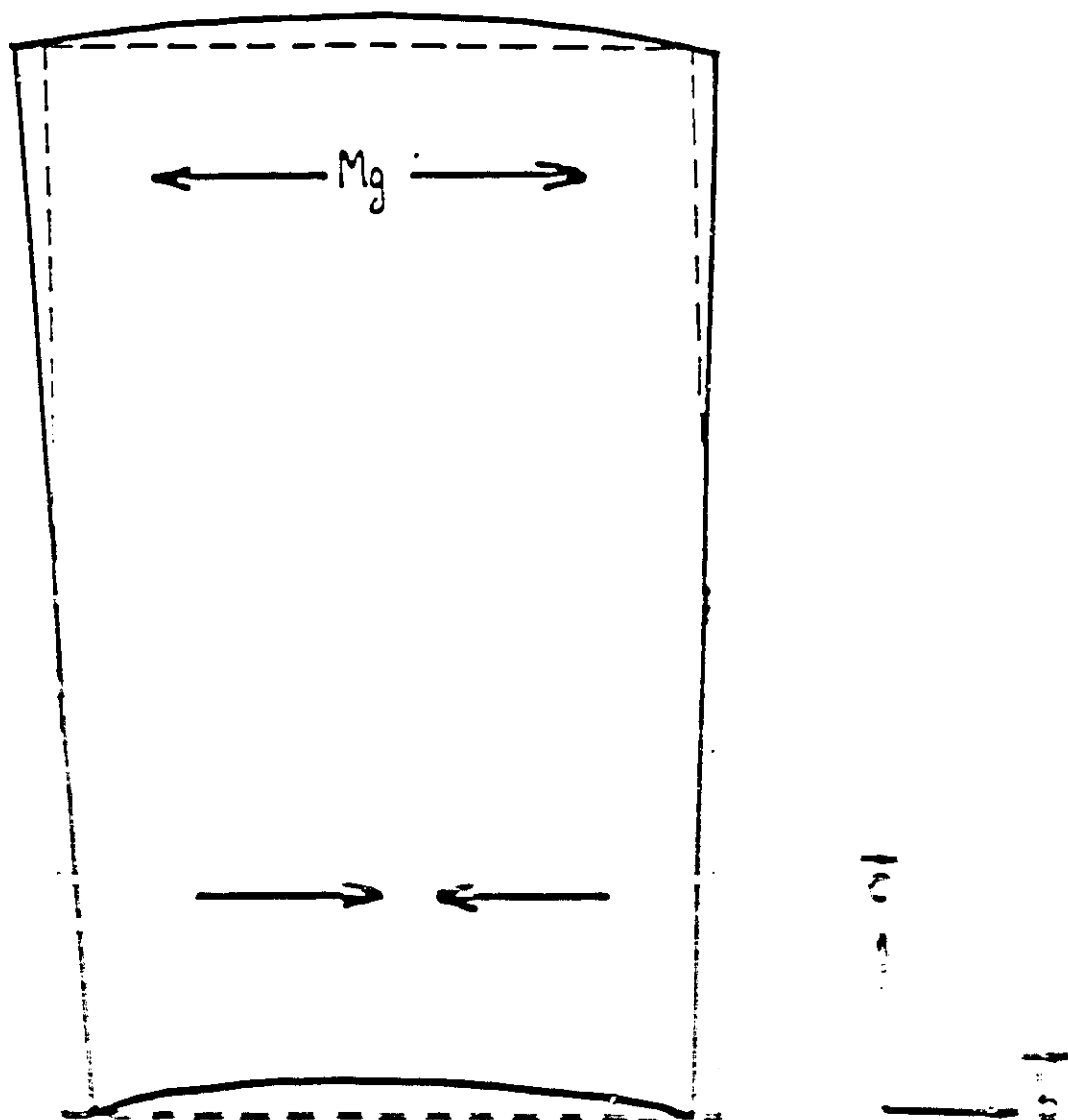


Figure 1 : Schematic diagram of the experimental setup.

electron microscopy (fig. 3.7 [24]). Some of the strain created by bulky magnesium could also disturb the d-spacing along \vec{c} , however, comparison of the line broadening of (0 2 0) and (0 0 1) peaks shows that this is minor. In addition, since there is no bonding between the layers that are stacked onto one another by the winding of the sheet, it is quite possible that there can be some variations in the interlayer spacing. This would result in stacking disorder, and would spread the (0 0 1) d-spacing over some range and would further increase the broadening of these lines. Therefore, it is possible that some of the broadening observed was due to stacking disorder and a minor amount of strain.

3.2 LEACHED CHRYSOTILE ASBESTOS: ALIX MATERIALS

3.2.1 The leaching process.

Acid leaching, prior to the crystallization of different types of zeolites, is an important step because it regulates the magnesium content and porosity of the chrysotile used as matrix for the formation of zeolitic particles. For a better understanding of the properties of the zeolites prepared using leached asbestos materials (hereafter called "Alix"), the acidic properties of leaching medium as well as its temperature and the duration of leaching were previously studied [11] and correlated to some physico-chemical characteristics of the Alix. In order to further and complete the study, we have carried out a detailed investigation of the properties of leached asbestos as a function of leaching conditions. Bulk density measurements were used to correlate the loss of magnesium to the compactness and porosity of the materials. The degree of crystallinity in chrysotile, obtained from X-ray powder diffraction (XRD), gives a measure of the breakdown of the chrysotile structure.

It was observed in an earlier study [5] that the zeolites with the most interesting catalytic properties were obtained when the XRD of the Alix used for the synthesis was in the range 22 to 24%. Within this range, the 11% led to chrysotiles having a zeolite degree of crystallinity higher than 10-12% [11].

Therefore, the main objective of the work presented is

this chapter is to establish the correlations between the magnesium leaching degree (MLD), i.e. the extent of the magnesium removal, upon various acid treatments (strong mineral acids and weak acids), and the physico-chemical characteristics of the resulting Alix materials, and to propose a structural mechanism of leaching.

3.2.2 Definition of the MLD.

Elemental analysis by atomic absorption spectrophotometry (AAS), showed the effect of leaching conditions on the magnesium content, and as a result, the magnesium content could be used to identify the extent of leaching [10,11].

The magnesium leaching degree (MLD), which expresses the extent of the leaching process as the percentage of magnesium which has gone into solution during the leaching process relative to the initial magnesium content, is defined as:

$$\text{MLD}(\%) = \frac{(\text{MgO})_i - (\text{MgO})_f}{(\text{MgO})_i} \times 100 \quad (3.3)$$

where $(\text{MgO})_i$ and $(\text{MgO})_f$ are, respectively, the initial and final magnesium contents based on the dried oxide.

This parameter was chosen because, in previous work, a strong dependence was observed between the extent of magnesium content in the Alix used for the synthesis of zeolite catalysts and the product selectivities in the conversion of methanol and light alcohols to hydrocarbons [10].

3.2.3 Leaching process with strong mineral acids.

The acidic attack of chrysotile asbestos by two different acids, hydrochloric acid and sulfuric acid, was performed by Kipkemboi [11]. The ratio of acid solution to chrysotile (volume (ml)/weight (g)) was kept equal to 10 for the complete study. The variable conditions were (i) acid concentration, (ii) temperature and/or (iii) reaction time. Under such experimental conditions, it appeared that the decomposition of chrysotile asbestos depended on the three intrinsic leaching parameters, namely : acid normality, temperature of the solution and reaction time.

Some impurities, such as free brucite, $\text{Mg}(\text{OH})_2$, were very rapidly dissolved by the acidic reagent, and since they contain magnesium, the MLD was related to them as well as to the two different structural magnesium components of the zeolite. In fact two thirds of the magnesium atoms, contained in the chrysotile phase, labelled as "skeletal" Mg, are part of the two dimensional framework, as they are structurally linked on the one hand, to silicon via oxygen bridges, and, on the other hand, they are coordinated to only one hydroxyl group. The second kind called "brucite-type" Mg is inserted in the Mg containing layers, between the skeletal magnesium atoms, and is connected to these via oxygen bridges as shown in Figure 1.1. It should be pointed out that the name "brucite-type" was chosen to emphasize the fact that the coordination of this Mg is the

same as in $\text{Mg}(\text{OH})_2$ brucite, ie. pseudo-octahedral with two axial hydroxyl groups and four equatorial shared oxygen atoms. However, it should be clear that the brucite-type magnesium is contained in the chrysotile phase, and it should not be confused with free brucite phase $\text{Mg}(\text{OH})_2$, which is found mixed with the chrysotile phase. Because of the absence of linking to silicon dioxide, and the more basic character due to coordination to two hydroxyl groups instead of only one, the "brucite-type" Mg appears to be more labile than the "skeletal" Mg.

Kipkemboi's results [11] showed that with strong mineral acid such as HCl and H_2SO_4 , the leaching process was strongly dependent on the acid normality, the reaction time, and temperature: an increase in MLD values with increasing acid normality, temperature, and time was obtained. The acid leaching process was also found to be thermally activated. In addition, Kipkemboi determined that the nature of the strong mineral acid did not seem to affect significantly the extent of leaching except for lower concentrations, in which dissolution of Mg containing impurities was more effective with H_2SO_4 than with HCl [11]. The final solid residue was found to be a collapsed macrostructure and a chemical composition close to silica gel [11].

The chemical composition of all the Alix materials synthesized by Kipkemboi and studied in this section are summarized in Appendices 2 and 3.

3.2.4 X-Ray Diffraction.

3.2.4.1 Effect of leaching on chrysotile asbestos.

After leaching, the Bragg peaks of the chrysotile phase are strongly depressed, showing a progressive loss of crystallinity as magnesium is removed (fig. 3.9). As shown by chemical analysis, chrysotile asbestos contains some impurities, some of which may be crystalline. The presence of significant amounts of iron in asbestos (Appendices 2 and 3) raises the possible presence of crystalline iron oxides. In addition, the molar ratio MgO/SiO_2 in unleached asbestos is 1.80, i.e. significantly larger than the theoretical value of 1.50 for pure chrysotile. The peak labelled "B" on figure 3.9 a) is the (0 0 1) peak for free brucite, $\text{Mg}(\text{OH})_2$, and shows that brucite is the main impurity responsible for the abnormally high MgO/SiO_2 ratio. From the chemical analysis results, one can determine that magnesium in unleached asbestos is distributed over about 83.3% chrysotile and 16.7% brucite and other Mg containing impurities such as pyroaurite, in molar percent. Two weak peaks, labelled "P" on Figure 3.9 a) belong to pyroaurite, $\text{Mg}_6\text{Fe}_2\text{CO}_3(\text{OH})_{16.4}\text{H}_2\text{O}$ with an indexation of (0 0 3) at $\theta = 5.70^\circ$ and (0 0 6) at $\theta = 11.43^\circ$ (see Section 3.1.1) [6,28,66]. It is important to mention the lack of Bragg peaks for iron oxides in unleached chrysotile asbestos, despite their fairly high content. The main reason is probably the distribution of iron over several phases, including pyroaurite and probably several types of

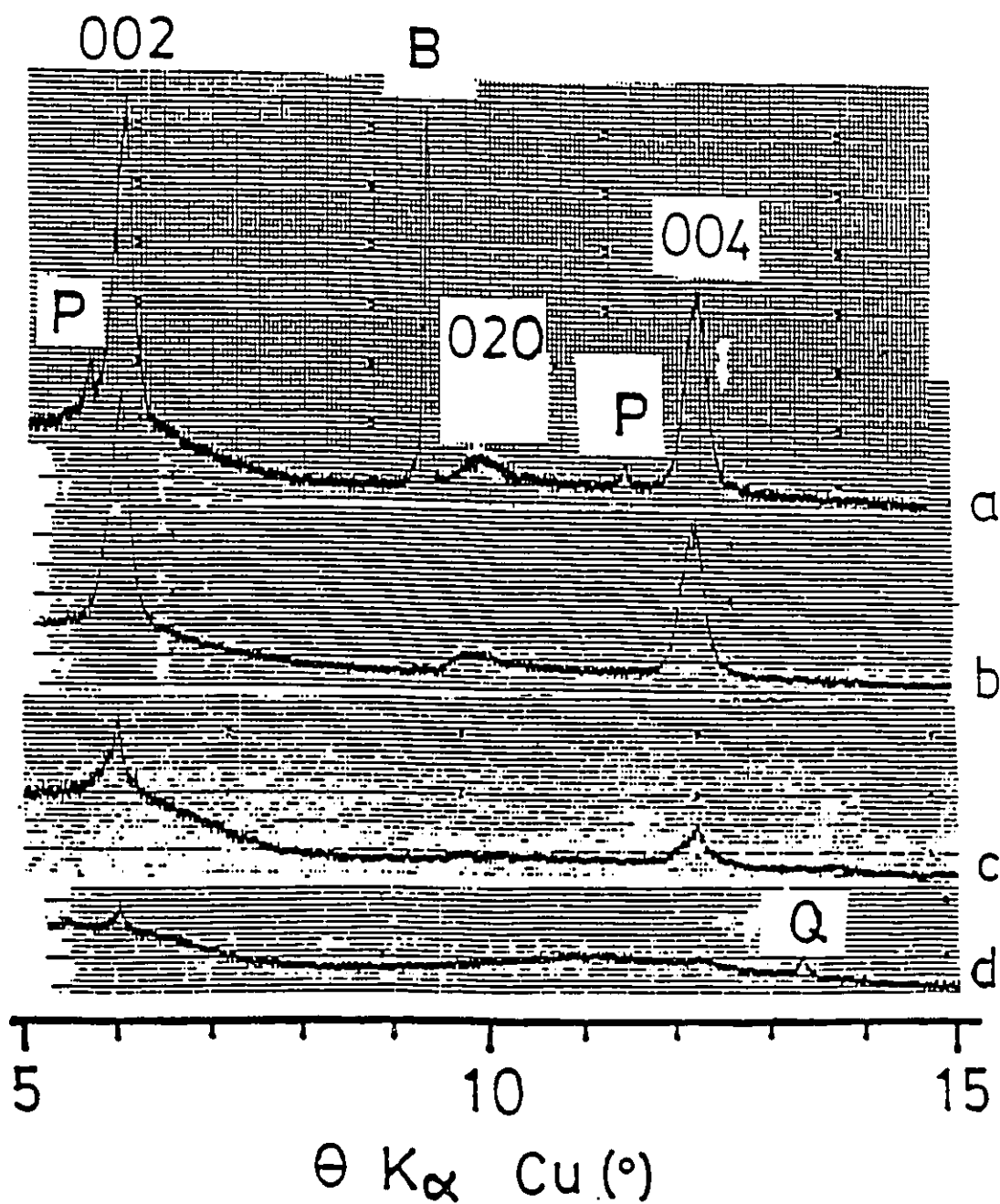


Figure 3.9 X-ray powder diffraction pattern of leached chrysotile asbestos versus MLD: (a) MLD=0%, (b) MLD=14%, (c) MLD=55%, (d) MLD=97.2%.

iron oxides (FeO , Fe_2O_3 , Fe_3O_4), resulting in a low amount for each of them, probably below the detection limit by XRD (estimated to be around 5% for each species). In addition, iron fluoresces when it is irradiated with the K_{α} radiation of copper, which strongly depresses the Bragg peaks of iron phases and increases the background. In order to counteract the fluorescence problem, another X-ray tube target such as Mo or Fe should be used, however, this could not be done since no X-ray powder diffractometer equipped with an X-ray tube other than Cu was available for this work. Pyroaurite and brucite dissolve easily in strong acids since only chrysotile peaks are observed for MLD values as low as 14.0% (fig. 3.9 b)). This could be expected since brucite is a hydroxide and pyroaurite is a hydroxycarbonate. At MLD=14.0%, the molar ratio MgO/SiO_2 is equal to 1.34 showing that there is no free brucite or pyroaurite left, as shown by XRD, and that a little of the chrysotile magnesium has been leached out. Only at very high MLD (fig 3.9 d)), a new and weak peak is observed (labelled "Q" on fig. 3.9 d), which is an indication of the formation of a small amount of crystalline product which is α -quartz [67]. The only other peak is a weak remnant of the (0 0 2) Bragg peak of chrysotile. Since this is the strongest peak of chrysotile, it is clear that the destruction of the crystalline chrysotile structure by strong mineral acids used in severe conditions was almost complete. At MLD=99%, no chrysotile peak could be observed.

The resulting product, when all the magnesium has been leached out, is amorphous silicon dioxide hemihydrate, $\text{SiO}_2 \cdot 0.5\text{H}_2\text{O}$. The water content was determined by dehydration experiments (900 °C for 4 hours) [11]. The formation of an amorphous form of silica is in good agreement with literature [68].

3.2.4.2 Degree of crystallinity studies by

XRD: Case of leaching by strong mineral acids.

The measurement of the degree of crystallinity (DC), provides a good way to correlate the amount of magnesium remaining in the asbestos fiber to the loss in crystallinity recorded. The samples used for the degree of crystallinity studies were first leached at 80 °C for 4 hours in a solution of a strong mineral acid. This was followed by filtration and drying overnight in a furnace at 110 °C. Mechanical grinding was performed on the Alix for two minutes, prior to the addition of the exact amounts of internal standard (NaCl). Then, the mixture, Alix-standard, was ground in a mortar for ca. 5 minutes before the DC analysis. The DC method used is described in detail in the experimental section (2.3.2.1).

Figure 3.10 illustrates the change in crystallinity of chrysotile asbestos when leached with strong mineral acids such as HCl and H₂SO₄. There is no significant difference between the two strong acids, as expected. A sharp decrease in degree of crystallinity is obtained with an increase in acid normality. This decrease is quasi-linear up to normality 2N and slows down above and changes much less rapidly above 3N. However, a slow but real decrease of DC (from ca. 20% to zero) is observed above normality 3N, whereas no significant change of MLD occurs. This seems to indicate that particle fragmentation to a highly

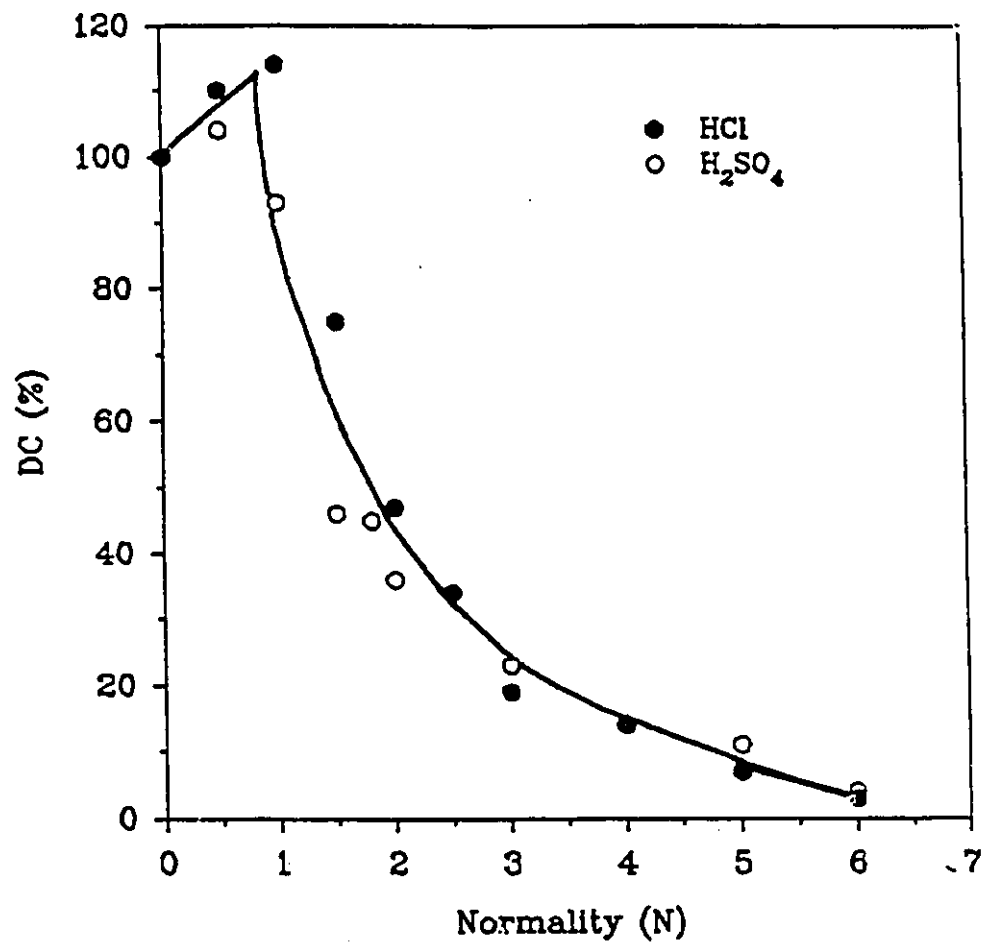


Figure 3.10 Chrysotile degree of crystallinity (DC) versus the normality of the acid used for leaching at 80 °C for 4 hours.

microcrystalline or amorphous state occurs above 3N, even though no further loss of Mg is detected. It should be noted that, above 3N at least 95% of the Mg content was lost. The points of fig. 3.10 located above DC=100% at low normalities (in the 1N region) have an overrated degree of crystallinity due to the rapid weight loss, at low acid normality, due to the rapid dissolution of the basic impurities (brucite and pyroaurite), whereas little magnesium from the chrysotile phase (and therefore little crystallinity) is lost under these conditions. Since we established from chemical analysis (see section 3.2.4.1) that only 83.3% of the unleached samples are made of the chrysotile phase, corrections of DC values for the crystallinity of chrysotile can be made, by multiplying the observed DC by 0.833. The corrected results shown on fig. 3.11 are much less flawed by the highly soluble impurities; all values of DC are lower than 100% as expected, and there is little loss of crystallinity below acid normality 1N; otherwise the behavior is similar to that found using uncorrected data. The acid attack starts with the easy elimination of brucite and pyroaurite. In fact these impurities are dissolved quasi-instantaneously into an acidic solution. Next, the following components to be dissolved are preferentially the "brucite-type" magnesium part of the structural chrysotile asbestos, which are the magnesium atoms positioned in the external layer of the monofiber since these are immediately exposed to the acidic solution. When DC is down to about 20%, further

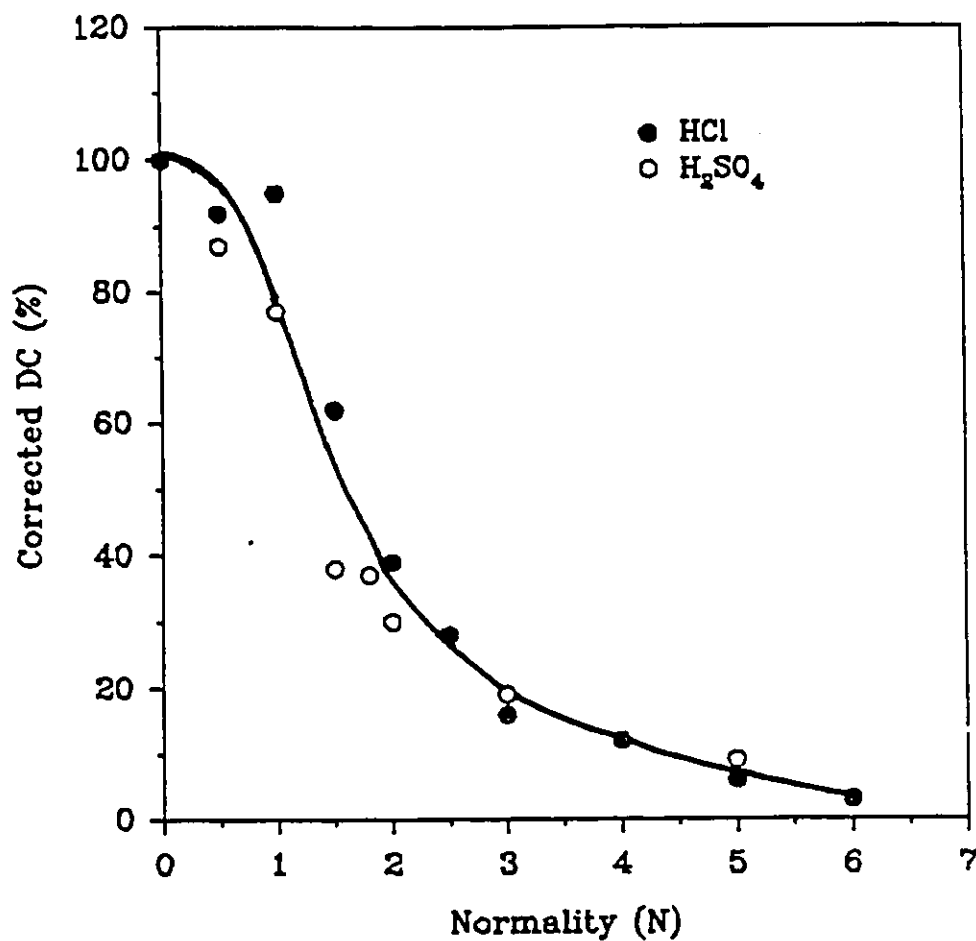


Figure 3.11 Corrected Chrysotile degree of crystallinity (DC) versus the normality of the acid used for leaching at 80 °C for 4 hours. The correction is explained in the text.

decrease is much slower. This can be related to the difficulty in removing the last magnesium atoms remaining in the chrysotile structure. The magnesium atoms that resist leaching best are "skeletal" magnesium which are less basic, are linked to Si via oxygen bridges, and are positioned in the internal layer of the fiber, and are therefore shielded from acidic attack. Indeed, more external layers have to be deteriorated before the internal layers can be exposed to the acidic medium.

Figure 3.12 and Tables 3.5 and 3.6 illustrate the relationship between the corrected degree of crystallinity (DC) and MLD for HCl and H₂SO₄ acids. Figure 3.12 shows a progressive loss of crystallinity with leaching.

In a first step, a rapid loss of crystallinity down to about 40% occurs from very low MLD values up to about 50% for HCl, and from MLD of 25% to about 65% for H₂SO₄. This corresponds to the removal of "brucite-type" magnesium primarily. Since, only one third of the total magnesium content of chrysotile asbestos is of "brucite-type", this initial phase should be completed at MLD = 33.3%. However, since 16.7% of the initial magnesium was contained in impurities, which are rapidly dissolved upon exposure to the acid, the real MLD of the chrysotile phase was lower than that of the sample mixture. Using the 16.7% content of magnesium in the impurities, the real MLD of the chrysotile phase was calculated to be 41% for HCl and 54% for H₂SO₄. These values are still higher than the theoretical prediction

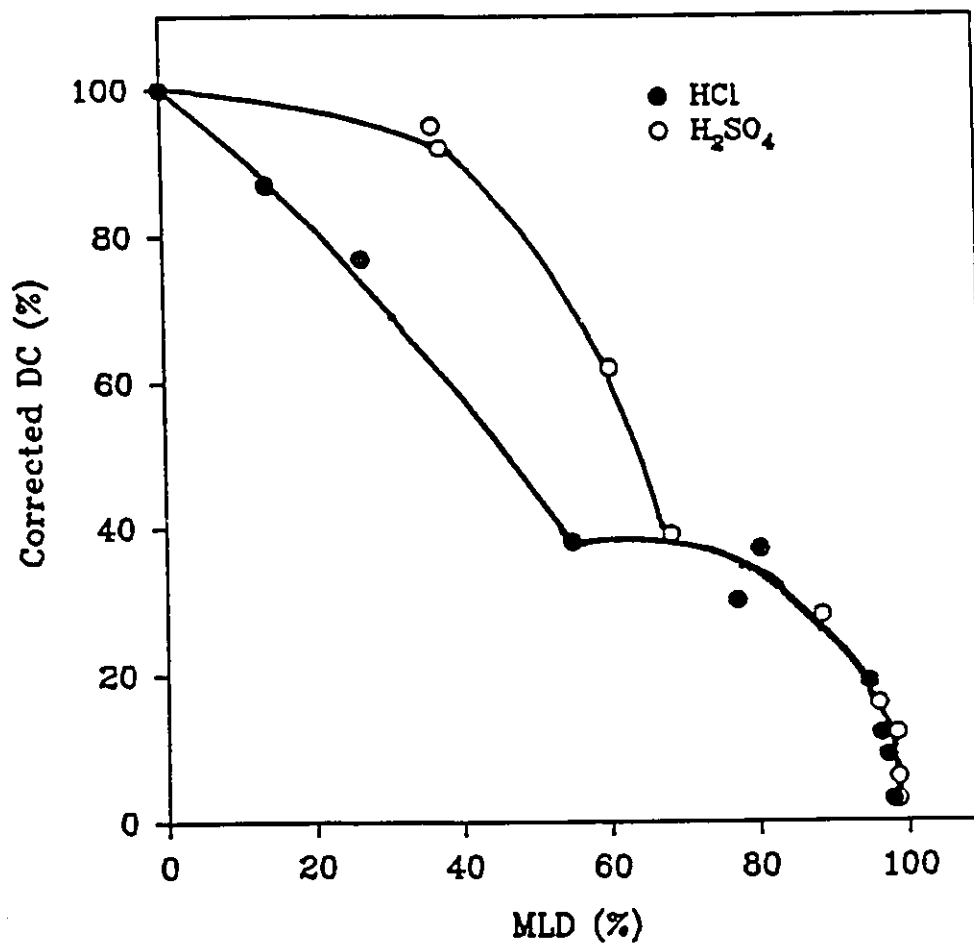


Figure 3.12

Relationship between the corrected degree of crystallinity and MLD for HCl and H₂SO₄ acid solutions for a reaction time of 4 hours at 80 °C.

ALIX #	Normality N	DC (%)	Corrected DC (%)	MLD (%)
76	0.5	104	87	14.0
77	1.0	93	77	26.7
67	1.5	46	38	55.0
68	1.8	45	37	80.3
78	2.0	36	30	77.2
72	3.0	23	19	94.8
73	4.0	14	12	96.3
74	5.0	11	9	97.2
75	6.0	4	3	97.9

Table 3.5 Relationship between the degree of crystallinity (DC) and the corrected degree of crystallinity (corrected DC) versus acid normality and MLD, for a reaction time of 4 hours, and a reaction temperature of 80 °C.

ALIX #	Normality N	DC (%)	Corrected DC (%)	MLD (%)
112	0.5	110	92	37.6
113	1.0	114	95	36.6
114	1.5	75	62	60.2
115	2.0	47	39	68.3
116	2.5	34	28	88.5
117	3.0	19	16	96.0
118	4.0	14	12	98.5
119	5.0	7	6	98.6
120	6.0	3	3	98.6

Table 3.6 Relationship between the degree of crystallinity (DC) and the corrected degree of crystallinity (corrected DC) versus acid normality and MLD for a reaction time of 4 hours, and a reaction temperature of 80 °C in H₂SO₄.

of 33.3%. However, considering the sources of experimental errors (temperature fluctuations during leaching, difficulties in stirring due to the interaction of magnetite impurities with stirring bar, the amount of impurities is an estimation), the value of 40% for HCl is remarkably close. It must also be pointed out that leaching of some of the skeletal magnesium probably occurs before all the "brucite-type" magnesium is reached. After the first rapid loss of crystallinity, the decrease of the degree of crystallinity is much slower up to MLD = 90%. This probably corresponds to the removal of more tightly held skeletal magnesium, and the chrysotile structure does not collapse completely until most of them have been removed.

As MLD approaches 100%, DC falls abruptly to zero. Above a MLD=85%, i.e. below DC=30%, the rapid loss in crystallinity indicates an important structural destruction or collapse of the chrysotile structure and an amorphization of the solid residue. This is due to the removal of the last 15% "skeletal-magnesium" remaining in the chrysotile structure, which are linked to silicon atoms via oxygen. In this range of MLD (above .85%), a considerable amount of $\text{SiO}_2 \cdot 0.5\text{H}_2\text{O}$ is formed, and is the remaining product obtained after complete leaching, in addition to a minor amount of α - quartz, which was detected by X-ray diffraction of the Alix for a MLD=97.2% (fig. 3.9 d)). Silicon dioxide hemihydrate, the final amorphous product was obtained after complete leaching for both HCl and H_2SO_4 [11]. All

divergences of behavior between H_2SO_4 and HCl curves of Figure 3.12, are observed at $\text{MLD} < 67\%$. They result from the difference in MLD observed between the two acids for $N \leq 1$ (Tables 3.5 and 3.6) and show the effectiveness of H_2SO_4 compared to HCl to dissolve the initial impurities as well as to initiate the removal of the brucite-type Mg, part of the chrysotile structure.

-

3.2.5 Bulk density and surface area of chrysotile asbestos leached by strong mineral acids.

Bulk density measurements, used for the determination of the density of powdered materials, are described in detail in section 2.4. It is obvious that the structural desintegration of leached asbestos that was observed by other techniques, should also affect the bulk density. Measurement of the density can support some structural changes and provide additional information on the transformations taking place upon leaching, provided the method is sensitive enough. Since the morphology and texture of the final porous material are of great interest, some important information concerning its porosity can also be deduced from the bulk density. For example, the packing efficiency of a material such as $\text{SiO}_2 \cdot 0.5\text{H}_2\text{O}$ can be investigated, in comparison with other polymorphs of silicon dioxide.

For these experiments, the same Alix materials were used as for the study of the degree of crystallinity, i.e. after leaching with HCl or H_2SO_4 at a constant temperature of 80 °C for a reaction time of 4 hours.

The measured density versus the normality of the strong mineral acids HCl and H_2SO_4 are shown on Figure 3.13 and in Tables 3.7 and 3.8. The density versus acid normality gives a similar pattern for both acids. For concentrations < 1 N, (region A on fig. 3.13) only a very slight decrease of bulk density is observed. At that stage, the main species dissolved are the basic impurities, with maybe, a minor part

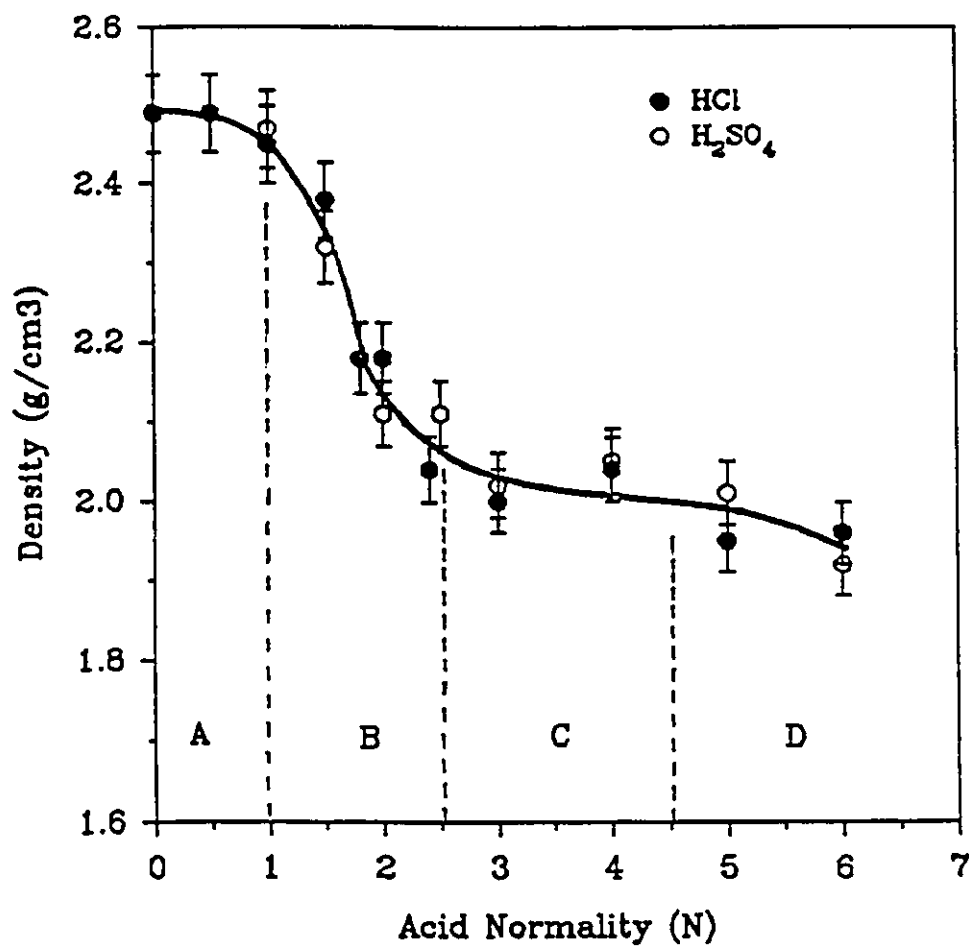


Figure 3.13 Bulk density of chrysotile asbestos versus acid normality for a reaction time of 4 hours at 80 °C.

ALIX #	Normality N	Density (g/cm ³)	MLD (%)
Asbestos	0.0	2.49	0.0
76	0.5	2.49	14.0
77	1.0	2.45	26.7
67	1.5	2.38	55.0
68	1.8	2.18	80.3
78	2.0	2.18	77.2
61	2.4	2.04	91.6
72	3.0	2.00	94.8
73	4.0	2.04	96.3
74	5.0	1.95	97.2
75	6.0	1.96	97.9

Table 3.7 Bulk density of chrysotile asbestos when HCl was used as leaching reagent. (Temperature = 80 °C, reaction time = 4 hrs)

ALIX #	Normality N	Density (g/cm ³)	MLD (%)
Asbestos	0.0	2.49	0.0
112	0.5	2.49	37.7
113	1.0	2.47	36.6
114	1.5	2.32	60.2
115	2.0	2.11	68.3
116	2.5	2.11	88.5
117	3.0	2.02	96.0
118	4.0	2.05	98.5
119	5.0	2.01	98.6
120	6.0	1.92	98.6

Table 3.8 Bulk density of chrysotile asbestos when H₂SO₄ was used as leaching reagent. (Temperature = 80 °C, reaction time = 4 hrs)

of the "brucite-type" structural magnesium. Therefore, little change in density would be expected if the density of the impurities were close to that of chrysotile. The main impurity which is rapidly dissolved is $\text{Mg}(\text{OH})_2$ brucite; its density, $\rho = 2.36 \text{ g/cm}^3$ [69], is close enough to that of unleached asbestos ($\rho = 2.49 \text{ g/cm}^3$) to give a negligible change upon dissolution of brucite. The other impurity that could be suspected to initiate considerable changes would be pyroaurite with its bulk density ranging from 2.13 to 2.18 g/cm^3 , depending on the crystal lattice involved [70]. However, the small amount of this mineral would not be enough to decrease significantly the obtained bulk density value for chrysotile asbestos. For concentrations of 1 to 2.5N (region B on fig. 3.13) a sharp decrease in bulk density is observed leading to the obvious conclusion that the effective removal of the magnesium is really coming from the initial fibrous structure of chrysotile. In that concentration range, most of the magnesium leached out is the "brucite-type" magnesium. Its removal first creates some empty spaces or vacancies in the sheets of the chrysotile fibers without affecting the initial framework, which does not collapse at this stage. This results in a considerable reduction in weight without reduction in volume, and hence, a decrease in density. For normalities higher than 2.5N, (region C on fig. 3.13) removal of Mg results in a gradual collapse of the fibrous structure. This large reduction in volumes compensates the reduction of weight due to further loss of Mg, and its results in a quasi-

constant density. At very high normalities (5 - 6N), a further small decrease in density is observed (region D on fig. 3.13), which corresponds to the disappearance of the last remnants of chrysotile and the appearance of the less dense highly porous $\text{SiO}_2 \cdot 0.5\text{H}_2\text{O}$.

The final density of ca. 1.9 g/cm^3 is significantly lower than the values reported for various crystalline, vitreous or amorphous varieties of silica (Table 3.9) thus indicating the completely leached Alix (MLD=100%) is less compact and more highly porous [71].

When plotted against MLD, the bulk density for the H_2SO_4 system (fig. 3.14), shows clearly the four regions identified on fig. 3.13. This is less clear for the Alix leached with HCl (fig. 3.15). The four regions are the following:

- A (MLD = 0-45%) : dissolution of basic impurities
(brucite and pyroaurite) and the most outer part of "brucite-type" magnesium which is the most exposed to the acid: slow decrease in density and removal of strain in silicate sheets;
- B (MLD = 45-65%): leaching out of "brucite-type magnesium": no structural collapse, creation of many Mg vacancies, giving a rapid decrease in density;
- C (MLD = 65-90%): removal of "skeletal magnesium" and structural collapse: the loss of weight due to removal of Mg is compensated by

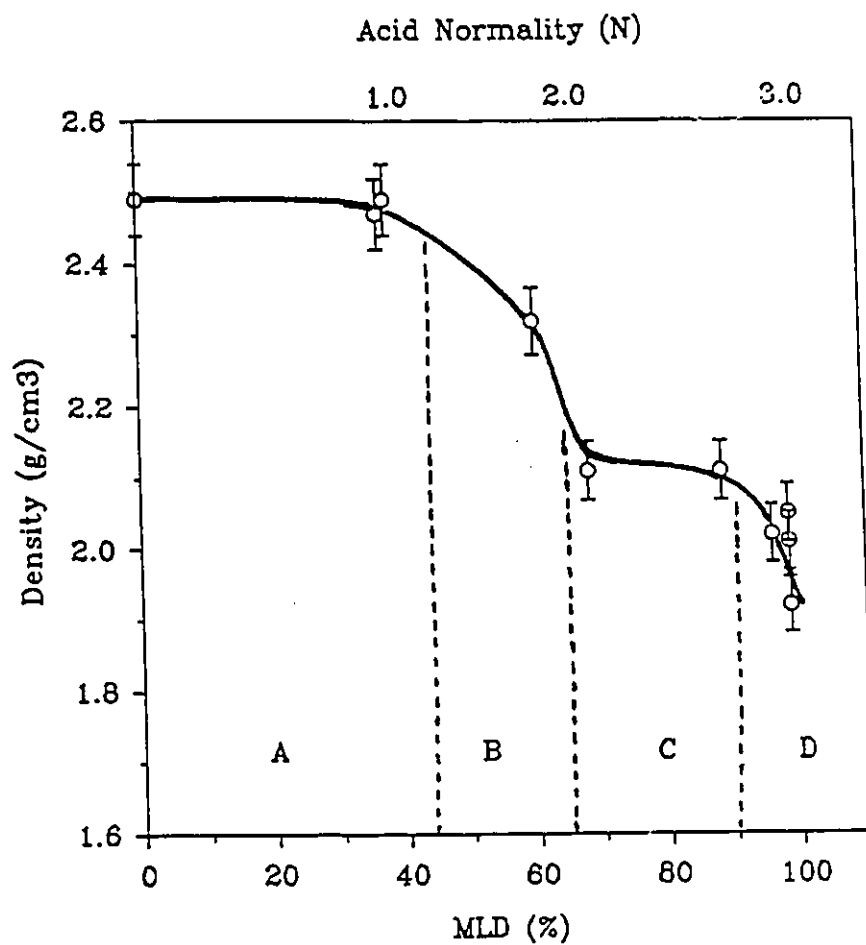


Figure 3.14 Bulk density versus MLD for chrysotile leached by using H_2SO_4 solutions at 80 °C for 4 hours.

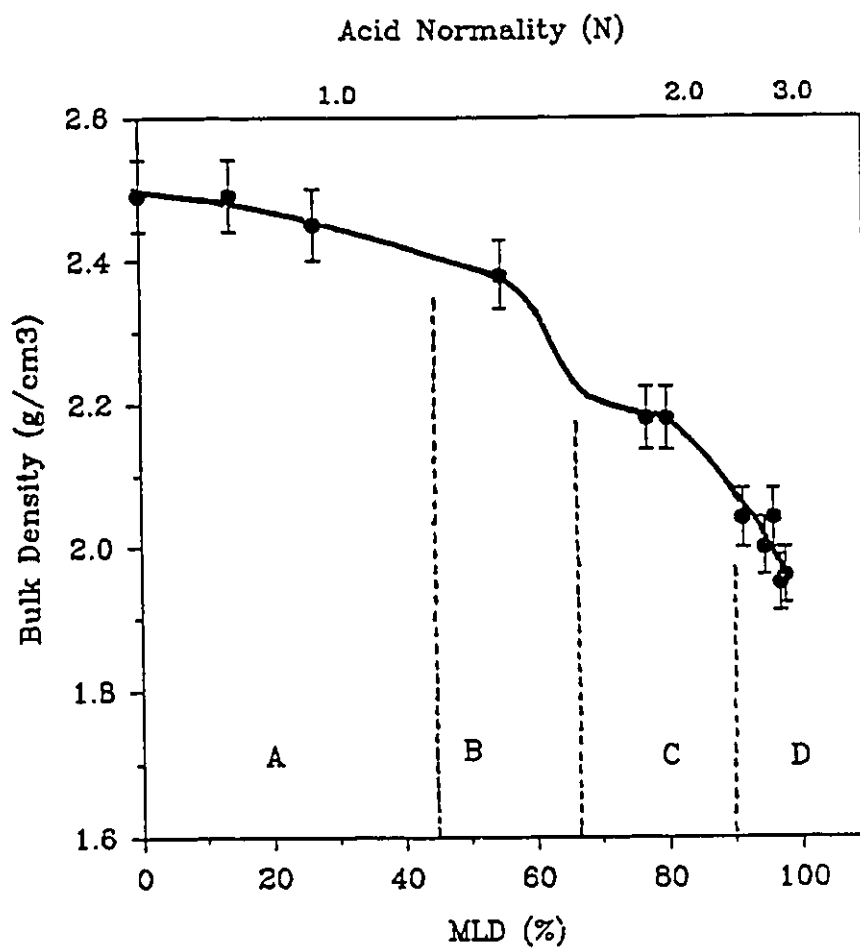


Figure 3.15 Bulk density versus MLD for chrysotile leached using HCl solutions at 80 °C for 4 hours.

Varieties of SiO ₂	Bulk Density (g/cm ³)
cristobalite	2.32
vitreous lechatelierite	2.19
tridymite	2.26
SiO ₂ . xH ₂ O opal	2.17 - 2.20
quartz	2.635 - 2.660

Table 3.9 Bulk density values of various types of silica. [71]

the loss of volume due to structural collapse leading to fairly constant density;

- D (MLD = 90-100%): complete disappearance of chrysotile, large production of amorphous porous silica hemihydrate: further decrease in density.

Comparison of Figure 3.13 with Figures 3.14 and 3.15 shows a similar behavior with the exception that regions A and B are stretched over a large part of Figures 3.14 and 3.15 because MLD versus normality is strongly non-linear. On Figures 3.14 and 3.15, normality 2N corresponds to about MLD = 77% and 68% respectively i.e. normalities 2N to 6N are squeezed in the regions of MLD = 77% to 98% for HCl and 68 to 99% for H₂SO₄.

The variation of the BET specific surface area of the material versus the compactness results obtained from the bulk density study are compared on Figure 3.16 and in Table 3.10. The surface area increases slowly from values up to 40 to 120 m²/g in the first phase of leaching (MLD=0 to 45%). This corresponds to the dissolution of the basic impurities, followed by the beginning of the leaching of "brucite-type" magnesium (region A figs. 3.13 to 3.15). Since no major structural reorganization occurs in that stage and the density change is minor (region A), no drastic change of surface area is expected. As more drastic structural changes take place, i.e., removal of most of the "brucite-type" Mg,

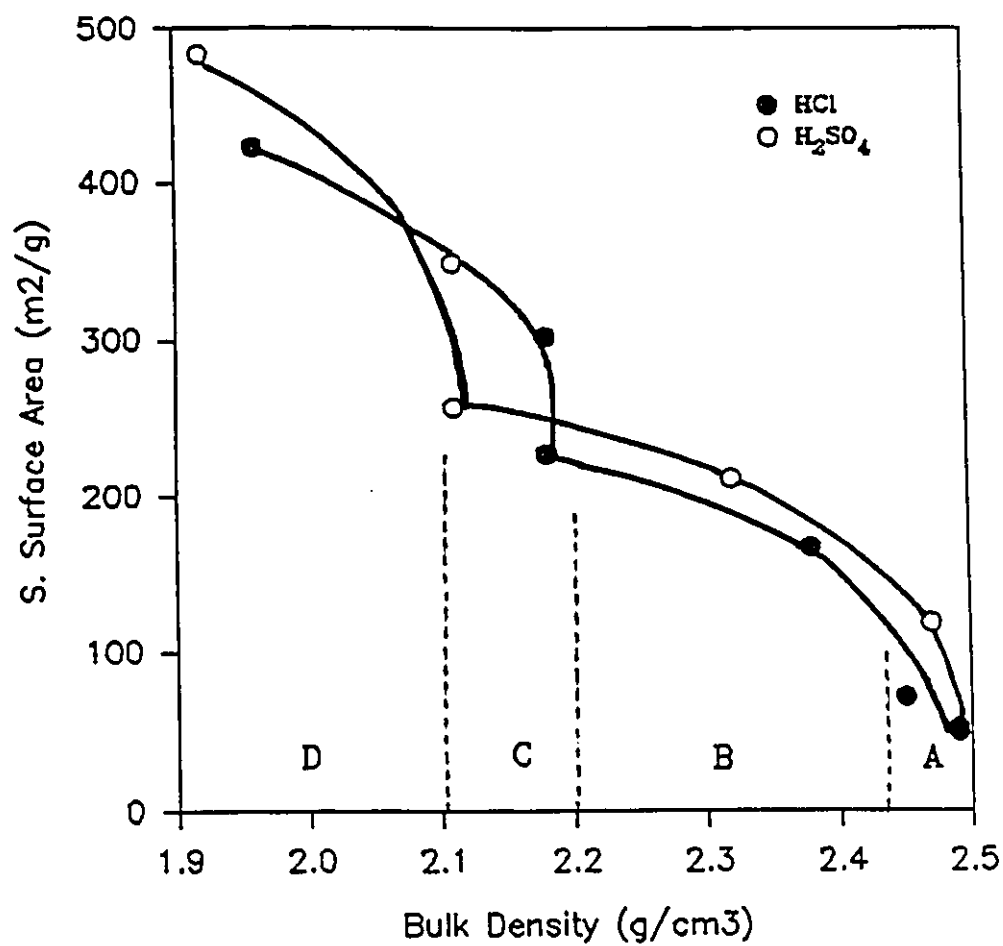


Figure 3.16 BET specific surface area versus bulk density for chrysotile leached with HCl and H₂SO₄ solutions at 80 °C for 4 hours.

Strong Mineral Acid	Normality (N)	Alix #	MLD (%)	Surface Area (m ² /g)	Bulk Density (g/cm ³)
chrysotile	---	--	0	49	2.49
HCl	0.5	76	14.0	52	2.49
	1.0	77	26.7	71	2.45
	1.5	67	55.0	167	2.38
	1.8	68	80.3	227	2.18
	2.4	61	91.6	302	2.18
	6.0	75	97.9	423	1.96
H ₂ SO ₄	1.0	113	36.6	118	2.47
	1.5	114	60.2	211	2.32
	2.0	115	68.3	257	2.11
	2.5	116	88.5	349	2.11
	6.0	120	98.6	483	1.92

Table 3.10 Specific surface area of Alix samples. [6,11,28]
 (temperature = 80 °C, reaction time = 4 hrs)

a more porous structure results and a large increase of specific surface area takes place (section B), however, as the collapse of the chrysotile structure starts, no further pores are created and the specific surface area levels off at about $250 \text{ m}^2/\text{g}$ (end of region B and C). With the removal of skeletal magnesium, a considerable amount of non-crystalline $\text{SiO}_2 \cdot 0.5\text{H}_2\text{O}$ is produced and an abrupt increase of specific surface area to about $400 \text{ m}^2/\text{g}$ occurs, showing the exceptionally high porosity of the Alix material (region D).

Kipkemboi reported that the specific surface area increased monotonously versus MLD [11], whereas this is not the case when it is plotted versus bulk density (fig. 3.16). This is not surprising since the bulk density study and the surface area do not probe the same way the changes taking place and the density does not change linearly with MLD. Indeed, the density measures the weight per unit volume, and therefore is sensitive to changes of both weight and volume and to the way they vary relative to one another. On the other hand, the surface area is a measure of the surface of the crystallites available for gas adsorption and is therefore sensitive to creation of pores and particle size decrease. Therefore, part B results in a sudden decrease of density because atoms of Mg are removed but the volume remains essentially the same. This creates a large increase in porosity and, as expected, gives a much higher surface area. Further removal of Mg collapses the structure (part C) which drastically reduces the volume and gives a constant density due to

compensation of weight loss by volume decrease. However, this phenomenon reduces further the particle size of the material and therefore increases the surface area. A similar interpretation can be made for part D. It may be concluded that parts B, C, and D, which are very different from one another in terms of density behaviour, all contribute to increase the surface area.

3.2.6 Secondary leaching of chrysotile asbestos with weak organic acids.

A weak organic acid, such as acetic acid, EDTA or oxalic acid, when used in high concentration, can decompose chrysotile, because of its low resistance to acidic attacks. Since the use of strong mineral acids does not make possible a fine tailoring of MLD because of their high leaching power, a two-step leaching method of chrysotile asbestos was designed by Kipkemboi [11]. In the first step, a mineral acid, under very mild conditions, is used in order to obtain a medium MLD value of around 50-60%; this is followed, in a second step, by a fine tailoring of MLD by leaching with a weak organic acid, in order to have a better control of the rate of magnesium removal. The three weak acids used in the secondary leaching process were acetic acid (ACA), oxalic acid (OXA), and ethylene diamine tetraacetic acid (EDTA). In addition to the three main parameters, i.e. acid normality, reaction time, and temperature, secondary leaching with an organic acid involves an additional parameter, i.e. the pH of the leaching solution.

The reaction conditions and the analytical results obtained by Kipkemboi [11] are found in Appendices 4 and 5. In these results, the iron content in the resulting Alix samples appeared as only weakly dependent on the leaching parameters, but was strongly dependent on the nature of the organic acid [11].

It should be mentioned that one of the ultimate aims of leaching by weak organic acids was to prepare Alix samples with MLD in the range of 60-85% for use as source of SiO_2 in the synthesis of chryso-zeolites. In this respect, the two-step leaching was highly reproducible and accurate. In order to further the understanding of the properties of these materials, which were prepared and characterized by Kipkemboi [11], XRD and bulk density measurements of samples leached by OXA and ACA have been carried out and are presented here.

3.2.7 Degree of crystallinity of Alix materials leached with weak organic acid.

For this study, only the samples of chrysotile leached with acetic acid and oxalic acid have been used. When the degree of crystallinity (DC) is plotted against normality (fig. 3.17 and Tables 3.11 and 3.12) wiggles are obtained (solid lines on fig. 3.17). These are probably due to the fact that the temperature of the reaction was not accurately controlled by Kipkemboi [11] when secondary leaching was carried out. Indeed, the temperature of the reaction medium was controlled using a heating plate. However, the temperature setting is not accurate and the actual temperature could change by as much as 10 °C with the exact position of the reaction vessel on the plate [8]. However, dashed curves of Figure 3.17 show that a clear trend is visible, i.e., the degree of crystallinity decreases with increasing acid normality. This behavior could have been expected. A remarkable difference can be observed between the two acids: the loss of crystallinity is small for ACA (56.8 to about 40%), whereas a drastic drop of degree of crystallinity to about 10% occurs for OXA at 1.5N and no significant further change occurs up to normality 6N. The drastic difference of reactivity between the two acids is in agreement with the higher reactivity of OXA reported in the literature [11,72,73]. The degree of crystallinity converges to non-zero values, in contrast to the results obtained with strong acids. With oxalic acid, the minimum degree of

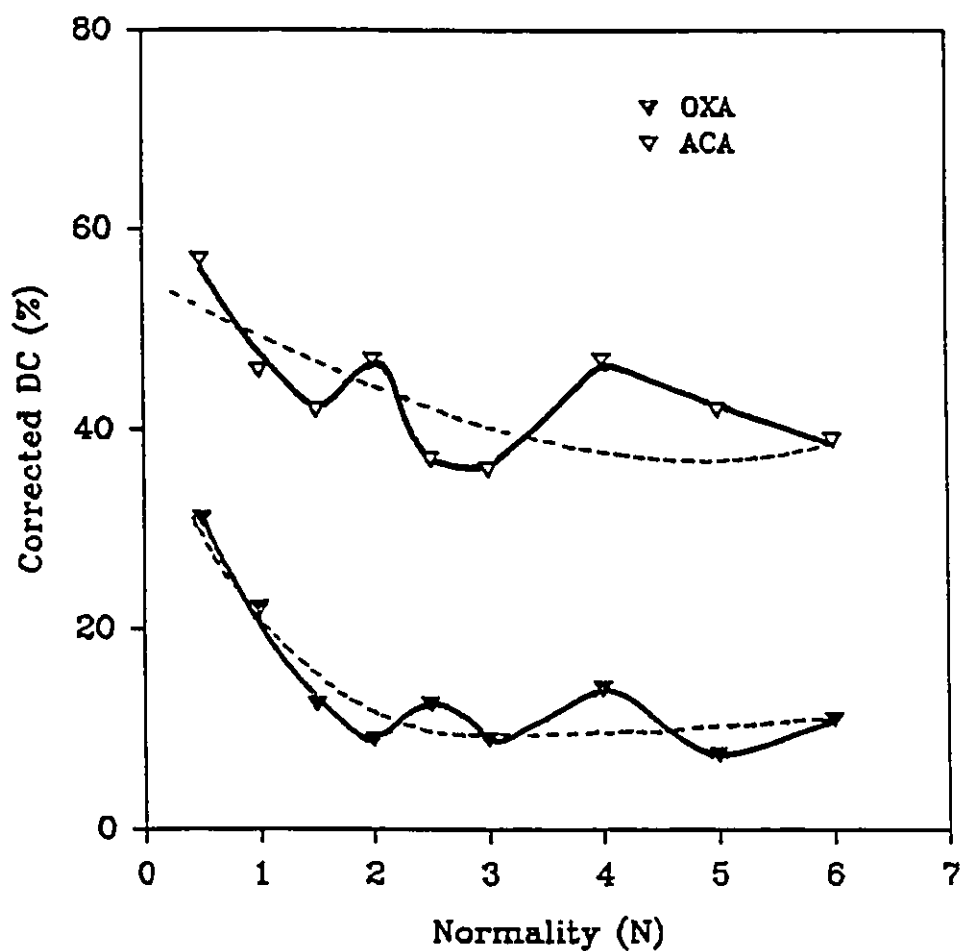


Figure 3.17 Corrected degree of crystallinity versus the normality of the weak acid used for secondary leaching of chrysotile at 80 °C for 4 hours.

ALIX #	Normality N	Corrected DC %	MLD %
150	0.5	57	67.2
122	1.0	46	70.7
123	1.5	42	74.1
124	2.0	47	74.4
125	2.5	37	74.9
126	3.0	36	75.8
127	4.0	47	75.4
128	5.0	42	79.1
129	6.0	39	79.6

Table 3.11 Corrected degree of crystallinity (corrected DC) versus MLD and the normality of the acetic acid used for secondary leaching of chrysotile at 80 °C for 4 hours.

ALIX #	Normality N	Corrected DC %	MLD %
149	0.5	31	66.1
130	1.0	22	71.1
131	1.5	13	72.7
132	2.0	9	73.0
133	2.5	13	76.2
134	3.0	9	77.2
135	4.0	14	79.2
136	5.0	8	76.4
137	6.0	11	77.2

Table 3.12 Corrected degree of crystallinity (corrected DC) versus MLD and the normality of the oxalic acid used for secondary leaching of chrysotile at 80 °C for 4 hours.

crystallinity is around 10% compared to the value of about 42% for acetic acid. This comparison illustrates the importance of the acid strength on the destruction of the chrysotile lattice and it also shows the opportunity provided by their milder reactivity for fine tuning the final value of MLD. Because of its higher acidity, OXA seems to be more efficient in destroying the fibrous structure of chrysotile.

When DC is plotted versus MLD (fig. 3.18), it is found that the degree of crystallinity decreases with increasing MLD; this trend was also observed for strong acids. The decrease is slow and continuous when ACA is used, whereas it is much more rapid and then levels off in the case of OXA. This is probably due to the higher reactivity of OXA. The points appear scattered, however, we are examining only a narrow range of MLD values (65-80%). The difference in acid strength is also clearly reflected on the difference in degree of crystallinity obtained at a given MLD: for any MLD value in the range of MLD covered by secondary leaching, i.e. 65% to 80%, the degree of crystallinity is about 30% higher when ACA is used. This shows a clear difference between the action of the two acids: although the same amount of magnesium is removed with both acids, the chrysotile structure collapses faster with OXA. We have no explanation for this phenomenon. It should be noted that the degree of crystallinity versus MLD for strong acids gives values similar to those obtained with weak acids (fig. 3.18), with , may be , HCl behaving more like ACA and H_2SO_4 like OXA,

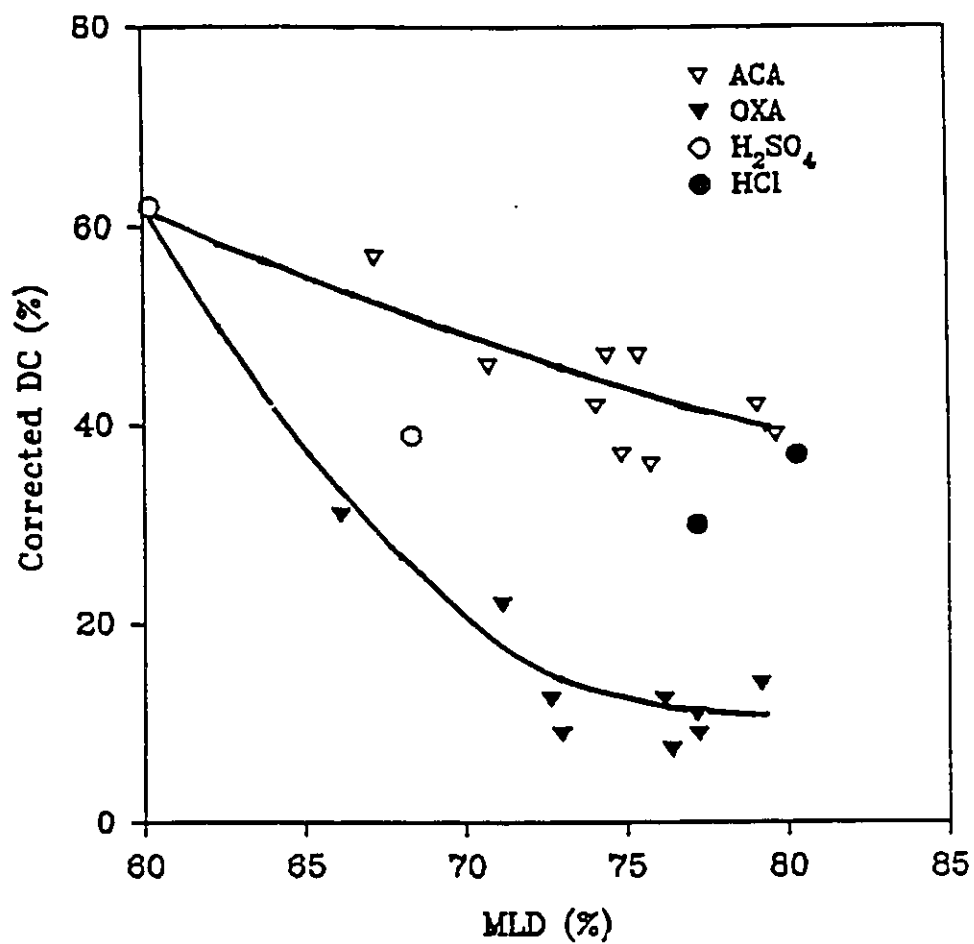


Figure 3.18 Corrected degree of crystallinity versus MLD for chrysotile after secondary leaching with OXA and ACA at 80 °C for 4 hours. The points for HCl and H_2SO_4 are given for comparison.

although this could be just a coincidence since there are only two points for each strong acid in the range $MLD = 60$ to 85% (fig.3.18).

3.2.8 Bulk density of asbestos chrysotile
leached with weak organic acids.

Bulk density measurements have been performed in order to evaluate changes in packing and porosity occurring upon secondary leaching with weak acids. The first impression one gets from the results of fig. 3.19 and Table 3.13 is that there is little change in the density versus normality of the weak acid ACA and there is a large initial decrease for OXA at very low normality (0.5N), then no further change at higher concentrations. The clear difference between the density obtained with the two acids for any acid normality can, again, be explained by the higher reactivity of OXA. Oxalic acid gives density values that are lower and closer to the density of the final residue, $\text{SiO}_2 \cdot 0.5\text{H}_2\text{O}$. This can be explained by its higher strength and is in agreement with the lower degree of crystallinity (fig. 3.17). In addition, the higher efficiency of oxalic acid (relative to acetic acid) for dissolving the iron containing impurities (other than pyroaurite which was dissolved by the strong acid in the first step of leaching), i.e. iron oxides, and the fact that iron oxides and their hydrates have a density clearly higher than that of chrysotile [74], explains the lower density measured for samples leached with oxalic acid. EDTA should give even lower densities, since it removes iron even better than oxalic acid.

The wiggles on the curves of fig. 3.19 are probably due to the temperature fluctuations mentioned in 3.2.7 (fig.

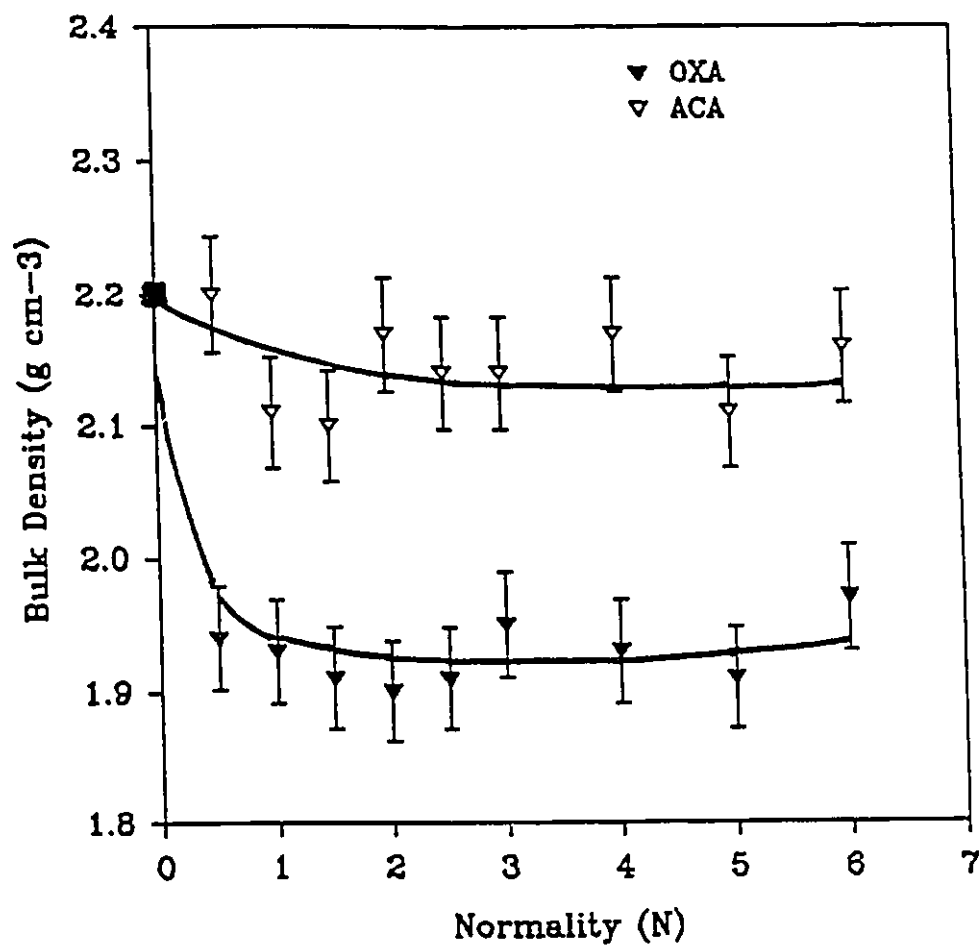


Figure 3.19 Bulk density of chrysotile versus the normality of the acid used for secondary leaching at 80 °C for 4 hours.

Leaching reagent	ALIX #	Normality N	Bulk Density (g/cm ³)	MLD %
Oxalic Acid	149	0.5	1.94	66.1
	130	1.0	1.93	71.1
	131	1.5	1.91	72.7
	132	2.0	1.90	73.0
	133	2.5	1.91	76.2
	134	3.0	1.95	77.2
	135	4.0	1.93	79.2
	136	5.0	1.91	76.4
	137	6.0	1.97	77.2
Acetic Acid	150	0.5	2.20	67.2
	122	1.0	2.11	70.7
	123	1.5	2.10	74.1
	124	2.0	2.17	74.4
	125	2.5	2.14	74.9
	126	3.0	2.14	75.8
	127	4.0	2.17	75.4
	128	5.0	2.11	79.1
	129	6.0	2.16	79.6

Table 3.13 Effect of secondary leaching at
80 °C for 4 hours on bulk density.

3.17) and can be considered meaningless; therefore one could say there is no significant change of density versus acid normality. The plot of the density versus MLD (fig. 3.20) also shows little change for samples leached with ACA, whereas a much more drastic decrease, then stabilization, occurs with OXA. The values for H_2SO_4 and HCl available for the region 65 to 80% MLD are also shown for comparison. It can be seen that the nearly constant density accross the MLD region 60 to 80% parallels the behavior of strong acids (fig. 3.14 and 3.15) and corresponds to removal of some "skeletal magnesium" coupled with partial structural collapse, such that the decrease of weight due to loss of magnesium is compensated by a loss of volume. The sudden drastic decrease of density observed with OXA can be explained by its high efficiency for removing high density iron oxides. The slow attack of "skeletal magnesium" by the weak acids explains their capability for fine tailoring of MLD in the range 60-80%. This, in addition to the high efficiency of OXA and EDTA for removing iron oxides, makes secondary leaching a necessary step in the preparation of the Alix to be used for the synthesis of zeolite catalysts.

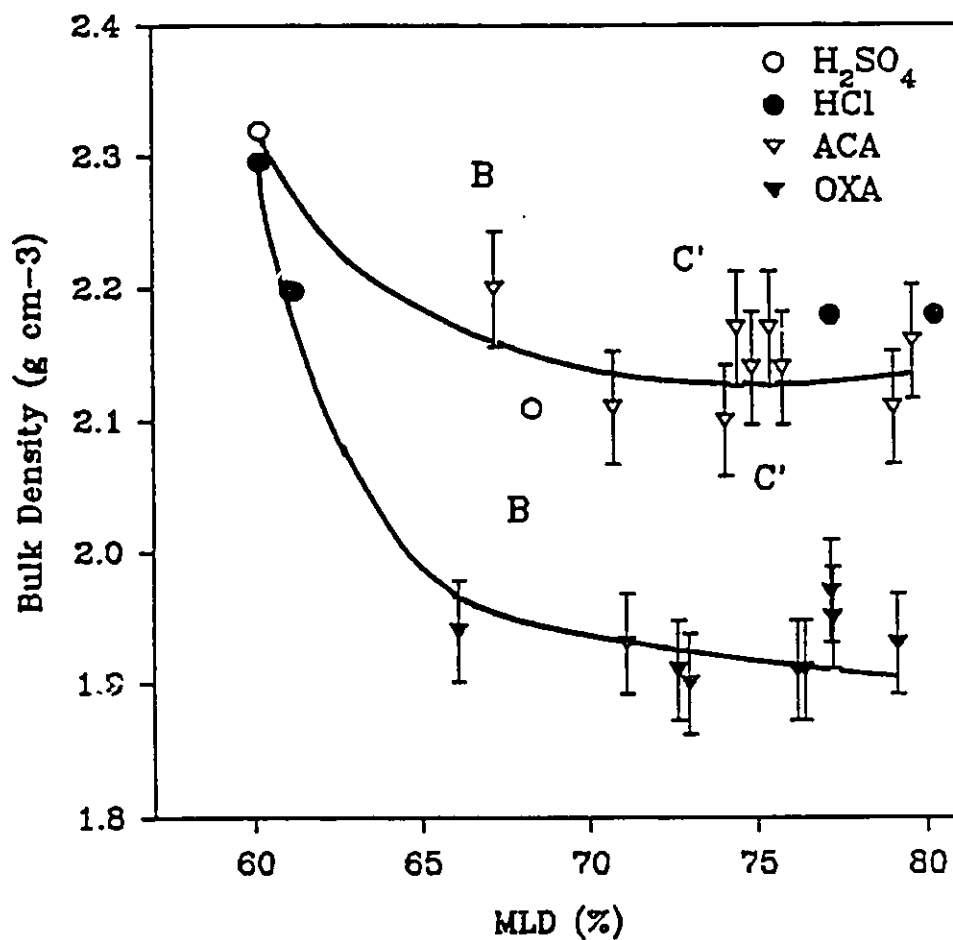
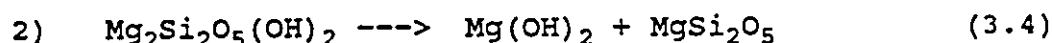
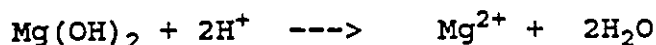
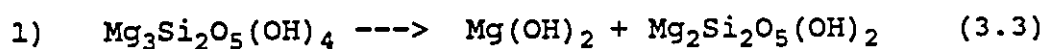


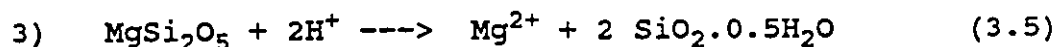
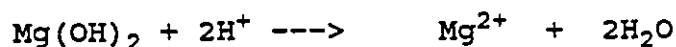
Figure 3.20 Bulk density of chrysotile versus MLD in the case of secondary leaching at 80 °C for 4 hours.

3.2.9 A proposed mechanism.

A very interesting mechanism based on the crystal structure and stoichiometry of the parent chrysotile asbestos as well as the physico-chemical properties of the resulting leached asbestos materials was proposed by Kipkemboi [11], in order to try and explain the results of leaching of chrysotile in the presence of acids. As shown below, our results corroborate this mechanism and offer additional information and propose some limitations. The mechanism proposed by Kipkemboi contains three main steps as described in the following equations:



(porous framework)



microporous

Of course, it should be clear that for steps 1 and 2, dissociation to give off $\text{Mg}(\text{OH})_2$ does not occur prior to dissolution of $\text{Mg}(\text{OH})_2$ by the acid.

This above mechanism proposes that in the presence of H^+ ions, the acid attack occurs on the outer layers of $\text{Mg}(\text{OH})_2$, which are sandwiched between the silicate sheets in chrysotile, and results in the dissolution of Mg^{2+} ions. The acid affects the brucite-type magnesium first i.e. the most vulnerable Mg atoms, which carry two hydroxyl groups and

appears as $\text{Mg}(\text{OH})_2$ molecules sandwiched between the "skeletal-type magnesium". Removal of "brucite-type magnesium" results in the following situations (fig. 3.21.a to b):

- the product obtained is $\text{Mg}_2\text{Si}_2\text{O}_5(\text{OH})_2$ as suggested by Kipkemboi [11], however, the octahedral coordination of Mg must be completed by water molecules, to give the hydrated product, $\text{Mg}_2\text{Si}_2\text{O}_5(\text{OH})_2 \cdot 4\text{H}_2\text{O}$.
- The removal of bulky Mg releases the strain that forced the sheets to bend and wind around themselves to give fibers, therefore it makes unwinding of the fibers possible, which allows acid attack on the next layer of $\text{Mg}(\text{OH})_2$ groups and so on.
- Unwinding results in a minor decrease of the volume of the unit cell, and the loss of "brucite-type magnesium" results in a net decrease of the weight of the unit cell with little change in volume. The result is a net decrease in bulk density (region B on fig. 3.13 to 3.15).
- The residual chrysotile, although more porous remains structurally unchanged despite the loss of one-third of its Mg atoms, hence only a minor decrease of the degree of crystallinity results (left hand side of fig. 3.12).

The second major step of the mechanism involves the cleavage of all the structural hydroxyl groups together with half of the "skeletal Mg" atoms which are linked to silicon via oxygen bridges (fig. 3.21.c). The remaining solid

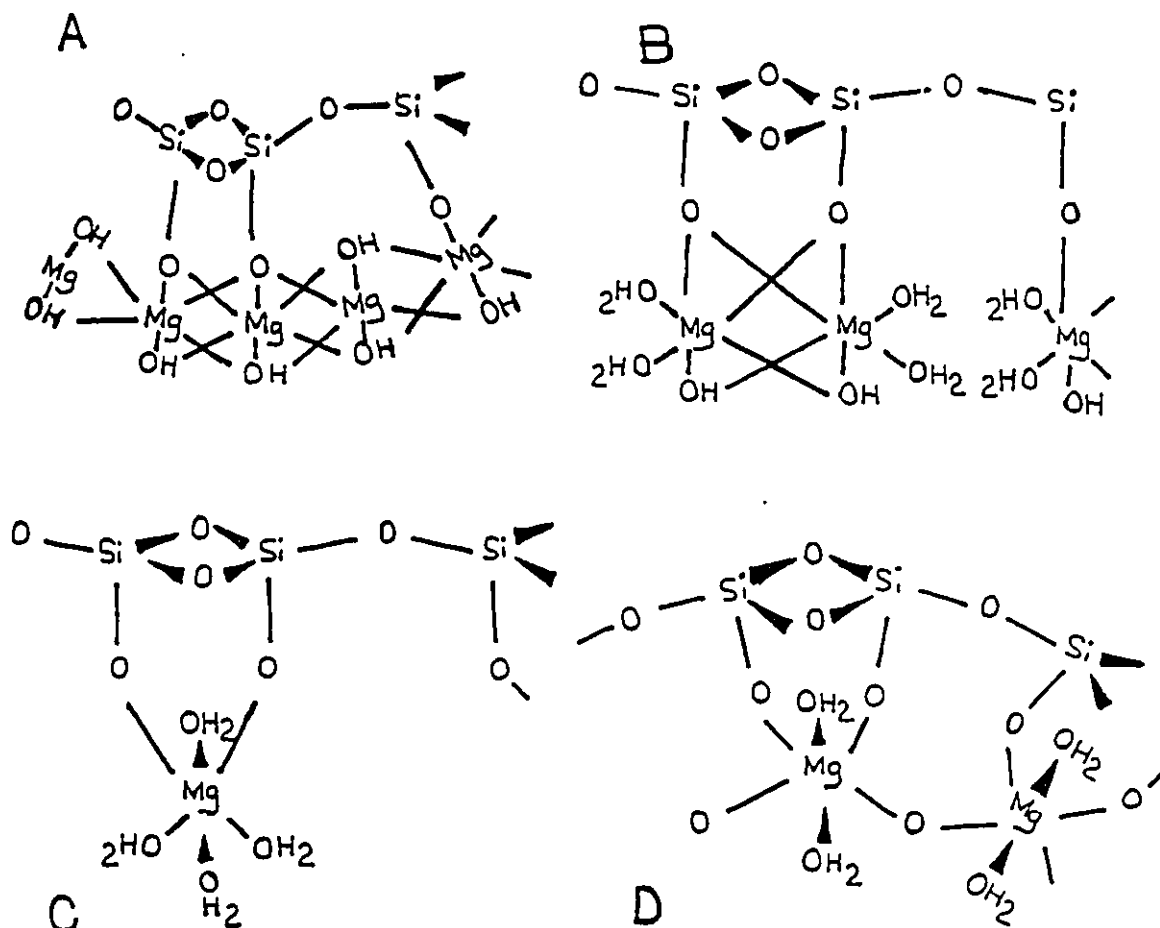


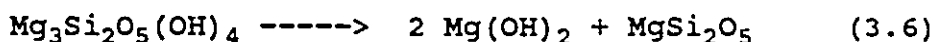
Figure 3.21 Proposed steps for acid leaching of chrysotile asbestos: (a) unleached asbestos, (b) $\text{Mg}_2\text{Si}_2\text{O}_5(\text{OH})_2 \cdot 4\text{H}_2\text{O}$ obtained after leaching of "brucite like magnesium"; (c) $\text{MgSi}_2\text{O}_5 \cdot 4\text{H}_2\text{O}$ obtained after leaching half of the "skeletal magnesium"; (d) $\text{MgSi}_2\text{O}_5 \cdot 2\text{H}_2\text{O}$ compacted form of (c) after forming Mg - O - Mg links.

appears as a very porous and siliceous residue which basically retains the fibrillar morphology of the parent chrysotile. Fig. 3.21.c shows that the remaining solid, $\text{MgSi}_2\text{O}_5 \cdot 4\text{H}_2\text{O}$, tetrahydrated after completing the magnesium coordination to six, using H_2O , is likely unstable. At this stage, one can expect a partial collapse of the asbestos structure, with breaking of the sheets to smaller pieces and bending of the sheets in the direction opposite to that of unleached asbestos (fig. 3.21.d) to form $\text{Mg} - \text{O} - \text{Mg}$ links, which would reduce the volume and therefore result in little change of bulk density (region C on fig. 3.13 to 15). The results of this reaction brings about the splitting of the fiber into fibrils and a moderate loss in the degree of crystallinity. Finally, in step 3, the dissolution of $\text{MgSi}_2\text{O}_5 \cdot 4\text{H}_2\text{O}$ requires an excess of H^+ ions; it is a very slow reaction, difficult to complete, and normally does not occur unless severe leaching conditions are used. The end product obtained when MLD is equal to 98% or larger, is a highly microporous and amorphous material. This end product is identified as being $\text{SiO}_2 \cdot 0.5\text{H}_2\text{O}$. When heated at 900°C , dehydration is complete and irreversible and SiO_2 is obtained. However, dehydration at lower temperatures i.e. at $100\text{--}200^\circ\text{C}$, although also complete, is partially reversible.

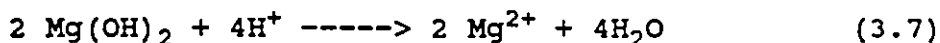
An interesting point is the comparison of the above mechanism with that proposed by Pundsack and Reimschuessel [75], who suggested that the acid attack of chrysotile takes place as follows, in two steps, following a slow dissociation

of chrysotile:

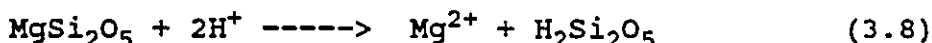
1) dissolution step:



2) step 1:



3) step 2:



Both mechanisms propose the presence of distinctive steps however, the model of Kipkemboi [11] implies the presence of an intermediate product, $\text{Mg}_2\text{Si}_2\text{O}_5 \cdot (\text{OH})_4$. None of these mechanisms has provision for overlapping between the reactions involved. Overlap between the reactional steps which was evidenced from different physical characterization techniques such as IR, ^{29}Si NMR and SEM in Kipkemboi's work [11].

The main reason for overlap between the reaction steps is due to the heterogeneous nature of the reaction, which is strongly enhanced by the shape of the crystallites. The rolled up double layers of chrysotile are made of alternating layers of SiO_4 tetrahedra, and two kinds of $\text{MgO}_2(\text{OH})_4$ octahedra. Only two thirds of these octahedra are bound to Si through the sharing of an oxygen atom ("skeletal-type Mg"), whereas one third is bound only to the two neighboring "skeletal Mg" and not to Si ("brucite-type Mg"). The outermost magnesium - containing layer situated on the outermost side of the fibril, is attacked first by the acid. On that layer, the "brucite-type" Mg is preferentially leached out

	Mole of MgO	Mole of SiO ₂	MgO/SiO ₂
Mg ₃ Si ₂ O ₅ (OH) ₄	3	2	1.50
Mg ₂ Si ₂ O ₅ (OH) ₂	2	2	1.00
MgSi ₂ O ₅	1	2	0.50
Starting material Chrysotile (7TF-12)	1.25	0.69	1.80

Table 3.14 Theoretical MgO/SiO₂ ratios based on
the proposed mechanism.

because of its stronger basicity (it is bonded to two OH^- groups) and the absence of $\text{Mg} - \text{O} - \text{Si}$ links. This starts the unfolding of the fibers, which exposes new layers of magnesium. However, of the first exposed layer, some "skeletal" Mg is most likely leached out before complete dissolution of the "brucite-type" Mg in the second layer, and so on. Following the acidic attack on the outer Mg layer, a silica layer is the next outermost part of the fibril, and it probably results in some fiber degradation leading to deposition of amorphous silica, while deeper layers are still undergoing the first step of the attack, i.e. leaching of "brucite-type magnesium".

From all the physical and chemical characterization techniques used in this work, one can agree on the complexity of the leaching reaction and the production of silicon dioxide hemihydrate as the final remaining solid material after complete leaching. The main conclusion concerning the complex reaction mechanism is the evidence of the involvement of several steps in the mechanism which are not necessarily well separated.

Table 3.14 gives the MgO/SiO_2 molar ratio for each of the intermediate products involved in the steps of the reaction mechanism we propose (equations 3.3 and 3.5). For comparison purposes, the same molar ratio has been calculated from the analytical results obtained when HCl and H_2SO_4 were used as leaching reagent and is given as a function of MLD (Table 3.15). The results of Table 3.15 are plotted on fig.

Leaching reagent	MLD values %	Mole of MgO	Mole of SiO ₂	MgO/SiO ₂
Sulfuric Acid	37.6	0.78	1.00	0.78
	36.6	0.79	1.01	0.78
	60.2	0.50	1.24	0.40
	68.3	0.39	1.32	0.30
	88.5	0.14	1.53	0.09
	96.0	0.05	1.59	0.03
	98.5	0.02	1.63	0.01
	98.6	0.02	1.63	0.01
	98.6	0.02	1.63	0.01
Hydrochloric Acid	14.0	1.07	0.80	1.34
	26.7	0.91	0.91	1.00
	55.0	0.56	1.15	0.49
	80.3	0.24	1.36	0.18
	77.2	0.28	1.38	0.20
	91.6	0.10	1.53	0.07
	94.8	0.07	1.59	0.04
	96.3	0.05	1.62	0.03
	97.2	0.04	1.62	0.02
	97.9	0.03	1.63	0.02

Table 3.15 MgO/SiO₂ ratios versus MLD in leached chrysotile based on analytical results.

3.22 (curve 1), which also gives the theoretical functions (straight lines) for leaching of pure chrysotile $\text{Mg}_3\text{Si}_2\text{O}_5(\text{OH})_4$ (line 2), pure $\text{Mg}_2\text{Si}_2\text{O}_5(\text{OH})_2$ (line 4) and pure MgSi_2O_5 (line 5). The regions A,B,C and D of figs. 3.13 - 3.15 are also shown. The first conclusion from Figure 3.22 is that there is no significant difference between the results of the two strong acids, HCl and H_2SO_4 , and that the experimental points are nicely approximated by a single curve (1) that follows none of the models (straight lines 2, 4 and 5). A closer examination shows that the experimental results (curve 1) follow a straight line from MLD of ca. 25% to 70%, and this straight line (line 3) has the same slope as the theoretical line (2) for pure chrysotile. The non linear part with a higher slope at low MLD (< 25%) is due to the dissolution of the basic impurities (free brucite and pyroaurite); this also shifts the line 3 below its theoretical location (line 2). Curving at high MLD (> 70%), gives another quasi-linear part which follows perfectly the theoretical line 4 for $\text{Mg}_2\text{Si}_2\text{O}_5(\text{OH})_2$. No evidence of line 5 is found, however, this would occur at very high MLD (region D of fig. 3.13 - 15), i.e. > 90%, and would span too narrow a range of MLD in a region where the four lines converge, to give a clear picture.

Fig. 3.22 confirms our previous conclusions based on a variety of physico-chemical measurements:

- 1) Leaching of chrysotile asbestos is a multistep procedure including:

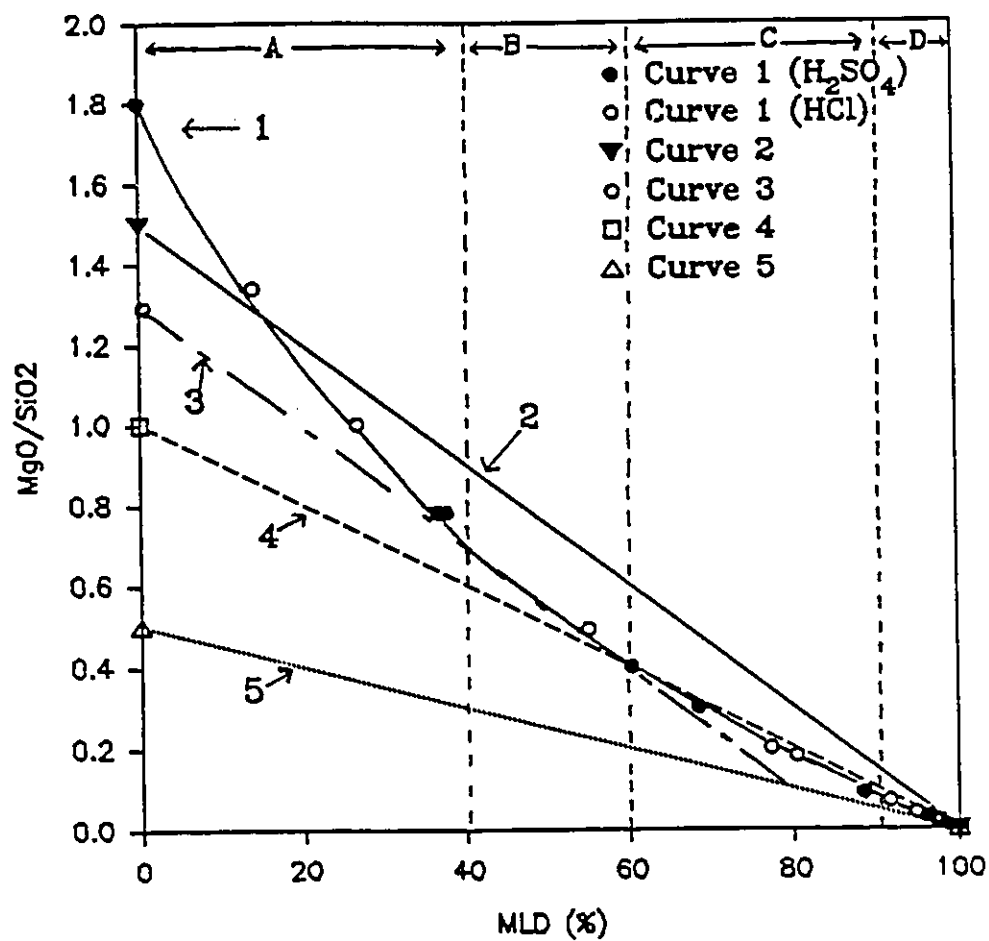
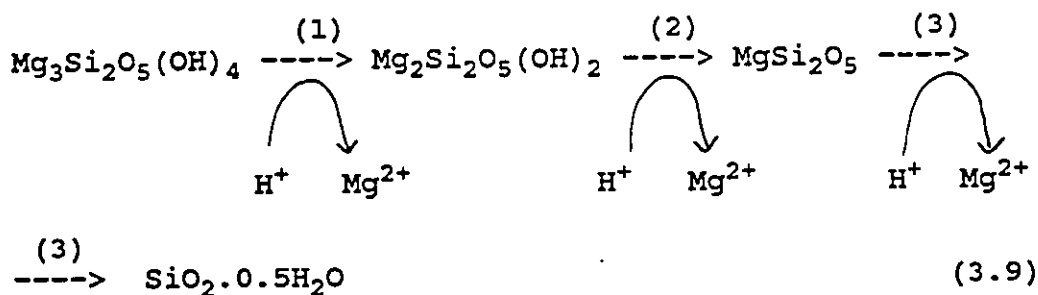


Figure 3.22 Interpretation of the ratio MgO/SiO_2 during leaching of chrysotile with strong acids.

- quick dissolution of basic impurities (brucite and pyroaurite);
 - acid leaching of chrysotile $\text{Mg}_3\text{Si}_2\text{O}_5(\text{OH})_2$ starts with the preferential dissolution of the most labile "brucite-type magnesium", to give $\text{Mg}_2\text{Si}_2\text{O}_5(\text{OH})_2$, which is probably hydrated; in this first step of leaching, the asbestos fibers start unfolding, however, the basic structure remains the same;
 - removal of "skeletal-type magnesium: this causes a structural collapse with the fibers breaking down to smaller pieces, giving amorphous silica hemihydrate $\text{SiO}_2 \cdot 0.5\text{H}_2\text{O}$ as the final solid product. We could not confirm or refute unambiguously the involvement of MgSi_2O_5 in an intermediate step.
- 2) The above multistep mechanism is probably quite realistic at the level of one double layer (OH - Mg layer and O - Si - O layer), however, the overall mechanism should include the diffusion of the acid to inner layers, which become exposed as the outer layers undergo the first step and unfold. X-ray diffraction shows that no other crystalline species, such as $\text{Mg}_2\text{Si}_2\text{O}_5(\text{OH})_2$ or MgSi_2O_5 , are formed as intermediate crystalline phases. Therefore, if such phases are indeed formed, they must be amorphous or microcrystalline. However, all our results clearly indicate that the leaching reaction [equations (3.3), (3.4), (3.5)] is

valid only locally on a part of Mg silicate sheet.



In any case, it cannot describe the overall reaction process in a model of a homogeneous reaction with well separated steps. Because of the particular structure of the chrysotile fibers, the reaction is highly heterogeneous. It is probably already finished at the outer layers before it has started in the most inner layers. the physical characteristics of the Alix products reflect this complexity due to the overlap between the reaction steps. In the initial stages of leaching, after the quick dissolution of the basic impurities, step 1 is predominant. As the reaction proceeds, the importance of step 2 and later step 3 (if it really occurs) increases and that of step 1 decreases. In the later stages, step 1 has been completed and only step 2 and/or step 3 is/are important.

The mechanism we have proposed above, i.e. multistep reaction with strong overlapping between the steps, especially for mid-values of MLD, explains the complex behavior of most of our physical measurements, which cannot be explained based on a simple model of well separated reaction steps. Our model is in perfect agreement with the special structure and texture of chrysotile.

3.3 ZEOLITE SYNTHESSES

3.3.1 General information

Zeolites are usually synthesized from a reactive gel which can be defined as a hydrous metal aluminosilicate prepared from either aqueous solutions, reactive solids, colloidal sols, or reactive aluminosilicates. For example, silica gel, which was widely used in this work as a source of silica, is classified as a colloidal system.

Crystallization from aluminosilicate gels can be discussed in terms of the free energy relations [76]. The initial reaction mixture is made of components which, in a first step, form a metastable phase "a", which may convert to the thermodynamically more stable products "b" or "c" after enough time. In the temperature region where a or b can both form, both the nucleation and growth rates are important; the metastable phase a, which forms preferentially, may be transformed to the more stable b and subsequently to c.

The free energy relations shown on Figure 3.23 are derived directly from the "simplicity principle" of Goldsmith, which relates the ease of crystallization to "disorder, structural simplicity or high entropy" [76-78]. Since the nucleus of the disordered structure should be smaller than the corresponding nucleus of the ordered structure which would require the need of a large number of atoms, the structurally disordered form, the metastable phase a, is more likely to attain the critical size necessary for growth than is the nucleus of the ordered form, b or c.

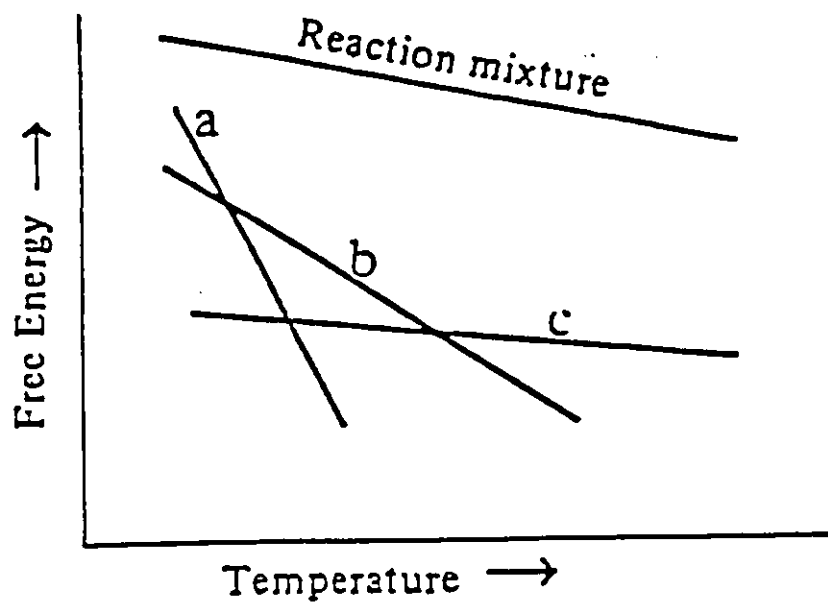


Figure 3.23 Schematic free energy relations between reaction mixtures and various zeolite phases, represented by a, b, c. [76]

There are four general conditions for the synthesis of zeolites:

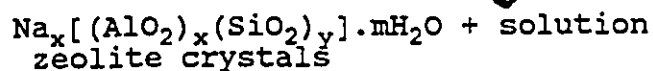
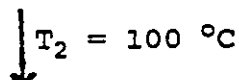
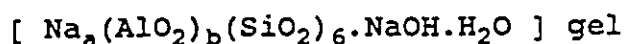
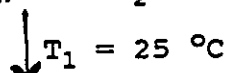
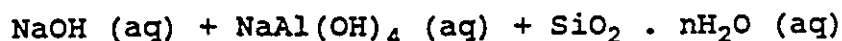
1. the use of reactive starting materials such as freshly coprecipitated gels, or amorphous solids;
2. relatively high pH introduced in the form of a strongly basic alkali metal hydroxide such as NaOH;
3. low temperature hydrothermal conditions i.e. lower than 200 °C [79,80] with concurrent low autogeneous pressure at saturated water vapor pressure;
4. a high degree of supersaturation of the components of the gel leading to the nucleation of a large number of crystals.

When the source of silica (silica gel or Alix material which are amorphous solids) are mixed with a source of alumina such as sodium aluminate, in a relatively strong alkaline medium, an aluminosilicate gel is formed. Then, these aluminosilicate gels are crystallized in a closed hydrothermal system at temperatures varying generally from room temperature to about 175 °C. In some cases, higher temperatures, up to 300 °C, are used. The pressure is generally the autogeneous pressure approximately equivalent to the saturated vapor pressure of water at the designated temperature. The reaction time for crystallization can vary from a few hours to several days and is mainly dependent on temperature and/or the type of zeolite being synthesized.

The type of zeolites synthesized in this work were Na-X, Na-Y and mostly Na-A zeolites. This was done in a

hydrothermal reactor (section 2.2) operated at 100 °C, which corresponds to the boiling point of water at 1 atmosphere pressure. In addition, the synthesis of zeolites in that temperature range usually produces crystals in the size range of 0.1 - 10 μm , which are the most suitable for applications as catalysts, sorbents and ion exchangers [80].

The preparation and crystallization of the gel can be represented schematically as follows, using the $\text{Na}_2\text{O} - \text{Al}_2\text{O}_3 - \text{SiO}_2 - \text{H}_2\text{O}$ system:



In this work, all zeolites synthesized by using Alix materials as the source of silica, are designated as chryso-zeolites.

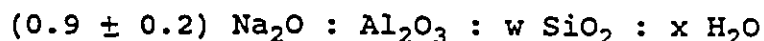
The X-ray diffraction technique was used for identification of the crystalline phases. Appendix 6 gives the list of Bragg peaks from literature for the zeolites Na-Y, Na-X, Na-A, Pt and HS. Zeolites P_t and HS were found as impurities in some of our preparations and their X-ray powder diffraction was required for phase identification of the zeolites.

From the usual sources of silica and alumina [41,82], sodium aluminate and silica gel were used in this work.

3.3.2 Na-Y chrysozeolites

Silica gel was used as the source of silica and sodium aluminate as the source of alumina. The reaction temperature was kept constant at 100 °C, since the optimum temperature range for the production of zeolite Y is between 80 and 125 °C [42]. The choice of the reactant mole ratios was determined from the literature, which gives some preferred compositions when silica gel is used as a silica source for zeolite Y synthesis [42]. The applied reaction time was 72 hours, and the other experimental parameters are summarized in Table 3.16.

The chemical formula of zeolite Na-Y can be normally expressed as follows in terms of mole of oxides:



where w is a value larger than 3 and up to 6, and x may take values up to about 9.

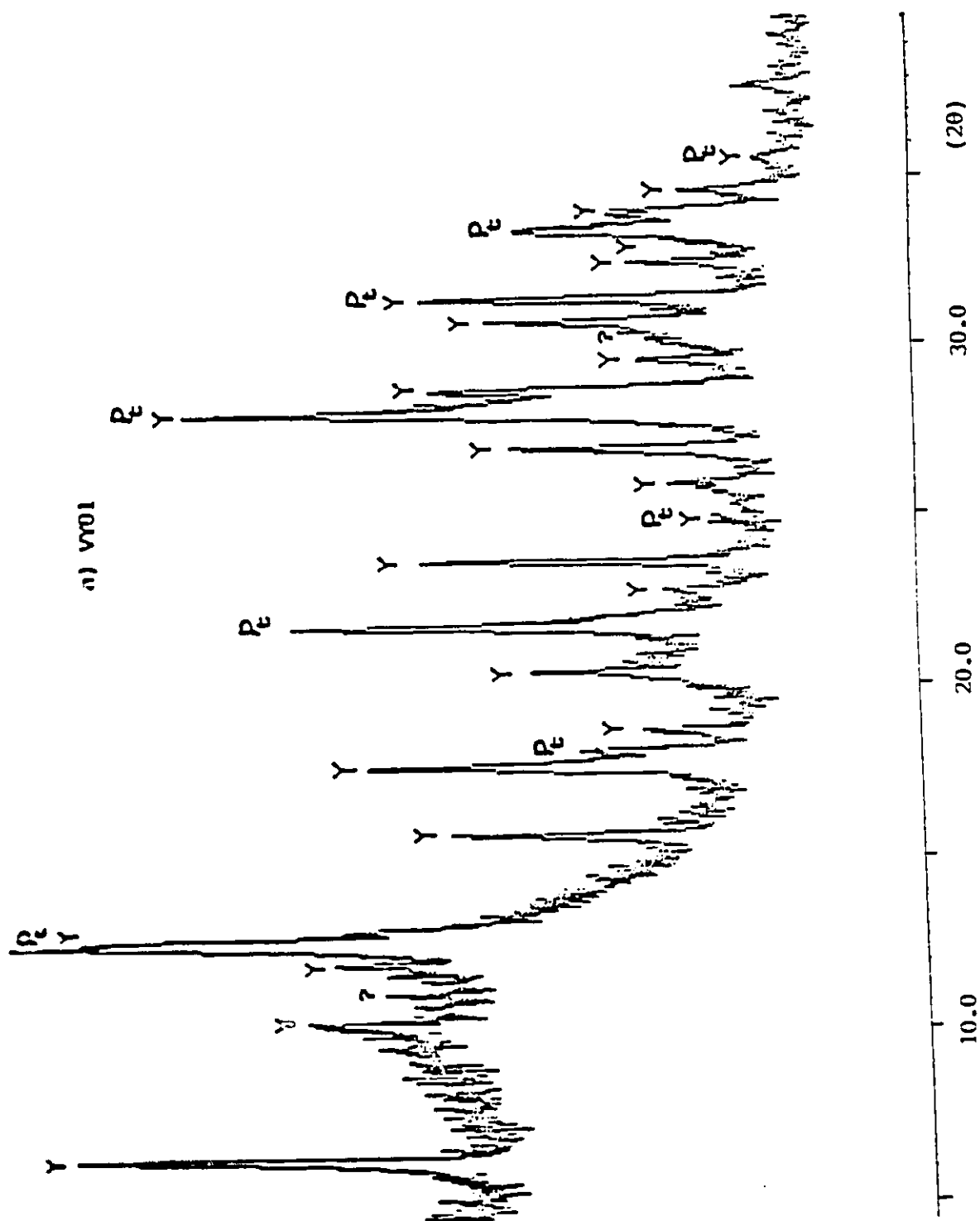
All attempts to synthesize zeolite Na-Y resulted in mixtures of phases, making it meaningless to carry out elemental analysis.

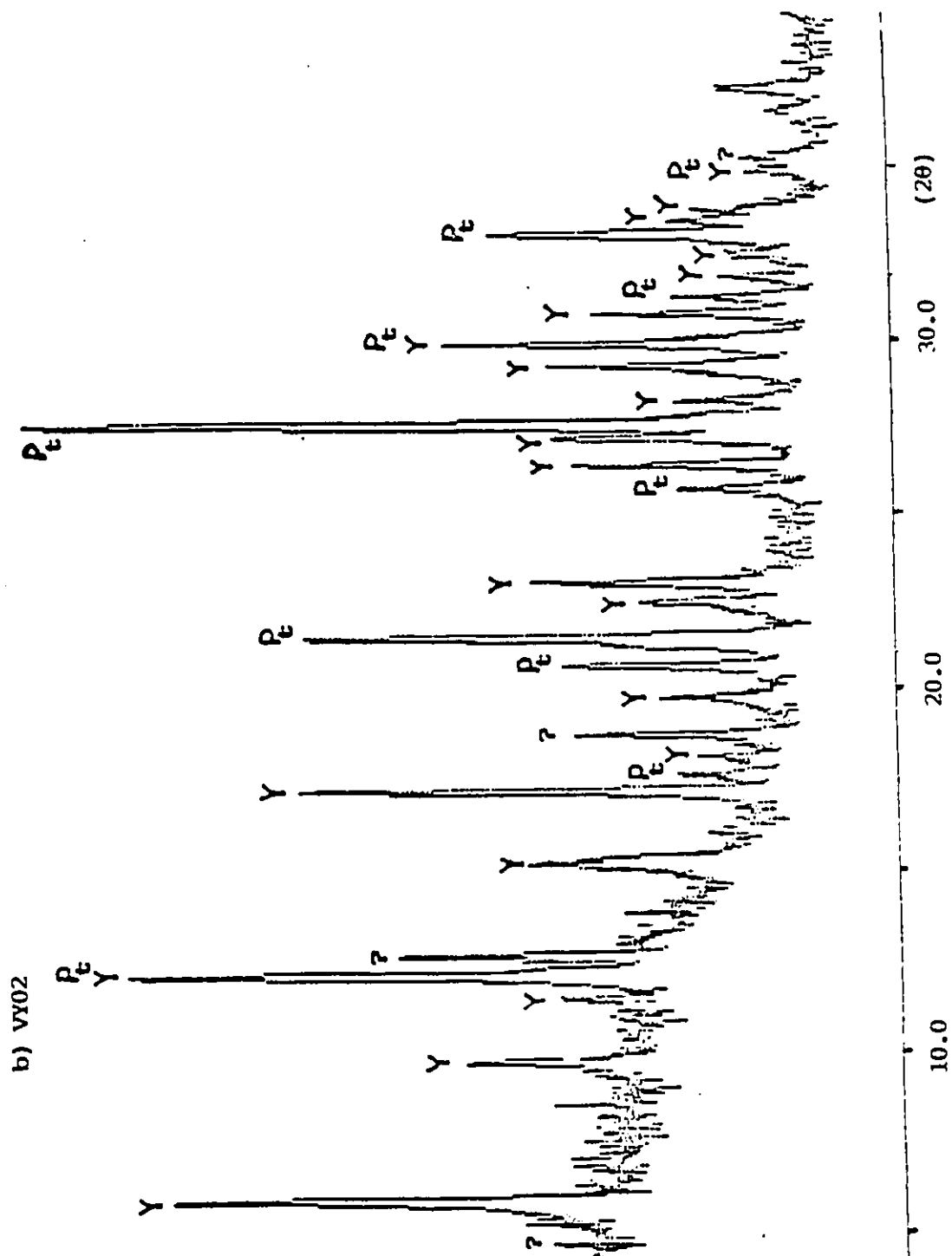
X-Ray powder diffraction was very useful for identifying the different constituents in the mixture of phases that were obtained. Phase identification was made by comparing the observed diffraction patterns with the literature for zeolites Na-P_t and Na-Y (Appendix 6 and Figure 3.24) [83-85]. In each diffraction pattern, zeolite P_t (tetragonal form of zeolite P) was identified by its Bragg peaks as an impurity present in significant amounts, whereas the others could not

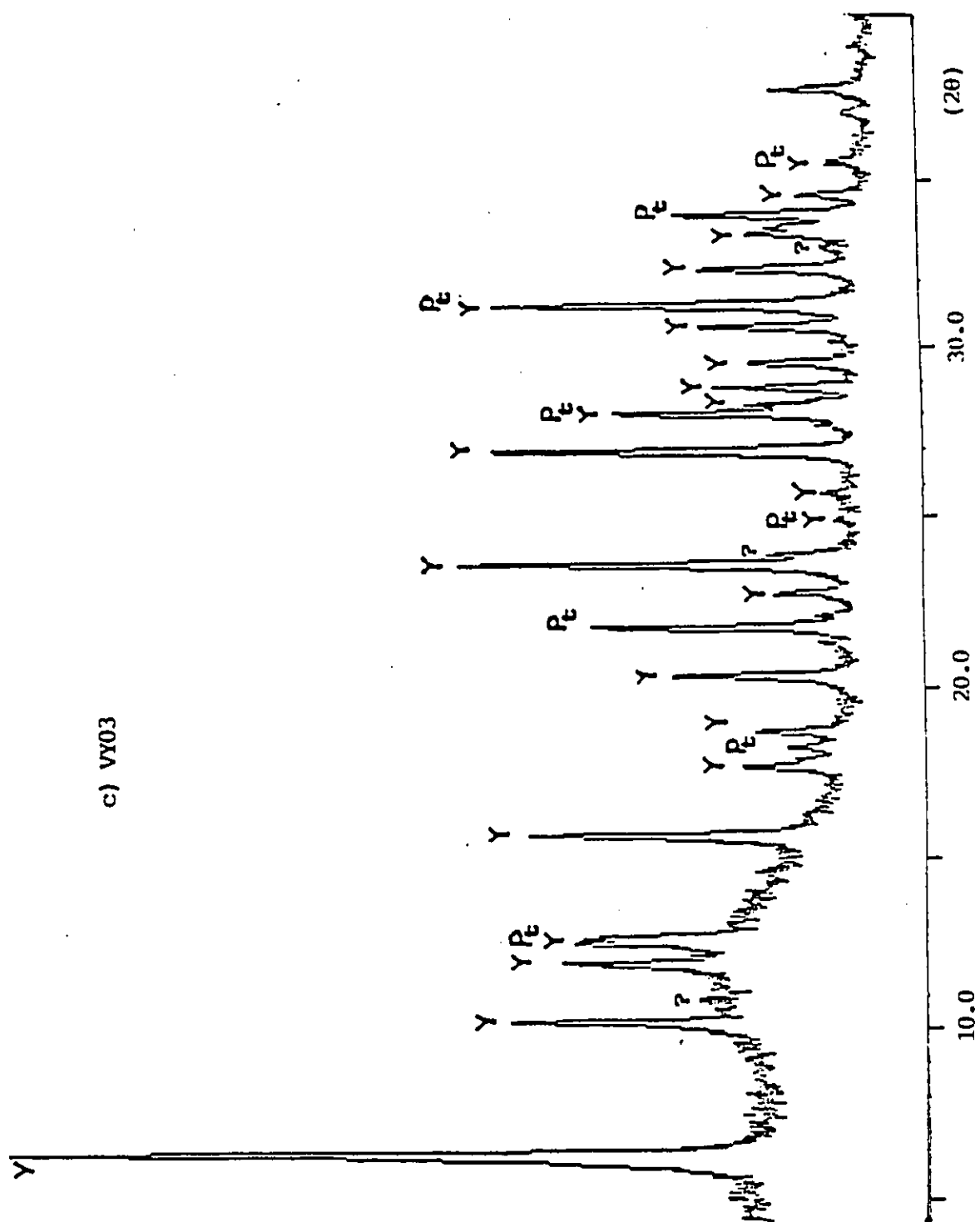
Sample #	Aging Time (Hours)	Gel Composition (mole ratios)		
		SiO ₂ /Al ₂ O ₃	Na ₂ O/SiO ₂	H ₂ O/Na ₂ O
VY01	0	15	0.8	50
VY02	0	15	1.6	35
VY03	24	15	1.6	35

Table 3.16 Experimental parameters for zeolite Na-Y syntheses. The reaction time was 72 hours, the reaction temperature was 100 °C, and the source of silica was silica gel. An aging time of the reaction mixture for 24 hours at room temperature prior to heating was used for VY03 sample.

Figure 3.24 X-ray powder diffraction patterns of the synthesized Na-Y zeolites: a) VY01 , b) VY02 , c) VY03.







be identified. The presence of the tetragonal form of zeolite P is in agreement with the free energy curve (Figure 3.23) [31,76,78,86,87]: in our experimental conditions, zeolite Na-Y corresponds to phase a, zeolite P to phase b and analcime (another type of zeolite) to phase c. In the experimental conditions favorable for the formation of zeolite Na-Y, the free energy curves for b and c should intercept at about 175 °C and for a and b, at about 100 °C, which corresponds to our reaction temperature. At that experimental temperature, zeolite P_t is thermodynamically more stable than zeolite Na-Y.

Silica gel was the only source of silica used for the synthesis of zeolite Y. For the same concentration of reactants, and same reaction temperature, a different zeolitic phase distribution may have been expected with the use of other sources of silica, since, according to literature [32,33,41], the type of reactant silica seems to control which species nucleate.

In the literature, the difficulty to synthesize pure zeolite has been mentioned for Na-Y [42]. The failure in obtaining zeolite Na-Y as a pure phase indicates the need for considerable refinement of the experimental parameters such as:

- 1) the gel composition, expressed in molar ratios
- 2) the aging time
- 3) the reaction temperature
- 4) the reaction time

5) mixing of the reaction mixture

Gel composition.

The gel composition depends on the composition of the reaction mixture and controls the type of zeolite synthesized. The starting compositions are usually expressed as NaO/SiO_2 , $\text{SiO}_2/\text{Al}_2\text{O}_3$, and $\text{H}_2\text{O}/\text{Na}_2\text{O}$ mol ratios [42,81]. Variations of these ratios, while keeping the other experimental parameters constant, would lead to changes in the products obtained, which would be identified by XRD, if crystalline. Some reactant compositions may also favor formation of amorphous materials, which could not be detected by XRD diffraction, due to their lack of crystallinity.

Aging or room temperature digestion.

An important step in the synthetic procedure of zeolite Y is the digestion of the reaction mixtures at ambient temperature prior to heating, this is also referred to as aging. The importance of aging for controlling the purity and/or composition of zeolites has already been reported [30,42]. In fact, aging seems to result in a purer zeolite Y, with a higher silica-to-alumina molar ratio.

At room temperature, the digestion period for reaction mixtures should be a minimum of 16 hours, and preferably 24 to 32 hours [42]. Room temperature aging longer than 40 hours might be undesirable, especially for commercial production scale preparations.

The effect of aging can be seen by comparing samples

VY02 and VY03, the only difference in their experimental parameters being the room temperature digestion of 24 hours performed for VY03 (Table 3.16 and fig. 3.24.b and c).

Zeolites Y and P_t can be identified by their XRD patterns, however, a net decrease in the relative intensity of the peaks for zeolite P_t , compared to the desired zeolite Y, is observed after room temperature digestion was performed (VY03). This observation is in agreement with the literature [30,42].

Reaction time.

It is reported that if crystallization also called "elevated temperature digestion" is too short, amorphous aluminosilicates may be formed, whereas prolonged periods usually result in a decrease in $\text{SiO}_2/\text{Al}_2\text{O}_3$ content of zeolite Y, and affect the conversion of the sodium zeolite Y to other types of zeolites, which are thermodynamically favored. [42]

Reaction temperature.

Crystallization can be carried out by maintaining the reaction mixture in a temperature range of about 20 to 125 °C, until the crystalline product is obtained. The preferred range is 80 to 125 °C.

At lower temperatures, crystallization times are somewhat longer than is usually considered desirable in commercial practice. Zeolite Y prepared at these lower temperatures contains particles which are smaller than those

prepared at higher temperatures.

Mixing of reaction mixture

All other impurity phases present in VY01, VY02 and VY03, other than zeolite P_t , are mainly due to improper mixing of the reaction mixture during crystallization. Our experimental set-up only allowed mixing by convection, which represented a high risk for producing heterogeneous mixtures.

3.3.3

Na-X Chrysozeolites

Crystalline zeolite Na-X was produced from two different sources of silica i.e. silica gel and Alix materials. The only source of alumina used was sodium aluminate.

The experimental conditions were a reaction time of 72 hours and a reaction temperature of 100 °C.

The basic formula for zeolite X may be expressed as follows in terms of mole of oxides:



where w is about within the range of 2.0 to 3.0 and x may take any value up to 6, when sodium type zeolite is considered [44].

Table 3.17 gives the reaction mixture compositions and the sources of silica for the different syntheses of zeolites Na-X. With silica gel, the only variable parameter was the gel composition; three different gel compositions were used, based on the preferred composition ranges reported in literature [44].

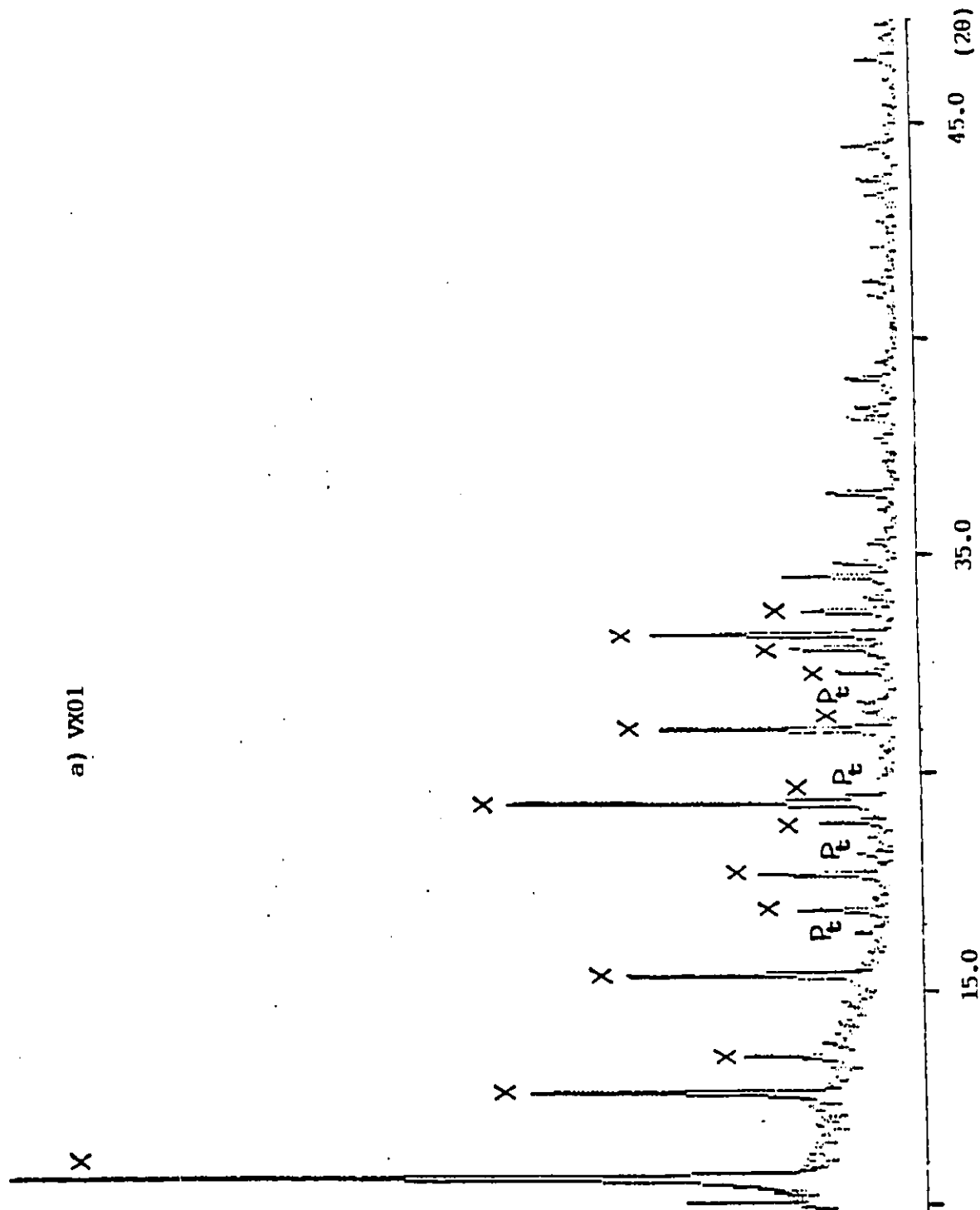
The successful synthesis of zeolite Na-X, was established by X-ray powder diffraction. Other phases present as impurities could also be detected and, in some cases, identified.

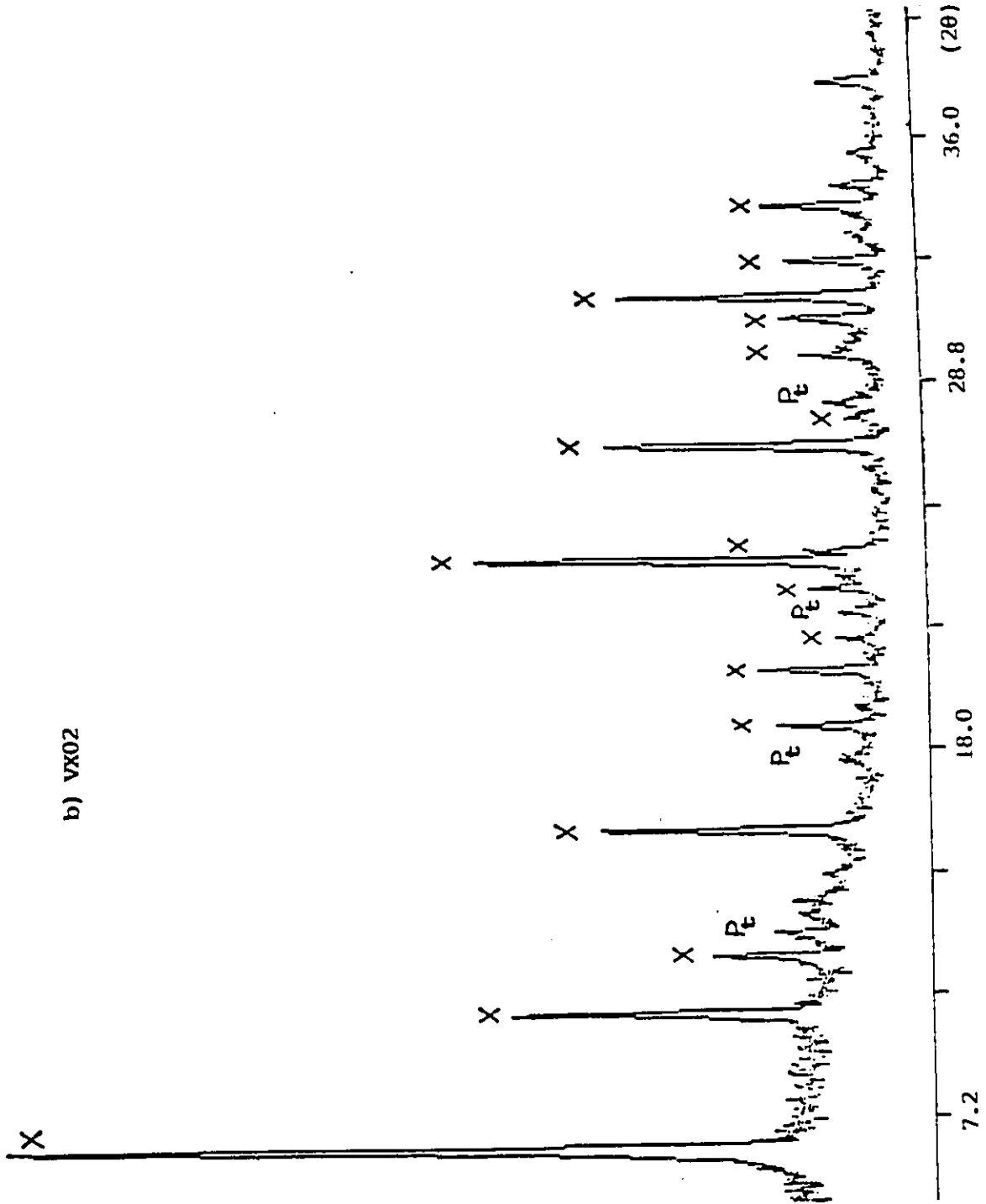
The gel composition used for VX01 sample was the most suitable choice when compared to the others (VX02 and VX03), as shown on Figure 3.25. Its X-ray powder diffraction pattern revealed the presence of zeolite Na-X as the major component and of zeolite P_t as an impurity. All samples

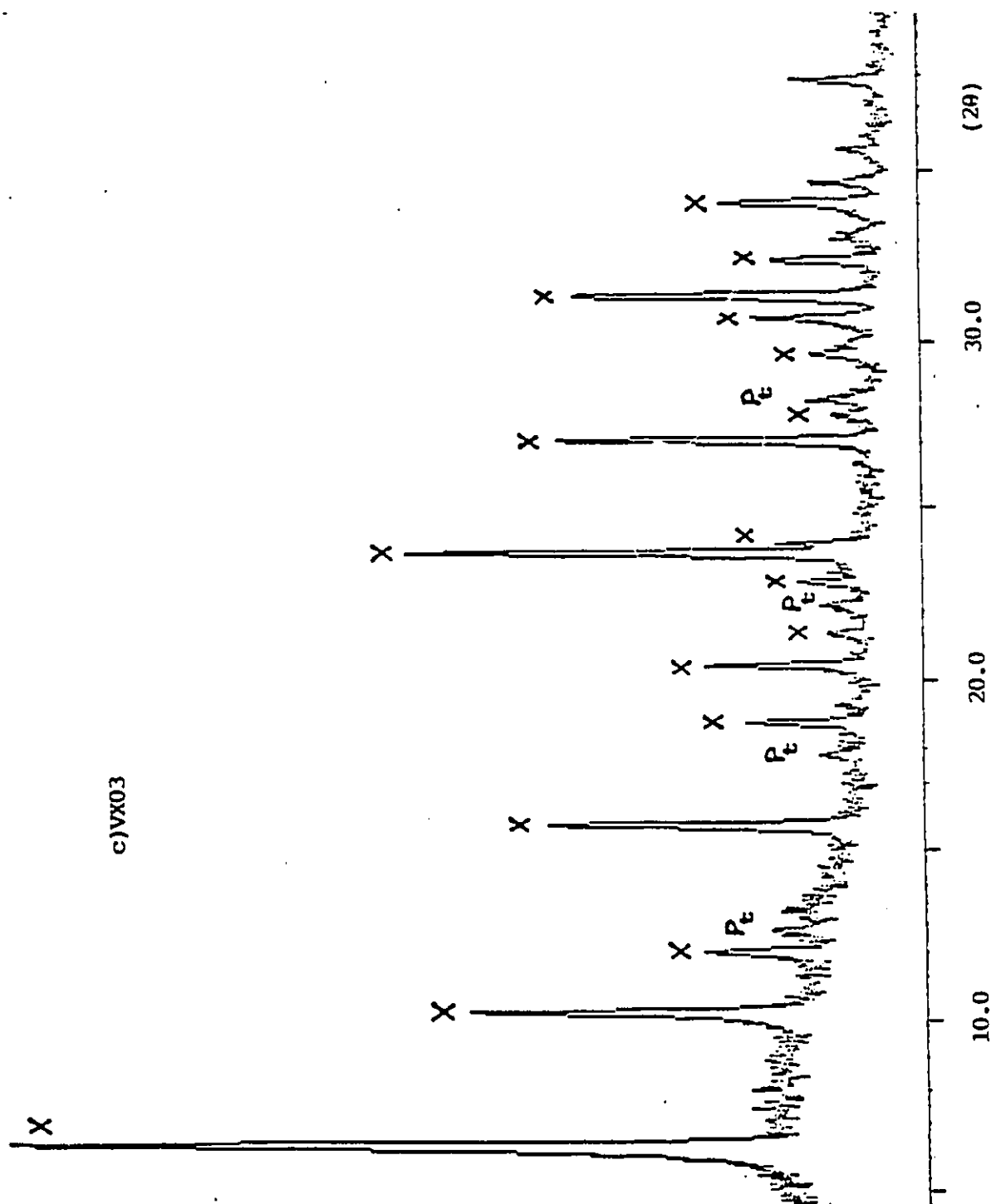
Sample #	MLD (%)	Source of silica	Gel Composition(mole ratios)		
			SiO ₂ /Al ₂ O ₃	Na ₂ O/SiO ₂	H ₂ O/Na ₂ O
VX01	--	gel	4.8	0.9	47.4
VX02	--	gel	4.9	0.8	51.1
VX03	--	gel	4.8	1.0	44.1
VAX01	98.7	Alix 167	4.8	0.9	47.4
VAX02	84.2	Alix 071	4.8	0.9	47.4

Table 3.17 Experimental parameters used for zeolite Na-X syntheses. The reaction time used was 72 hours and temperature was 100 °C for all reactions. Two sources of silica were used (silica gel and Alix materials).

Figure 3.25 X-ray diffraction pattern of the Na-X Zeolites : a) VX01 , b) VX02 , c) VX03.



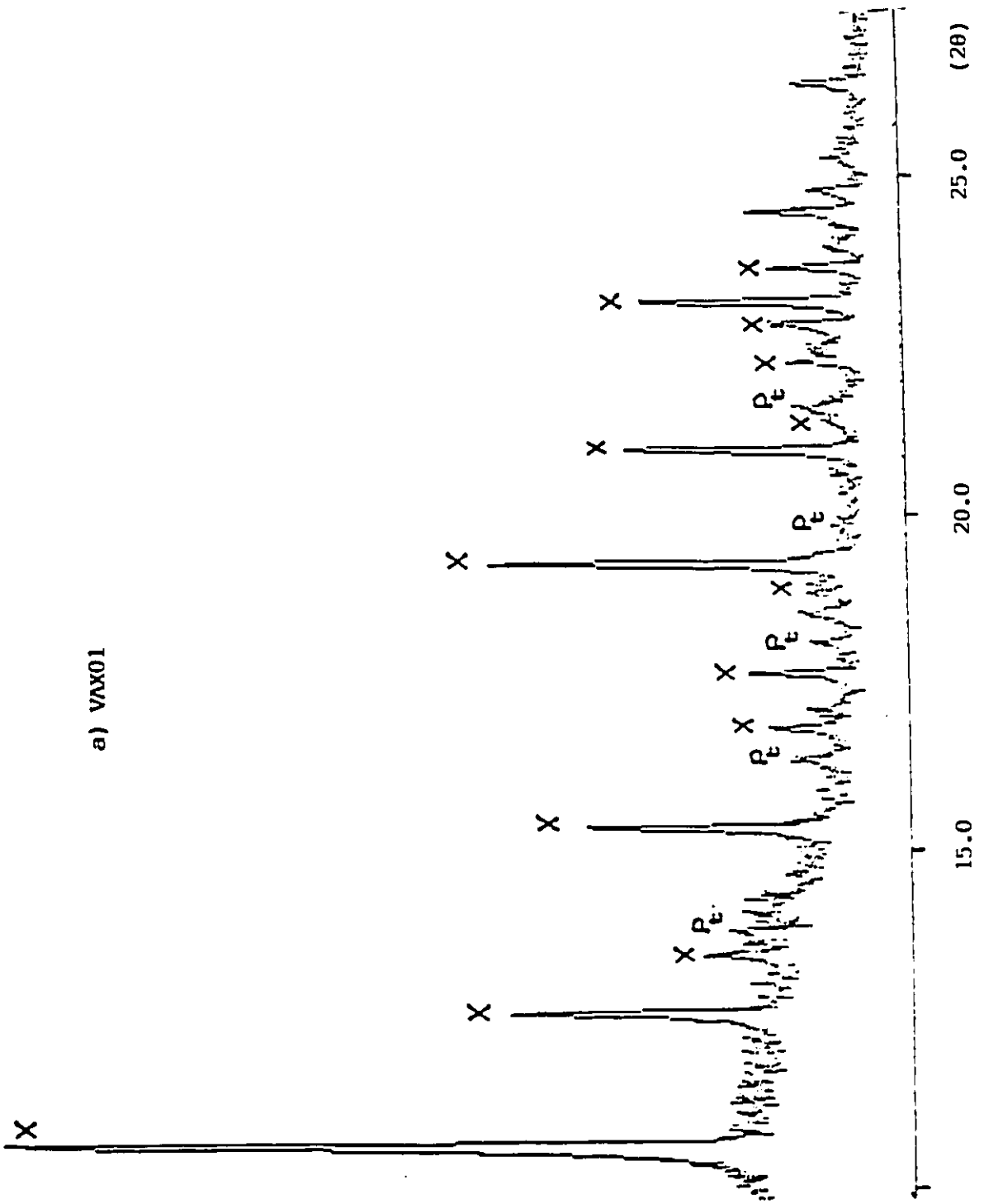




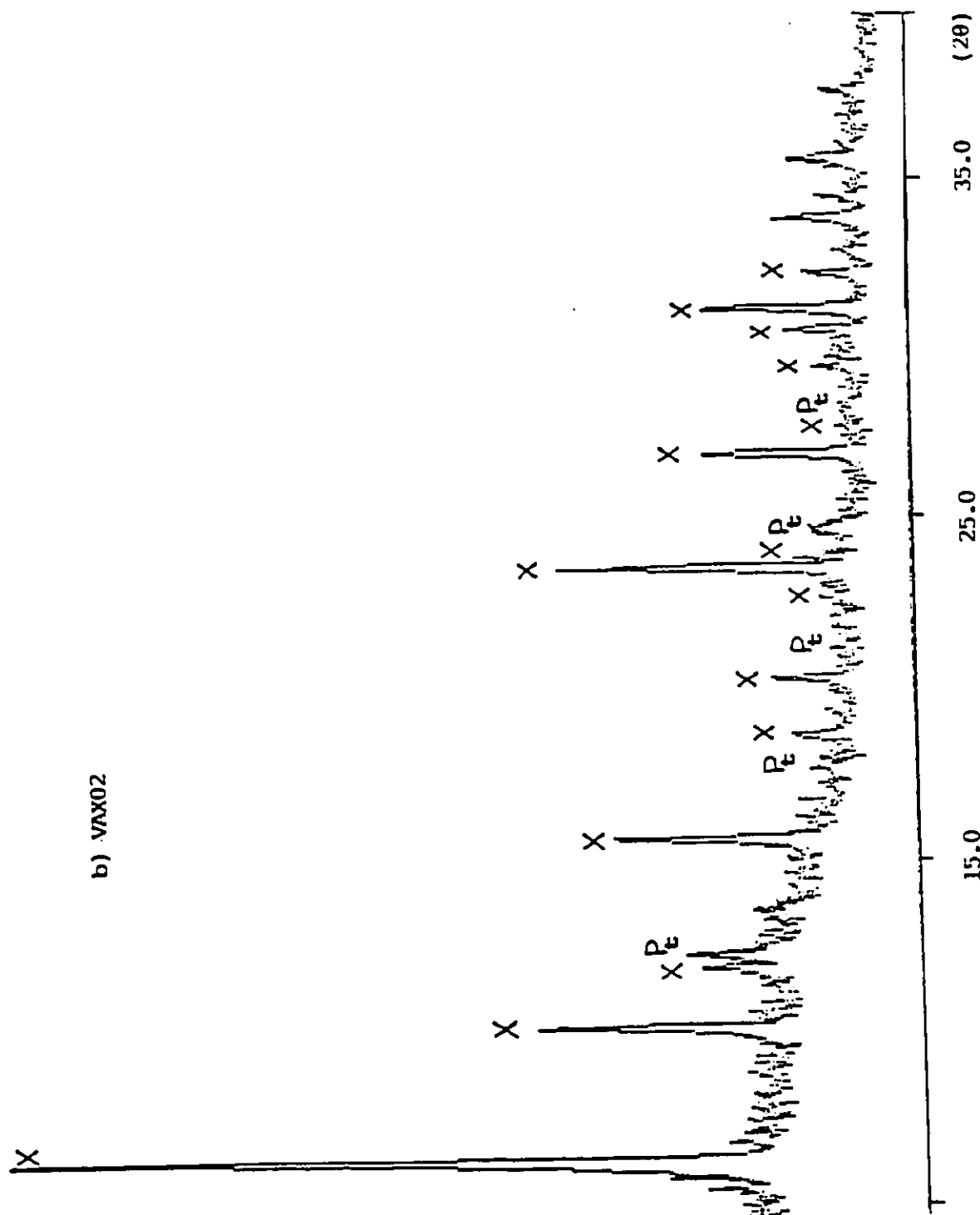
(VX01,VX02 and VX03) show the presence of at least another crystalline impurity which could not be unidentified.

Another set of experiments, (VAX01 and VAX02) was performed using Alix materials as the source of silica, and the same gel composition as in sample VX01 (Table 3.17). The results obtained for VAX01 and VAX02 (Figure 3.26) are similar to those prepared from silica gel. The X-ray diffraction patterns show that variations of the MLD values do not seem to affect the final product since similar mixtures of crystalline phases were formed for the two samples. Zeolite Na-X is the major crystalline phase, and zeolite P_t is found as the major impurity. In addition to zeolite P_t , at least one additional unidentified crystalline phase is also detected, which also appear in samples VX01, VX02 and VX03.

Figure 1.26 X-ray powder diffraction patterns of the synthesized Na-X chrysoccolites: a) VAX01 b) VAX02.

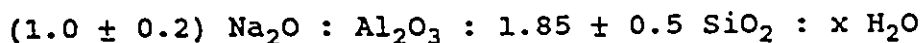


a) VAX01



3.3.4 Na-A Chrysozeolites

The formula for zeolite Na-A may be expressed as follows in terms of mole of oxides:



In this formula, x may take any value up to 5.1 for a sodium type of zeolite A [43].

All syntheses were carried out at 100 °C for 72 hours. As shown on Table 3.18, the only experimental variables were the source of silica and the gel composition.

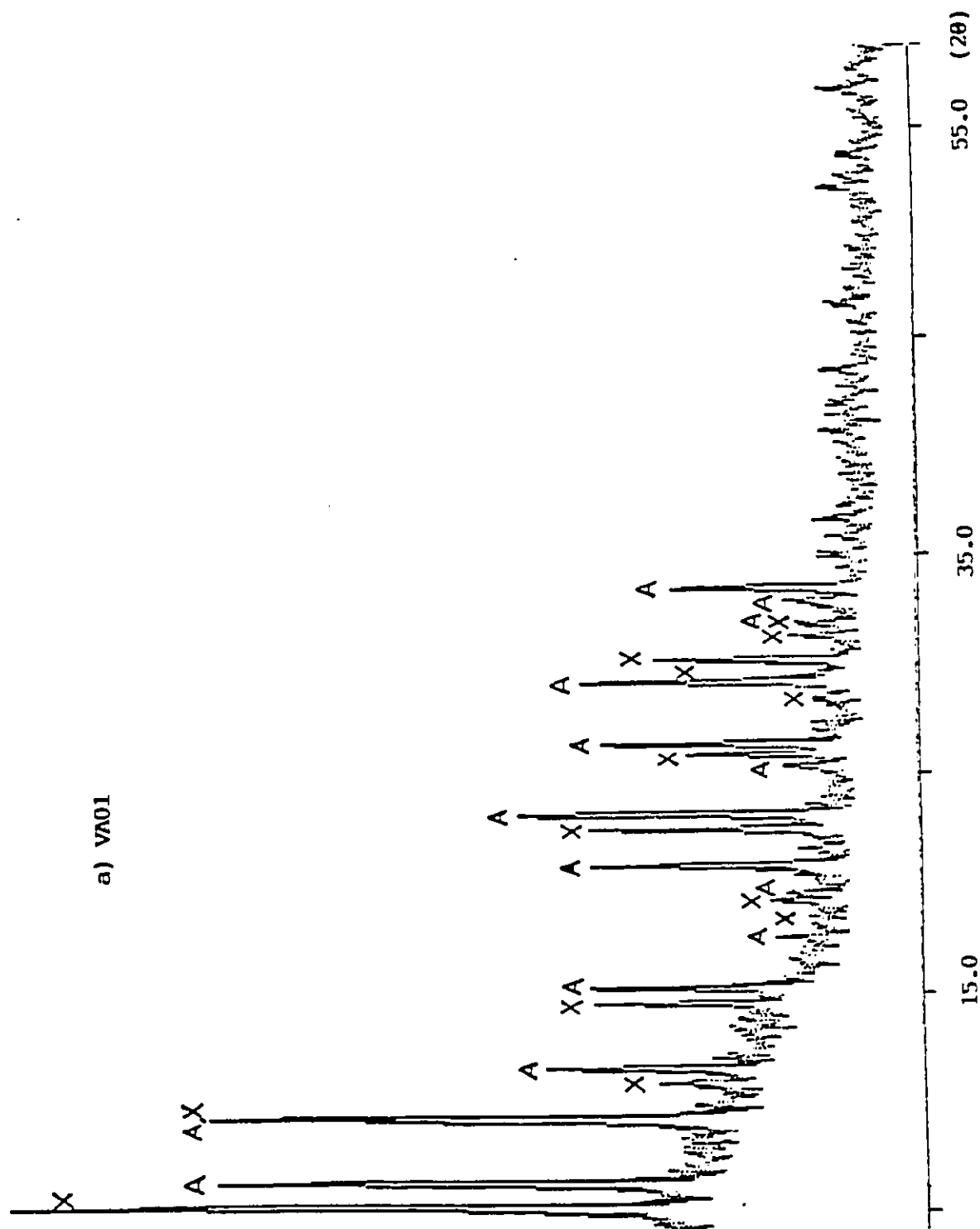
VA01 was synthesized by using silica gel as the source of silica. Its high silica to alumina ratio of 1.9 and its low concentration in alkali ($\text{Na}_2\text{O}/\text{SiO}_2 = 0.7$) seem to favor the formation of zeolite Na-X instead of zeolite Na-A (fig. 3.27.a). In order to avoid this, the alkali to silica ratio was raised to 1.2 and the silica to alumina ratio was reduced to 1.9 and 1.5 as shown on Table 3.18 for VA02, VA05, and VA06. This modification was based on some reported ranges of gel composition [43]. By raising the alkali content and by reducing the silica to alumina ratio, zeolite Na-X was no longer formed as shown on Figure 3.27.b, d, and e, and zeolite Na-A was found to be the major crystalline phase. However, crystalline by-products could be detected, several Bragg peaks could not be attributed to zeolite Na-A. Among these impurities, zeolite HS and at least another unidentified crystalline phase were found in the samples.

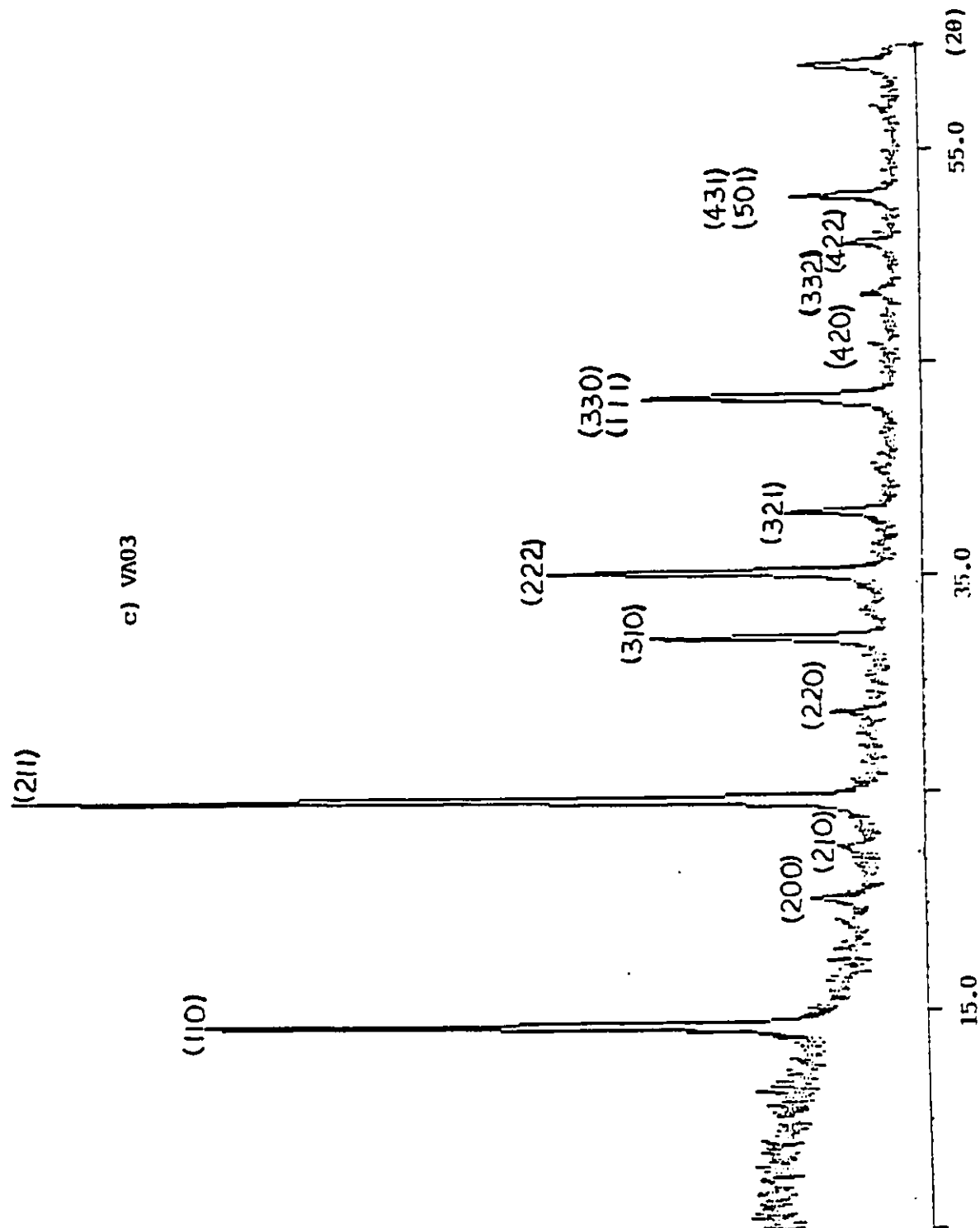
For VA03 and VA02, the same gel composition was used, the only difference between the two samples being that VA03

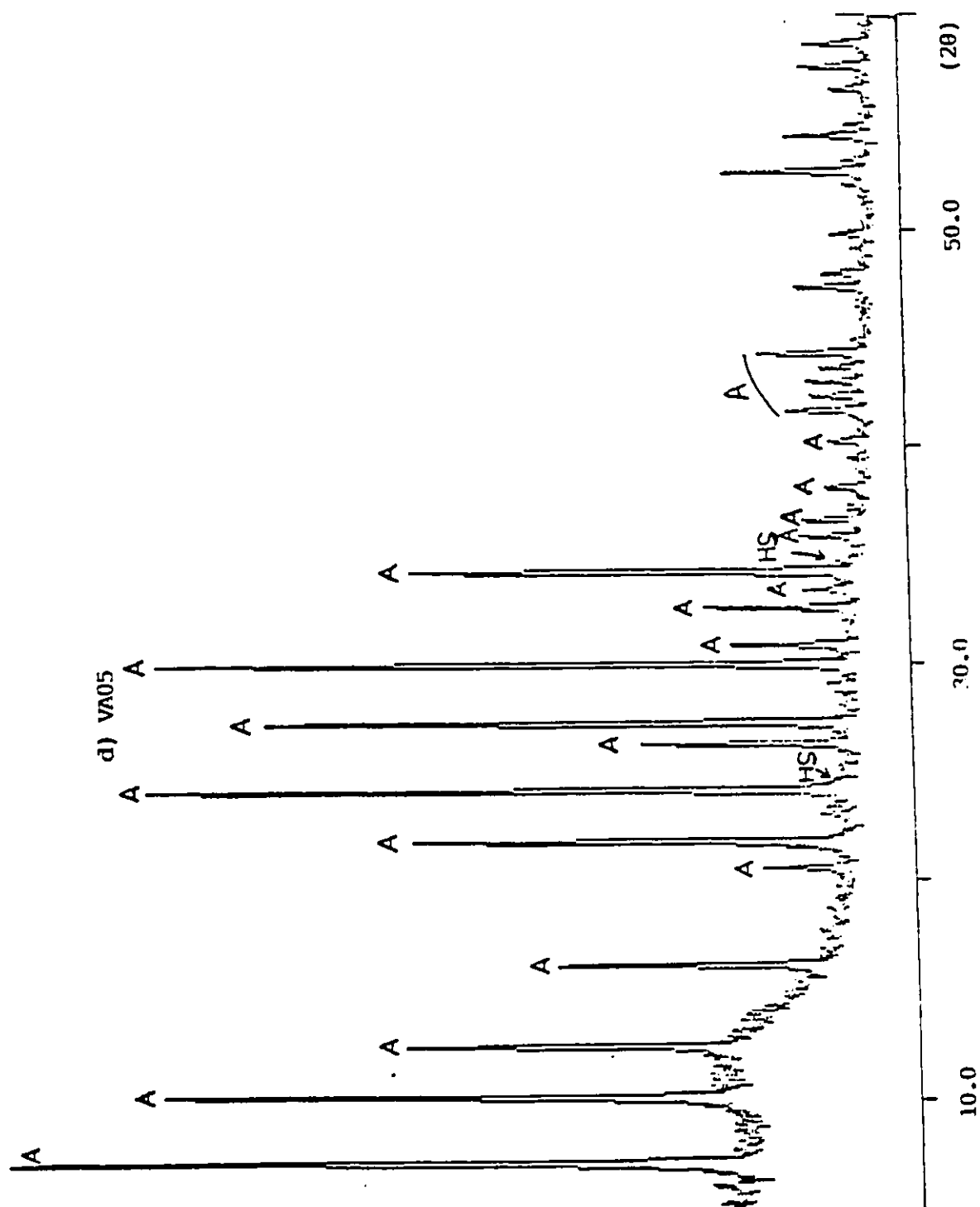
Sample #	Source of silica	MLD (%)	Gel Composition(mole ratios)		
			SiO ₂ /Al ₂ O ₃	Na ₂ O/SiO ₂	H ₂ O/Na ₂ O
VA01	gel	--	1.9	0.7	59.3
VA02	gel	--	1.5	1.2	36.0
VA03	silicate	--	1.5	1.2	36.0
VA05	gel	--	1.6	1.2	45.0
VA06	gel	--	1.8	1.2	45.0
VAA01	Alix 066	99.0	1.2	1.2	36.0
VAA02	Alix 162	94.8	1.2	1.2	36.0
VAA05	Alix 071	84.0	1.2	1.2	36.0
VAA06	Alix 168	94.0	1.6	1.2	45.0
VAA07	Alix 167	98.7	1.6	1.2	45.0

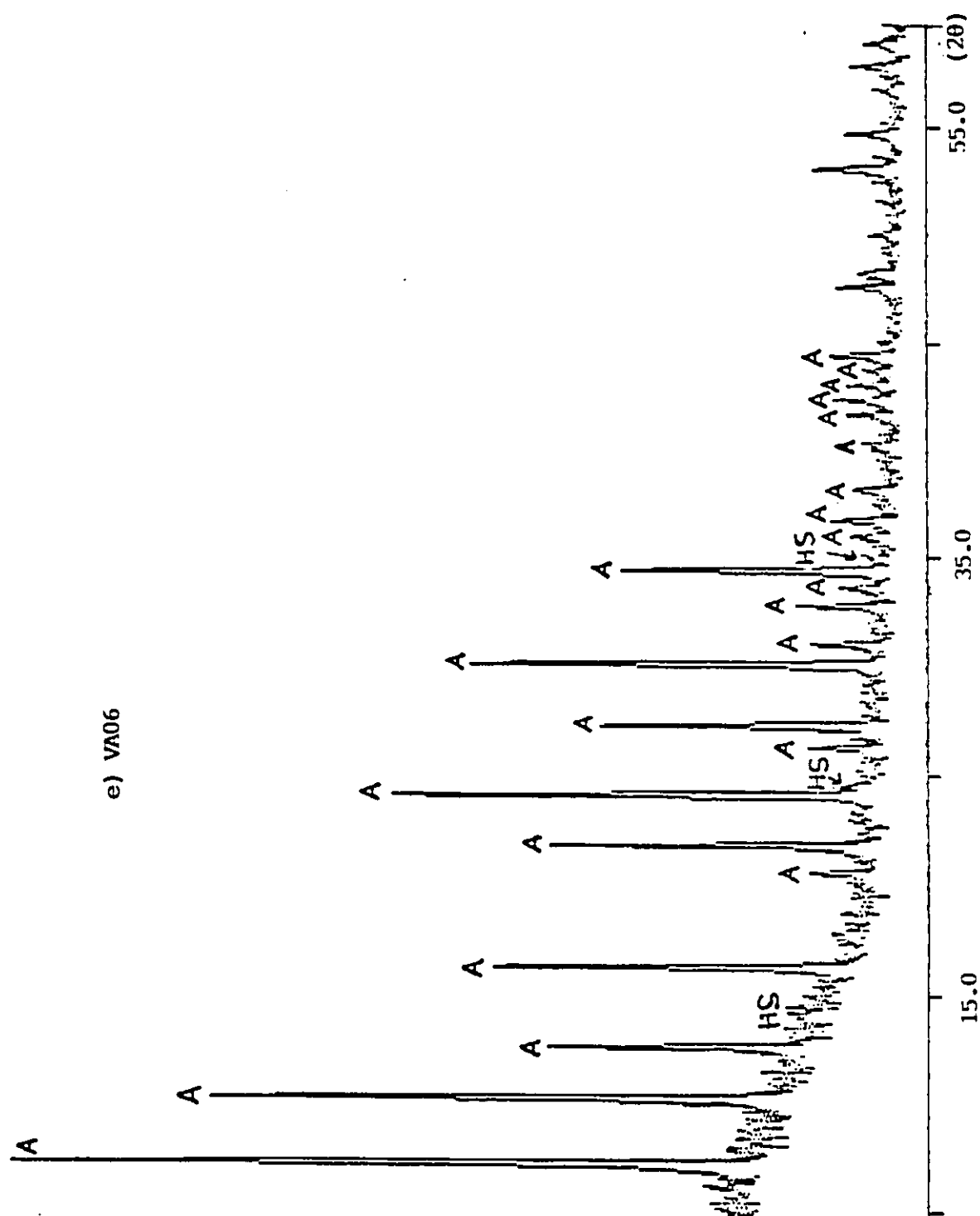
Table 3.18 Experimental parameters used for zeolite Na-A syntheses. The reaction time and temperature used were 72 hours and 100 °C respectively for all samples. The source of silica was silica gel, sodium silicate, or Alix materials.

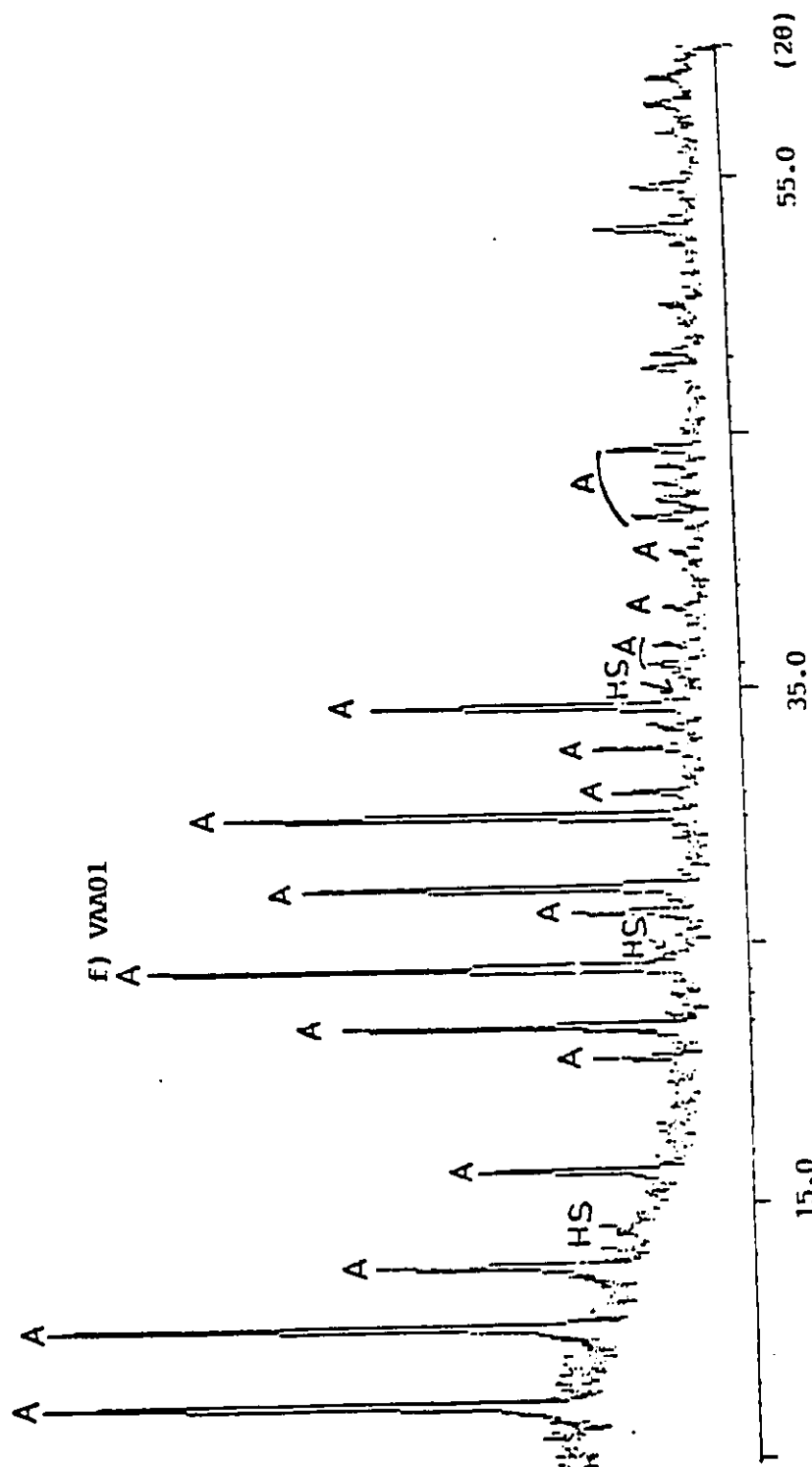
Figure 3.27 X-ray powder diffraction patterns of the synthesized Na-A zeolites and chryso-zeolites: a) VA01, b) VA02, c) VA03, d) VA05, e) VA06, f) VAA01, g) VAA02, h) VAA05, i) VAA06, j) VAA07.

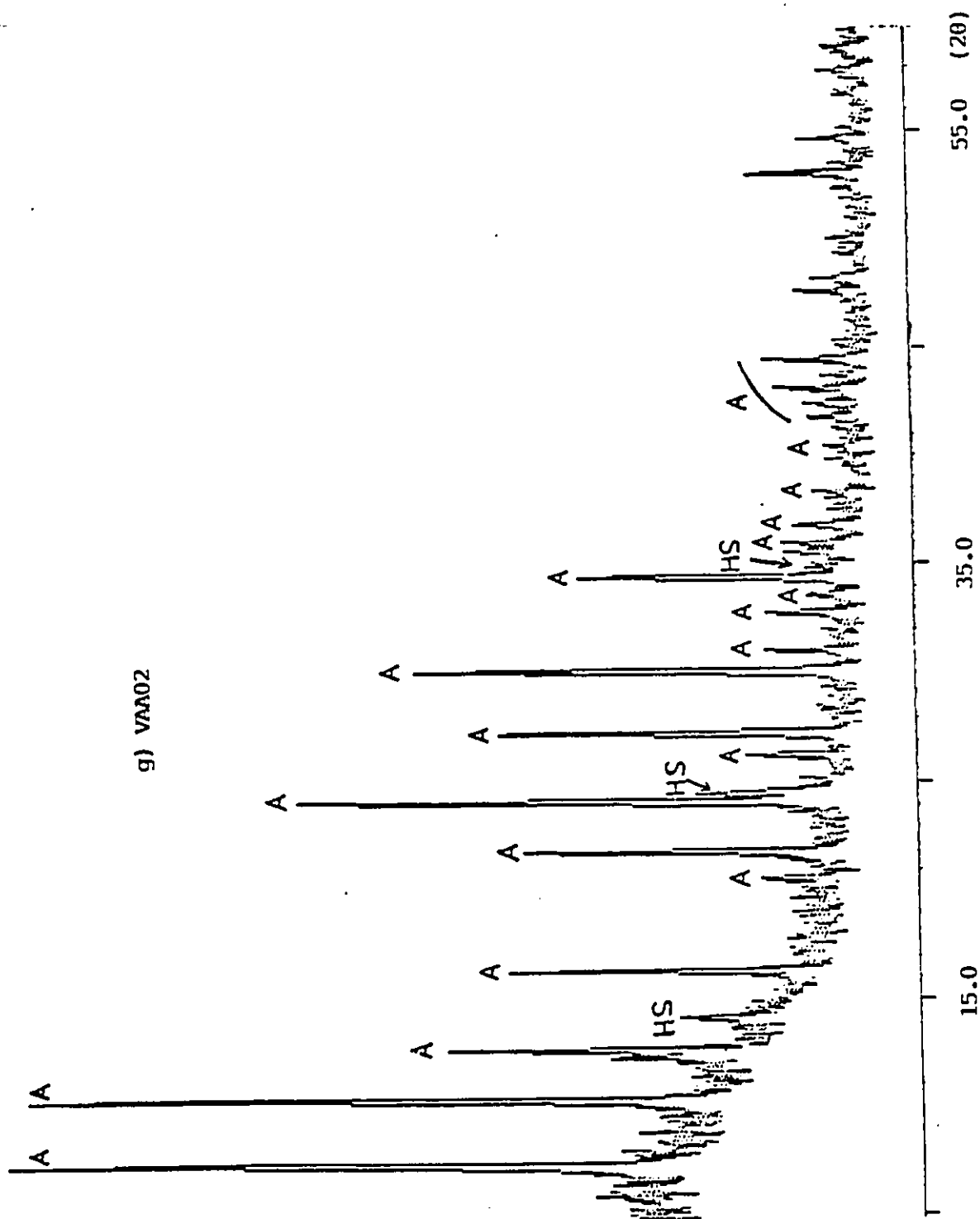


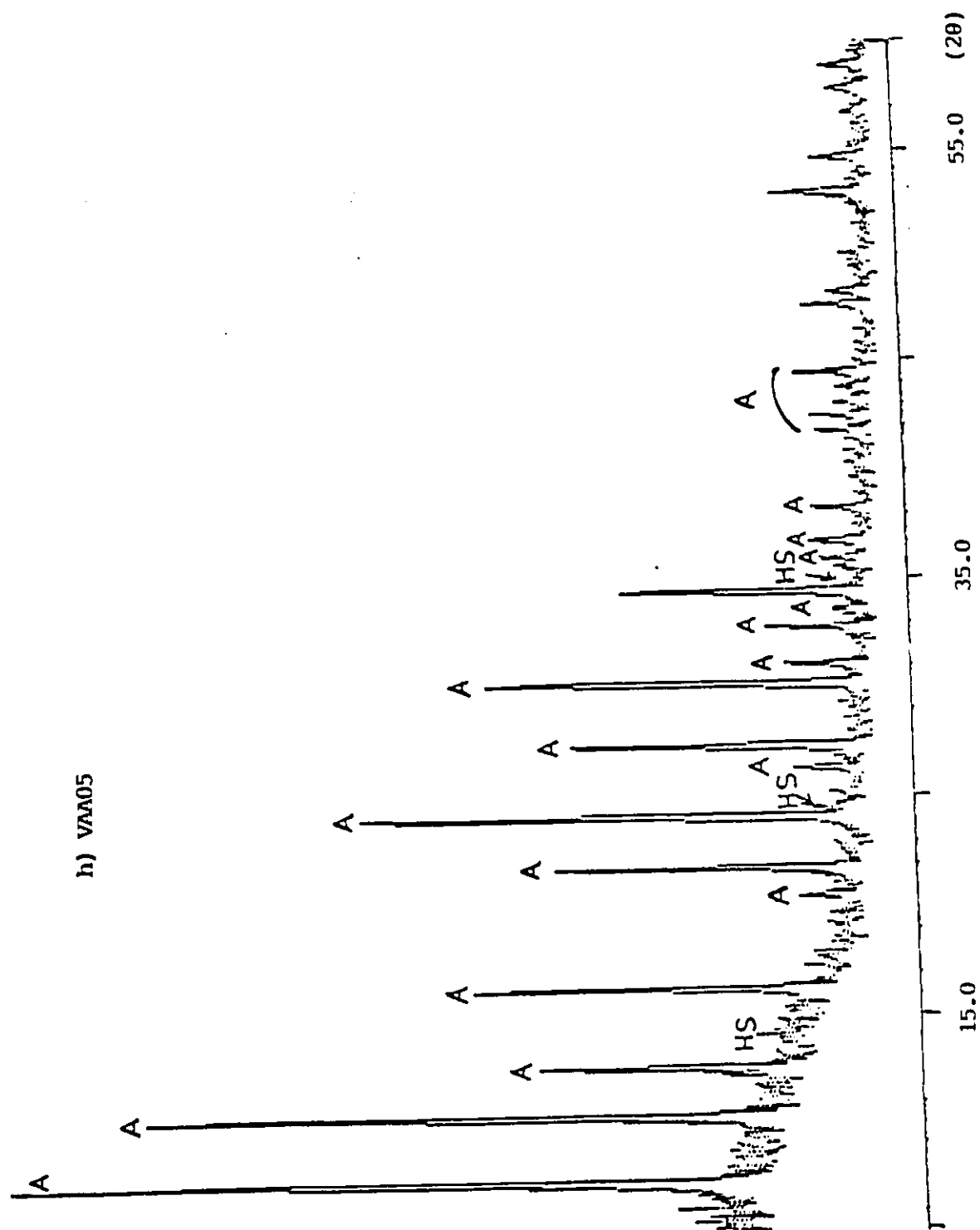


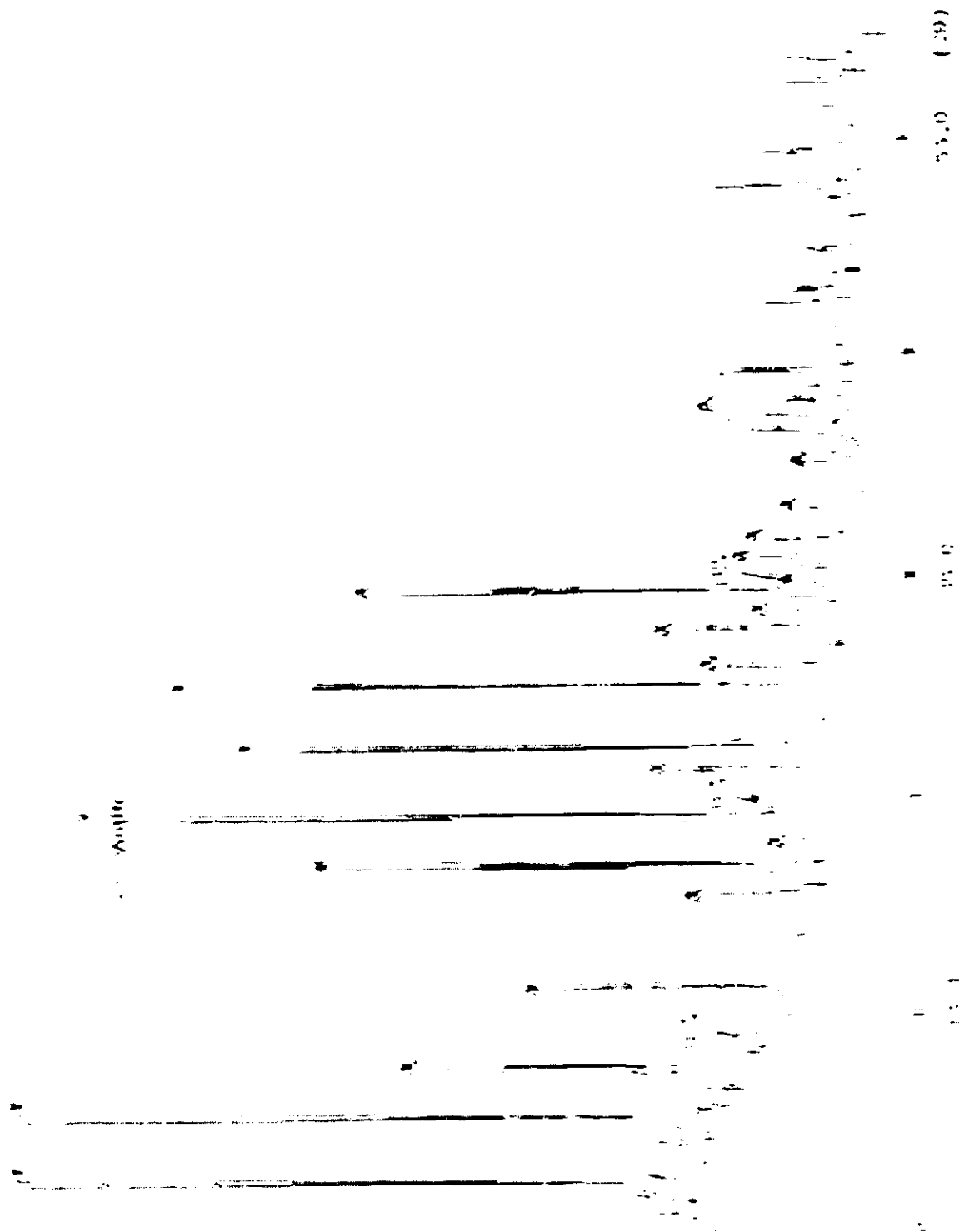


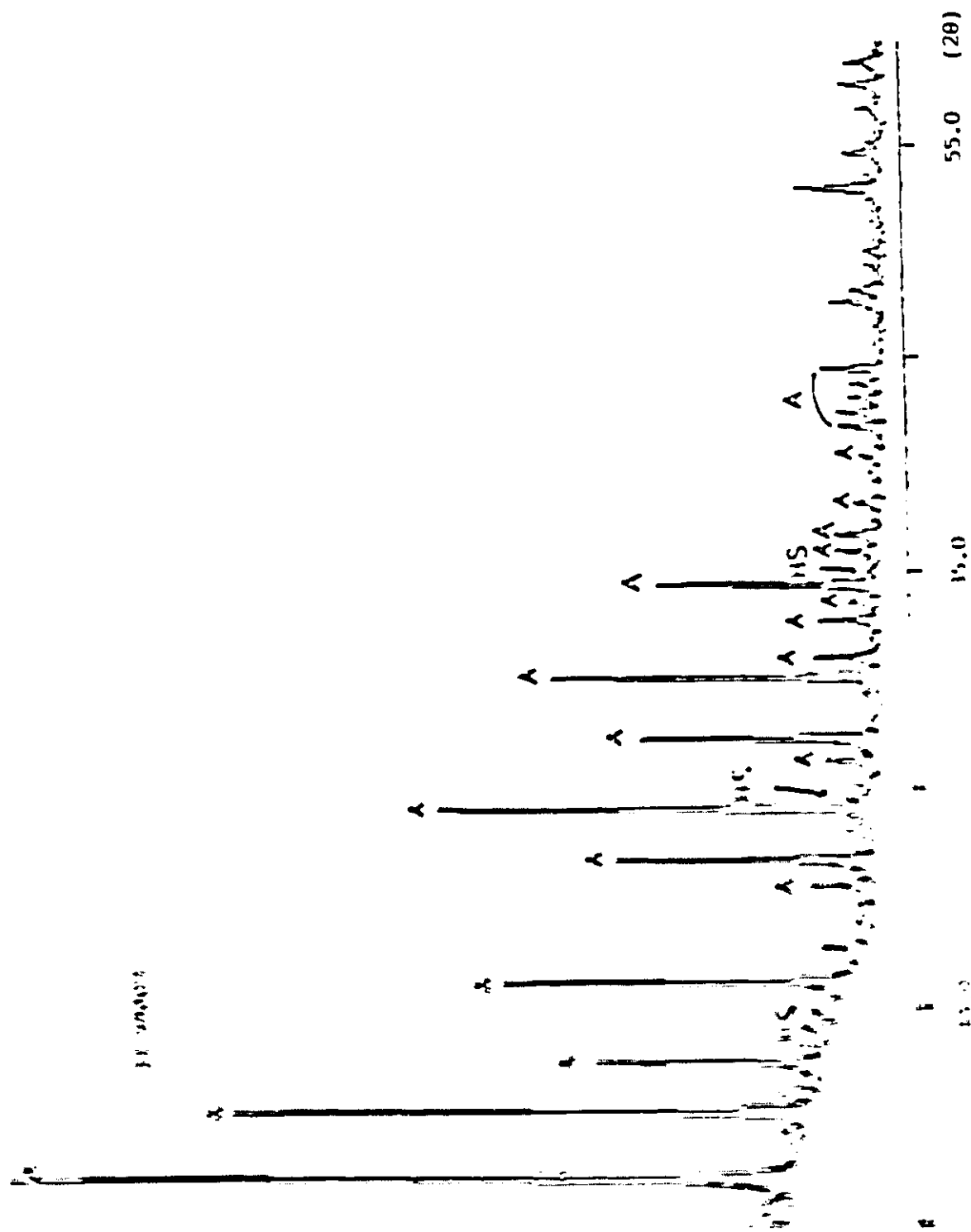












was synthesized by using sodium silicate as the source of silica. The XRD pattern of VA03 (fig. 3.27.c) show that zeolite HS was the only crystalline phase obtained when sodium silicate was used, whereas zeolite Na-A was obtained as the major component when silica gel was used as source of silica (fig. 3.27.b). VA02 also contains some other crystalline phases: zeolite HS (hydrosodalite), and at least another unidentified crystalline phase. Its XRD pattern was similar to the ones obtained with VA05, and VA06.

Silica gel was used for the preparation of VA01, VA02, VA05, and VA06. In order to study the effect of the source of silica on the nature of the product, Alix materials with MLD from 84.0 to 99.0% were used for the synthesis of VAA01, VAA02, VAA05, VAA06, and VAA07 as mentioned in Table 3.18. In order to keep the other experimental parameters constant, only two gel compositions were considered. The X-ray powder pattern of the products for the five samples (fig. 3.27.f to j) were similar to those obtained when the source of silica was silica gel (fig. 3.27.a, b, d, and e). Compared to the case where zeolite Na-A was synthesized from Alix material, the (111) Bragg peak of chrysotile asbestos situated at $2\theta = 10.1^\circ$ could not be detected when Na-A zeolite was synthesized. Zeolite Na-A is the major crystalline phase in all samples synthesized using Alix materials, along with some crystalline impurities, one of which could be identified as being zeolite HS. The intensity of the peaks and of the gel composition (fig. 3.27.f to j) and of the zeolite Na-A (fig. 3.27.f to j) are similar to those obtained when silica gel was used as source of silica (fig. 3.27.a, b, d, and e).

45.0) do not seem to have much influence on the final product e.g. the same crystalline phases were obtained.

The results of elemental analysis done by using Atomic Absorption Spectrometry are available in Appendix 7, for most of the zeolite Na-A synthesized in this work. The composition of the samples was determined in order to verify if the ratio $\text{Na}_2\text{O}/\text{Al}_2\text{O}_3$ was equal to 1.0 ± 0.2 as mentioned in the literature [43,86]. Appendix 7 shows that most of the samples are in agreement with the literature. For the samples that deviate from the ideal composition, the reaction time was not sufficient to form zeolite Na-A, e.g. VA10 (reaction time = 35 minutes) which was used for the study of the kinetics of crystallization (section 3.4). Excess washing may remove some sodium which is ion exchanged by hydrogen to give a ratio $\text{Na}_2\text{O}/\text{Al}_2\text{O}_3$ below 1. On the other hand, insufficient washing may result in some sodium from the mother liquor to be deposited on the zeolite particles when the samples are dried. This would result in an excess sodium ($\text{Na}_2\text{O}/\text{Al}_2\text{O}_3 > 1$). These results show the importance of appropriate monitoring of the pH while the hot reaction mixture is being filtered and washed [43].

3.4 A Study of the Kinetics of the Crystallization of Na-A zeolite.

3.4.1 Introduction

The successful attempts of synthesizing Na-A zeolite of an acceptable degree of purity, from Alix materials with variable MLD values, as well as from silica gel, opened the way for comparisons about the kinetics of crystallization that might be influenced by the source of silica.

It is reported in the literature [29,88] that the crystallization of Na-A zeolite is a two step process and obeys a sigmoidal law. The first step is the nucleation and consists of an induction period in which stable nuclei of zeolite Na-A are formed. The second step is the crystallite growth step which occurs after nucleation and results in an increase in the size of the zeolitic crystallites. The rate of increase of the size of the crystallites depends on the classical variables such as reaction time, temperature, reactant composition (molar ratios), and pressure, as well as on others such as the alkalinity (pH), nature of reactants stirring during the reaction, etc... [34,35,36,88].

The choice of Al_2O_3 and SiO_2 sources should be made in terms of the specific zeolite to be synthesized, because of their influence on the course of reaction.

In an alkaline medium such as the one used for Na-A zeolite synthesis, it has been established [29,88] that aluminate solutions have a relatively simple composition with $Al(OH)_4^-$ as the dominant anionic species. With silicates,

this is certainly not the case since various polymeric species are known to occur, depending on the origin and the history of the starting material (thermal treatment, etc... [29,88]).

The depolymerized and hydrated Al and Si anions, designated as precursors, condense together to give polymeric aluminosilicate species (solid or solute) which reacts with other aluminosilicate species, as shown on Figure 3.28 to give 4-membered rings also designated as a type of secondary unit building [14,16]. These 4-membered rings can be polymerized with other similar units to give more complex species which represents the basic cubic unit found in zeolite A as shown on Figure 3.29.

When the reaction mixture is relatively rich in Al as is the case for the Na-A zeolite synthesis, the ratio $\text{SiO}_2/\text{Al}_2\text{O}_3$ must be equal to 2 ($\text{Si}/\text{Al}=1$) in order to satisfy Loewenstein's rule [43,37].

The experimental parameters used in this kinetic study are listed in Table 3.19. It can be seen from the above table that the only experimental variables were the source of silica and the reaction time, which was varied from 35 minutes to 72 hours (i.e. 4,320 minutes). Hydrothermal syntheses were carried out in the reactor described in section 2.2. The optimization of molar ratios was carried out by analyzing the Na-A zeolite purity by X-ray diffraction versus the composition of the reaction mixture in SiO_2 , Na_2O , H_2O , Al_2O_3 , when silica gel was used as the source of silica

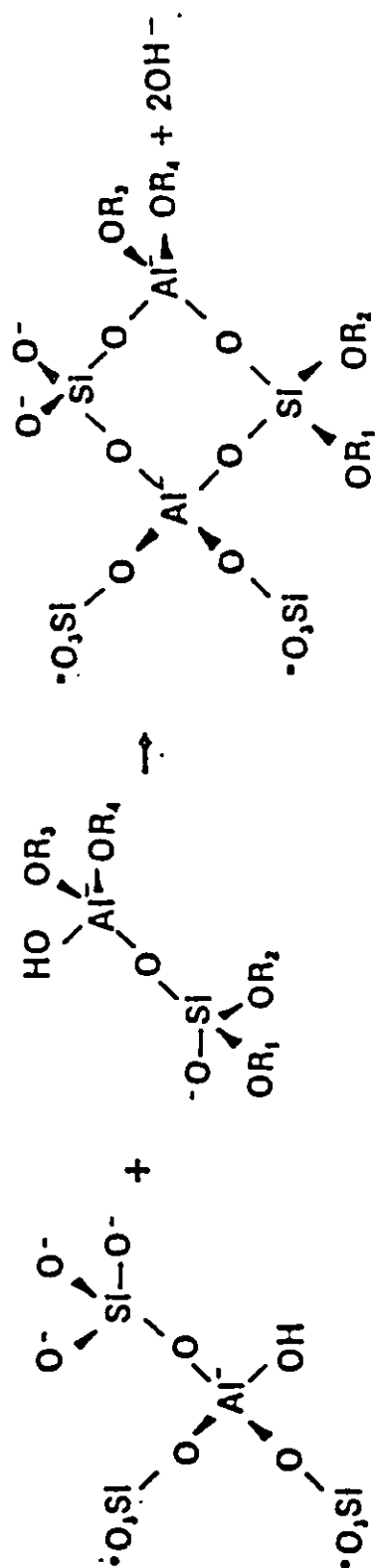


Figure 3.28 Condensation of precursor aluminosilicates to give 4 ring units. 37

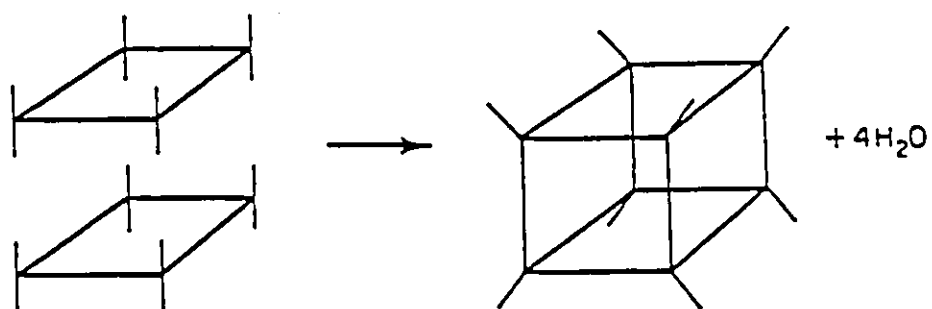


Figure 3.29 Polymerization of 4-membered aluminosilicate rings to give more complex units. 29

Sample #	Source of Silica	Reaction Time (min)	Gel Composition (mole ratios)		
			SiO ₂ /AlO ₃	Na ₂ O/SiO ₂	H ₂ O/Na ₂ O
VA10	gel	35	1.6	1.2	45.0
VA09	gel	60	1.6	1.2	45.0
VA07	gel	90	1.6	1.2	45.0
VA08	gel	120	1.6	1.2	45.0
VA05	gel	4320	1.6	1.2	45.0
VAA16	Alix	60	1.6	1.2	45.0
VAA15	Alix	90	1.6	1.2	45.0
VAA17	Alix	120	1.6	1.2	45.0
VAA06	Alix	4320	1.6	1.2	45.0

Table 3.19 Experimental parameters used for the kinetic study of the crystallization of Na-A zeolite. Two sources of silica were used i.e. silica gel and Alix 168 (MLD=94). The reaction temperature was kept at 100 °C for all samples.

(VA05 and VA06). The purpose of the optimization was to obtain a Na-A zeolite with the best possible degree of purity necessary for kinetic studies.

3.4.2 Comparative kinetic study by XRD

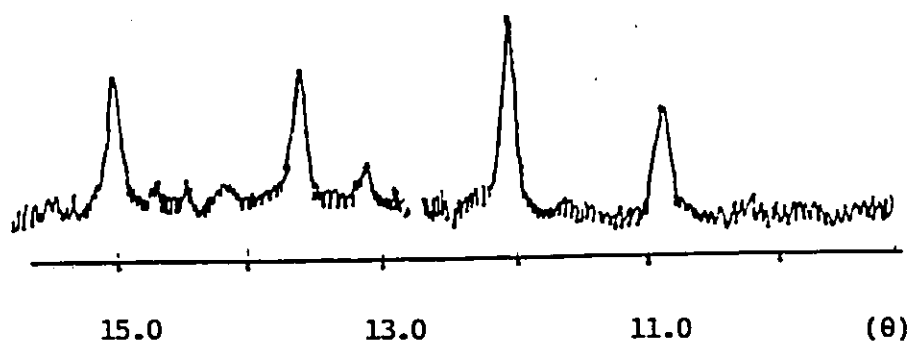
For the comparative kinetic study, syntheses were carried out by varying only the source of silica and/or the reaction time as summarized in Table 3.19. The choice of silica gel for comparative studies is based on its use in a routine preparation of Na-A zeolite [43]. The choice of Alix materials is due to its use in this laboratory, where it was designed, and led to a completely new path for the formation of Na-A zeolite. All samples were investigated by X-ray powder diffraction by following the intensity of the Na-zeolite peaks as the reaction time increases, for the samples prepared from silica gel (Figure 3.30 a, b, c, and d) and from Alix 168 (Figure 3.31 a, b, c, and d). X-ray Diffraction was a very useful technique for the qualitative evaluation of the degree of purity of the Na-A zeolite synthesized and for the measurement of its content in the sample. The increase in intensity of the Na-A zeolite Bragg peaks with reaction time can be observed in Figures 3.30 and 3.31 as the quantity of the zeolite in the sample increases. The rate of production of Na-A zeolite can be measured by plotting the degree of crystallinity (DC) versus reaction time (Table 3.20, Figures 3.32 and 3.33): an increase in DC with reaction time is observed. The degree of crystallinity increases from 0 to 81%, relative to the external standard, which is a commercial zeolite Na-A with a pore size of 4 Å.

When silica gel was used as the source of silica, no Bragg peak was observed after a reaction time of 35 minutes,

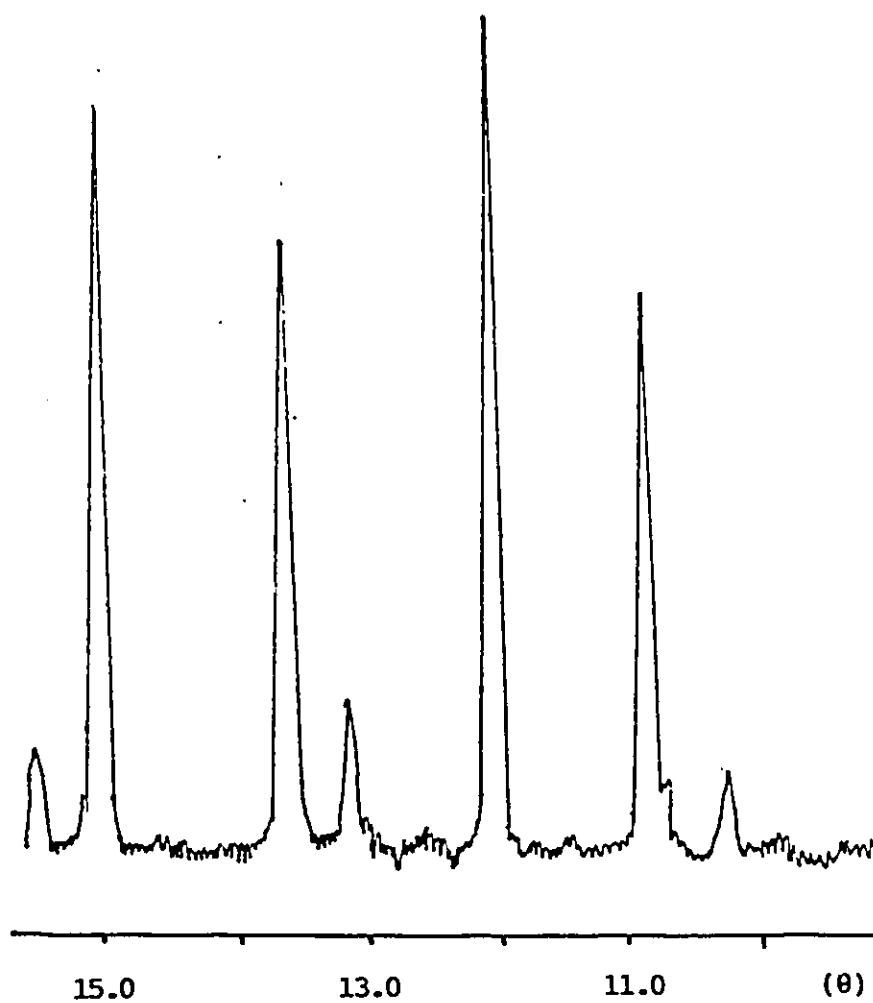
Figure 3.30 X-ray powder diffraction patterns of Na-A zeolite samples used for the comparative kinetic study: a) VA09, b) VA07, c) VA08, and d) VA05.



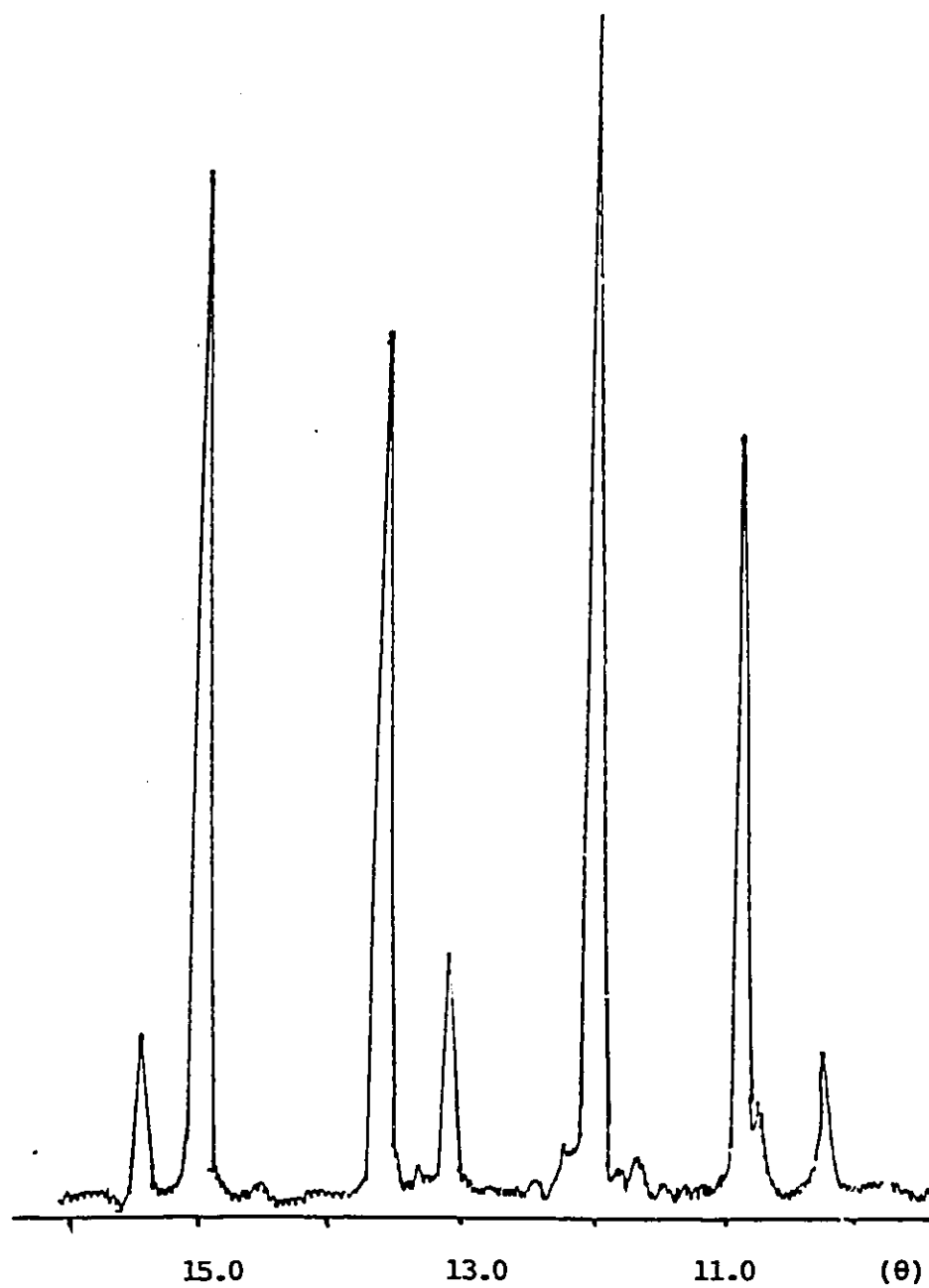
a) VA09, reaction time = 60 minutes



b) VA07, reaction time = 90 minutes

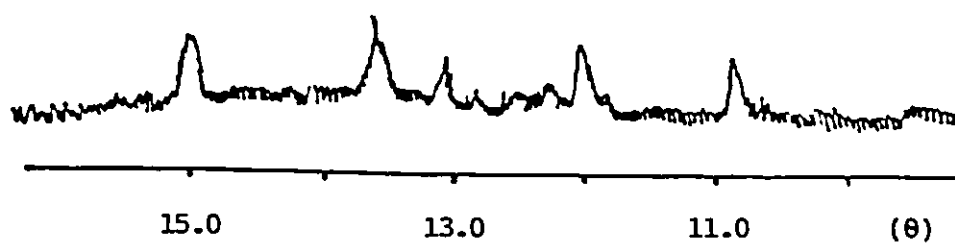


c) VA08, reaction time = 2 hours

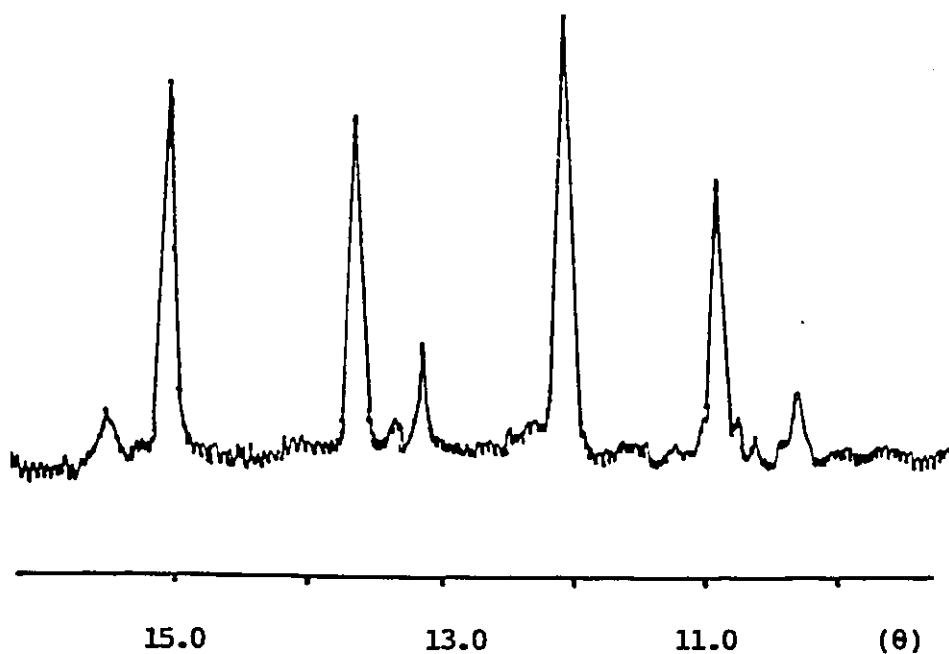


d) VA05, reaction time = 72 hours

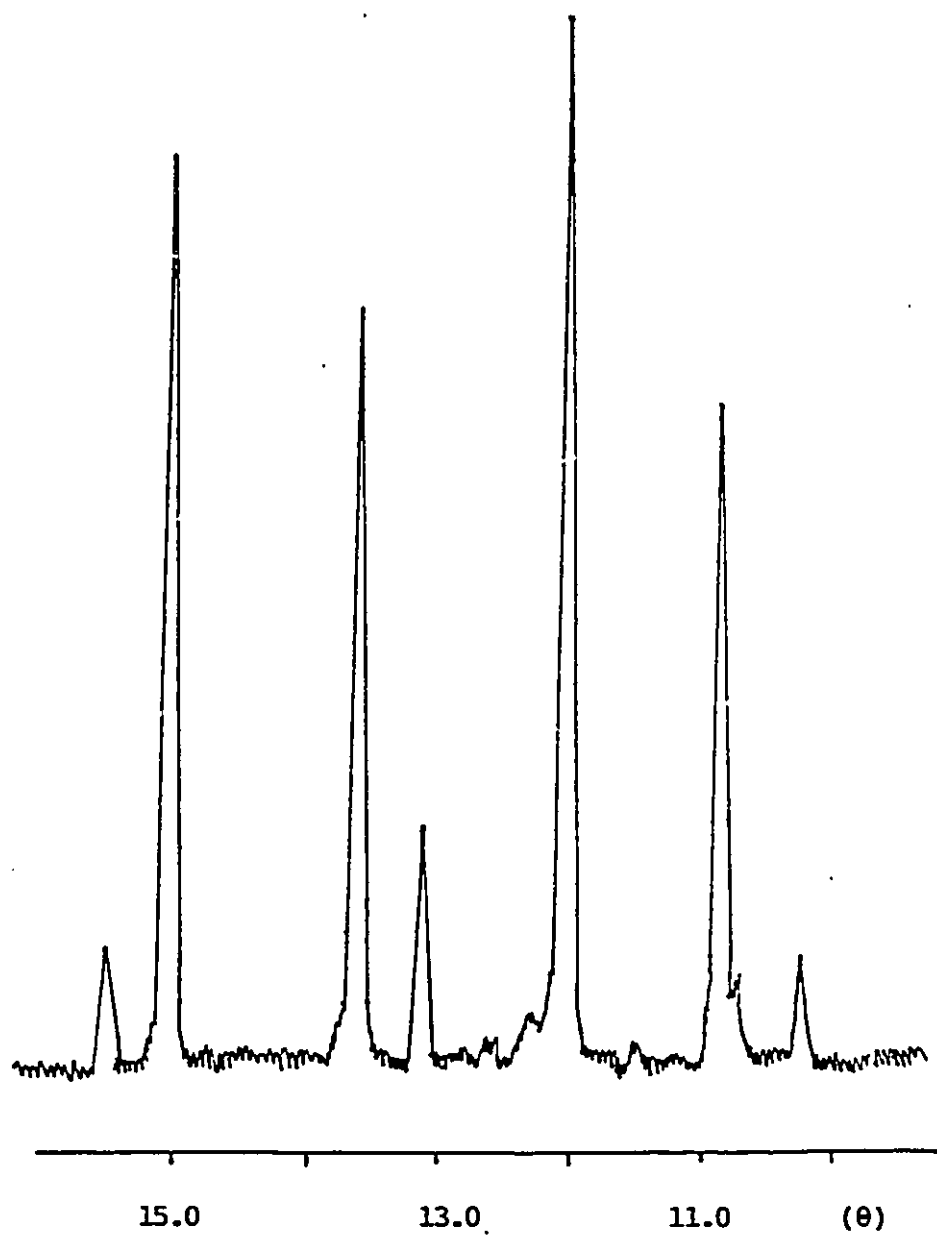
Figure 3.31 X-ray powder diffraction patterns of Na-A chrysozeolite samples used for the comparative kinetic study: a) VAA16, b) VAA15, c) VAA17, and d) VAA06.



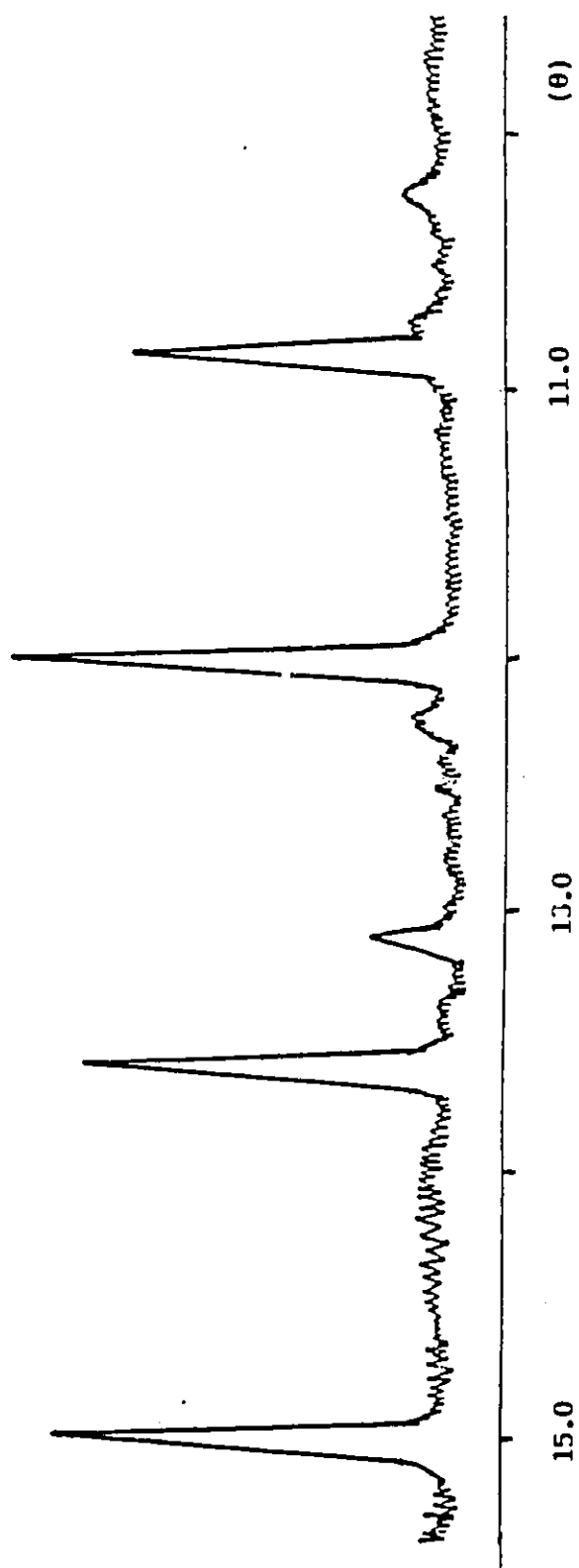
a) VAA16, reaction time = 60 minutes



b) VAA15, reaction time = 90 minutes



c) VAA17, reaction time = 2 hours



d) VAA06, reaction time = 72 hours

which indicates either that the sample is amorphous (no crystalline phase) or that the microcrystalline particles are smaller than the critical size for detection of $40 - 50 \text{ \AA}$ [46].

When Alix 168 (MLD = 94%) was used as the silica source, the same trend in DC values was obtained (Table 3.20, Figures 3.32 and 3.33), i.e. DC increases with reaction time.

Very weak diffraction peaks were observed, which could not be attributed to Na-A zeolite, and are crystalline impurities. Zeolite HS (hydrosodalite) was identified as being one of the by-products.

When the degree of crystallinity is plotted versus reaction time, sigmoidal curves are obtained for both sources of silica, in agreement with the literature [29-34,88].

One important observation from the curves is the shorter induction period observed when Alix material was used as the source of silica, compared to the one of about one hour obtained when silica gel was used. Since identical experimental conditions, such as mole ratios of oxides, temperature, and set of reaction times for the two concerned systems were used, only one explanation can be offered to explain the difference in precursor behaviors, i.e. the difference in silica solubility.

Sample #	Source of Silica	Reaction Time (minutes)	D.C. (%)	Δ (DC) (%)
VAA10	silica gel	35	0	2.5
VAA09	silica gel	60	5.8	2.8
VAA07	silica gel	90	28.7	3.9
VAA08	silica gel	120	72.9	6.1
VAA05	silica gel	4320	80.8	6.5
VAA16	Alix 168	60	15.6	3.3
VAA15	Alix 168	90	58.3	5.4
VAA17	Alix 168	120	74.3	6.2
VAA06	Alix 168	4320	66.8	5.8

Table 3.20 Effect of reaction time on the degree of crystallinity. The reaction temperature was kept at 100 °C for all samples. Δ (DC) is the maximum error allowed on the degree of crystallinity DC, calculated according to the description in section 2.3.3

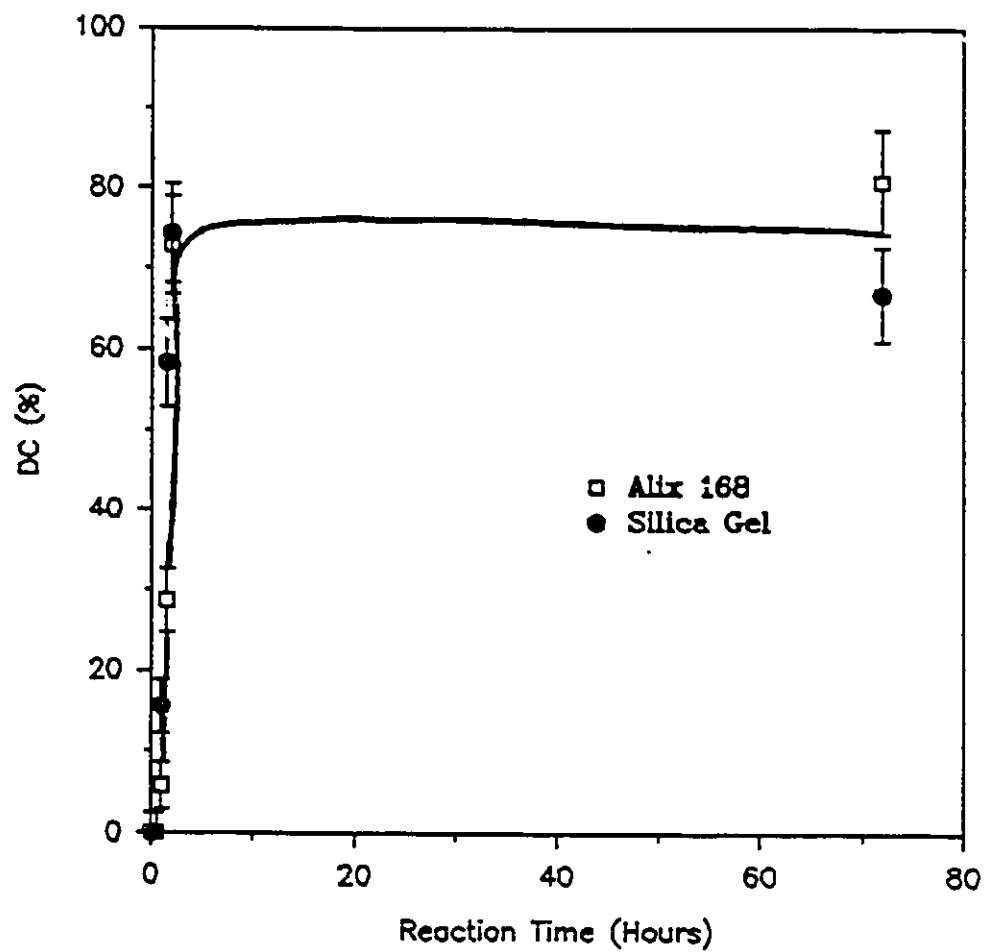


Figure 3.32 Plot of the degree of crystallinity (DC) of Na-A zeolite versus reaction time from 0 to 72 hours. The error bar is the maximum error allowed.

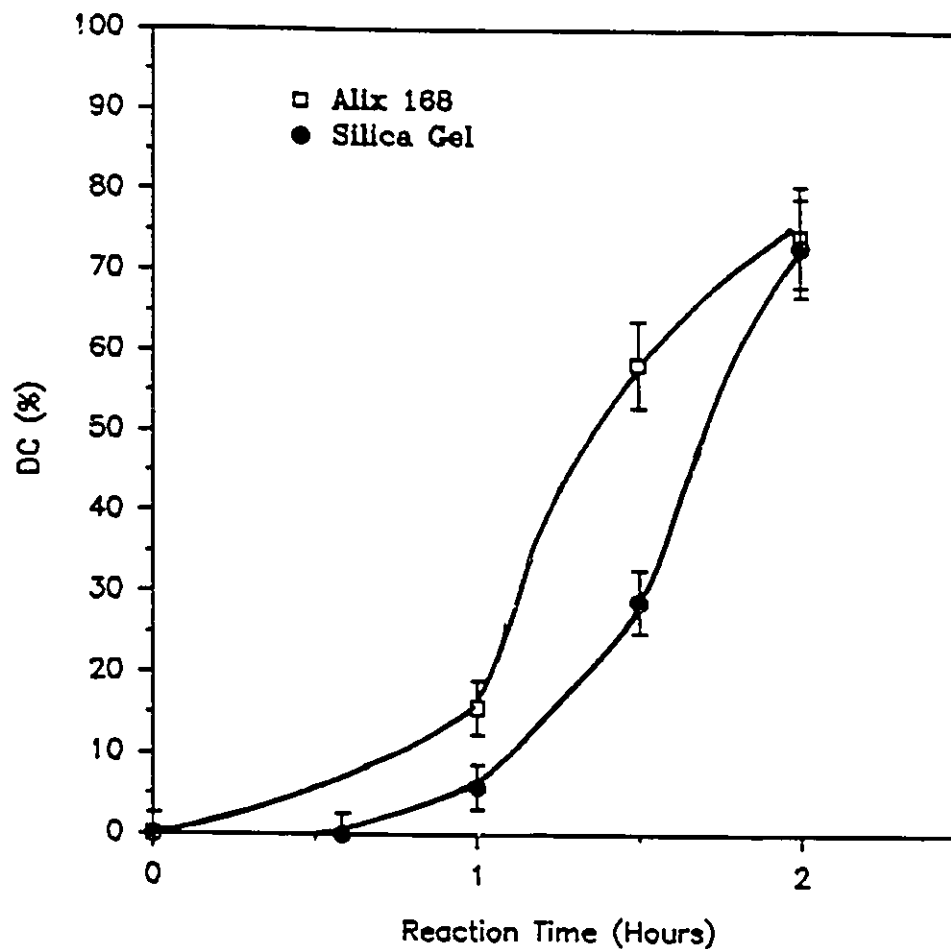
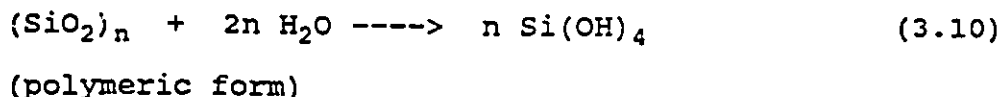


Figure 3.33

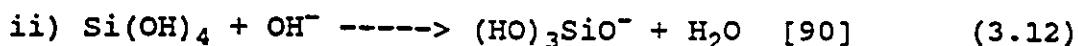
Plot of the degree of crystallinity (DC) of Na-A zeolite versus reaction time from 0 to 2 hours. The error bar is the maximum error allowed.

3.4.3 Solubility of silica

In non basic aqueous solutions, silica exists as the tetrahydroxide monomer, Si(OH)_4 , and as silicate anions in solutions of high pH (i.e. $>10.5-11$) [88,89]. The solubility of silica, particularly amorphous forms, has been studied extensively. In the case of silica gel, the dissolution might involve a simultaneous hydration and depolymerization. Dissolution is catalyzed by the presence of a strong base such as sodium hydroxide and when the pH exceeds about 10.5 - 11, silica dissolves extensively. This probably involves depolymerization through hydration to form Si(OH)_4 , followed by the addition of an OH^- ion to form the silicate anion. The depolymerization reaction can be represented as follows:



Various dissolution reactions have been proposed by different authors:



iii) and the possible production of Si(OH)_6^{2-} which is analogous to SiF_6^{2-} . [89]

In the case of the Alix material, the depolymerization step (equation 3.10) probably has little significance or is

not required. Indeed initially, the silica matrix seemed to be mostly present as the monomeric form in the reaction mixture. If these hypotheses were verified, it would lead to a significant decrease in the induction period when Alix material is the source of silica compared to the silica gel.

In order to investigate the reason for the difference in induction period between the two systems, the measurement of the solubility of silica was made with Alix material and with silica gel. The hydrothermal reactor mentioned in section 2.2 was used for the experiment (fig. 2.1). The same experimental conditions as for the syntheses of Na-A zeolite were used. The source of silica, either the Alix material or silica gel, was mixed separately with NaOH and water in the same molar ratios used for the kinetic studies of the crystallization of Na-A zeolites (Table 3.19), and the mixtures were held at 100 °C for the same periods of time as the ones used for the kinetic study. After the dissolution step, a hot filtration was performed, followed by washing with H₂O and drying at 110 °C overnight. Then, the solid residue (undissolved silica) was cooled in a dessicator, and weighed. The weight of the solid was obtained by subtracting the weight of the filter paper which was measured prior to filtering. The weight of dissolved silica is equal to the weight used minus the undissolved part. The percent of dissolved silica gel and Alix 168 is shown in Table 3.21. The results highlight that silica solubilization is initially (i.e. in the first 30 min.) a lot more efficient

TIME (minutes)	Amount of material dissolved (%)	
	Alix 168	silica gel
10	69	41
20	87	43
30	88	49
40	88	88

Table 3.21 Solubility of Alix 168 and silica gel in the reaction mixture used for the synthesis of Na-A zeolite. determined.

when Alix material is used as the source of silica. After a solubilization time of 10 minutes, 69% of Alix 168 had dissolved compared to 41% of silica gel. After 20 to 30 minutes, dissolution of 87-88% of Alix material was completed, compared to 43-49% silica gel. After 40 minutes, the percent dissolved was the same for both (88%), showing that after 40 minutes, the same amount of SiO_2 was present in solution for both systems. The difference in silica solubility between 0 and 30 minutes supports the hypothesis that when silica gel is considered, subsequent hydration and depolymerization occur. With Alix material, it seems that mainly hydration is involved and most of the silica is already present in the monomeric form. This is reflected by the ease of solubilization of Alix materials, compared to silica gel.

The experimental induction period depends on the silica solubility. The degree of hydration and depolymerization of silica has a direct effect on the induction time observed: a longer induction period was observed with the use of silica gel compared to Alix material. This difference can be attributed to the fact that hydration and depolymerization must take place for silica gel whereas mainly only hydration is required for Alix material.

Further investigation regarding silica solubility would be possible by using ^{29}Si NMR on the remaining mother liquor samples after filtration. This could give the distribution of the different structural units of silicate anions in the

mother liquor. The results expected from this type of experiment may be summarized as follows: lower molecular weight silicate anions should be found in the case of Alix materials [91].

3.4.4 Study of the kinetics of crystallisation of Na-A zeolite: sigmoidal shaped curve

Not enough data points were available for fitting the experimental curves to a sigmoidal function. In addition, it has been reported there are no valuable mathematical models of the curve, which are in agreement with the experimental results. Quantitative evaluation of the kinetics of formation of zeolite A were investigated by Meise and Schwochow [77,78]. They attempted to describe both, the curves of yield of crystals against time and the final distribution of crystal sizes. Although qualitative agreement to their model has been observed, large deviations from the experimental curves have been reported to occur.

The effect of parameters such as temperature, the type of cations (K^+ instead of Na^+), the alkalinity (pH), and the source of silica on the nucleation and/or on the growth steps could be predicted:

temperature: with an increase in temperature, both nucleation and crystal growth accelerate, i.e. the crystallization of zeolite A is thermally activated;

alkalinity and SiO_2 source: as the alkalinity or as the activity of silica rises, the induction period is reduced. These parameters would affect nucleation more than crystal growth [77,78];

type of cation: potassium compared to sodium ions would slow down nucleation at a given alkalinity. The steric factors probably play a decisive role, particularly since this effect is exerted only when K^+ ions are present in the reaction batch at the beginning of the synthesis.

The evaluation of the induction period in zeolite synthesis must be based on the kinetics of nucleation but though qualitatively obvious from the sigmoidal shaped kinetic curves, the sigmoidal shape makes a quantitative evaluation difficult. The usual way to evaluate the induction period is by extrapolating to the time axis, the tangent representing the maximum rate of deposition of crystals. However, this procedure is not based upon the quantitative formulation of nucleation kinetics so that the significance of the induction period is quite ambiguous, and its evaluation is fairly empirical. From our results (Figures 3.32, 3.33 and Table 3.21) one can observe that the induction period was shorter when Alix material was used. The exact induction time is somewhat difficult to evaluate due to the above ambiguity in the determination method, and to the low number of data points.

3.4.5 Evaluation of the crystallization constant.

A study of the rate of crystallization of zeolite A was done by Kerr [88,89], by using a reaction mixture prepared from an amorphous sodium aluminosilicate of composition $\text{NaAlO}_2 \cdot 0.82 \text{ SiO}_2$ and aqueous NaOH.

At 100 °C he found that the rate of formation in the growth step followed approximately a first-order kinetics and was proportional to the quantity of crystalline zeolite present in the system. The formation occurred rapidly after an induction period called the nucleation step, which is due to the formation of nuclei of zeolite. Schwochow and Meise [34,36] also found a first order kinetics for the growth step and a higher order for the nucleation step.

Since we measured the quantity of crystalline zeolite present in the system (zeolite degree of crystallinity), the same type of study could be done, which would make it possible to evaluate the rate constant of crystallization.

The kinetics of a reaction is described by the general mass action rate law, which gives the rate R of a reaction at constant temperature as a function of the chemical composition of the system [92]:

$$R = \frac{-d(A)}{dt} = \frac{d(D)}{dt} \quad (3.13)$$

where,

A is a reactant and D is a product.

The expression can be written as

$$R = k (A)^x (B)^y \quad (3.14)$$

If the reaction follows a first order kinetics, as proposed in previous references [34,36,88,89], the rate law is then given by the expression:

$$\frac{d(A)}{dt} = -k (A) \quad (3.15)$$

when the reactant is involved or

$$\frac{d(D)}{dt} = k (D) \quad (3.16)$$

when the product is considered.

Since the degree of crystallinity (DC) is related to the concentration of A-type zeolite product, one can consider the equation:

$$\frac{d(DC)}{dt} = k (DC) \quad (3.17)$$

which can be rewritten as

$$\frac{d(DC)}{(DC)} = k \int dt \quad (3.18)$$

and gives upon integration

$$\ln (DC) = kt + \text{constant} \quad (3.19)$$

Thus, for a first order reaction, a plot of $\log (DC)$ versus t (time) gives a straight line of slope equal to k , the rate constant of crystallization.

In this work, when silica gel was used as the source of silica, a first order kinetics for the formation rate seems to be well supported by the straight line obtained when $\log (DC)$ is plotted against reaction time (Figure 3.34 and Table

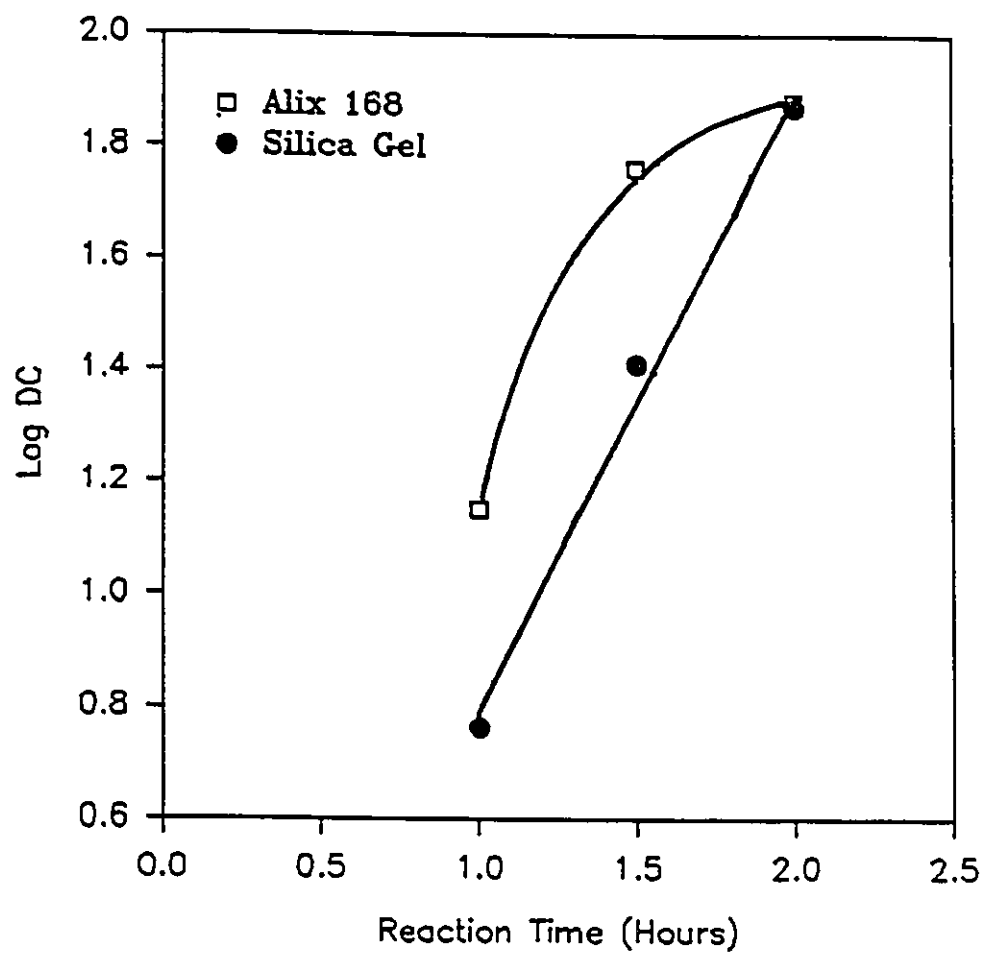


Figure 3.34 Plot of log (DC) versus reaction time.

Source of Silica	Sample #	Log DC	Time (minutes)
Silica gel	VA09	0.76	60
	VA07	1.41	90
	VA08	1.87	120
	VA05	1.89	4320
ALIX 168	VAA16	1.15	60
	VAA15	1.76	90
	VAA17	1.88	120
	VAA06	1.85	4320

Table 3.22

Evaluation of the crystallization constant for Na-A zeolites. Alix 168 and silica gel were the two sources of silica compared in this study.

3.22). The slope of the line gives a rate constant of crystallization k of 1.0 sec^{-1} .

When Alix 168 (MLD = 94%) was used as the source of silica (Figure 3.34 and Table 3.22), the three experimental points are not aligned and therefore the reaction does not appear to follow a first order kinetic law. However, the number of experimental points is too few, and more would be needed to draw meaningful conclusions. As mentioned in section 3.4.4, the activity of the source of silica should affect nucleation more than crystal growth, therefore it is quite possible that the effect of the nature of the source of silica on the rate of crystal growth is minor, may be even negligible, however, we do not have enough data to support these ideas.

3.4.6 Morphological study and particule size distribution by Scanning Electron Microscopy (SEM).

Several micrographs at magnifications of X350 and X5000 (Figure 3.35) were taken in order to follow the morphological changes occuring in the solid during the zeolite Na-A synthesis with reaction time (kinetic study).

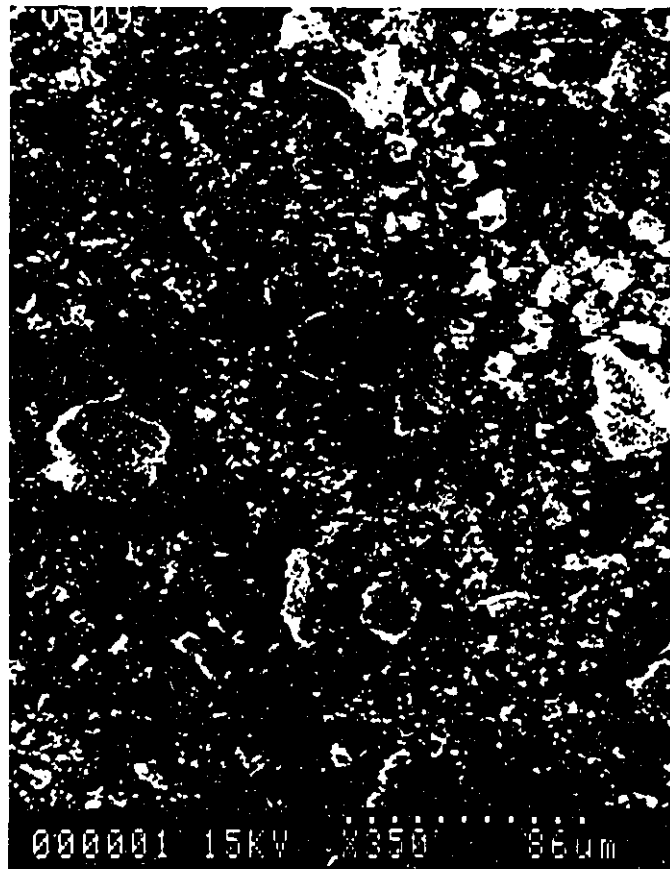
For short reaction times (ca. 1 hour), a cake-like solid is observed, which is the amorphous aluminosilicate gel. This gel is visible in several micrographs (a,b,e, f,i,j,m,n). For a reaction time of 1 hour, no Na-A zeolite could be detected when silica gel was used as the source of silica , whereas a small amount is present in the same time period when the Alix material was used for the reaction (i).

After a reaction period of 1.5 hours, some crystallites of zeolite Na-A are formed in all samples. These crystallites can be easily differentiated from the amorphous aluminosilicate gel by their regular cubic shape. A large amount of amorphous aluminosilicate gel was still present in the samples, especially when silica gel was used (b,f,j,n).

Both sources of silica gave similar results after a reaction period of 2 hours (c,g,o,k). Regular cubic crystallites were obtained with comparable dimensions ranging from 1.5 to 6.0 μm in diameter, both for silica gel and Alix 168.

Finally, after a reaction time of 3 days (d,h,l,p) crystal size is about the same as for a reaction period as

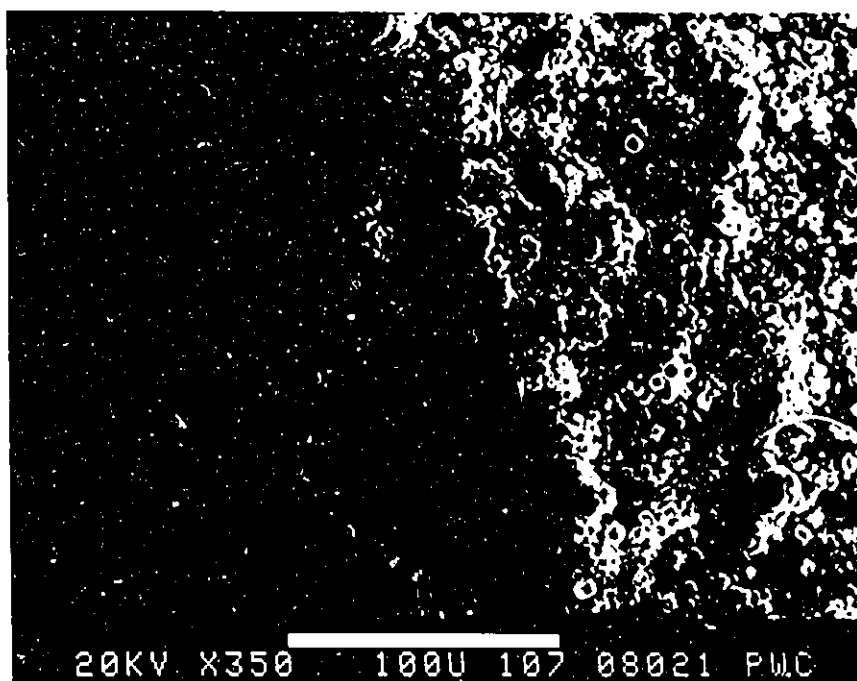
Figure 3.35 Scanning electron micrographs of the solid obtained in the Na-A zeolite synthesis versus reaction time, for two sources of silica i.e. silica gel and Alix material. VA stands for silica gel and VAA for Alix material.



VA09, 1 hour
X350



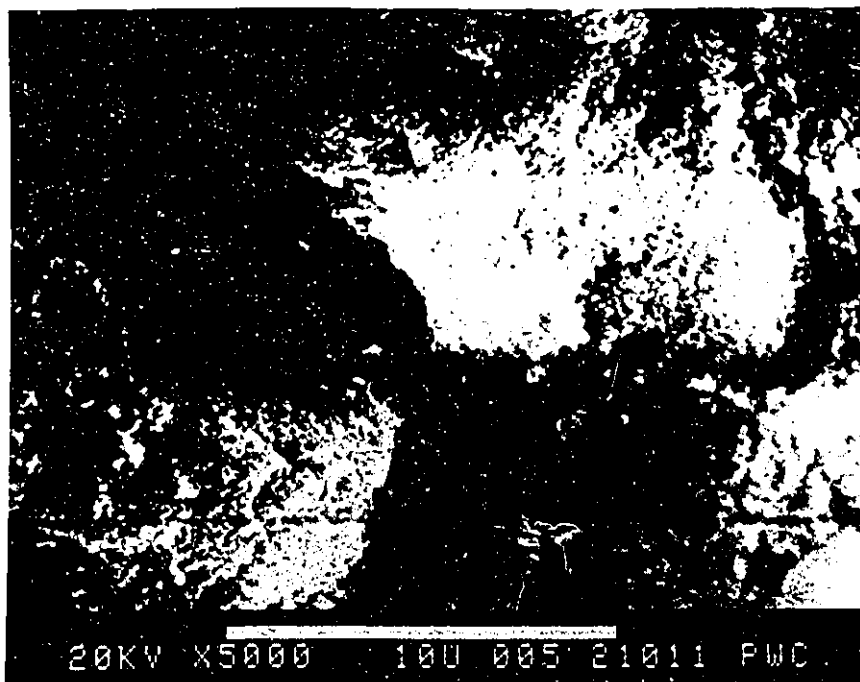
VA07, 1.5 hour
X350



VA08, 2 hours
X350



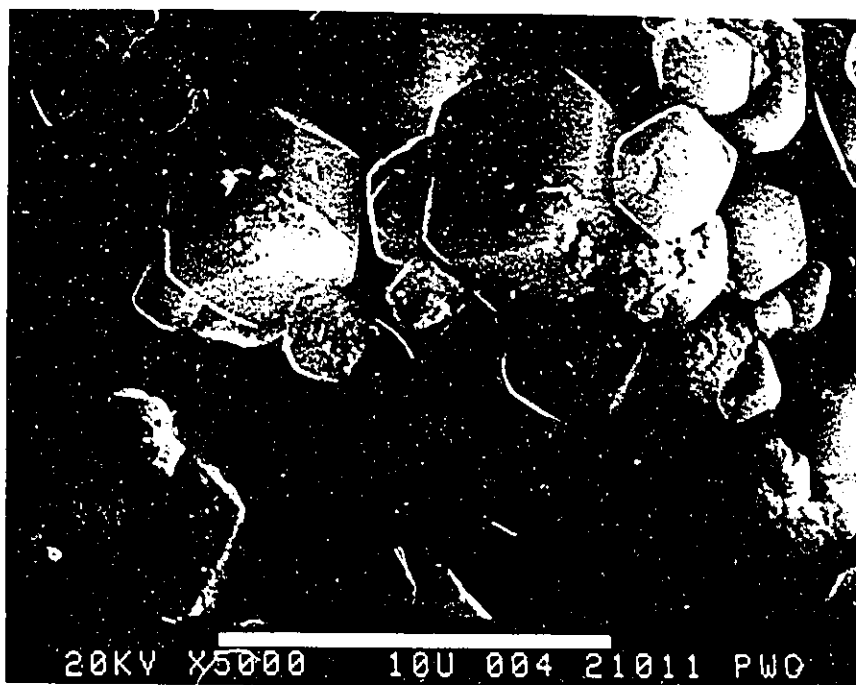
VA05, 72 hours
X350



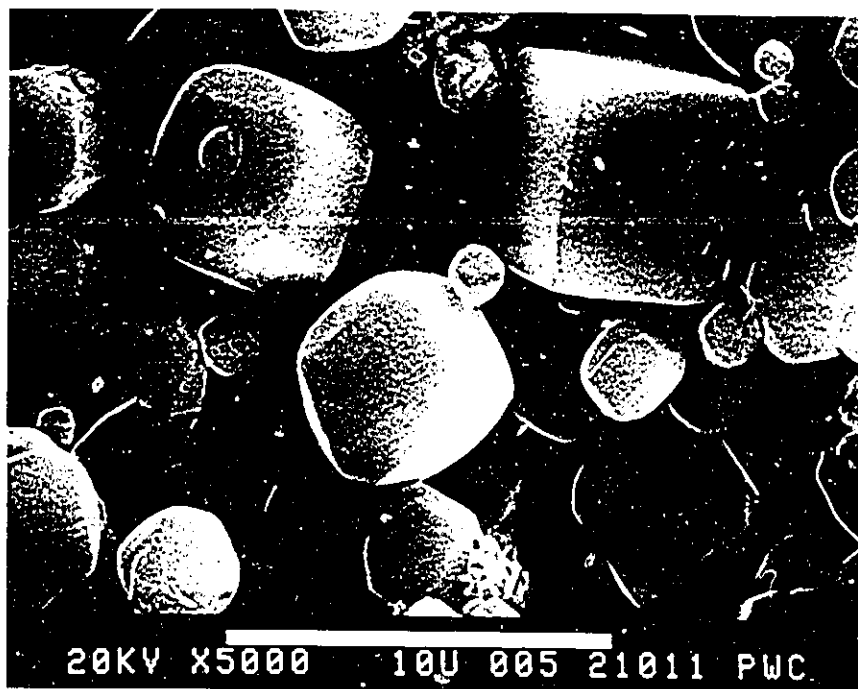
VA09, 1 hour
X500



VA07, 1.5 hour
X500



VA08, 2 hours
X5.00K



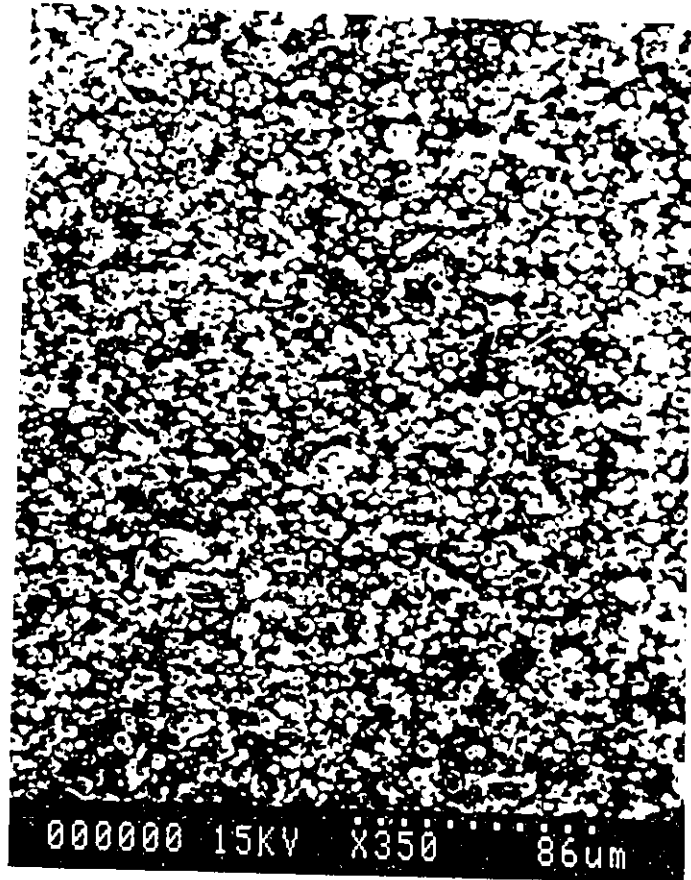
VA05, 72 hours
X5.00K



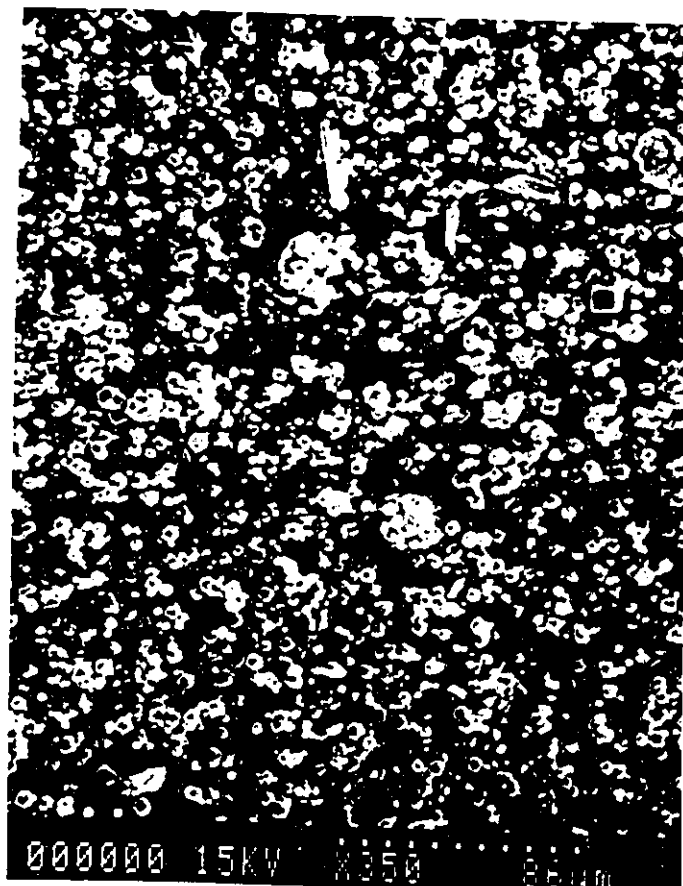
VAA16, 1 hour
X350



VAA15, 1.5 hour
X350



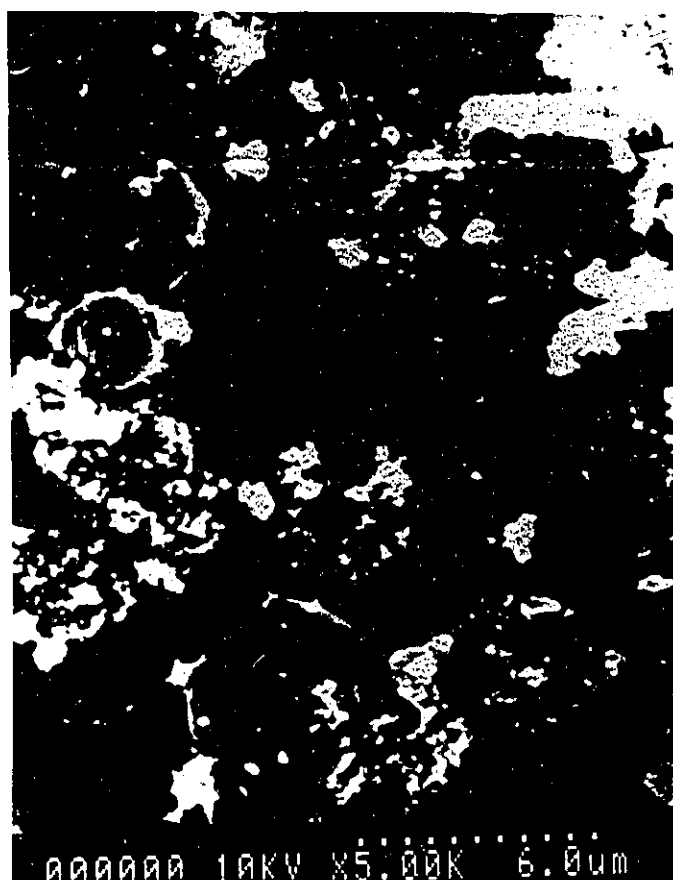
VAA17, 2 hours
X350



VAA06, 72 hours
X350



VAA16, 1 hour
X5.00K



VAA15, 1.5 hour
X5.00K



VAA17, 2 hours
X5.00K



VAA06, 72 hours
X5.00K

low as 2 hours. The main difference between the two sources of silica concerns the cleanliness of the zeolite crystals. In fact, Figure 3.34 and the SEM micrographs represented on Figure 3.35 show that when silica gel was used, crystallization was still taking place at its maximum rate for a reaction period as high as 2 hours. This results from the fact that a straight line was observed at a 2 hour reaction time, as expected from the relation given in equation (3.19), for a first order kinetics. When Alix material was used as the source of silica, the agreement with first order kinetics could not be verified because of insufficient data. However, for a reaction time of 2 hours, a decrease of the crystallization rate was observed.

From the SEM micrographs, it is impossible to differentiate between zeolite Na-A and zeolite HS (Hydrosodalite), which is the major impurity phase found in our samples, since the crystals of both zeolites are cubic-shaped.

From the SEM micrographs, it was easy to evaluate the frequency factor of particle sizes, which expresses the average diameter of the particles (\varnothing_{av}) by the relation [8]:

$$\varnothing_{av} = \frac{\varnothing_i n_i + \varnothing_j n_j + \varnothing_k n_k + \dots}{n_i + n_j + n_k + \dots} \quad (3.20)$$

where

n_i, n_j, n_k, \dots = number of particles with an average particle sizes of $\varnothing_i, \varnothing_j$, or \varnothing_k , respectively.

$\bar{\sigma}_1, \bar{\sigma}_j, \bar{\sigma}_k, \dots$: average particle size of a given range of crystal dimensions, measured on the electron micrographs.

A plot of $\bar{\sigma}_{av}$ against reaction time can be done in order to see the trend and be able to compare between silica gel and Alix material.

From equation (3.20), some values of $\bar{\sigma}_{av}$ were calculated and are listed in Table 3.23. The plots of $\bar{\sigma}_{av}$ versus reaction time are shown on Figures 3.36 and 3.37. The results show that the average particle size changes with reaction time practically the same way regardless of the type of silica used for the synthesis (silica gel or Alix material). The general trend of these curves consists in a slow growth of the particles from 30 to 90 minutes, after an induction period of about 30 minutes. Then, a very fast growth occurs between 90 and 120 minutes, which ends rapidly after 2 hours; very little increase in size is observed up to 72 hours. For both sources of silica, and at a reaction time of 1 hour the frequency factor $\bar{\sigma}_{av}$ (equation 3.20) gives an average particle size of $<0.1 \mu\text{m}$ ($<1000 \text{ \AA}$). Average particle dimensions can also be obtained from the broadening of the Bragg peaks (XRD), using the Scherrer method, after correction for instrumental broadening as described in Section 3.1.2.1, however, this technique is limited to the range ca. $40 - 1000 \text{ \AA}$. The above XRD method gave a crystallite size of 861 \AA for both sources of silica, which is in agreement to the value obtained by using the frequency

Sample #	Source of Silica	Reaction Time (Hours)	ϕ_{av} (μm)
VA09	Silica gel	1.0	<.1
VA07		1.5	0.5
VA08		2.0	2.2
VA05		72.0	2.6
VAA16	ALIX 168	1.0	<.1
VAA15		1.5	0.3
VAA17		2.0	2.0
VAA06		72.0	2.9

Table 3.23 Study of the average particle dimension of Na-A zeolite versus reaction time. The reaction temperature was kept constant at 100 °C.

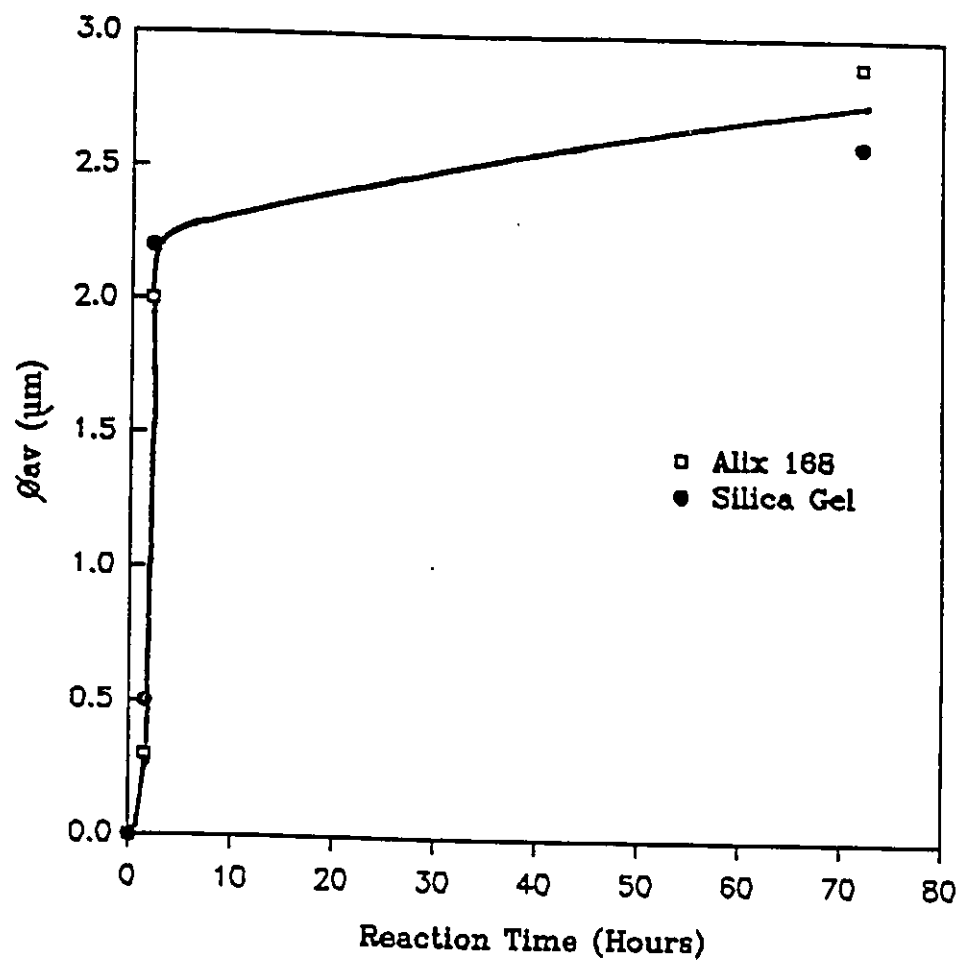


Figure 3.36 Average particle dimension of Na-A zeolite versus reaction time.

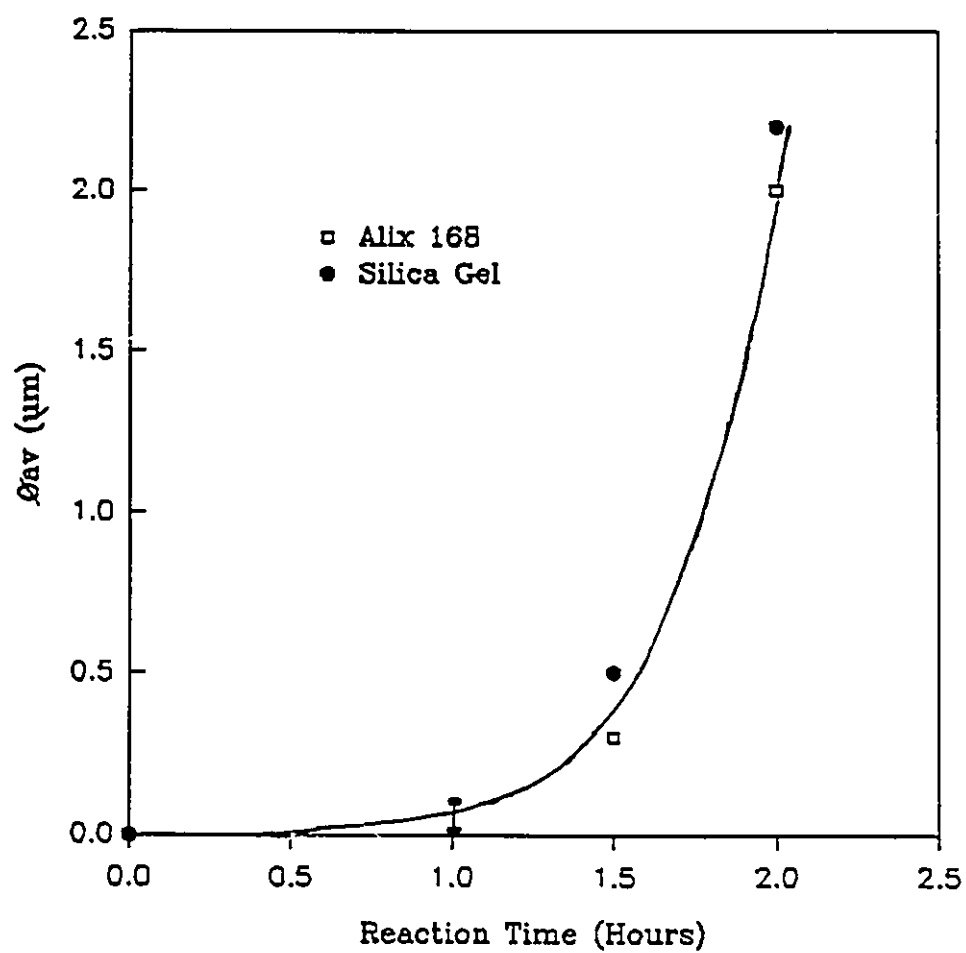


Figure 3.37 Average particle dimension of Na-A zeolite versus reaction time in the first two hours.

factor method ($< 1000 \text{ \AA}$). The good correlation between the two methods supports the validity of the techniques used.

3.4.7 Kinetic study by bulk density measurements

It has been reported in the literature [43] that the density of a fully hydrated zeolite Na-A is $1.99 \pm 0.1 \text{ g/cm}^3$, when measured by the flotation method. Since only polycrystalline samples were prepared in this work and the flotation technique requires single crystals, we used the Archimedean method, which consists in measuring the weight of liquid displaced by the sample. This technique is described in detail in section 2.4.

No significant change of density is observed versus reaction time or with the nature of the source of silica (Table 3.24). In most cases, the density is in the range $1.9 - 2.0 \text{ g/cm}^3$, which compares well with literature values: Alix with MLD=94% ($\rho=2.0$) and Na-A zeolite ($\rho=1.99$) [43].

Fluctuations within this range look erratic; this is probably due to a variable degree of hydration, which is difficult to control. Adsorption of water in the pores of the zeolite increases the weight of the sample without changing its volume, and therefore leads to an increase in density. Desorption has the opposite effect. Since the densities of both silica sources and that of the final zeolite are approximately the same, the density changes little during the reaction and therefore cannot be used as an indicator for the advancement of the reaction.

Sample #	Source of Silica	Reaction Time (Hours)	Bulk Density (g/cm ³)
VA10	Silica gel	0.6	1.97
VA07		1.5	1.91
VA08		2.0	2.04
Alix 168		0	2.00
VAA16	ALIX 168	1.0	2.00
VAA15		1.5	1.93
VAA17		2.0	1.97
VAA12		3.0	1.90
VAA11		6.0	1.93
VAA10		18.0	1.99
VAA14		24.0	2.00
VAA09		48.0	1.88
VAA06		72.0	2.02
Na-A zeolite	commercial		1.99

Table 3.24 Bulk density of Na-A zeolites versus reaction time and the source of silica used.

3.4.8 Specific surface area of Na-A zeolites by BET.

BET experiments were carried out in order to determine the influence of reaction time on the specific surface area when Na-A zeolite was synthesized from different sources of silica.

Commercial Na-A zeolite with a 4 \AA pore size (Type 4A LINDE) was first used as a standard control. This pore size is too small to allow for any adsorption of nitrogen molecules. As expected, no specific surface area higher than $114 \text{ m}^2/\text{g}$ was obtained even if the degassing time and/or the temperature were increased, because of the difficulty in nitrogen adsorption due to the small pore apertures (Table 3.25).

BET experiments were performed by using a commercial Ca exchanged A type zeolite of pore size of 5 \AA (Type 5A LINDE). This consists of zeolite Na-A partially cation exchanged with Ca^{2+} in order to have increased pore apertures relative to the sodium form. For the Ca exchanged A type zeolite, surface areas as high as 635 to $630 \text{ m}^2/\text{g}$ were recorded, since it has pore dimensions wide enough to allow a comfortable fit for N_2 molecule.

The N_2 molecular diameter reported in the literature varies from 3.15 to 3.75 \AA , depending on the reference [92,94]. This is close enough to the pore size of 4 \AA to prevent the nitrogen molecules from entering the pores. This emphasizes the necessity to have pore sizes large enough to

Sample and pore size (Å)	Specific Surface Area (m ² g ⁻¹)	Degassing Time (Hours)	Degassing Temperature (°C)
Na-A, 4 Å	69.5	3.0	250
Na-A, 4 Å	31.6	4.0	152
Na-A, 4 Å	62.9	4.0	225
Na-A, 4 Å	79.7	4.0	225
Na-A, 4 Å	114.2	4.0	225
Na-A, 4 Å	85.6	14.0	225
Na-A, 4 Å	66.2	14.0	225
Na-A, 5 Å	680.0	4.0	225
Na-A, 5 Å	634.6	4.0	225
Na-A, 5 Å	668.7	4.0	225
VA08, --	82.3	4.0	225

Table 3.25 Specific surface area measurements of zeolite Na-A using the BET technique.

allow entry of the gaseous molecules to where the adsorption sites are located.

A BET experiment was run on a zeolite synthesized using silica gel as source of silica (VA08). The measured specific surface area value of $82.3 \text{ m}^2/\text{g}$ was quite similar to the values obtained when commercial Na-A zeolite with pore size of 4 \AA was used. This result suggests that the pore size for Na-A zeolites prepared using silica gel is not larger than 4 \AA .

The small pore sizes created a difficulty in getting an efficient nitrogen adsorption on most of the samples. This made it impossible to get valuable information regarding variations of BET specific surface areas with reaction time, and to compare specific surface area values between the zeolites prepared using the two sources of silica.

3.4.9 ^{29}Si Magic Angle Spinning Solid State NMR study of the formation of Na-A zeolite.

^{29}Si Magic Angle Spinning Solid State NMR was used to investigate the crystallization of Na-A zeolite. The instrumentation and experimental parameters were discussed in Section 2.8.

The results are listed in Table 3.26 and shown on Figure 3.38. After a reaction time of 1 hour at 100 °C, X-ray diffraction showed that only little zeolite had been formed and SEM data supported the presence of mostly amorphous alumino-silicate gel for both sources of silica, silica gel and Alix 168. This is in agreement with the observation of a single broad NMR signal, near -85 ppm relative to tetramethylsilane, TMS (fig. 3.38.a and e). The broadening of the peak is caused by a distribution of slightly different chemical shifts related to the presence of different environments of Si, i.e. $(\text{SiO})_{4-n}\text{Si}(\text{OAl})_n$ units in the amorphous structure. The peak position of -85 ppm relative to TMS is in agreement with the presence of an amorphous form of alumino-silicate that contains a significantly high amount of aluminium (Si/Al=1) [91,95].

When the reaction was carried out over 1.5 hours, two peaks were detected for both sources of silica (fig. 3.38.b and f). One of the peaks, located near -85.0 ppm is the broad peak of amorphous alumino-silicate. The other, very narrow, peak located near -89 ppm relative to TMS, was

Sample#	Source of silica	reaction time (Hours)	peak position (ppm)	peak assignment
VA09	silica gel	1.0	-84.7	Al-Si
VA07	silica gel	1.5	-84.6 -89.3	Al-Si Na-A zeolite
VA08	silica gel	2.0	-89.4	Na-A zeolite
VA05	silica gel	72.0	-89.6	Na-A zeolite
VAA16	Alix 168	1.0	-84.6	Al-Si
VAA15	Alix 168	1.5	-84.8 -89.0	Al-Si Na-A zeolite
VAA17	Alix 168	2.0	-89.2	Na-A zeolite
VAA06	Alix 168	72.0	-89.2	Na-A zeolite
Na-A zeolite [95]			-88.9±0.5	Na-A zeolite

Table 3.26 ^{29}Si Solid State NMR of synthesized Na-A zeolite. Silica gel and Alix 168 were the two sources of silica used. Al-Si in the above table stands for amorphous aluminosilicate.

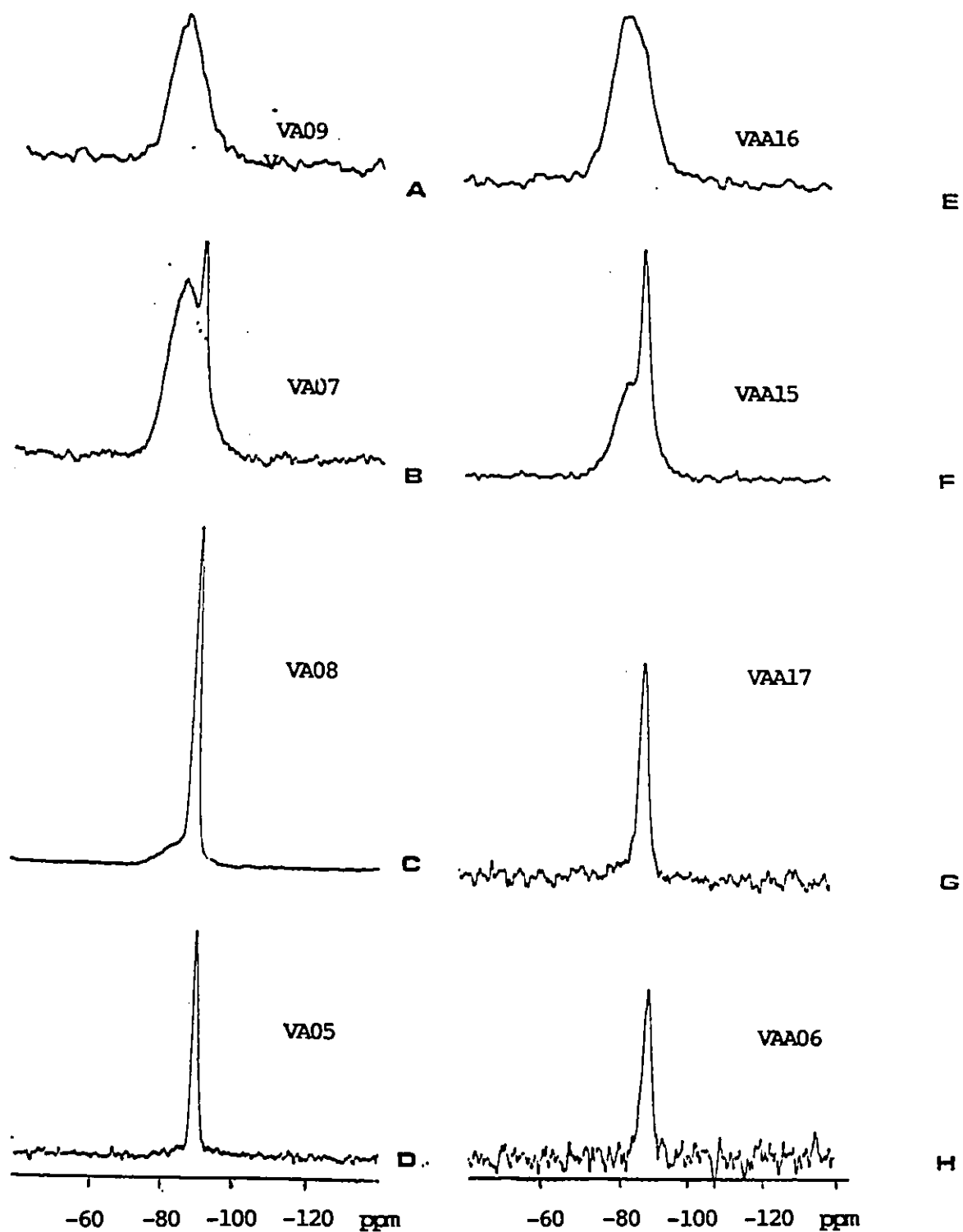


Figure 3.38 ^{29}Si Magic Angle Spinning NMR of Na-A zeolite samples obtained from silica gel and Alix 168.

attributed to the formation of some zeolite Na-A crystallites. The chemical shift of -88.9 ± 0.5 ppm relative to TMS reported in literature for Na-A zeolite [96] is in good agreement with our experimental value. The ratio of the intensities of the two types of Si is 1 : 2.4 when Alix 168 was used compared to the 1 : 1.2 when silica gel was the source of silica. The higher ratio obtained for samples originating from Alix 168 confirms the larger amount of zeolite measured by X-ray diffraction (DC = 58.3%) after a reaction time of 1.5 hours compared to silica gel (DC = 28.7%).

After a 2 hour reaction, only a small remnant of the amorphous alumino-silicate gel is still evident when silica gel was used, for longer reaction times (72 hours) the only peak observed was that of Na-A zeolite at around -89 ppm [91,92-99].

The presence of a single ^{29}Si resonance in the spectrum of zeolite A shows that Si and Al are ordered and the chemical shift corresponds to the Si(4Al) signal, which is in agreement with the suggested Loewensteinian principle [96,97].

The impurity phases detected by X-ray diffraction (Section 3.3.4) could have expected to give rise to extra NMR peaks due the existence of several Si environments. However, the experimental results for reaction times of 2 hours or longer show no evidence of additional peaks. This is in agreement with the low amount of impurity observed by X-ray

diffraction, but it could also mean that the Si environment is very similar in all phases, i.e. in 13A zeolite and the impurities, although this is an unlikely situation.

CHAPTER 4 Conclusion

A detailed investigation of the X-ray powder diffraction pattern of chrysotile asbestos, in the light of structural and textural information known from earlier works, has led to a full interpretation of all lines, including their particular line broadening pattern. The batch 7TF12 of chrysotile from Asbestos contains orthochrysotile-20_{C1} $\text{Mg}_3\text{Si}_2\text{O}_5(\text{OH})_4$, brucite $\text{Mg}(\text{OH})_2$ and pyroaurite $\text{Mg}_6\text{Fe}_2\text{CO}_3(\text{OH})_{16} \cdot 4\text{H}_2\text{O}$. Brucite is commonly found in chrysotile asbestos, however, this is the first report of the presence of pyroaurite impurity in chrysotile; although its peaks were observed by others, they had not been identified.

The peculiar pattern of the linewidth has been fully explained. Brucite is found to be fully crystalline, and free of strains and stacking faults. The average particle diameter of pyroaurite is slightly smaller than 1,000 Å. For chrysotile, because of the fibrous structure, the broadening of the Bragg peaks is a function of direction and has a different origin for each direction:

- along the \vec{a} axis: the helicoidal winding of the sheets along the \vec{a} axis destroys the periodicity in this direction, and as a result, no (h 0 0) peak is observed;
- along the \vec{b} axis: the curvature of sheets, due to bulky magnesium ions, creates a very large non-uniform internal strain along \vec{b} , which results in a very large broadening; some uniform strain is

also probably present and is responsible for the lineshift;

- along the \vec{c} axis: the line broadening is due to the small diameter of the fibers; the result from X-ray diffraction (average diameter of 170 Å) is in good agreement with the value of 200 Å found by electron microscopy.

The study of leaching of chrysotile asbestos has shown that the reaction is a multistep process which is thermally activated. First, the basic impurities contained in the mineral asbestos, are dissolved. This is followed by leaching of the "brucite-type" magnesium, which is more basic and less strongly bound to the lattice than the "skeletal" Mg, since it is not linked to the silicon oxide layer. This results in minor structural modifications only, and has no major effect on the morphology and crystallite shape. On the other hand, a net decrease of compactness (i.e. density) and degree of crystallinity result and the porosity and surface area show a large increase. The second step is mostly concerned with the removal of the skeletal magnesium, which is linked to silicon via oxygen bridges. This causes a structural collapse, resulting in the formation of finely divided amorphous silicon dioxide hemihydrate $\text{SiO}_2 \cdot 0.5\text{H}_2\text{O}$. In that step, designated as "degradation of the fiber", some important changes have been observed in morphology [11], in crystallinity, as well as in porosity.

Results from bulk density measurements strongly supports the presence of the two main structural steps in the leaching process. The four regions observed when bulk density is plotted against MLD values provide a better understanding of the leaching process. The first part of the curves (fig. 3.13, 3.15, and 3.15) show little changes in density and correspond mostly to the dissolution of basic impurities. Then, a drastic decrease in bulk density is observed, as "brucite-type Mg" is leached without major structural modifications. Then, leaching of some of "skeletal-type Mg" results in an increase in compactness, which cancels the weight loss and results in little change in density. Finally, the end of the removal of "skeletal-type Mg" leads to a material with a density significantly lower than for other types of silica usually encountered, which shows the high porosity and the low compactness of the final product obtained. This conclusion was also suggested from measurements of high values of specific surface area [11,28], however the present work is the first direct measurement of the compactness of the materials.

The study of the crystallinity supports these results by the considerable losses in DC obtained (reduced nearly to zero), due to the formation of a final amorphous material.

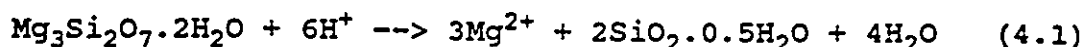
The study of leaching of chrysotile asbestos has been done by using two different types of system [11]:

- 1) The use of strong mineral acids such as HCl and H₂SO₄ leads to an aggressive leaching, which can be complete

if harsh conditions are used (high temperature, high concentration, long reaction time), however, it gives poor control for fine tailoring of MLD of intermediate values (50-80%). The results are usually weakly dependent on the nature of the strong acid.

- 2) A two step leaching process has been designed in order to make fine tailoring possible of the MLD of the final product. For this purpose, a first attack of the parent chrysotile asbestos with a mineral acid under very mild conditions is performed in order to obtain a MLD value of about 50 - 60%. The following step is the fine tuning of leaching with a weak organic acid such as acetic acid (ACA), oxalic acid (OXA), and ethylenediamine tetraacetic acid (EDTA), in order to have a better control of the extent of magnesium removal. In this process it appeared that the nature of the acid is also a main experimental parameter, i.e. its strength (the pH of its solution) and the chelating effect (for removal of iron oxides).

The acid leaching equation (4.1) as stated in [11] and in section 3.2.9 just describes the overall stoichiometry of the reactions, however, it does not provide information about its mechanism.



Leaching obviously occurs according to a mechanism

involving several steps. Based on our experimental results, the most probable mechanism has been proposed in section 3.2.9, and which involves three distinctive steps, in addition to removal of impurities. However, most of our results also show that the validity of well defined steps is strongly questioned and strong overlap is evident from the wealth of physico-chemical characterization techniques we or Kipkemboi [11] have used, namely IR, ^{29}Si MAS NMR, SEM, bulk density and X-ray diffraction.

The main reason for the reactional overlaps is the rolled up double layered structure of chrysotile. The first Mg containing layer situated on the outermost side of the fibril, is first attacked by the acid. On that layer, the "brucite-type" Mg atom are preferentially leached out compared to "skeletal" Mg due to their stronger basicity and absence of links to Si. Although the multistep reaction mechanism is most likely valid on one given layer only, i.e. the layer directly exposed to the acid, it cannot account for the whole solid because unwinding of the fibers has to occur before deeper layers are exposed to the acid, which delays the reaction for the deeper layers. Some "skeletal" Mg is obviously leached out before complete dissolution of all of the "brucite-type" Mg, as we have observed for a MLD as low as 55%.

Interpretation of the results was made more complex by the presence of two magnesium containing impurities, $\text{Mg}(\text{OH})_2$ brucite and $\text{Mg}_6\text{Fe}_2\text{CO}_3(\text{OH})_{16} \cdot 4\text{H}_2\text{O}$ pyroaurite, which give

unleached asbestos a higher Mg content than the theoretical value. They also add an undesired component to DC (values larger than 100% after mild leaching), however, when appropriately accounted for, the distortion they cause to the result could be minimized. All the Alix samples studied in this work were prepared by Kipkemboi [11]. He could probably have selectively eliminated the basic impurities by a quick and very mild acid attack, for example by using a low concentration (0.5 N) of a strong acid at ambient temperature for a short period of time (30 minutes).

The preparation of the Alix material is a necessary intermediate step in the synthesis of chryso-zeolite. Alix are used as a source of silica for the synthesis of the zeolites, and also as a matrix for the growth of zeolite crystallites. The properties of the final chryso-zeolites are strongly dependent on the properties of the Alix used for the synthesis, and they differ if silica gel is used instead of an Alix.

In the second part of the work presented in this thesis, hydrothermal syntheses of chryso-zeolites of types A,X, and Y have been performed.

Sodium aluminate was the only source of alumina used whereas two different sources of silica were compared for zeolite synthesis. Alix materials previously obtained from acid leaching of chrysotile asbestos was one source of silica, the other was commercial silica gel. The zeolites prepared from Alix material were grouped under the generic

name "chryso-zeolites". In these syntheses, Alix materials were not only used as source of silica but also as a matrix support for the growth of zeolite crystallites.

The first type of zeolite synthesized was Na-Y zeolite, using silica gel as the source of silica. All samples obtained were identified by their X-ray powder diffraction patterns and they contained significant amounts of impurities. The major side-product was identified as zeolite P_t . The formation of several crystalline phases in each sample showed the lack of refinement of the experimental parameters such as gel composition, reaction time, reaction temperature and mixing.

The effect of aging or digestion of the reaction mixture at room temperature prior to synthesis on the purity of Na-Y zeolite was also investigated. A net decrease of the relative intensity of the Bragg peaks of all undesired phases (zeolite P_t , and the others) compared to the desired Na-Y zeolite phase was observed when room temperature digestion was performed for 24 hours.

The second type of zeolite prepared was Na-X zeolite. Two sources of silica were used and their effect compared, i.e. silica gel and Alix materials. Silica gel was used in order to define optimum gel composition requirements based on the appropriate composition range reported in the literature. The major impurity phase found in these syntheses was zeolite P_t , which could be expected based on the free energy relations discussed in Section 3.3.1.

The formation of zeolite P_t in the synthesis of zeolite Na-Y can also be related to the above free energy relations, phase a, being zeolite Na-X or Na-Y depending on the initial gel composition, which represents the most stable of the metastable phases. This metastable phase was the first one to be formed. The use of an experimental temperature of 100 °C was in principle, a sufficient factor to allow the formation of zeolite P_t phase, which is the most thermodynamically stable phase b since for these systems, the transition temperature between a and b is around 100 °C.

Na-X chrysozeolites were also synthesized by using Alix materials of variables MLD values, varying from 84 to 99 %. Since similar X-ray diffraction patterns were obtained regardless of MLD (within the range 84 to 99%), variations in Mg content in the lower range of Mg concentration does not seem to affect the nature of the final product. However, for the same gel composition between samples such as VX01 synthesized from silica gel, and VAX02 and VAX03 synthesized from Alix materials, similar XRD patterns were obtained regardless of the source of silica. In these samples, Na-X zeolite was obtained as the major phase. Several undesired phases can be detected, in which only one could be identified as zeolite P_t .

The third type of zeolite that was prepared was Na-A zeolite using three sources of silica, silica gel, Alix materials and sodium silicates. Several samples were prepared by using silica gel, and this study showed that for

the same source of silica, i.e. silica gel, variations in the chemical composition of the reaction mixture leads to the formation of different zeolitic phases. In this case, Na-X was formed instead of Na-A at high silica to alumina ratio and at low concentration in alkali.

For most reactions using silica gel, Na-A zeolite was obtained as the major crystalline phase. However, crystalline by-products were detected, by the presence of several Bragg peaks which could not be attributed to Na-A zeolite. Only one of these impurities could be identified, and it was zeolite HS (hydrosodalite).

When another source of silica, i.e. sodium silicate, was used, with the same gel composition, surprisingly, the only crystalline phase obtained was zeolite HS, whereas Na-A zeolite was found to be the major crystalline phase when silica gel was used. This result showed that the required initial gel composition may differ with the type of silica source used. Therefore, the source of silica is influential on the type of zeolite phase that will be obtained from synthesis.

A third source of silica was used for the synthesis of Na-A zeolite. Synthesis was carried out by using the same gel composition as above by using Alix materials with MLD values of 94.0 and 98.7 %. The corresponding XRD patterns showed the formation of similar phases as with silica gel. When Alix materials were tested versus MLD, all other experimental parameters being identical, there was absolutely

no difference in the diffraction patterns that could be related to the variable MLD in the range 84 to 100%. This result is consistent with our study of Na-X zeolite in the same MLD interval.

A kinetic study of the synthesis of Na-A zeolite was performed. This study is exploratory because a detailed investigation would have required a much larger number of experiments, well beyond the scope of this M.Sc. thesis.

The difference in the rate of formation of Na-A zeolite between the two different sources of silica used, i.e., silica gel and Alix material, was found to be related to their difference in solubility in the aqueous reaction mixture. Alix material was found to be far more soluble than silica gel and therefore more reactive. After 10 minutes, 69% of Alix material was in solution, compared to a value of 41% for silica gel. After 20 minutes, the solubility of Alix material increased from 69 to 87%, whereas for silica gel, in the first 40 minutes in solution, no appreciable increase in silica solubility occurred, which stayed below 50%. The difference in solubility between the two materials is probably related to the degree of polymerization of silica species: the longer solubilization time observed with silica gel probably indicates a higher degree of polymerization. Therefore, in this case, depolymerization must occur, leading to dissolution. The requirement for depolymerization was also evidenced by the longer induction times found when silica gel was used as source of silica for the synthesis of

zeolites, and by the lower intensities of Bragg peaks observed in the diffraction patterns for a reaction time of 90 minutes or shorter.

At this point, it is quite clear that the silica available from silica gel is more polymerized than that existing in Alix materials. However, we have no evidence that Alix materials produced only monomeric forms of silicate species: low molecular weight polymerized silicate species may also be found if the acid attacks during leaching of chrysotile does not break all Si - O - Si bridges.

Further investigation using ^{29}Si NMR on the remaining mother liquor samples after filtration in the solubility experiments would probably be suitable for a detailed investigation of the distribution and type of structural silicate units present in the mother liquor. Lower molecular weight silicate anions would be expected to be found in the mother liquor in the case of Alix materials than in the case of silica gel.

The curves for the kinetics of crystallization are sigmoidal for both sources of silica, as expected, and in agreement with literature. However, mathematic deviations of that type or curves have been reported. Unfortunately, the low number of experimental points obtained in this exploratory work did not make possible a detailed analysis of the kinetics.

Evaluation of the induction period is usually done by extrapolating to the time axis, the tangent representing the

maximum rate of deposition of crystals. However, this procedure is not based upon the quantitative model of kinetics of nucleation, making its evaluation empirical. Our results show a shorter induction period when Alix material was considered. This observation is supported by the higher solubility of Alix materials, compared to silica gel.

The determination of the rate of formation of Na-A zeolite was not possible because of the low number of data available. However, it appears that the reaction with silica gel follows a first order kinetic law in the initial stages (< 2 hours). When Alix 168 was used, the reaction rate was much lower at 2 hours, in agreement with the shorter induction period and larger solubility of Alix materials.

The morphological study of the samples yielded similar results regarding the comparison of the two sources of silica considered. Using the electron micrographs, it was possible to follow the formation of cubic shaped crystallites of Na-A zeolite with time.

From the same micrographs it was possible to evaluate the frequency factor of particle sizes (ϕ_{av}), i.e. the average diameter of particles. When ϕ_{av} is studied with respect to reaction time, one can observe a drastic increase in the average diameter of particles in the range 1.5 to 2 hours. For longer reaction times, only a moderate increase in average diameter of particles occurred, i.e. a maximum size has been reached. The behavior of the two sources of silica was similar. For a reaction time as low as 1 hour, the

average diameter of the particles was evaluated from the SEM micrographs to be $< 1000 \text{ \AA}$. This was double-checked by the Scherrer method, using the broadening of the X-ray diffraction peaks, which gave a crystallite size of 861 \AA for both sources of silica.

Bulk density measurements were made, however, the progression of the reaction cannot be evaluated by this technique since both sources of silica and Na-A zeolite have very similar densities. In addition, erratic fluctuations of the measured density were observed, which are probably due to the variable degree of hydration of the zeolite tested.

Since the pore sizes of 4 \AA were too small to allow entry of nitrogen molecules, the specific surface areas of Na-A zeolites could not be measured by the BET technique.

On the other hand, ^{29}Si Solid State NMR was a useful technique for following the formation of Na-A zeolite. After a reaction time of 1 hour, only the broad band near -85 ppm (relative to TMS) of amorphous alumino-silicate gel was observed. This is supported by the corresponding SEM micrographs which show only an amorphous solid, and by X-ray diffraction. At longer reaction times a considerable amount of Na-A zeolite was produced. This was measured by the appearance of the characteristic narrow peak in the -89 ppm region. As the reaction progressed, the intensity of this peak increased and the broad band (at -85 ppm) decreased. After a reaction time of 1.5 hours a relatively higher band ratio for amorphous/zeolite of 1 : 2.4 was found for Alix

material, compared to a 1 : 1.2 ratio for silica gel. This further evidenced that a greater amount of Na-A zeolite had been formed from the Alix material than from the silica gel.

In summary, zeolite was synthesized in a comparative study of the effect of two sources of silica on the course of reaction, i.e. on the nature of the products and on the kinetics of formation of zeolites. The conditions of the reaction were optimized and the products were studied. The techniques that were most useful for the characterization of the products were identified. A detailed study of the kinetics of crystallization of zeolites would have required a much larger number of reactions, well beyond the scope of the study undertaken for this project, therefore this part of this thesis should be considered as being exploratory. More data must be obtained in order to determine the order of reaction for crystal growth, the activation energy and the significance of the induction period, for the various sources of silica. It has been established that leached asbestos (Alix) can be used for the synthesis of zeolites, and it is more efficient than silica gel, a conventional commercial source of silica. This procedure also has the advantage of using an abundant natural resource of Quebec, Chrysotile asbestos. Because it is carcinogenic many uses of asbestos have been banned. Upon acid leaching, the fibrous structure of chrysotile is destroyed, which results in a complete disappearance of its carcinogenic properties. Therefore, its use as a source of silica for the synthesis of zeolites (we

call "chryso-zeolite") provides a useful and safe application of this otherwise nefarious material.

Further studies would require more work to determine the ideal conditions for the synthesis of these zeolites, in order to eliminate impurities. Finally, a ^{29}Si NMR spectrum of the mother liquor obtained upon filtration of the undissolved silica could give indications about the degree of polymerization of silicate species for each source of silica.

REFERENCES

1. "Chrysotile Asbestos: a Material for Today and Tomorrow", Direction des Communications du Ministère de l'Energie et des Ressources, #15BN 2-550-16034-7, M 826, Quebec, (1986).
2. "Asbestos", Energy, Mines and Resources Canada, # M35-28, 1986E, Ottawa, (1986).
3. W.E. Sinclair, "Asbestos its Origin, Production and Utilization", Mining Publications, LTD, London, 2^e ed., 1959, pp. 277-315.
4. R. Le Van Mao and P.H. Bird, U.S. Pat. 4511667, April 16, (1985).
5. P. Levesque, Ph.D. Thesis, Concordia University, Montreal, Canada, Septembre 4, 1987.
6. R. Le Van Mao, P. Kipkemboi, A. Vaillancourt, P. Levesque, and G. Denes, "Leached Asbestos Materials: Precursors of Zeolites.", Zeolites, 9, pp. 405-411, (1989).
7. E.M. Flanigen, "Molecular Sieve Zeolite Technology: The First Twenty Five Years", in "Zeolites: Science and Technology, NATO ASI Series, no. 80, (1984), pp. 3-34.
8. R. Le Van Mao, Private Communication.
9. R. Le Van Mao, U.S. Pat. 4615995, October 7, (1986).
10. R. Le Van Mao, P. Levesque, B. Sjiariel and P.H. Bird, Can. J. Chem., 63, (1985), pp.3464-3470.
11. P. Kipkemboi, M.Sc. Thesis, Concordia University, Montreal, Canada, March 1988.
12. G.T. Kokotailo, "Zeolite crystallography", in "Zeolites: Science and Technology, NATO ASI Series, no. 80, (1984), pp.83-108.
13. W.M. Meier, "Molecular Sieves", Society for Chemical Industry, London, (1968), p. 10.
14. D.W. Breck, " Zeolite Molecular Sieves", John-Wiley and Sons, New-York, (1974), pp. 29-133.

15. J.V. Smith, "Origin and Structure of Zeolites". in "Zeolite Chemistry and Catalysis, J. A. Rabo, ACS Monograph, 171, Am. Chem. Soc., (1976), pp.1-79.
16. R.M. Barrer, "Molecular Sieves", Society of Chemical Industry, London, (1968), pp.1-42.
17. W.A. Wachter, "Statistical and Topological Approaches to Modelling Zeolite Acidity, Activity and Stability", in "Proceedings of the Sixth International zeolite Conference, D. Olson and A. Bisio, Butterworths, (1984), pp. 141-150.
18. P. Aitcin, F. Kimmerly, "L'Amiante Chrysotile", Universite de Sherbrooke, November 1981, p. 6-2.
19. P. Kipkemboi, M.Sc. Thesis, Concordia University, Montreal, Canada, March 1988, p.11.
20. Bragg and al., Krist. 76, p. 201, (1930).
21. B. Warren and K.W. Herring, Phys. Rev., 59, p. 925, (1941).
22. P. Aitcin, F. Kimmerly, "L'Amiante Chrysotile", Universite de Sherbrooke, November 1981, p. 8-6.
23. E.J. Whittacker and J. Zussmann, "The Characterization of Serpentine Minerals by X-ray Diffraction", Mn. Mag., 31, (1956).
24. K. Yada, "Study of Chrysotile Asbestos by a High Resolution Electron Microscope", Acta. Crysta., 23, (1967), pp. 704-707.
25. P. Aitcin, F. Kimmerly, "L'Amiante Chrysotile", Universite de Sherbrooke, November 1981, p. 8-10.
26. J. Assad and all, "Etude Mineralogique de l'Amiante au Quebec en Relation avec son Exploitation, Extraction et Utilisation", Universite Laval, Octobre 1976, p.25.
27. J. Assad and all, "Etude Mineralogique de l'Amiante au Quebec en Relation avec son Exploitation, Extraction et Utilisation", Universite Laval, Octobre 1976, p.19.
28. G. Denes, P. Kipkemboi, R. Le Van Mao, and A. Vaillancourt, "Magnesium Leaching of Asbestos Chrysotile as a New Route to Microcrystalline Silicon Dioxide.", in "Proceedings of International Symposium on the Production and Processing of Fine Particles", Montreal, 28-31 August 1988, pp. 599-607.

29. R.M. Barrer, "Hydrothermal Chemistry of Zeolites", Academic Press Inc., London, (1982).
30. L.D. Rollmann, "Synthesis of Zeolites, an Overview", in "Zeolites: Science and Technology", NATO ASI Series, no. 80, (1984), p. 114.
31. D.W. Breck, "Zeolite Molecular Sieves", John-Wiley and Sons, New-York, (1974), pp. 266-267.
32. R.M. Barrer, "Hydrothermal Chemistry of Zeolites", Academic Press Inc., London, (1982), pp. 133-185.
33. L.D. Rollmann, "Synthesis of Zeolites, an Overview", in "Zeolites: Science and Technology", NATO ASI Series, no. 80, (1984), p. 110.
34. W. Meise and F.E. Schwochow, "Kinetic Studies on the Formation of Zeolite A", in "Molecular Sieves", W.M. Meier and J.B. Uytterhoeven (eds), Advances in Chemistry series, no. 121, Am. Chem. Soc., USA, (1973), pp. 169-178.
35. A. Culfaz and L.B. Sand, "Mechanism of Nucleation and Crystallization of Zeolites from Gels", in "Molecular Sieves", W.M. Meier and J.B. Uytterhoeven (eds), Advances in Chemistry series, no. 121, Am. Chem. Soc., USA, (1973), pp. 140-151.
36. E.M. Flanigen, "A Review and New Perspectives in Zeolite Crystallization", in "Molecular Sieves", W.M. Meier and J.B. Uytterhoeven (eds), Advances in Chemistry series, no. 121, Am. Chem. Soc., USA, (1973), pp. 119-139.
37. F. Roozeboom, H.E. Robson, S.S. Chan, "Study on the Mechanism of Crystallization of Zeolites A, X and Y", in "Zeolites: Science and Technology", NATO ASI Series, no. 80, (1984), pp. 127-150.
38. D.W. Breck, "Zeolite Molecular Sieves", John-Wiley and Sons, New-York, (1974), pp. 249-251.
39. D.W. Breck and E.M. Flanigen, "Molecular Sieves", Society of Chemical Industry, London, (1968), p. 47.
40. E. Roland, "Industrial Production of Zeolites", in "Zeolites as Catalysts, Sorbents and Detergent Builders. Applications and innovations", H.G. Karge and J. Weitkamp, Elsevier, Amsterdam, (1989), pp. 645-659.
41. D.W. Breck, "Zeolite Molecular Sieves", John-Wiley and Sons, New-York, (1974), pp. 245-378.
42. D.W. Breck, U.S. Pat. 3,130,007 (1964).

43. R.M. Milton, U.S. Pat. 2,882,243 (1959).
44. R.M. Milton, U.S. Pat. 2,882,244 (1959).
45. D.W. Breck, "Zeolite Molecular Sieves", John-Wiley and Sons, New-York, (1974), p. 278.
46. B.D. Cullity, "Elements of X-ray Diffraction", 2^e ed., Addison-Wesley, Reading, Ma, (1959), pp.192-284.
47. G.S. Rajhans and J.L. Sullivan, "Asbestos Sampling and Analysis", Ann Arbor Science, (1981), pp. 204-231.
48. "Standard Test Method for Relative Zeolite Diffraction Intensities", in "Annual Book of ASTM Standards", Part 25, Petroleum Products and Lubricants (III), (1980), D 3906-8, pp. 970-977.
49. G.S. Rajhans and J.L. Sullivan, "Asbestos Sampling and Analysis", Ann Arbor Science, (1981), pp. 215-217.
50. G. Denes, Private Communication.
51. J.R. Anderson and K.C. Pratt, "Introduction to Characterization and Testing of Catalysts", Academic Press, Australia, (1985), pp. 169-173.
52. "International Critical Tables of Numerical Data", Physics, Chemistry and Engineering, Vol III, NRC, USA, McGraw-Hill, New-York, (1928), pp. 27-28.
53. G.S. Rajhans and J.L. Sullivan, "Asbestos Sampling and Analysis", Ann Arbor Science Publishers Inc., Michigan (1981), p. 216.
54. A.P. Middleton, "The Identification of Asbestos in Solid Materials", in "Asbestos", Volume 1: "Properties, Applications, and Hazards", L. Michaels and S.S. Chissick, ed., Wiley-Interscience, New-York (1979), p. 266.
55. JCPDS Powder Diffraction File, International Centre for Diffraction Data, Swarthmore, PA (1989).
56. J. Zussman, "The Mineralogy of Asbestos", in "Asbestos", Volume 1: "Properties, Applications and Hazards", L. Michaels and S.S. Chissick, ed., Wiley-Interscience, New-York (1979), p. 59.
57. G.S. Rajhans and J.L. Sullivan, "Asbestos Sampling and Analysis", Ann Arbor Science Publishers Inc., Michigan, (1981), pp. 11-12.

58. A.A. Hodgson, "Chemistry and Physics of Asbestos", in "Asbestos", Volume 1: "Properties, Applications and Hazards", L. Michaels and S.S. Chissick, ed., Wiley-Interscience, New-York (1979), pp. 75-79.
59. E.W. Nuffield, "X-ray Diffraction Methods", John-Wiley and Sons, New-York, (1966).
60. A.R. West, "Solid State Chemistry and its Applications", John-Wiley and Sons, (1984), pp. 115-186.
61. A.R. West, "Solid State Chemistry and its Applications", John-Wiley and Sons, (1984). pp. 173-175.
62. B.D. Cullity, "Elements of X-ray Diffraction", Addison-Wesley, Reading, MA (1959), pp. 96-103 and 261-263.
63. B.D. Cullity, "Elements of X-ray Diffraction", Addison-Wesley, Reading, MA (1959), pp. 263-269 and 444-453.
64. M.E. Lines and A.M. Glass, "Principles and Applications of Ferroelectrics and Related Materials", International Series of Monographs on Physics, Oxford Science Publications, Clarendon Press, Oxford (1979), pp. 155-160 and 364.
65. J. Zussman, "The Mineralogy of Asbestos", in "Asbestos", Volume 1: "Properties, Applications and Hazards", L. Michaels and S.S. Chissick, ed., Wiley-Interscience, New-York (1979), pp. 49-51.
66. ASTM 14-293, from Neumann and Bergstol, Mineral, Museum, Oslo, Norway, (sample from Langban, Sweden).
67. Swanson and Fuyat, NBS Circular 539, Vol. III, (1953), (ASTM 5-0490).
68. P. Aitcin, F. Kimmerly, "L'Amiante Chrysotile", Universite de Sherbrooke, November 1981, pp. 8-24 to 8-27.
69. R.O. Weast (ed.), "CRC Handbook of Chemistry and Physics", 61nd ed., CRC Press, (1980-1981), Florida, USA, p. B-116.
70. J.D.H. Donnay, G. Donnay, E.G. Cox, O. KenNard and M.V. King, "Crystal Data, Determinative Tables", ACA Monograph, no 5, 2nd ed., Washington, 1963.
71. R.O. Weast (ed.), "CRC Handbook of Chemistry and Physics", 61nd ed., CRC Press, (1980-1981), Florida, USA, p. B-143.

72. R.O. Weast (ed.), "CRC Handbook of Chemistry and Physics", 62nd ed., CRC Press, (1981-1982), Florida, USA, pp. D-142 to 143.
73. W.E. Harris and B. Kratochvil, "Chemical Separations and Measurements: Background and Procedures for Modern Analysis", Saunders Golden Series, Saunders College, Philadelphia, (1974), p. 67.
74. G. Denes, "Preparation, Characterization, Magnetic and Mossbauer Spectroscopic Studies of Microcrystalline and Amorphous Iron Trihydroxide", in "Proceedings of the International Symposium on the Production and Processing of Fine Particles", Vol. 7, (1988), pp. 615-626.
75. F. Pundsack and G. Reimschuessel, J. Phys. chem., 60, 1218 (1956).
76. D.W. Breck, "Zeolite Molecular Sieves", John-Wiley and Sons, New-York, (1974), pp. 247-251.
77. J.R. Goldsmith, J. Geol., 68, 533 (1960).
78. D.W. Breck, "Zeolite Molecular Sieves", John-Wiley and Sons, New-York, (1974), pp. 277-279.
79. E.M. Flanigen, "Molecular Sieve Zeolite Technology: The First Twenty Five Years", in "Zeolites: Science and Technology, NATO ASI Series, no. 80, (1984), p. 15.
80. D.W. Breck, "Zeolite Molecular Sieves", John-Wiley and Sons, New-York, (1974), p. 246.
81. R.M. Barrer, "Hydrothermal Chemistry of Zeolites", Academic Press Inc., London, (1982), p. 176.
82. L.D. Rollmann, "Synthesis of Zeolites, an Overview", in "Zeolites: Science and Technology", NATO ASI Series, no. 80, (1984), pp. 109-126.
83. D.W. Breck, "Zeolite Molecular Sieves", John-Wiley and Sons, New-York, (1974), pp. 347-378.
84. D.W. Breck, "Zeolite Molecular Sieves", John-Wiley and Sons, New-York, (1974), pp. 72-74.
85. R.M. Milton, U.S. Pat., 3,008,803, (1961).
86. D.W. Breck, "Zeolite Molecular Sieves", John-Wiley and Sons, New-York, (1974), pp. 273-277.

87. E. Roland, "Industrial Production of Zeolites", in "Zeolites as Catalysts, Sorbents and Detergent Builders. Applications and innovations", H.G. Karge and J. Weitkamp, Elsevier, Amsterdam, (1989), p. 651.
88. D.W. Breck, "Zeolite Molecular Sieves", John-Wiley and Sons, New-York, (1974), pp. 333-345.
89. G.G. Alexander, W.M. Heston, Jr., and R.I. Iler, J. Phys. Chem., 58, (1954), p. 453.
90. P.S. Roller, Jr and G. Ervin, J. Am. Chem, 62, 468 (1940).
91. G. Engelhardt, B. Fablke, M. Magi, and E. Lippmaa, "High-Resolution Solid-State ^{29}Si and ^{27}Al N.M.R. of Aluminosilicate Intermediate in the Synthesis of zeolite A. Part II", Zeolites, Vol. 5, January 1985, pp. 49-52.
92. A.W. Adamson, "A Textbook of Physical Chemistry", 2nd ed., Academic Press, USA, (1979).
93. "Density of Liquid Mixture", Acta Crystallographica, Vol. 4, (1951), p. 565.
94. R.O. Weast (ed.), "CRC Handbook of Chemistry and Physics", 62nd ed., CRC Press, (1981-1982), Florida, USA, p. F-172.
95. C.H. Hsin and Y.L. Ting, Ind. Eng. Chem. Res., Vol. 29, No. 5, (1990), pp. 749-754.
96. J. klinowski, "Nuclear Magnetic Resonance Studies of Zeolites", in "Progress in NMR Spectroscopy", Vol. 16, (1984), pp. 237-309.
97. C.A. Fyfe, "Solid State NMR for Chemists", C.F.C. Press, Guelph, Ontario, Canada, (1983), pp. 337-361.
98. E. Lippmaa, M. Magi, A. Samoson, M. Tarmak, and G.J. Engelhardt, Am. Chem. Soc., 103, p. 4992.
99. C.A. Fyfe, G.C. Gchbi, J.S. Hartman, J. Klinowski, and J.M. Thomas, J. Phys. Chem., 86, (1982), p. 1247.

APPENDICES

APPENDIX 1

EVALUATION OF THE ERROR ON DENSITY MEASUREMENTS. [52]

1. Evaluation of the error of ρ_{solvent} .

$$\rho_1 \text{ CCl}_4 = 1.63255 - 0.001911 T - 0.69 \times 10^{-6} T^2$$

$$\rho_1 20^\circ\text{C} = 1.594054$$

$$\rho_1 22^\circ\text{C} = 1.590174$$

$$\rho_1 24^\circ\text{C} = 1.5862886$$

$$S_o \Delta \rho \text{ CCl}_4 = .002 \text{ g / cm}^3 \cdot \text{C}$$

2. Evaluation of $\Delta \rho$

$$\ln = \ln (m_3 - m_1) + \ln \rho_1 - \ln (m_3 - m_4 - m_1 + m_2)$$

$$\frac{d\rho}{\rho} = \frac{d(m_3 - m_1)}{(m_3 - m_1)} + \frac{d\rho_1}{\rho_1} - \frac{d(m_3 - m_4 - m_1 + m_2)}{(m_3 - m_4 - m_1 + m_2)}$$

$$\frac{\Delta \rho}{\rho} = \frac{\Delta(m_3 - m_1)}{(m_3 - m_1)} + \frac{\Delta \rho_1}{\rho_1} + \frac{\Delta(m_3 - m_4 - m_1 + m_2)}{(m_3 - m_4 - m_1 + m_2)}$$

$$\Delta \rho = \rho \left[\frac{m_3 + m_1}{m_3 - m_1} + \frac{\Delta \rho_1}{\rho_1} + \frac{\Delta m_3 + \Delta m_4 + \Delta m_1 + \Delta m_2}{m_3 - m_4 - m_1 + m_2} \right]$$

gives densities within 1-2 % error.

ALIX #	SiO ₂	Al ₂ O ₃	Na ₂ O	Fe ₂ O ₃	MgO
76	48.16	0.10	0.15	8.34	43.25
77	54.87	0.23	0.13	7.98	36.79
67	68.95	0.12	0.08	8.27	22.58
68	81.57	0.12	0.11	6.75	9.86
78	83.03	0.24	0.11	5.30	11.32
61	91.83	0.25	0.08	3.63	4.21
72	95.36	0.29	0.10	1.63	2.62
73	97.39	0.31	0.10	0.34	1.86
74	97.25	0.60	0.09	0.64	1.42
75	98.12	0.50	0.06	0.27	1.05
93	54.61	0.14	0.13	8.17	36.95
94	79.46	0.20	0.11	4.41	15.82
95	82.54	0.10	0.14	4.28	12.94
96	92.53	0.25	0.21	5.70	7.90
97	89.37	0.29	0.17	2.63	7.54
98	92.56	0.31	0.12	0.63	6.38
99	94.09	0.35	0.14	0.41	5.83
112	59.80	0.37	0.13	8.39	31.31
113	60.78	0.38	0.15	6.84	31.85
114	74.65	0.41	0.18	4.79	19.97
115	79.06	0.39	0.14	4.51	15.90
116	91.74	0.45	0.15	1.87	5.79
117	95.30	0.50	0.12	2.09	1.99
118	97.82	0.37	0.16	0.91	0.74
119	97.79	0.41	0.15	0.92	0.73
120	97.94	0.43	0.17	0.74	0.72
107	56.24	0.32	0.09	7.78	35.57
78	63.86	0.44	0.16	7.68	28.88
108	74.40	0.43	0.20	7.15	17.02
79	73.07	0.48	0.09	6.68	18.68
109	90.05	0.41	0.11	5.35	4.08
81	90.00	0.41	0.10	4.79	2.71
82	97.32	0.43	0.18	0.71	1.36
110	97.97	0.39	0.12	0.27	1.25
111	98.25	0.39	0.16	0.00	1.20

Appendix 2 Chemical composition of Alix materials (wt%, on dried oxides basis). Samples related to acid concentration experiments. [11]

ALIX #	SiO ₂	Al ₂ O ₃	Na ₂ O	Fe ₂ O ₃	MgO
86	77.02	0.57	0.10	7.57	14.74
87	80.19	0.36	0.12	7.11	11.76
88	83.35	0.35	0.15	6.55	9.60
63	87.93	0.50	0.10	4.04	7.43
89	88.73	0.43	0.18	4.22	3.61
90	90.97	0.54	0.12	4.84	3.53
61	91.83	0.25	0.08	3.63	4.21
60	93.69	0.32	0.11	1.89	3.99
62	94.57	0.42	0.09	1.38	3.54
91	93.91	0.61	0.08	2.97	2.43
92	95.33	0.20	0.09	2.23	2.15
100	67.39	0.29	0.13	5.33	26.86
101	78.09	0.21	0.12	5.79	15.79
102	84.51	0.51	0.15	4.77	13.45
95	84.99	0.10	0.14	4.28	10.49
103	87.13	0.14	0.18	4.07	8.48
104	89.69	0.16	0.11	4.12	5.92
105	90.37	0.20	0.09	3.51	5.83
138	79.34	0.26	0.10	6.42	13.88
139	80.37	0.29	0.10	5.81	13.43
140	82.18	0.31	0.13	6.15	11.23
141	84.75	0.29	0.11	5.75	9.10
142	88.43	0.36	0.10	3.70	7.41
143	88.39	0.37	0.12	3.88	7.24
144	88.35	0.36	0.11	4.75	6.43
145	88.44	0.41	0.12	4.64	6.39
146	90.78	0.39	0.12	4.32	4.39
147	91.49	0.43	0.13	3.39	4.56
148	92.74	0.45	0.10	3.11	3.60

Appendix 3 Chemical composition of Alix materials (wt%, on dried oxides basis). Samples related to leaching time experiments. [11]

Nature of the acid	Normality N	pH	Chemical composition of final Alix (wt %)					MLD %
			SiO ₂	Al ₂ O ₃	Na ₂ O	Fe ₂ O ₃	MgO	
Acetic Acid (a)	0.5	2.65	78.01	0.39	0.11	5.01	16.47	67.2
	1.0	2.50	78.68	0.50	0.15	5.97	14.70	70.7
	2.0	2.25	80.47	0.50	0.20	5.99	12.84	74.4
	3.0	2.00	81.22	0.47	0.17	5.98	12.16	75.8
	4.0	1.95	81.56	0.41	0.16	5.52	12.35	75.4
	5.0	1.90	84.69	0.43	0.12	3.63	11.13	77.8
Oxalic Acid (a)	0.5	1.40	79.78	0.41	0.15	2.64	17.02	66.1
	1.0	1.25	82.87	0.39	0.16	2.08	14.50	71.1
	2.0	1.10	83.97	0.42	0.15	1.90	13.56	73.0
	3.0	1.00	86.40	0.42	0.16	1.59	11.43	77.2
	4.0	0.70	87.43	0.41	0.19	1.51	10.46	79.2
	5.0	0.60	86.91	0.38	0.14	2.28	10.29	79.5
EDTA (b)	1.0	2.70	78.80	0.17	0.28	0.92	19.81	60.5
	2.0	2.60	80.02	0.22	0.38	0.67	18.71	62.7
	3.0	2.35	82.73	0.31	0.39	0.80	15.77	68.6
	4.0	2.30	85.03	0.26	0.41	0.56	13.74	72.6
	5.0	2.30	85.74	0.23	0.44	0.69	12.90	74.3

APPENDIX 4 Secondary leaching of chrysotile asbestos with weak organic acids. (volume of the acid solution was 100 ml, and the weight of the starting material was 10 g. In the case of (a) the starting material had a MLD=56.8%, and a MLD=55.0% when (b) was involved.)[11]

Nature of the acid	Leaching Time (hours)	Chemical composition of final Alix (wt %)					MLD %
		SiO ₂	Al ₂ O ₃	Na ₂ O	Fe ₂ O ₃	MgO	
Acetic Acid	1.0	85.20	0.48	0.12	5.47	11.64	76.8
	2.5	85.10	0.50	0.11	4.50	9.79	80.5
	4.0	86.70	0.43	0.13	4.13	8.63	82.8
	5.5	88.00	0.42	0.12	4.47	6.99	86.1
	7.0	89.2	0.44	0.10	4.38	5.97	88.1
Oxalic Acid	1.0	87.10	0.43	0.12	2.33	10.03	80.0
	2.5	88.60	0.49	0.15	2.32	8.47	83.1
	4.0	90.30	0.51	0.14	2.34	6.69	86.7
	5.5	91.20	0.45	0.14	2.30	5.95	88.2
	7.0	91.50	0.47	0.13	2.29	5.63	88.8

APPENDIX 5 Effect of time on the second leaching step with an organic acid. The volume of the acid solution was 100 ml, and the weight of the starting material was 10 g of Alix with a MLD=70.6. The concentration of organic acid was 3.5N and the temperature of the solution 80 °C. [11]

h k l	d (Å)	I (%)
1 1 1	14.29	100
2 2 0	8.75	9
3 1 1	7.46	24
3 3 1	5.68	44
3 3 3,	4.76	23
5 1 1		
4 4 0	4.38	35
6 2 0	3.91	12
5 3 3	3.775	47
4 4 4	3.573	4
7 1 1,	3.466	9
5 5 1		
6 4 2	3.308	37
7 3 1,	3.222	8
5 5 3		
7 3 3	3.024	16
8 2 2,	2.917	21
6 6 0		
7 5 1,	2.858	48
5 5 5		
8 4 0	2.767	20
9 1 1,	2.717	7
7 5 3		
6 6 4	2.638	19
9 3 1	2.595	11

APPENDIX 6 a) Zeolite Na-Y, $a = 24.73 \text{ Å}$; $\text{Si/Al} = 2$ [41]

h k l	d (Å)	I (%)
1 1 1	14.465	100
2 2 0	8.845	18
3 1 1	7.538	12
3 3 1	5.731	18
3 3 3,	4.811	5
5 1 1		
4 4 0	4.419	9
5 3 1	4.226	1
6 2 0	3.946	4
5 3 3	3.808	21
6 2 2	3.765	3
4 4 4	3.609	1
7 1 1,	3.500	1
5 5 1		
6 4 2	3.338	8
7 3 1,	3.253	1
5 5 3		
7 3 3	3.051	4
8 2 2,	2.944	9
6 6 0		
7 5 1,	2.885	19
5 5 5		
8 4 0	2.794	8
9 1 1,	2.743	2

APPENDIX 6 b) Zeolite Na-X $a = 24.93 \text{ Å}$; $\text{Si/Al} = 1.25$ [41]

h k l	d (Å)	I (%)
1 0 0	12.29	100
1 1 0	8.71	69
1 1 1	7.11	35
2 0 0	-----	--
2 1 0	5.51	25
2 1 1	5.03	2
2 2 0	4.36	6
2 2 1,	4.107	36
3 0 0		
3 1 0	-----	--
3 1 1	3.714	53
2 2 2	-----	--
3 2 0	3.417	16
3 2 1	3.293	47
4 0 0	-----	--
4 1 0,	2.987	55
3 2 2		
4 1 1,	2.904	9
3 3 0		
4 2 0	2.754	12
4 2 1	2.688	4
3 3 2	2.626	22
4 2 2	2.515	5
4 3 0,	2.464	4
5 0 0		
4 3 1,	-----	--
5 1 0		
5 1 1,	2.371	3
3 3 3		
5 2 0,	2.289	1
4 3 2		
5 2 1	2.249	3
4 4 0	2.177	7
4 4 1,	2.144	10
5 2 2		
5 3 0,	2.113	3
4 3 3		
5 3 1	2.083	4
6 0 0,	2.053	9
4 4 2		

APPENDIX 6 c) Zeolite Na-A a = 12.32 Å [41]

h k l	d (Å)	I (%)
1 1 0	7.132	85
1 0 1	7.047	83
1 1 1	5.776	5
2 0 0	5.048	51
0 0 2	4.914	26
1 0 2	4.420	8
2 1 1	4.108	94
1 1 2	4.049	22
2 0 2	3.527	4
2 1 2	3.328	18
3 1 0	3.194	100
1 0 3	3.117	64
3 1 1	3.036	10
1 1 3	2.979	5
3 0 2	2.776	3
2 0 3	2.750	5
3 2 1	2.694	46
3 1 2	2.679	28
2 1 3	2.653	21
4 0 0	2.531	6
3 2 2	2.435	5
1 0 4	2.387	4
4 2 0,	2.257	2
4 0 2		
4 2 1	2.206	2
2 1 4	2.159	2
4 2 2	2.055	1
5 1 0	1.982	2
4 1 3	1.966	2
1 0 5	1.929	1

APPENDIX 6 d) Zeolite P_t [41]

h k l	d (Å)	I (%)
1 1 0	6.28	80
2 0 0	4.44	30
2 1 0	3.97	5
2 1 1	3.63	100
2 2 0	3.13	5
3 1 0	2.81	60
2 2 2	2.56	80
3 2 1	2.37	30
3 3 0,	2.09	80
4 1 1		
4 2 0	1.99	5
3 3 2	1.888	9
4 2 2	1.814	30
5 0 1,	1.737	40
4 3 1		
5 2 1	1.623	5
4 4 0	1.573	30
5 3 0,	1.523	30
4 3 3		
4 4 2,	1.480	30
6 0 0		
5 3 2,	1.439	30
6 1 1		
6 2 0	1.402	5
5 4 1	1.371	30

APPENDIX 6 e) Zeolite HS a = 8.86 Å [41]

Sample #	SiO ₂ (mole) x10 ⁻⁴	Al ₂ O ₃ (mole) x10 ⁻⁴	Na ₂ O (mole) x10 ⁻⁴	H ₂ O (mole) x10 ⁻⁵	Fe ₂ O ₃ (mole) x10 ⁻⁶	MgO (mole) x10 ⁻⁵	A/B (mole)
VA05	8.49	4.17	4.07	8.22	0.42	-----	0.98
VA06	7.85	4.19	4.27	10.80	0.34	-----	1.02
VA07	6.20	3.31	3.33	6.00	0.26	-----	1.01
VA08	6.00	3.51	3.26	8.10	0.47	-----	0.93
VA09	5.04	2.54	2.59	16.67	0.32	-----	1.02
VA10	-----	2.50	10.00	8.84	11.70	-----	4.00
VAA06	6.12	2.99	3.01	10.20	17.60	2.50	1.01
VAA08	7.07	2.69	2.96	4.68	25.60	9.88	1.10
VAA10	6.34	2.50	2.93	8.84	17.10	3.05	1.17
VAA11	6.40	2.79	3.09	6.70	15.20	2.95	1.11
VAA12	5.82	3.12	3.40	7.14	17.30	3.01	1.09
VAA15	5.64	3.45	3.00	6.78	15.40	1.79	0.87
VAA16	5.97	3.43	3.08	6.03	16.70	1.78	0.90
VAA17	6.59	2.61	2.91	9.14	3.55	0.20	1.11
Na-A*	7.56	2.63	2.53	8.53	2.41	0.49	0.96

Appendix 7 Chemical Composition of the Na-A zeolite synthesized.
Na-A* stands for (Type 4A LINDE). A/B = molar ratio
NaO/AlO. [11]